Visualising the role of presynaptic calcium in the cerebellar cortex using a novel transgenic mouse

Thesis submitted for the degree of Doctor of Philosophy

By

Salem Hamad Mohamed

Department of Neuroscience, Psychology and Behaviour

College of Medicine, Biological Sciences and Psychology

University of Leicester

United Kingdom

February 2020

Abstract

Topic: Visualising the role of presynaptic calcium in the cerebellar cortex using a novel transgenic mouse

Author: Salem Hamad

Evidence suggests that CB1Rs and NMDARs may be expressed at PF presynaptic terminals and that these receptors may modulate synaptic transmission at synapses formed with cerebellar PCs. Presynaptic effects of receptors and signalling pathways are hard to establish because synaptic terminals are generally too small to allow direct electrical recording. We have explored the use of a transgenic mouse (SyG37) that expresses a ratiometric calcium indicator selectively in presynaptic terminals. Using a combination of fEPSP recordings, fluorescence measurements of presynaptic calcium and pharmacological manipulation, we have explored the use of SyG37 mice for measuring presynaptic activity and synaptic modulation in the cerebellar cortex. We first established that this sensor was widely expressed in the cerebellum but crucially within PF terminals. In response to different patterns of electrical stimulation, calcium dependent responses were reliably detected within ensembles and even single presynaptic boutons. The effects of changing the intensity, frequency and number of stimuli to PF terminals were studied. SyGCaMP2 responses were calcium dependent and inhibited by application of TTX. Direct activation of the GCL produced responses that propagated directly above the point of stimulation through ascending axons. Signals then bifurcated to spread in either direction along PFs. Direct activation of the ML produced responses that propagated along PFs. Activation of NMDARs reduced synaptic transmission through a direct effect on PF terminals since the effect was maintained when all excitatory and inhibitory synaptic transmission was blocked. This effect was due to a decrease in the number of presynaptic boutons that responded to stimulation. Activation of CB1Rs also produced a reduction in synaptic activity that remained when inhibitory and excitatory synaptic transmission was blocked, also suggesting a direct effect on PF terminals. In this case, both the number of boutons responding to stimulation and the amount of calcium entering single terminals was reduced.

Acknowledgements

Foremost, I would like to express my deep and sincere gratitude to my primary thesis supervisor, Prof Nicholas Hartell. He was always incredibly helpful and constantly looking to get the best out of me. He was both an excellent supervisor and an excellent teacher. His guidance helped me throughout my research and the writing of this thesis. This thesis would not have been possible without the help, support and patience of my principal supervisor.

Besides my advisor, I would also like to thank my co-supervisor Dr. Martine Hamann, for the all general help, encouragement and advice.

My grateful thanks also go to the lab members for their assistance and support. In addition, I am grateful to my committee members, Dr. McCutcheon James and Dr. Marra Vincenzo, for offering suggestions and guidance on how to improve my thesis.

I am extending my thanks to all the members of Neuroscience, Psychology and Behaviour departments.

I would like to acknowledge the Libyan Ministry of Higher Education Scholarship Programme for funding my PhD and thus making this research possible.

Finally, my biggest thanks go to my parents, brothers, sisters and friends for their love, prayers, support, caring and sacrifices for educating and preparing me for my future. I am very much thankful to my wife for her love, understanding, prayers and continuing support to complete this research work.

Last but not least, my thanks go to all the people who have supported me to complete the research work directly or indirectly.

Table of contents

Abstract i
Acknowledgements ii
Table of contents iii
List of Figures 1
List of abbreviations 6
Chapter 1: Introduction 9
1.1 Anatomical structure and function of the cerebellum 9
1.1.1 Afferent input and efferent outputs from the cerebellum 11
1.1.2 Cellular structure of cerebellum 13
1.1.3 Information flow in the cerebellum 17
1.2 Evidence for a functional difference between ascending axon and parallel fibre synapses 21
1.3 The use of calcium imaging techniques to monitor synaptic signalling and transmission 22
1.3.1 The dual roles of calcium in triggering and modulating transmitter release 24
1.3.1.1 The mechanism of calcium-dependent transmitter release at presynaptic terminals 28
1.3.1.2 The role of residual calcium in modulating transmitter release 32
1.4 SyGCaMP2-mCherry as a tool for monitoring presynaptic calcium 34
1.5 Presynaptic modulation of synaptic release 35
1.5.1 Evidence for NMDAR located on presynaptic elements modulating synaptic release 40
1.5.2 Evidence for CB1R located on presynaptic elements modulating synaptic release 42
1.6 Summary of aims 46
Chapter 2: Materials and methods 47
2.1 Experimental animals used in this study 47
2.2 Genotyping 49
2.3 Preparation of acute brain slices 51
2.3.1 Solutions and equipment 51
2.3.2 Dissecting and slicing 52

2.4 Reagents 53
2.5 Extracellular field potential recordings 53
2.6 Ca^{2+} Imaging 56
2.6.1 Epifluorescence microscopy 56
2.6.2 Multiphoton microscopy imaging recordings 58
2.6.3 Expression of SyGCaMP2-mCherry in the SyG37 mouse's brain cerebellum slice 59
2.7 Data analysis 60
2.7.1 Field potential data 60
2.7.2 Ca^{2+} imaging data 61
2.7.2.1 Epifluorescence imaging data 61
2.7.2.2 Multiphoton microscopy imaging data 63
2.7.2.3 Subtracting images 65
2.8 Experimental design and statistical analysis 66
Chapter 3: Expression patterns of SyGCaMP2-mCherry in the cerebellar cortex of the SyG37 transgenic mouse line 67
3.1 Introduction 67
3.2 Results 68
3.2.1 Expression patterns of SyGCaMP2-mCherry in cerebellar coronal slices of SyG37 mice 68
3.2.2 Visualisation of neuronal activity in the cerebellar cortex in SyG37 mice using a wide-field epifluorescence microscope 75
3.3. Discussion 81
Chapter 4: Pharmacological and electrophysiological investigation of the characteristics of SyGCaMP2 signalling in the cerebellar cortex of SyG37 mice 83
4.1 Introduction 83
4.2 Results 85
4.2.1 Pharmacological and electrophysiological investigation of SyGCaMP2 responses to ML stimulation 85
4.2.1.1 The effects of the sodium channel blocker tetrodotoxin (TTX) on SyGCaMP2 fluorescence and field potential responses to ML stimulation 85
4.2.1.2 The effects of lowering extracellular calcium on SyGCaMP2 fluorescence and field potential responses to ML stimulation 89

4.2.1.3 The effects of pharmacological inhibition of AMPA, $GABA_A$ /Glycine and NMDA receptors on the SyGCaMP2 fluorescence and field potential of the PF responses to ML stimulation 93

4.2.1.4 The effects of the NMDAR antagonist DL-AP5 on SyGCaMP2 fluorescence and field potential responses to ML stimulation 96

4.2.2 Measurements of calcium transients within the ML and GCL regions to different patterns of stimulation using the SyGCaMP2 sensor 98

4.2.2.1 The effects of increasing stimulus intensity on both SyGCaMP2 fluorescence and fEPSP responses to direct stimulation of the ML 98

4.2.2.2 The effects of increasing stimulus intensity on SyGCaMP2 fluorescence responses to direct stimulation of the GCL 104

4.2.2.3 The effects of increasing stimulus number and frequency on SyGCaMP2 fluorescence within the ML and GCL to direct and indirect stimulation of GCL and ML 108

4.2.2.4 The effects of increasing stimulus intensity on individual presynaptic boutons within the ML to direct stimulation of the ML 111

4.2.2.5 The effects of increasing stimulus number on individual presynaptic boutons within the ML to direct stimulation of the ML 113

4.3. Discussion 115

4.3.1 SyGaMP2 as a sensor for measuring presynaptic calcium in the cerebellar cortex 115

4.3.2 Using SyG37 mice to visualise activity in the cerebellar cortex 118

Chapter 5: Investigating the Role of Presynaptic NMDA Receptors at Cerebellar PF-PC Synapses 121

5.1 Introduction 121

5.2 Results 123

5.2.1 Effects of NMDA receptor activation with extracellular perfusion with NMDA and glycine 123

5.2.2. Effects of AMPA receptor inhibition 129

5.2.3 Effects of NMDA/Gly application in during pharmacological blockade of AMPA and $GABA_A$ receptors. 131

5.2.4 Effects of NMDAR activation in the presence of NMDAR antagonist AP5 133

5.2.5 Effects of activation of NMDAR with and without the presence of AP5 on baseline level of SyGCaMP2: mCherry Ratio 136

5.2.6 Effects of NMDAR activation on single presynaptic bouton responses ... 139

5.3 Discussion ... 141

Chapter 6: Investigating the Role of Presynaptic CB1R at Cerebellar PF-PC Synapses using SyG37 mice ... 148

6.1 Introduction ... 148

6.2 Results ... 149

6.2.1 Effects of activation of CB1Rs with extracellular perfusion with endocannabinoid agonist WIN55, 212-2 ... 150

6.2.2 Effects of CB1R activation in the presence of pharmacological blockade of AMPA, NMDA and GABAA receptors ... 154

6.2.3 Effects of CB1R activation in the presence of pharmacological blockade of CB1R blocker ... 156

6.2.4 Effects of activation of CB1Rs with and without AM251 on the baseline SyGCaMP2: mCherry Ratio ... 159

6.2.5 Effects of CB1R activation on single presynaptic bouton responses ... 161

6.3. Discussion ... 163

Chapter 7: General Discussion ... 170

References ... 178

List of Figures

Figure 1.1. Schematic representation of the major anatomical subdivisions of the cerebellum……..10

Figure 1.2. Schematic diagram of input and output connections of the cerebellum……13

Figure 1.3. A schematic diagram of the major neurones in the cerebellar cortex…17

Figure 1.4. A schematic diagram of a cerebellar glomerulus……..18

Figure 1.5. Diagram of Information flow in the cerebellum…….. 20

Figure 1.6. Schematic diagram of the structural organization of a presynaptic terminal of a neuron……..25

Figure 1.7. The principal stages of the vesicle cycle……..…28

Figure 1.8. Model of the SNARE/SM protein cycle and the function interaction of complexion and synaptotagmin 1 in calcium fusion triggering……..32

Figure 1.9. Schematic diagram of neurone structure and synapses between neurones…….36

Figure 1.10. Schematic representation of the structure and NMDAR activation…39

Figure 1.11. Inhibition of synaptic release linked to NMDA receptor activation……42

Figure 1.12. Possible model for the endocannabinoid mechanism of action……45

Figure 2. 1. Schematic diagram of SyGCaMP2-mCherry construction…….....…48

Figure 2.2. Typical example of a genotyping gel used for identification of transgenic mice from SyG37 colonies……..…51

Figure 2.3. A typical trace for an extracellular field potential response evoked by the activation of the cerebellar PFs……..55

Figure 2.4. Photographs of the imaging and electrophysiological recording system used for experiments……..…..…57

Figure 2.5. Multiphoton microscope system and control software used to obtain images of single boutons……59

Figure 2. 6. Analysis steps for SyGCaMP2 imaging……..……64

Figure 2.7. Typical trace for a SyGCaMP2 fluorescence response……..…65

Figure 3.1. Expression pattern of SyGCaMP2-mCherry in cerebellar coronal slices of SyG37 and wildtype mice using epifluorescence microscope……..……..….69

Figure 3.2. Expression pattern of SyGCaMP2 in cerebellar coronal slices as shown using multiphoton microscopy…….…..…71

Figure 3.3. Expression pattern of SyGCaMP2-mCherry in sagittal slices of SyG37 and WT mice using multiphoton microscopy…….……73

Figure 3.4. Expression pattern of SyGCaMP2-mCherry in coronal slices of SyG37 and WT mice using multiphoton microscopy……...….74

Figure 3.5. Expression pattern of SyGCaMP2 in coronal slices of SyG37 mice obtained using multiphoton microscopy…….75

Figure 3.6. The time course of changes in SyGCaMP2 and mCherry fluorescence in response to electrical stimulation of the ML of the cerebellum of SyG37 mice …76

Figure 3.7. Visualisation of neuronal activity in the cerebellar cortex in SyG37 mice using epifluorescence microscopy…….78

Figure 3.8. Visualisation of neuronal activity in the cerebellar cortex of SyG37 mice using multiphoton microscopy…….80

Figure 4.1. Schematic diagram of parallel fibres - Purkinje cell synapses……..…86

Figure 4. 2. Effects of 0.1 μM TTX on SyGCaMP2 fluorescence and corresponding field potential responses to ML stimulation in sagittal cerebellar slices…..…….88

Figure 4.3. Effects of lowering extracellular calcium on SyGCaMP2 fluorescence and field potential responses to ML stimulation in sagittal cerebellar slices…...…90

Figure 4.4. The effects of lowering extracellular calcium with increased of concentrations magnesium on SyGCaMP2 fluorescence and field potential responses to ML stimulation in sagittal cerebellar slices……92

Figure 4.5. Effects of 10 μM NBQX, 10 μM PTX then 50 μM DL-AP5 on SyGCaMP2 fluorescence and corresponding field potential responses to ML stimulation in sagittal cerebellar slices…….……..…95

Figure 4.6. Effects of AP5 on SyGCaMP2 fluorescence and corresponding field potential responses to ML stimulation in sagittal cerebellar slices…….…….97

Figure 4.7. Visualization of the effects of direct activation in the ML of coronal cerebellar slices on SyGCaMP2 fluorescence……99

Figure 4.8. Schematic diagram for direct activation of the molecular layer in coronal cerebellar slices of SyG37 mice……100

Figure 4.9. Effects of increasing stimulus intensity on SyGCaMP2 fluorescence within the ML and GCL regions to direct activation of the ML in coronal cerebellar slices of SyG37 mice…….…….101

Figure 4.10. Effects of increasing stimulus intensity on peak SyGCaMP2 and fEPSP responses and the relationship between peak SyGCaMP2 and field of the PF responses to direct activation of the ML in coronal cerebellar slices of SyG37 mice…….……...…103

Figure 4.11. Visualization of the effects of direct activation in GCL of coronal cerebellar slices on SyGCaMP2 fluorescence……..…105

Figure 4.12. Schematic diagram for direct stimulation of the granule cell layer in coronal cerebellar slices of SyG37 mice…….……...106

Figure 4.13. Effects of increasing stimulus intensity on SyGCaMP2 fluorescence within the GCL and GCL regions to direct activation of the GCL in coronal cerebellar slices of SyG37 mice……..…107

Figure 4.14. Direct and indirect stimulation in the ML and GCL of SyGCMP2 responses in coronal cerebellar slices of SyG37 mice…….……108

Figure 4.15. The effects of increasing stimulus number and frequency on SyGCaMP2 fluorescence to a direct and indirect stimulation of GCL and ML…..110

Figure 4. 16. Effects of increasing stimulus intensity on individual presynaptic boutons within the ML to direct stimulation of ML…….……112

Figure 4. 17. Effects of increasing stimulus number on SyGCaMP2 responses in individual presynaptic boutons within the ML to direct stimulation of the ML…….114

Figure 5. 1. Effects of applications of NMDA and glycine on SyGCaMP2 fluorescence to molecular layer stimulation……...…126

Figure 5. 2. Visualization of the effects of NMDA/Gly on SyGCaMP2 fluorescence responses to cerebellar ML stimulation……...127

Figure 5.3. Effects of perfusion of NMDA and glycine on fEPSP responses…….…128

Figure 5.4. Effects of AMPA receptor inhibition…….....131

Figure 5.5. Effects of NMDA receptor activation in the presence of a pharmacological blockade of AMPA and GABAA receptors……..….133

Figure 5.6. Effects of NMDA receptor activation in the presence of a pharmacological blockade of NMDA receptor blocker……..……..….135

Figure 5.7. Pharmacological characterisation of the NMDA/Gly-induced depression of SyGCaMP2 and synaptic transmission responses……...136

Figure 5.8. Effects of activation of NMDAR with and without the presence of AP5 on the baseline ratios…….……..…...138

Figure 5.9. Positive modulation of NMDA reduces the number of responding puncta but fails to effect the puncta size in response to ML stimulation……..140

Figure 5.10. Positive modulation of NMDA reduces the number of responding puncta but fails to effect the puncta size in response to ML stimulation…….……141

Figure 5.11. Schematic diagram showing the glutamatergic synapse between parallel fibres and the Purkinje cell, as well as illustrating the location of the NMDA receptors at parallel fibres…….……..…….147

Figure 6.1. The effects of the CBR1 agonist WIN55, 212-2 on SyGCaMP2 fluorescence responses to ML stimulation in coronal cerebellar slices……...151

Figure 6.2. The effects of the CBR1 agonist WIN55, 212-2 on field potential responses to ML stimulation in coronal cerebellar slices…….……152

Figure 6.3. Visualization of the effects of WIN55, 212-2 on SyGCaMP2 fluorescence responses to cerebellar ML stimulation…….……..……153

Figure 6.4. CB1R activation modulates SyGCaMP2 fluorescence responses to ML stimulation in the presence of DNQX, AP5 and picrotoxin……..……155

Figure 6.5. Prevention of WIN55, 212-2-induced suppression of SyGCaMP2 fluorescence responses recorded from the ML region to electrical activation of the ML by prior bath application of 10 μM AM251……..…….157

Figure 6.6. Prevention of WIN55, 212-2-induced suppression of PF amplitude recorded from the ML region to electrical activation of the ML by prior bath application of 10 μM AM251…….……158

Figure 6.7. Pharmacological characterisation of the WIN55, 212-2 induced depression of SyGCaMP2 and synaptic transmission responses……..……159

Figure 6.8. Effects of activation of CB1R in the absence and presence of AM251 on the resting ratios of SyGCaMP2: mCherry…….……....161

Figure 6.9. CB1Rs activation reduces the number and size of single puncta responses that respond to ML stimulation……..…....162

Figure 6.10. Proposed scheme overview for the endocannabinoid mechanism…….……169

List of abbreviations

aCSF	Artificial cerebrospinal fluid
AMPA	α-amino-3-hydroxyl-5-methyl-4-isoxazole propionate receptors
AP	Action potential
AP5	2-amino-5-phosphono-valerate
ATP	Adenosine 5’ triphosphate
AUC	Area under the curve
AM251	N-(Piperidin-1-yl)-5-(4-iodophenyl)-1-(2,4-dichlorophenyl)-4-methyl-1H-pyrazole-3-carboxamide
BCs	Basket Cells
CB1R	Cannabinoid-1 receptor
Ca^{2+}	Calcium
CaM	Calmodulin
CaMK	Calcium calmodulin-dependent protein kinase
CaMKII	Calmodulin kinase 2
cAMP	Cyclic adenosine monophosphate
CAZ	Cytomatrix at active zones
CF	Climbing fibre
CNS	Central nervous system
cpEGFP	Circularly permuted enhanced green fluorescent protein
DAG	Diacylglycerol
DNA	Deoxyribonucleic acid
DNQX	6,7-dinitroquinoxaline-2,3-dione
DMSO	Dimethyl sulfoxide
DCN	Deep cerebellar nuclei
EPSPs	Excitatory postsynaptic potentials
ER	Endoplasmic reticulum
F	Fluorescence
fEPSP	Field excitatory post synaptic potential
EPSC	Excitatory postsynaptic current
GABA	Gamma-Aminobutyric Acid
GABAAR	Gamma-Aminobutyric Acid type A Receptor
GCaMP	GFP + Calmodulin + myosin protein
GC	Granular cell
GCL	Granular cell layers
GECI	Genetically encoded calcium indicator
GFP	Green fluorescent proteins
Gly	Glycine
GluRs	Glutamate receptors
GMP	Guanosine-5’-monophosphate
GoC	Golgi cell
GPCR	G-protein coupled receptors
GTP	Guanosine triphosphate
IP3	Inositol 1, 4, 5-trisphosphate

IO	Inferior olivary
K^+	Potassium
LTD	Long-term depression
LTP	Long term potentiation
MF	Mossy Fibre
Mg^{2+}	Magnesium
mGluRs	Metabotropic glutamate receptors
Min	Minutes
ML	Molecular layer
Munc13	Mammalian uncoordinated-13
Munc18	Mammalian uncoordinated-18
N1	First negative component of the fEPSP
N2	Second negative component of the fEPSP
NBQX	2,3-Dioxo-6-nitro-1,2,3,4-tetrahydrobenzo[f]quinoxaline-7-sulfonamide
NMDA	N-methyl-D-Aspartate receptor
NMDAR	N-methyl-D-aspartate- type ionotropic glutamate receptors
NO	Nitric oxide
ns	Not significantly different
NSF	N-ethylmaleimide-sensitive factor
NT	Neurotransmitter
PC	Purkinje cell
PCL	Purkinje cell layer
PCR	Polymerase chain reaction
PF	Parallel fibre
PIP2	Phosphatidylinositol 4, 5 bisphosphate
PKA	Protein kinase A
PKC	Protein kinase C
PKG	Protein Kinase G
PLA2	Phospholipase A2
PLC	Phospholipase C
PPD	Paired-pulse depression
PPF	Paired-pulse facilitation
PPR	Paired pulse ratio
PTX	Picrotoxin
Rab3a	Ras-related protein
Rim	Rab3-interacting molecule
ROIs	Regions of interest
RyR	Ryanodine receptor
s	Second
SC	Stellate cell
SEM	Standard error of means
SNAP-25	Synaptosomal-associated protein 25
SNAREs	Soluble N-ethylmaleimide-sensitive factor attachment protein receptors

STD	Short term depression
STP	Short term plasticity
SV	Synaptic vesicle
TAE	Tris base, acetic acid and EDTA
TRPCs	Transient receptor potential channels
TTX	Tetrodotoxin
THC	Tetrahydrocannabinol
t-SNAREs	Target membrane SNARES
UBCs	Unipolar brush cells
V	Voltage
VAMP	Vesicle-associated membrane protein
VAMP2	Vesicle-associated membrane protein 2
VDCC	Voltage-dependent calcium channels
VGCCs	Voltage-gated calcium channels
vGluT	Vesicular glutamate transporter
vGAT	Vesicular GABA transporter
v-SNARE	Vesicular SNARE
WT	Wild type
WIN 55,212-2	(R)-(+)-[2,3-Dihydro-5-methyl-3-(4-morpholinylmethyl) pyrrolo[1,2,3-de] 1,4-benzoxazin-6-yl] -1-naphthalenylmethanone mesylate

Chapter 1: Introduction

1.1 Anatomical structure and function of the cerebellum

The cerebellum (Latin for; “little brain”) is a mass of nervous tissue that covers most of the posterior surface of the brain stem. Although it comprises about 10% of the total volume of the human brain, it contains more than 50% of its neurons (Ito and Itō, 1984, Nolte, 1988, Wright et al., 2016). The cerebellum has a lot of different functions. It collects sensory and motor inputs from the entire body via the spinal cord and brainstem. With this collection of inputs, it performs various significant functions: for vision, it coordinates eye movements; in the body, it maintains balance, posture and coordinates movements; in motor learning, it helps the body to learn movements that need practice and fine tuning (Ito, 2006, Strick et al., 2009, Purves et al., 2008). Recent evidence also suggests that the cerebellum is involved in cognitive and emotive functions (Stoodley and Schmahmann, 2010, D‘Angelo and Casali, 2013). Damage to the cerebellar cortex can lead to many and various conditions, such as ataxia, loss of balance, dysmetria and motor learning deficiency (Schmahmann, 2004, Kreutz and Sala, 2012). At the anatomical level, the cerebellum is located behind the cerebrum. It occupies most of the posterior cranial fossa. The surface of the cerebellum has folds and fistulations that result in a massive increase in surface area of the cerebellum. It is composed of grey matter (cerebellar cortex), white matter (inner cortex) and three pairs of deep nuclei. The white matter contains a tract of myelinated nerve fibres while the grey matter contains cell bodies of neurons, dendrites and glial cells. Three pairs of deep nuclei include the fastigial, two interposed (the globose and emboliform) and the dentate nuclei. These pairs project out of the cerebellum (Kandel et al., 2000, Llinas and Negrello, 2015). There are three anatomical lobes that can be distinguished in sagittal sections of the cerebellum. These lobes include the anterior lobe (responsible for the tone of muscles), the posterior lobe (responsible for coordinating movement) and the flocculonodular lobe (responsible for maintaining balance). They are also separated by two fissures: the primary fissure, which is located on the upper surface and divides the corpus cerebelli anterior and posterior lobules; and the posterolateral fissure, which is located on the underside of the

cerebellum and divides the large posterior lobe from the small flocculonodular lobe. Shallower fissures subdivide the anterior and the posterior lobe into large numbers of lobules across species (see Figure 1.1). In mammals, anatomists have found 10 lobules that differ in size (Voogd and Glickstein, 1998, Kandel et al., 2000, Nieuwenhuys et al., 2007). The cerebellum can also be divided into medial and lateral regions by two longitudinal furrows that cut across the anterior, posterior and flocculonodular lobes. The vermis (Latin, "worm") is the middle zone of the cerebellum and has a major cerebellar hemisphere on each part. Each hemisphere consists of an intermediate and lateral segment. There is also a shallow groove which comprises the paravermis which helps to distinguish the separation between the central vermis and other two hemispheres (Kandel et al., 2000, Nieuwenhuys et al., 2007, Purves et al., 2008).

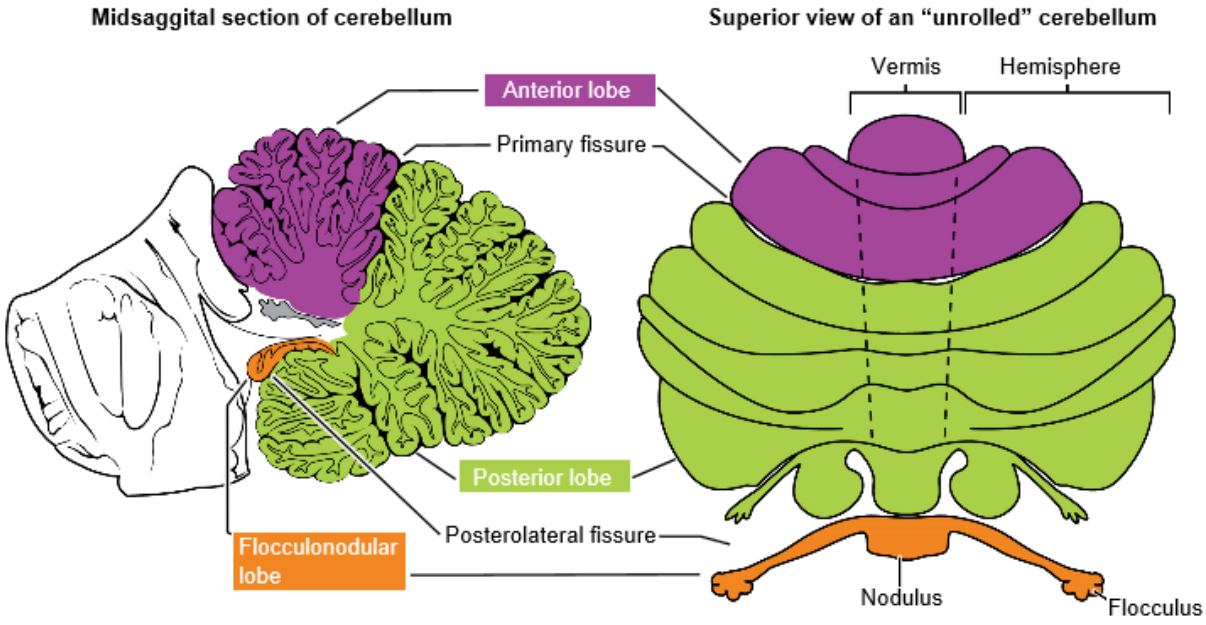

Figure 1.1. Schematic representation of the major anatomical subdivisions of the cerebellum. Midsagittal section of the cerebellum (left) showing the anterior lobe, posterior lobe and flocculo- nodular lobe. It also shows the primary fissure and the posterolateral fissure. The superior view (right) shows the vermis connecting with the hemispheres on either side. The paravermis is not shown. Adapted from https://en.wikipedia.org/wiki/Anterior_lobe_of_cerebellum#/media/File:1613_Major_Regions_of_the_Cerebellum-02.svg.

The cerebellum is highly regular in structure. It is made up of three main layers, the outer molecular layer (ML), the Purkinje cell layer (PCL) and inner granular layer (GCL). Each layer is composed of various cell types. In the following section, the input and output connections of the cerebellum, cellular structure of cerebellum and information flow in the cerebellum will be briefly described.

1.1.1 Afferent input and efferent outputs from the cerebellum

The connection of inputs and outputs to and from the cerebellum occur through three pairs of pathways that connect with the brain stem. These pathways, called the cerebellar peduncles, consist of the middle cerebellar peduncles (or brachium pontis), inferior cerebellar peduncles (or restiform body) and superior cerebellar peduncles (or brachium conjunctivum). The middle cerebellar peduncle is the largest of the three and carries afferent pathways that arrive from pontine nuclei. The inferior peduncle is both the smallest of the three and the most complex as it contains several afferent and efferent paths. The afferent pathways contain axons from the spinal cord, the vestibular nuclei and various areas of brainstem tegmentum, while the efferent pathways contain axons to the reticular formation and the vestibular nuclei (Purves et al., 2008). Finally, the superior cerebellar peduncles, which is an efferent pathway, carries cerebellar efferents from the deep cerebellar nuclei (DCN) to the upper motor neurons (Carleton and Carpenter, 1983, Kandel et al., 2000).

The entire output of the cerebellum acts initially on the DCN and vestibular nuclei. These nuclei then transmit the output to motor areas of the cerebral cortex and the brain stem. The activity of Purkinje cells (PCs), which represents the only output cell of the cerebellar cortex, is determined via two excitatory inputs, which are the climbing fibres (CFs) and mossy fibres (MFs) (Kandel et al., 2000, Purves et al., 2008). Afferent input to the cerebellum is basically supplied by CFs and MFs. MFs arise from many nuclei of the brainstem and spinal cord. They influence PCs indirectly via synapses with granule cells (GCs). MFs carry sensory information from precerebellar nuclei (i.e., such as the pontine and vestibular nuclei, etc.), spinal cord and the reticular formation, and supply GCs, which form ascending axons that

bifurcate to form parallel fibres (PFs) (Eccles et al., 1966). MF-GC synapses can be modulated by GABAergic inhibitory Golgi cells (GoCs) (Ito, 2006). The other excitatory inputs to the cerebellum come from CFs. They arise from the inferior olivary nucleus (IONs) in the medulla oblongata of the hindbrain. CFs are so named due to the morphology of their terminations on the PCs. Their axons spread into the cortex and wrap around the dendrites and the soma of the PCs, where they create many excitatory synapses (Strata and Rossi, 1998, Dittman and Regehr, 1998, Purves et al., 2008). The ION integrates sensory motor information from various areas of the brain such as the spinal cord, precerebellar nuclei and cerebral cortex (Dean et al., 2010). This information is conveyed by CFs which connect to the cerebellum and to the DCN. Apart from the direct projection from the cerebellum to the vestibular nuclei, the cerebellum projects to the DCN that projects, in turn, to the neurons of the upper motor cortex (by a relay in the thalamus) and brainstem (Purves et al., 2008). The DCN is the output gate from the cerebellum. All the Information processed in the cerebellum is sent out to the DCN where it is incorporated with the input of the cerebral MFs and CFs (Kandel et al., 2000, Brodal, 2004). Pathways leaving the DCN project to the reticular formation, the superior colliculus, the vestibular nuclei, and the upper motor neurons in the red nucleus (Voogd and Glickstein, 1998, Kandel et al., 2000, Purves et al., 2008). A diagram of the afferent and efferent connections of the cerebellum is shown in Figure 1.2.

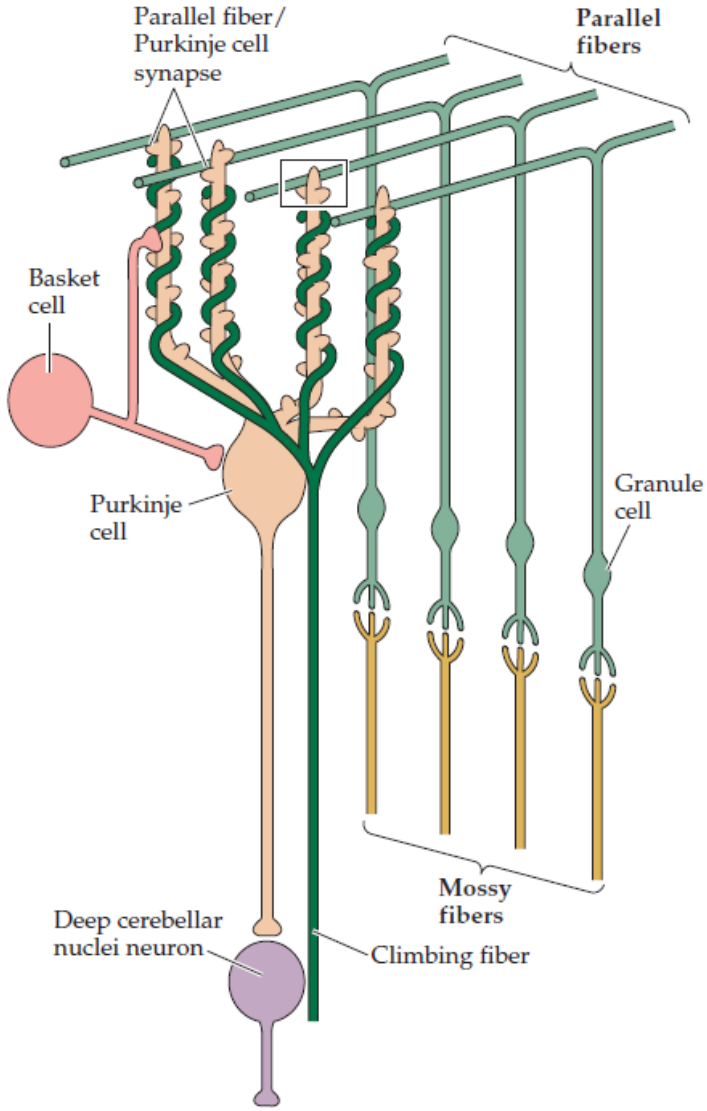

Figure 1.2. Schematic diagram of input and output connections of the cerebellum. The input information is supplied by the mossy fibres and climbing fibres, while the output information is carried out by Purkinje cells to the deep cerebellar nuclei neurons. Taken from (Purves et al., 2008).

1.1.2 Cellular structure of cerebellum

The three layers of the cerebellar cortex contain different types of neuron which include, firstly, the GCL, which contains GCs, GoCs, unipolar brush cells (UBCs) and Lugaro cells, and secondly the PCL, which contains PCs. Finally, the molecular layer (ML) contains stellate cells (SCs) and basket cells (BCs). In total, there are seven types of neuronal cells that will be briefly described in the following section.

i) Purkinje cells

PCs are the biggest neuron in the vertebrate CNS. They are the principle cells of the cerebellum, and the first discovered in 1837 by Johannes Evangelista Purkinje. PCs are essential because they represent the only output cell in the cerebellum. They have a big and wide dendritic arborisation that extends into the ML, where every single PC can receive about 200,000 excitatory synapses from the PFs in the rat (Napper and Harvey, 1988, Kandel et al., 1991). In striking contrast to the single contact formed by many PFs, CFs make only a single connection to each PC, but with around hundreds to thousands of synaptic release sites that cover particularly the more proximal the dendrites of the PC (Strata and Rossi, 1998, Kandel et al., 1991, Llinas and Negrello, 2015). PCs project to DCN neurons and create GABAergic inhibition in projection regions that contain a large number of different cell types within the DCN (Chaumont et al., 2013). Furthermore, PC axons make collaterals and can form synapses with many different cell types, such as GoCs, ML interneurons and Lugaro cells (Palay and Chan-Palay, 2012).

ii) Granule cells

GCs represent the largest single type of neuron in the mammalian brain; it is estimated that there are more than 50 billion in each individual. They fill up the area between the PCL and the white matter in the cerebellum, constituting around one-third of the latter. They are small in terms of cell body size, with a diameter of about 4-8 μm on average (Lamont and Weber, 2012, Llinas and Negrello, 2015, Sutton, 1971). During cerebellar development, GCs (in postnatal 10-day old mice) eventually migrate from their birthplace in the top of the external granular layer to their final destination at the bottom of the internal granular layer through the ML and the PCL (Komuro and Rakic, 1998, Komuro et al., 2001); for a review see Yacubova and Komuro (2002).

Each GC axon first ascends into the ML to form ascending axons which then bifurcate to form PFs. These then extend several millimetres in either direction of cerebellar folia. GCs receive the excitatory input from MFs. Both the PFs and

ascending axons form a large number of synapses with PCs (Eccles et al., 1967, Chan-Palay, 1974, Kandel et al., 1991).

iii) Golgi cells

GoCs are the second-most common cell in the GCL. It is the main inhibitory neuron in the cerebellum. It was discovered in 1873 by Camillo Golgi. It can receive excitation from both GCs and MFs. GoC neurons suppress the excitation of GC to MF input which ultimately arrives at the PC through PFs (Palkovits et al., 1971, Pellionisz and Szenta, 1973). Furthermore, GoCs also receive inputs from CFs, PCs and ML interneurons (Chan-Palay, 1974). GoCs are generally present in two sizes: smaller ones have a soma diameter that is about 6-11 μm and are located in the lower half of the GCL. Larger ones have a somatic diameter of 9-16 μm and their location is the top part of the GCL. GoC axons branch frequently in the GCL where they terminate on dendrites of GCs. The number of GoCs is roughly the same as that of PCs (Kandel et al., 2000, Lamont and Weber, 2012, Llinas and Negrello, 2015).

Finally, the GCL also contains UBCs and Lugaro cells. UBCs are generally associated with vestibular signalling and are found for the most part in the flocculonodular lobe. They are generally connecters for vestibular signals. The name UBC derives from the brush-like dendritic arbor that is spiny, tufty and short branched, creating synapses in the structures of glomerulae with which they connect to GCs. UBCs are usually thought to distribute and multiply the MF signals carrying vestibular input. Interestingly, UBCs are also found in the dorsal cochlear nucleus. However, neither of these cells have yet been fully described, for more details, see Hirono et al. (2012); Chan-Palay (1974); Lainé and Axelrad (2002); Llinas and Negrello (2015).

iv) Molecular layer interneurons: Basket cells and Stellate cells

BCs and SCs are interneurons that reside in the ML. Although the morphologies of these two cell types are different, extensive research has shown that they have an

almost identical functionality (Jörntell and Ekerot, 2003). Their neurotransmitter is γ-aminobutyric acid (GABA). They locally inhibit PCs. They are excited by PFs and then give feedforward inhibition onto PCs (Cohen and Yarom, 2000). The major inhibitory input to PFs is from GoCs and neighbouring interneurons. Previous research has established that interneurons can also be activated by CFs (Szapiro and Barbour, 2007). SCs are found in the most superior part of the ML. They have short axons and a few radial dendrites that make synapses with nearby dendrites of PCs in the ML. On the other hand, BCs are found to be located mostly in the lower part of the ML. They receive PF inputs as well as CF collaterals. BCs axons expand along the PCL at right angles to the direction of the PFs. As result, when PFs excite a row of PCs and neighbouring BCs, this inhibits the PC (Eccles et al., 1967, Kandel et al., 1991). Many studies suggest that as many as 50 different BCs wrap their terminals around each PC soma forming pinceau synapses (Szentágothai et al., 1966, Tigyi et al., 1990, Kandel et al., 2000, Buttermore et al., 2012). BC axons also ascend to connect to the PC dendritic tree (Hámori and Szentágothai, 1966). A diagram of the neurones in the cerebellar cortex is shown in Figure 1.3.

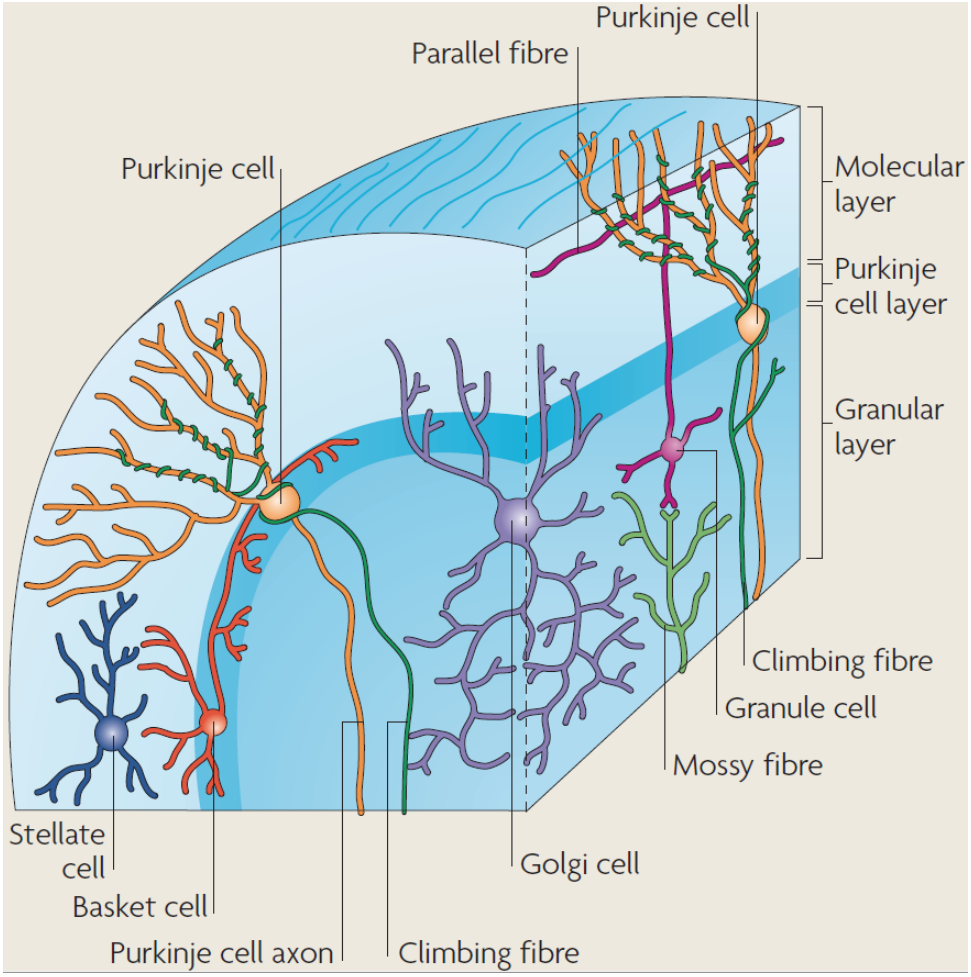

Figure 1.3. A schematic diagram of the major neurones in the cerebellar cortex. This diagram illustrates the location and connections of five of the main neuronal types that are found in the cerebellum, which are Purkinje cells, granule cells, Golgi cells, Basket cells, and Stellate cells. Lugaro cells and the unipolar brush cells are not shown. Adapted from Dean et al. (2010).

1.1.3 Information flow in the cerebellum

The cerebellum has an interestingly uniform structure in terms of cell structure and organization, as mentioned earlier. It is divided into three layers. The GCL comprises huge numbers of small GCs and fewer GoGs. The axon terminals of GCs, GoGs and MFs form synapses within a glomerulus (see Figure 1.4) in the granular layer (Jakab and Hamori, 1988, Tibbetts, 2013).

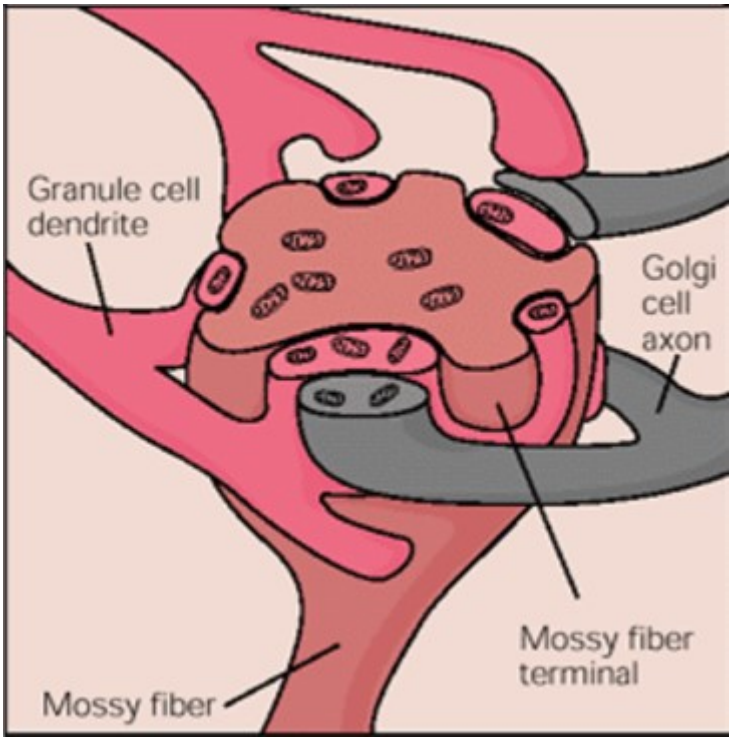

Figure 1.4. A schematic diagram of a cerebellar glomerulus. The glomerulus contains the bulbous terminals of mossy fibres that make synaptic contact with Golgi cell axon terminals and granule cell dendrites. Adapted from Tibbetts (2013).

GCs have specialized axons which ascend and bifurcate to form PFs. GC dendrites are excited by MF terminals and inhibited by the GoC axons (Ito, 2006). The activation of GoCs, however, can occur via two direct synapses, which are from MFs and/or GCs. As a result, GoGs trigger feedback inhibition in GCs (Shinoda et al., 1992, Hamann et al., 2002, Cesana et al., 2013). The cell bodies of PCs are located in the PCL. The dendrites of PCs project through into the ML, while their axons pass through the GCL. GCs also send their axons to the ML where they form PFs and excite PCs. There are two types of excitatory synaptic inputs received by PCs. The first is indirectly from PFs. The second is directly from CFs that originate from the ION and carry the motor information and sensory information required for learning(Purves et al., 2008, Dean et al., 2010). Neurotransmission in both PF-PC and CF-PC synapses is mediated by glutamate. CF inputs provide a very strong excitatory drive to PCs (Dittman and Regehr, 1998). GoGs receive input information from PFs and supply an inhibitory feedback to GCs (Pellionisz and Szenta, 1973, Kandel et al., 1991).

As mentioned above, there are two types of ML inhibitory interneuron, which are SCs and BCs. These are excited by PFs and then supply feedforward inhibition onto PC dendrites. Together, the two excitatory inputs from CFs and MFs and the two inhibitory inputs from BSs and SCs modulate ongoing PC activity according to their relative timings. GoC, SCs and BCs control the information flow through the cerebellum. When CF and PF inputs arrive simultaneously to a PC, PF-PC synapses may produce a long-term depression (LTD), whereas when PF inputs connect without concurrent CF input, PF-PC synapses can produce long-term potentiation (LTP) (Jacoby et al., 2001, Coesmans et al., 2004, Sims and Hartell, 2005, Sims and Hartell, 2006, Salin et al., 1996). Finally, the final destination of the input pathways to the cerebellum is the PCs. They represent the only output of the cerebellum and provide projections to the DCN, as mentioned earlier. PCs are inhibitory and release GABA from synapses formed within the DCN and their output represents an integration of inputs from PFs and CFs, as well as direct and indirect influences from BCs, SCs and GCs. For example, SCs and BCs have a direct inhibitory impact on PCs. However, GoCs also inhibit GCs and so this leads to an indirect modulatory effect (Nolte, 1988, Siegel and Sapru, 2015, Kandel et al., 1991, Purves et al., 2008). Figure 1.5 illustrates how information flows in the cerebellum.

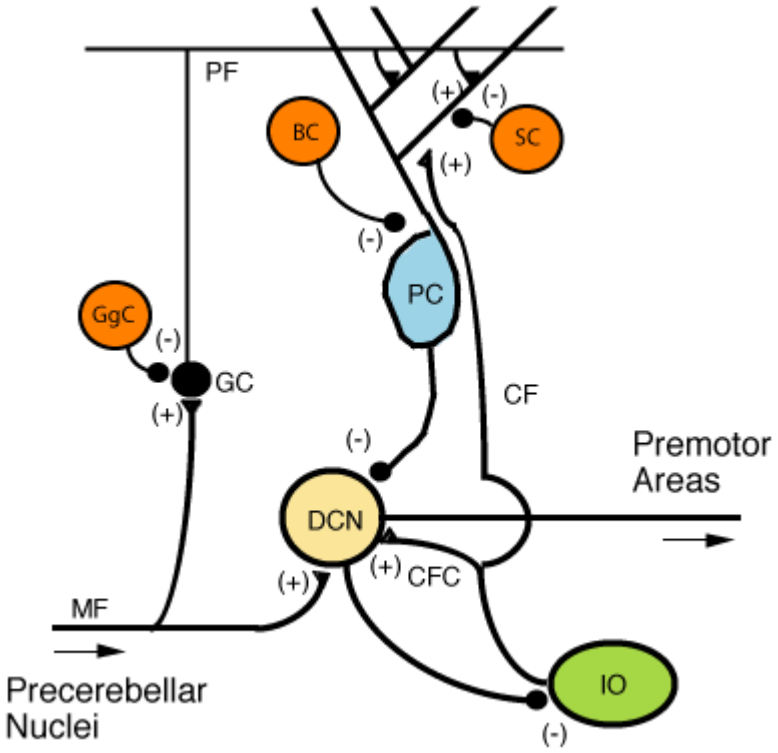

Figure 1.5. Diagram of Information flow to and from the cerebellum. This shows the excitatory and inhibitory connections in cerebellar circuits and in the deep cerebellar nuclei. MF inputs induce excitation in GCs and GgCs. GgCs then provide feedback inhibition to GCs. GC axons form PFs to stimulate PC dendrites, which then also get feedforward inhibition from BCs and SCs. CFs excite PCs. PC output is produced by the combination of inputs. The PC output is ultimately sent to the DCN. Figure adapted from Sachana et al. (2016).

Abbreviations

(+): excitatory; (-): inhibitory; GgC: Golgi cell; PC: Purkinje cell; GC: Granule cell; PF: Parallel fibre; MF: Mossy fibre; CF: Climbing fibre; CFC: Climbing fibre collateral; BC: Basket cell; SC: Stellate cell; IO: Inferior olive; DCN: Deep cerebellar nuclei.

There is also a number of neuromodulators that can influence the cerebellar circuitry such as acetylcholine, norepinephrine, serotonin, dopamine (Schweighofer et al., 2004) and adenosine (Dittman and Regehr, 1996, Wall et al., 2007).

1.2 Evidence for a functional difference between ascending axon and parallel fibre synapses

GCs have long axons that ascend into the ML and then bifurcate to form PFs, which extend for several millimetres across the cerebellar cortex. The PFs and ascending axons both make synapses with PCs. It is estimated that each PC receives converging input from upwards of 200,000 PFs (Napper and Harvey, 1988, Kandel et al., 2000). PFs make more synapses than the ascending segment of the same axon. This is due to the variation in the length of these axonal segments (Gundappa-Sulur et al., 1999). Ascending axon inputs form about 7-24% of the total GC inputs on the PC. Recently, several lines of evidence suggest that there is a functional difference in the transmission properties between synapses formed by ascending and PF segments of granule cell axons of a presynaptic nature. Sims and Hartell (2005) demonstrated that, in the same axon, ascending granule cell axon synapses release transmitters with higher release probabilities and amplitudes of mean quantal compared with PFs synapses. Furthermore, ascending granule cell axon synapses are more resistant to cerebellar LTD than PF synapses. This led to the suggestion that there is further level of functionality and complexity of cerebellar processing. Moreover, Sims and Hartell (2006) found that synapses formed via ascending GC axons to PCs were highly also resistant to forms of LTP compared with PFs at the same axon, further suggesting that the two segments of GC axons perform different functions in cerebellar signalling pathways. Several studies (Heck, 1995, Vranesic et al., 1994, Díez-García et al., 2005) have shown that although direct activation of PFs generate activation along beams of fibres over some distance, activation of the MFs produces only spatially restricted spots of stimulation above the region of the MF termination with in many cases only slight evidence of PF beam activation (Jaeger, 2003). Díez-García et al. (2005), on the other hand, found that the direct stimulation in the GCL produced local responses and beam responses in the ML. Synapses of the ascending granule cell axon are darker in their presynaptic terminal than those formed by PFs. This led to the suggestion that ascending axon synapses have a high release probability of transmitter (Gundappa-Sulur et al., 1999) and indeed experimentally, this was found to be the case (Sims and Hartell, 2005). Whilst evidence accumulates to indicate that there are

fundamental differences between these two synapse types formed in different segments of the same axon, the functional significance remains unclear.

1.3 The use of calcium imaging techniques to monitor synaptic signalling and transmission

Neural plasticity refers to the ability of synapses to change their transmission strength over time. It is thought to play critical functions in the early development of the brain and its neural circuitry; many studies have shown that failure of synaptic plasticity can contribute to various prominent neurological disorders. Consequently, clarifying the molecular mechanisms underlying synaptic plasticity in various brain regions is essential to understanding the nervous basis of normal and abnormal brain function (Citri and Malenka, 2008). Understanding the role and plasticity of neural networks requires the ability to monitor synaptic activity in a large range of identified neurons. Monitoring where, when and how synapses are active in neural networks is therefore the main technical challenge.

Calcium ions have several vital physiological roles in neuronal function, including neurotransmitter release, release modulation, and cell growth (Takei et al., 1998, Berridge, 1998). Ca^{2+} influx through several types of Ca^{2+} permeable membrane channels is necessary for different patterns of differential gene expression in neurons (Finkbeiner and Greenberg, 1998, Lerea and McNamara, 1993). Ca^{2+} is also an essential signal for plasticity at various synapses including those of the cerebellum and hippocampus (Bliss and Collingridge, 1993, Malenka and Nicoll, 1999, Simons, 1988). Due to the wide range of effects of Ca^{2+}, several techniques/methods for its measurement have been established including electrophysiological techniques (non-optical methods) and bioluminescent or fluorescent probes (optical techniques).

Ca^{2+} imaging enables us to monitor changes in calcium concentration that accompany neuronal activity (Tada et al., 2014). In most neurons, action potentials (APs) are closely coupled to rapid and huge increases in intracellular Ca^{2+} concentration. These Ca^{2+} transients can be measured as changes in the fluorescence in neuronal axons, dendrites and somata *in vivo* and/or *in vitro* in response to changes in underlying neuronal activity (Haag and Borst, 2000, Seelig

et al., 2010). Fluorescence changes can be measured by using various fluorescent Ca^{2+} indicators and various optical imaging techniques including epifluorescence microscopy and two-photon microscopy. Fluorescent Ca^{2+} indicators have the ability to change their properties when they react to calcium ions. These indicators can be divided into two main classes, which are genetically encoded calcium indicators (GECIs) and organic chemical (dye) indicators. Chemical indicators include such species as calcium green-1 acetoxymethyl (AM) ester, Indo-1, Fluo-4 AM, Fura-2 AM and Cal-520 (Stosiek et al., 2003, Russell, 2011) (for a review, see Russell, 2011). GECIs represent an alternative and now widely adopted method for imaging calcium. The green fluorescent protein (GFP) first discovered by Shimomura et al. (1962) from the jellyfish *Aequorea victoria*, is a protein composed of a small molecule of 238 amino acid units (26.9 kDa). It exhibits bright green fluorescence (508 nm) when exposed to light in the blue part of (470 nm) of the ultraviolet range. GFP has become one of the most widely studied and exploited proteins in cell biological studies as labels of cellular constructions, a mark of gene expression and fusion tag (Zapata-Hommer and Griesbeck, 2003). Mutagenesis and engineering of *Aequorea* GFP into a variety of proteins to render them more fluorescent has opened new vistas in biosensor technology (Baird et al., 1999). Several different forms of fluorescent protein-based Ca^{2+} sensors have been developed since GFP was discovered, ranging from the Cameleons (Tsien, 1998), Camgaroo (Baird et al., 1999, Griesbeck et al., 2001) and the GCaMP family (Akerboom et al., 2009, Tian et al., 2009, Ohkura et al., 2012, Dana et al., 2014, Tian et al., 2012, Nakai et al., 2001).

Genetically encoded calcium indicators (GECIs) provide certain advantages over chemical indicators. They can allow the activity between genetically identified subsets of cells to be monitored. Moreover, they allow Ca^{2+} dynamics in specific subcellular parts to be measured. Furthermore, they allow for long-term *in vitro* and *in vivo* Ca^{2+} responses to be reliably recorded (Mao et al., 2008, Tian et al., 2012). GECIs are now routinely used to image neuronal activity and indeed underlie many recent advances in cellular functional imaging. GECIs can be targeted to cell populations, identified populations of neurons and even in specific cellular compartments (Mao et al., 2008).

GECIs are typically delivered using population-specific viral vector methods. However, expression levels can be different and/or decline with time. Although the expression levels of GECIs in transgenic mice can be stable and reproducible during imaging neural activity over long periods of time, their expression levels tend to be much lower and are of lower sensitivity compared to those achieved with viral transduction methods. Finding ways and sensors to improve the sensitivity and utility of transgenic animals remains an important challenge. In recent years, the brightness and sensitivity of the GCaMP family have been improved to help overcome some of these limitations, resulting in the development of GCaMP1, GCaMP2, GCaMP3, GCaMP5, SyGCaMP2-mCherry and GCaMP6 (Nakai et al., 2001, Díez-García et al., 2005, Tian et al., 2009, Ohkura et al., 2012, Akerboom et al., 2012, Al-Osta et al., 2018). Díez-García et al. (2005), for instance, have used GCaMP2 to detect responses in cerebellar PFs through cell-specific expression in GGs, whilst Al-Osta et al. (2018) have used SyGCaMP2-mCherry to selectively detect responses in the presynaptic terminals of neurons. Furthermore, GCaMP6 is now widely used to report neuronal activity *in vivo* (Chen et al., 2013). Finally, the measurement of synaptic calcium transients can allow synaptic transmission to be quantified as there is a close linear relationship between calcium current and transmitter release (Llinas et al., 1981).

1.3.1 The dual roles of calcium in triggering and modulating transmitter release

Communication between neurons depends on chemical synapses and the release of neurotransmitter into at the presynaptic active zone of nerve terminals (Südhof, 1995). Synaptic neurotransmitters enable a dynamic process of information exchange and storage in the brain. Synaptic transmission initially occurs when APs trigger the release of a transmitter from the presynaptic side of neurons (Katz, 1969). APs start near the cell body of a neurone and propagate down axons to a nerve terminal. Presynaptic axon terminals are specialised to secrete neurotransmitters. The process of secretion is induced by invasion of an AP into a presynaptic bouton and is strictly Ca^{2+} transient dependent (Südhof, 2004, Dietrich et al., 2003). In most synapses, neurotransmitter release is triggered by Ca^{2+} influx

through calcium channels. According to their voltage dependency, voltage-gated calcium channels (VGCCs) can be divided into L, P/Q, R, T and N types. L, P/Q and N types are activated at high voltages, T-type channels are activated at low voltages and R- type channels are activated at an intermediate voltage (Katz, 1969, Iwasaki and Takahashi, 1998). Presynaptic terminals of neurons are composed of various functional and structural compartments. These contain the active zone (see Figure 1.6), where synaptic vesicles (SVs) undergo a trafficking cycle (dock, fuse and recycle) as well as there being a large reservoir of SVs that can be classified functionally into three pools. Firstly, the reserve pool, which contains synaptic vesicles which are away from active zones. They are located within this zone via microfilaments. Secondly, the release-ready pool, which contains synaptic vesicles that are docked at the active zone. Finally, the proximal pool, which contains synaptic vesicles that are located between the reserve pool and release-ready pool. They appear to be connected closely to the active zone by a matrix of thin filaments (Garner et al., 2000, Garner et al., 2002). The active zone can be defined as the area of presynaptic membrane where the regulated release of neurotransmitter takes place. Studies focussed on the molecular machinery of the presynaptic active zone have identified at least 100 proteins that contribute to exocytosis (Südhof, 2004). These proteins are briefly described in the following section.

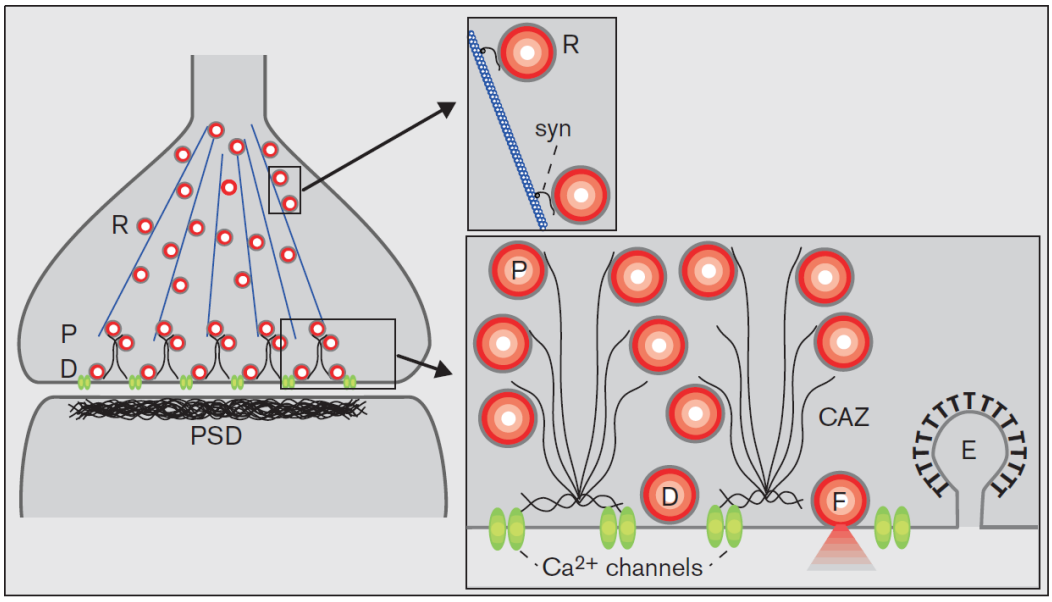

Figure 1.6. Schematic diagram of the structural organization of a presynaptic terminal of a neuron.

Upper inset: Synaptic vesicles (SVs) in the reserve pool (R) are tethered to microfilaments via

short filaments of syntaxin. Lower inset: a smaller proximal pool (P) of SVs is embedded in the meshwork of fine filaments. SVs of the third pool are physically docked (D) with the membrane of the active zone in a fusion-ready state They are very near to voltage-gated Ca^{2+} channels. After fusion (F), proteins of synaptic vesicles are recycled by clathrin (T)-dependent endocytosis (E). The postsynaptic membrane is associated with a cortical cytoskeletal structure called the postsynaptic density (PSD). Adapted from Garner et al. (2000).

SVs are the main organelles in neurotransmitter release. All functions of presynaptic terminals contain synaptic vesicles where neurotransmitters are stored (Garner et al., 2000). At presynaptic neurons, SVs pass through a complex cycle of trafficking that governs the release process. The trafficking cycle can be split into sequential steps (see Figure 1.7). Step 1: vesicles are likely generated via budding from initial endosomes. They are actively loaded with neurotransmitter. Step 2: vesicles are translocated to the active zone of the presynaptic plasma membrane. Step 3: SVs are filled with neurotransmitter and dock only at the active zone. Step 4: The docked vesicles pass through a maturing process which is named priming. At this stage, SVs stop and wait for a Ca^{2+} signal. Several features of the release process suggest that a distinct priming step is necessary including, a) the speed of calcium-elicited exocytosis of synaptic vesicles which is very quick for the complex multistep reaction; b) Ca^{2+} cannot immediately trigger the majority of docked synaptic vesicles to fuse. This is due to some synaptic vesicles not yet being fusion competent; c) during extensive stimulation, the exocytosis of synaptic vesicles slows down before the number of docked synaptic vesicles also declines. Step 5: fusion and exocytosis. In response to a rise in the intracellular Ca^{2+} concentration during an action potential, primed vesicles are activated for fast exocytosis fusion to release neurotransmitters. Step 6: kiss and stay is a local mechanism of recycling that requires exocytosis without synaptic vesicles fusing into the plasma membrane. Vesicles are reacidified and refilled with neurotransmitters without undocking. Therefore, these vesicles continue to stay within the readily releasable pool. Step 7: kiss and run is also a local mechanism of recycling that requires exocytosis without synaptic vesicles fusing into the plasma membrane. However, vesicles do not remain within the active zone. Additionally, they do not involve clathrin coating, which is an important step for endocytosis. Step 8: endosomal recycling, vesicle endocytosis occurs via presynaptic cisternae and clathrin-coated pits. They

reacidify and refill with neurotransmitters either via a direct route (step 9) or indirect route, which may hold after passing through an endosomal intermediate stage. The entire SV cycle takes about one minute, exocytosis/fusion takes place in less than 1 ms, whereas endocytosis occurs in less than 5s, with the remaining 55 s being used for the other cycle stages (Südhof, 2004, Garner et al., 2000, Li and Chin, 2003, Südhof, 1995). The release of neurotransmitter is greatly modulated by signals impinging on the presynaptic terminal region, as well as changes triggered by repetitive stimulation. There are two major points in modulating transmitter release which include the peak Ca^{2+} influx induced by the AP and the release probability for a given concentration of Ca^{2+} (Südhof, 2004). The concentration of the peak Ca^{2+} can depend on three parameters: first, the form of the AP; second, the open probability of VGCCs; and finally, the Ca^{2+} concentration that exists outside the plasma membranes at the time the Ca^{2+} channels open. Modulation of AP duration can in turn modulate the release of a neurotransmitter (Qian and Saggau, 1999). Activation of cannabinoid-1 receptors (CB1Rs), for example, can inhibit N-type Ca^{2+} channels (Wilson et al., 2001) and changes in residual calcium can result in the short-term plasticity (STP) of release (Zucker and Regehr, 2002). The release probability is also variable as it depends on the number of release-ready vesicles and the Ca^{2+} response of those vesicles. At rest, there is a low probability of spontaneous neurotransmitter release. This can be recorded via electrophysiology as miniature postsynaptic currents. Ca^{2+} influx can induce two means of release which are fast synchronous and slower asynchronous release. Most synapse communication is highly reliant upon the synchronous release of neurotransmitters which is induced rapidly, about 50 µs after an increase in Ca^{2+} concentration, at a presynaptic bouton. However, a slower asynchronous release can persist for > 1 s following an AP. Both these components are strictly Ca^{2+} dependent but can change differentially by the application of repetitive stimulation (Kaeser and Regehr, 2014, Li and Chin, 2003, Südhof, 2004). The mechanism of calcium-dependent transmitter release at presynaptic terminals will briefly be described in the following paragraph.

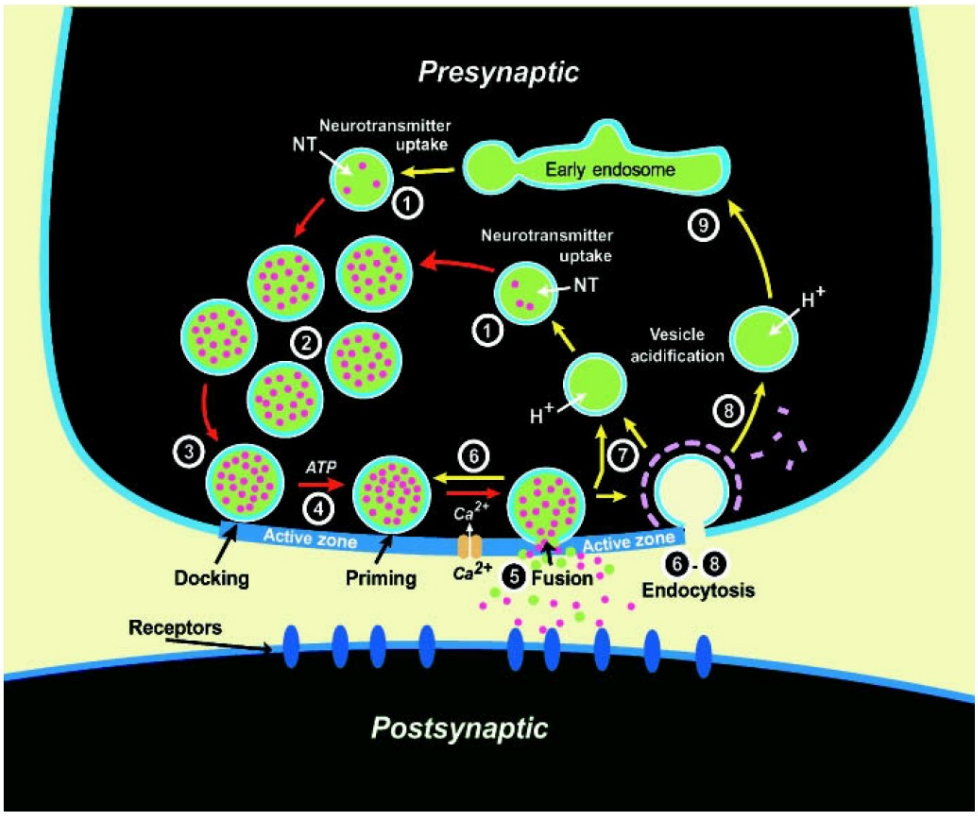

Figure 1.7. The principal stages of the vesicle cycle. (1) Active transport of neurotransmitters into vesicles. (2) Translocation of vesicles to the active zone. (3) Docking at the active zone. (4) Vesicles undergo a priming process (5) Calcium-triggered fusion pore opening. (6) Kiss and stay. (7) Kiss and run. (8) Vesicle endocytosis by clathrin-coated pits reacidify and refill with neurotransmitters directly, or (9) after passing through an endosomal intermediate stage. Adapted from Südhof (2004).

1.3.1.1 The mechanism of calcium-dependent transmitter release at presynaptic terminals

The release of neurotransmitter is mediated via exocytosis of SVs at the active zone of presynaptic nerve terminals. It is estimated that more than 1000 proteins function at the presynaptic active zone, hundreds of which are assumed to contribute to exocytosis (Südhof, 2004). The proteins of synaptic vesicles can be divided into transport and trafficking proteins. The transport proteins include neurotransmitter uptake. Trafficking proteins play an essential role in participating in synaptic vesicle cycles (Südhof, 2013, Li and Chin, 2003). While great strides towards understanding the molecular mechanisms governing synaptic vesicle trafficking and

neurotransmitter release have been made, the complete role of these proteins is not well characterised (Südhof, 2013). Recent studies focussed on the molecular composition of the presynaptic active zone have identified several proteins of general fusion machinery that contribute to exocytosis, including SNAREs (soluble N-ethylmaleimide–sensitive factor (NSF) attachment protein receptors), Munc18/nSec1, ATPase N-ethylmaleimide sensitive factor, Rab3 GTPase, Bassoon and Piccolo/Aczonin, the exocytotic proteins and membrane-associated guanylate kinases (MAGUK). In addition, SV exocytosis uses a set of exclusive components including complexin, synaptotagmin, RIM (Rab3-interacting molecule), and Munc13 (Li and Chin, 2003). For more information about the presynaptic active zone proteins involved in neurotransmitter release, see Südhof (1995), Südhof (2004), Li and Chin (2003), Brose et al. (2000) and Garner et al. (2000).

SNARE proteins are the core of the membrane fusion machinery. They play an essential role in the machinery for vesicular exocytosis. However, their specific role in the process of fusion and synaptic vesicle exocytosis remains controversial (Bruns and Jahn, 2002, Mayer, 2001). The SNARE family were initially divided into two groups based on their localization as v-SNAREs and t-SNAREs, and then later redivided into R-SNAREs and Q-SNAREs, based upon the presence of conserved glutamine or arginine amino acids in the middle of the SNARE structure (Fasshauer et al., 1998). The SNARE family is composed of syntaxin-1, SNAP-25 (a synaptosome-associated protein with a mass of 25 kDa), and vesicle-associated membrane protein (VAMP2), also referred to as synaptobrevin (Südhof, 2013). Initially, at the docking stage of the vesicle, syntaxin1 and SNAP-25 bind together to form a high-affinity binding site for synaptobrevin. Synaptobrevin is bound to synaptophysin, a synaptic vesicle protein (Becher et al., 1999). Synaptophysin is localized to synaptic vesicles with only slight expression on the surface of the membrane compared to synaptobrevin (Granseth et al., 2006). It also is thought to play an important role in SV endocytosis (Valtorta et al., 2004). At this stage, Munc-18 also binds selectively with monomeric syntaxin, keeping it in closed conformation and preventing it from forming SNARE complexes. This binding also confirms that synaptic vesicles are ready to fuse only when appropriately stimulated (Li and Chin, 2003, Südhof, 1995).

At the plasma membrane, the vesicular SNARE (v-SNARE) synaptobrevin forms a tight, four α-helix bundle with the target SNARES (t-SNARES) syntaxin and SNAP-25 present. This helps to pull the vesicle membrane into tight apposition with the plasma membrane. The four-helix bundle is formed by a step-wise zippering mechanism from the membrane distal ends to the membrane proximal ends of the SNARE proteins (Li and Chin, 2003).

Munc-13 plays a key role in priming synaptic vesicles by displacing the negative regulator Unc-18/Munc18 from syntaxin, allowing progression of the core complex formation to take place. Munc-13 is responsible for the establishment of a readily releasable pool of vesicles rather than their fusion. Munc-13 applies its priming role by promoting the assembly of the SNARE complex. Munc-13 can also binds to several proteins such as DOC2α, calmodulin and nsec7-1 (Brose et al., 2000). The fusion of SVs with the presynaptic membrane requires the formation of a stable soluble N- ethylmaleimide-sensitive factor attachment protein receptor (SNARE) complex and a local increase in calcium concentration. Synaptotagmin-1 is a popular candidate as a fast-release calcium sensor (Südhof, 2013); it is involved in regulating the SNARE proteins' zipping. It has two domains, C2A and C2B. Three calcium molecules can bind to the C2A domain whereas only two calcium molecules can bind the C2B domain (Tokuoka and Goda, 2003). One prevalent model of the fusion of the synaptic vesicle (see Figure 1.8) is that formation of a SNARE complex is stimulated by the interaction of active zone proteins including the Rab3-interacting molecule (RIM), mammalian uncoordinated-18 (Munc18), mammalian uncoordinated-13 (Munc13) and SM proteins. The complex formation of this is assumed to prime the vesicles, which mean the vesicles become ready for fusion and neurotransmitter release. The next step involves complexin linking to the SNARE complex, causing the vesicles to be "superprimed" as it stimulates the SNARE–SM protein complex (Südhof, 2013). When an AP arrives, the voltage-gated calcium channels are opened near the SNARE/complexion complex then the calcium binds to synaptotagmin-1 which leads to a change in the synaptotagmin-1 conformation (Atasoy and Kavalali, 2008, Südhof, 2013) These changes displace complexin and allow the membrane of the vesicle to fuse with the presynaptic membrane. This fusion leads to the pore in the membrane opening, after which the neurotransmitter can be released. The membrane pore continues to increase in size

until the membrane of the vesicle becomes indiscernible from the membrane of the presynaptic terminal. Finally, the SNARE complex will be dissociated when it binds with NSF/SNAPs, after which the SNARE proteins become ready to enter a new cycle of exocytosis (Carr and Munson, 2007, Atasoy and Kavalali, 2008, Pang and Südhof, 2010, Südhof, 2013).

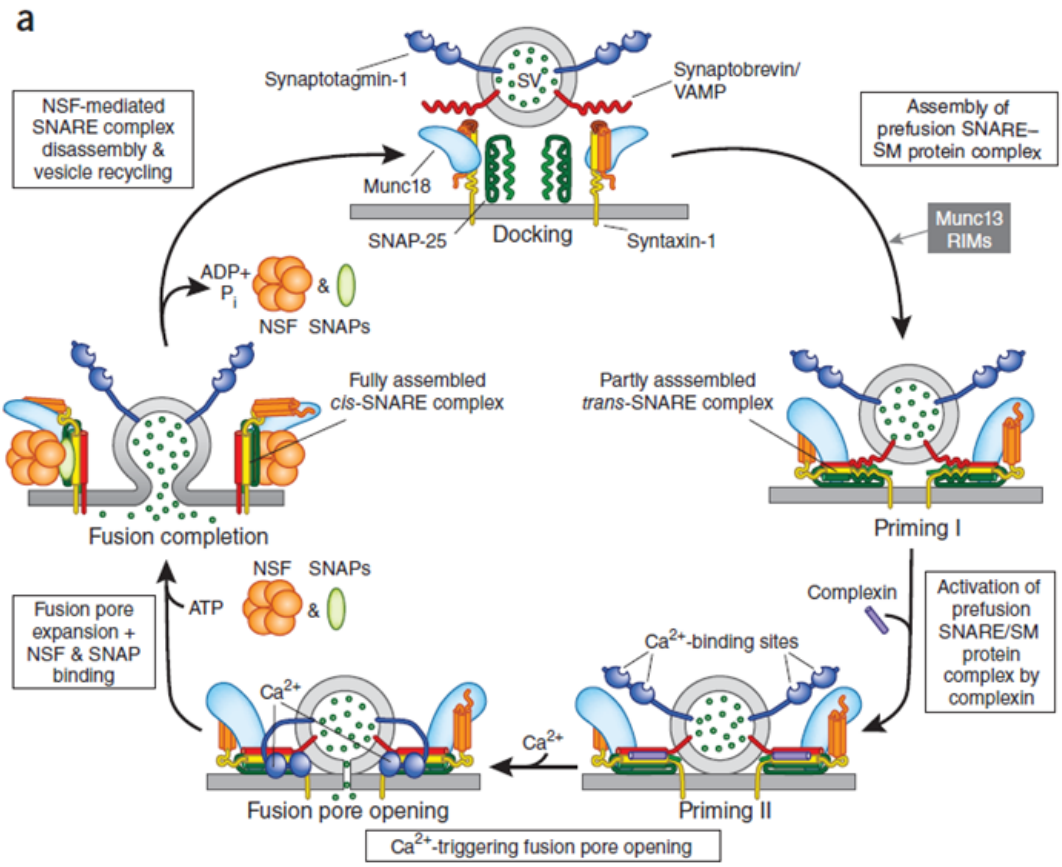

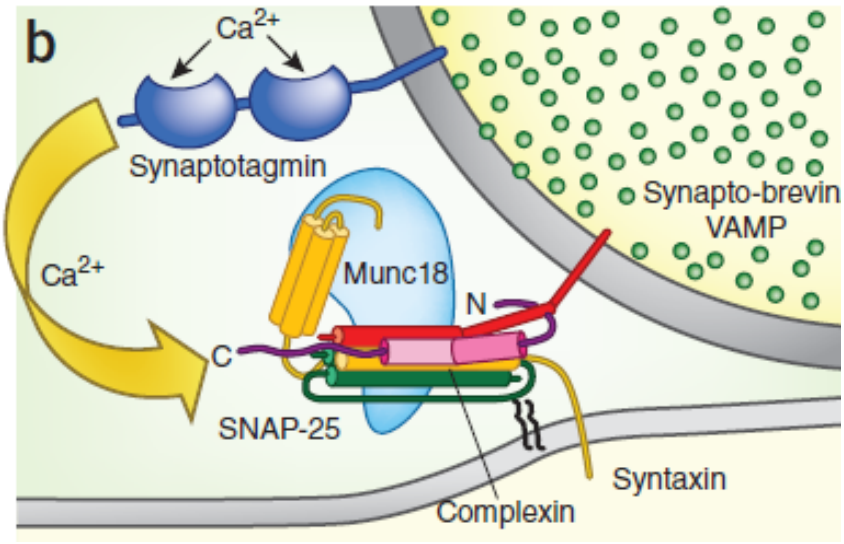

Figure 1.8. Model of the SNARE/SM protein cycle and the functional interaction of complexion and synaptotagmin 1 in calcium fusion triggering. (a) Docked vesicles containing complexes of unassembled soluble N-ethylmaleimide- sensitive factor attachment protein receptor (SNARE) (docking) are primed to release via assembly of a partial SNARE-complex catalysed via Munc13, Munc18 and RIM (priming I) followed by binding of complexins to the assembled SNARE complexes to form a metastable state (Priming II). Calcium triggering of release, through calcium binding to synaptotagmin 1, encourages synaptotagmin 1 binding to the SNARE complex and to membrane phospholipids. The later removal of complexin leads to fusion-pore opening (fusion pore opening) and expansion (fusion pore expansion). (b) The expanded view shows synaptotagmin with the fusion assembly of primed synaptic vesicle (Munc18-1, synaptobrevin, syntaxin and SNAP25 and complexin) poised to elicit the opening of the fusion pore upon Ca^{2+} binding. Modified from (Südhof, 2013).

Abbreviations: N-ethylmaleimide-sensitive factor (NSF); S-nitroso-penicillamine(SNAP); Synaptosomal-associated protein 25 (SNAP-25); Soluble N-ethylmaleimide- sensitive factor attachment protein receptors (SNAREs); Adenosine 5′-triphosphate (ATP); Mammalian uncoordinated (Munc); synaptic vesicle (SV); synaptobrevin (VAMP); Adapted from Südhof (2013).

1.3.1.2 The role of residual calcium in modulating transmitter release

Residual calcium concentration plays a critical role in synaptic transmission immediately after AP invasion of presynaptic nerve terminals and in modulating

forms of short-term plasticity (STP) within the central nervous system (CNS) (Regehr, 2012). Ca^{2+} influx through voltage-gated Ca^{2+} channels is induced by an AP initially generated near the soma (cell body) of a neurone that propagates down along the axon. The entry of Ca^{2+} increases the probability that vesicles located at active sites in the presynaptic terminal will fuse with the terminal membrane and release neurotransmitters into the synaptic cleft, as mentioned previously. Under certain conditions, the first pulse of the stimulus can trigger Ca^{2+} influx that can remain elevated in the presynaptic terminals for several hundred milliseconds, known as residual calcium (Zucker and Regehr, 2002, Zhang and Linden, 2012, Zukin and Bennett, 1995). While residual amounts of Ca^{2+} are generally not sufficient to induce any further neurotransmitter release in itself, it can combine with any fresh calcium that enters during a second stimulation pulse which leads to an increased probability of SVs fusing with the presynaptic terminal. If the second response is always higher than the first when paired stimuli are delivered in rapid succession then this phenomenon is referred to as pared pulse facilitation (PPF) (Katz and Miledi, 1968, Zucker and Regehr, 2002, Zhang and Linden, 2012). The opposite of this phenomenon is known as paired pulse depression (PPD). This occurs when the first AP successfully elicits release at most release sites resulting in the amplitude of the second response being smaller than the first response. The most widely accepted theory to explain the mechanism of PPD is that of a presynaptic transient decrease in release, likely caused by depletion of the release-ready pool of vesicles by the first stimulus in the pair (Zucker and Regehr, 2002, Mennerick and Zorumski, 1995, Debanne et al., 1996). The ratio of the amplitude of the second postsynaptic response to that of the first is referred to as the PPR. Data from several studies suggest that, in the mammalian CNS, PPR is inversely correlated with release probability (Zucker and Regehr, 2002, Dobrunz and Stevens, 1997, Zucker, 1989) and changes in PPR are often used as evidence for changes in release probability. The mechanism underlying this has been attributed to the impacts of presynaptic Ca^{2+} kinetics and depletion of a release-ready pool of vesicles (Debanne et al., 1996, Catterall and Few, 2008, Inchauspe et al., 2004).

Although changes in PPR are generally considered to be due to a presynaptic mechanism of action, alterations in the PPR are not exclusively mediated by a presynaptic change in release probability; for example, PPR can arise through

desensitization of the postsynaptic receptor (Trussell et al., 1993, Opazo et al., 2010), or could also be affected by other modifications which are not associated with alterations in release probability (Shin et al., 2010, Geppert et al., 1997). These limitations indicate that this method is inadequate, on its own, as evidence for a presynaptic mechanism (Yang and Calakos, 2013). Therefore, we have created a transgenic mouse (SyG37) that selectively expresses a ratiometric presynaptic calcium sensor SyGCaMP2-mCherry as an indicator which can be used to demonstrate a presynaptic site of action. SyGCaMP2-mCherry and the SyG37 mouse will be briefly described in the following paragraphs.

1.4 SyGCaMP2-mCherry as a tool for monitoring presynaptic calcium

GECIs have been widely used to report calcium changes *in vivo*, *ex vivo* or in live cells *in vitro* (Mao et al., 2008, Díez-García et al., 2007). Among GECIs, one of the most widely used calcium sensor families are the GCaMPs. This is due to the fact that GCaMPs are highly sensitive and respond rapidly to alterations in intracellular Ca^{2+} concentrations. GCaMP is composed of a circularly permuted enhanced green fluorescent protein (cpEGFP) fused to calmodulin (CaM) (calcium-binding protein) and a Ca^{2+}/CaM-binding myosin light chain kinase (Wang et al., 2008, Akerboom et al., 2009, Akerboom et al., 2012). This assembly provides insight into a sophisticated molecular mechanism of Ca^{2+} triggered fluorescence change. (Akerboom et al., 2009, Nakai et al., 2001).

Upon an increase in Ca^{2+} and binding to CaM, a conformational change occurs through calmodulin binding with M13 light chain kinase which consequently changes the fluorophore conformation of an attached fluorescent protein that leads to an increase in emission fluorescence intensity (Mao et al., 2008, Nakai et al., 2001). In recent years, the brightness and sensitivity of the GCaMP family have been improved considerably, leading to the development of GCaMP1, GCaMP2, GCaMP3, GCaMP5 and GCaMP6, as mentioned previously. However, well-performing ratiometric Ca^{2+} sensors are still rare (Thestrup et al., 2014). In the last few years, a new strain of a transgenic mice, named SyG37, was produced by our

laboratory. SyG37 mice selectively express a fluorescent protein-based, ratiometric calcium sensor (SyGCaMP2-mCherry) in the presynaptic terminals of neurones. Using this sensor, changes in presynaptic calcium levels at single and populations of synapses can be measured, even when synaptic transmission is inhibited (Al-Osta et al., 2018). This approach is complementary to electrophysiological techniques for measuring neuronal activity. The combination of both can help to establish the origin and mechanisms of changes in the strength of synaptic transmissions.

The generation and characteristics of SyG37 mice have been previously described in considerable detail by Okorocha (2016) and Al-Osta et al. (2018). Very briefly, SyGCaMP2 was created by the fusion of the calcium indicator GCaMP2 to the C-terminus of the vesicular protein synaptophysin-1 (Dreosti et al., 2009). The spectrally distinct red fluorescent protein mCherry was then fused to the C-terminus of SyGCaMP2. A Thy1.2 promoter was used to target the expression to neurones but non-specifically. The red fluorescence, which is calcium-independent, was designed to help identification of presynaptic boutons as GCaMP2 on its own exhibits very low fluorescence at lower Ca^{2+} concentrations. It can also be used to allow ratiometric measurement of Ca^{2+} as a proportion of the quantity of sensor expressed. The absolute ratio of SyGCaMP2: mCherry fluorescence is proportional to absolute Ca^{2+} levels (Al-Osta et al., 2018, Pereda et al., 2019).

1.5 Presynaptic modulation of synaptic release

Released neurotransmitter activates receptors on the postsynaptic side of the synapse. The process of presynaptic release and subsequent postsynaptic actions allow neurones to communicate with each other (see Figure 1.9).

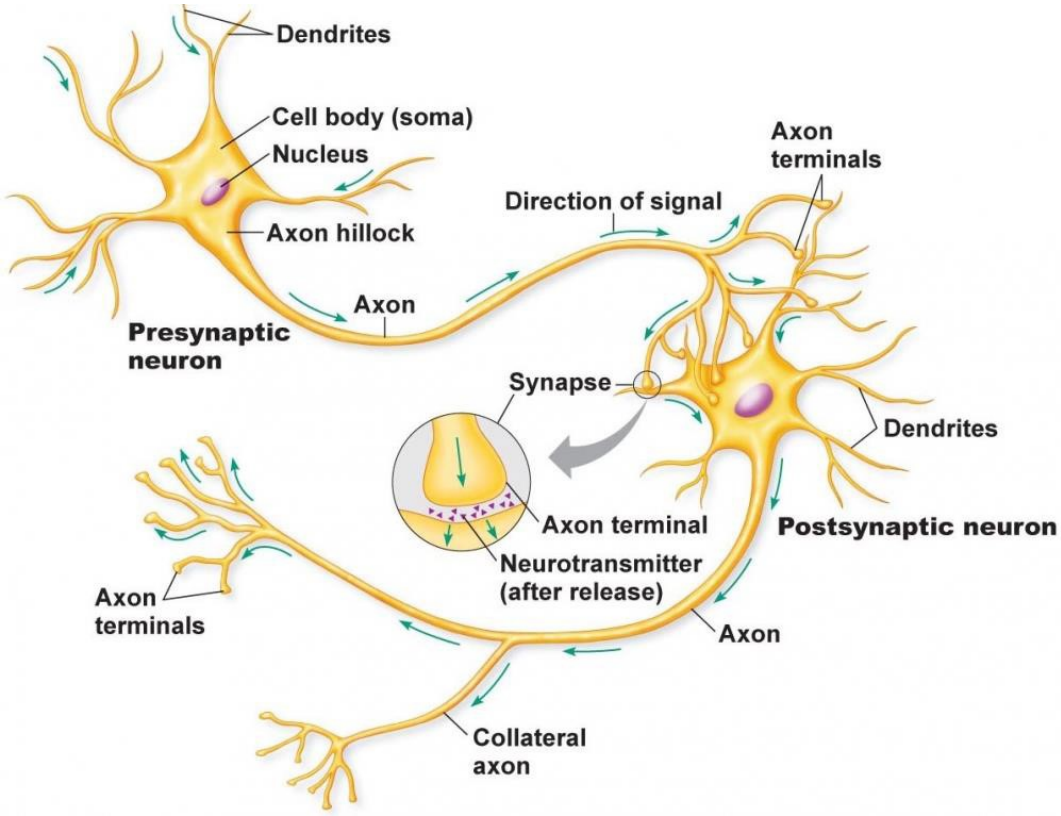

Figure 1. 9. Schematic diagram of neurone structure and synapses between neurones. The basic structure of a neurone, which generally consists of a cell body (soma), axon hillock, one long axon and numerous dendrites. Dendrites receive information from other neurones and axons carry information away from the soma to the axon terminals. It also shows that axon terminals connect with their target cells to form synapses, usually but not exclusively on dendrites. The green arrows illustrate the direction of information flow. Adapted from http://letsmaketech.com/index.php?controller=post&action=view&id_post=22.

Neurotransmitters can be excitatory or inhibitory depending on the neurotransmitters contained in their presynaptic vesicles. Glutamate is the major excitatory neurotransmitter. It forms more than 70% of all central nervous system synapses (CNS) while GABA and glycine are the main inhibitory neurotransmitters in the CNS. GABA receptors include $GABA_A$ (ionotropic), $GABA_C$ (ionotropic) and $GABA_B$ (metabotropic) receptors. $GABA_A$ and $GABA_C$ receptors lead to inhibition of postsynaptic cells via an increase in chloride ion conductance while $GABA_B$ receptors act via G-protein, which has an inhibitory effect on adenylyl cyclase (AC) leading to an alteration in potassium channel currents (Purves et al., 2008,

Terunuma et al., 2014). Glycine receptors include one type – analogous to $GABA_A$ whereas there is no metabotropic glycine receptor.

Glutamate receptors can be categorized as ionotropic (ligand-gated ion channels) and metabotropic (G-protein-coupled) receptors. Metabotropic glutamate receptors (mGluRs) can be also categorized into Group I (mGlu1 and mGlu5), group II (mGlu2 and mGlu3) and group III (mGlu4, mGlu6, mGlu7 and mGlu8). Stimulation of type I metabotropic glutamate receptors that are G-protein coupled initiates an intracellular signalling cascade where phospholipase (PLC) cleaves phosphatidylinositol 4,5-bisphosphate (PIP2) producing diacylglycerol (DAG) and inositol 1,4,5-trisphosphate (IP3). DAG stimulates protein kinase C (PKC), whereas IP3 binds to IP3R on the endoplasmic reticulum (ER) and releases stored calcium. Ryanodine receptors (RyR) can be bound by calcium and impact Ca^{2+}-induced Ca^{2+} release. The release of Ca^{2+} from the intracellular stores results in an additional influx of Ca^{2+} through the plasma membrane channels (Bouron, 2000, Baba et al., 2003). However, Group II and group III mGluRs act differently, producing slow inhibitory effects on AC which then leads to a reduction in the second messenger, cAMP. In general, activation of these groups leads to a decrease in $[Ca^{2+}]_i$ (Coutinho and Knöpfel, 2002).

Ionotropic receptors include α-amino-3-hydroxy-5-methyl-4-isoxazolepropionic acid (AMPA), Kainate and N-methyl-D-aspartic acid (NMDA) receptors. Ionotropic glutamate receptor subunits include AMPA receptors (GluA1/ GluR1, GluA2/ GluR2, GluA3/ GluR3 and GluA4/ GluR4), kainate receptors (GluK1/ GluR5, GluK2/ GluR6, GluK3/ GluR7, GluK4/ KA1 and GluK5/ KA2) and NMDA receptors (GluN1/NR1, GluN2A/NR2A, GluN2B/ NR2B, GluN2C/NR2C and GluN2D/NR2D). Within the CNS, fast excitatory synaptic potentials are mediated by AMPA receptor subtypes. They are principally permeable to sodium and potassium ions but can conduct Ca^{2+} depending on their subunit composition. They also display rapid activation and deactivation rates. In contrast, slower synaptic transmission is mediated by kainate receptors and NMDA receptors (Traynelis et al., 2010). NMDA receptors (NMDARs) are ligand-gated ionotropic glutamate receptors, and are named after the agonist molecule N-methyl-D-aspartate as this binds selectively to NMDAR and not to other types of glutamate receptors such as the AMPA and kainate receptors (Moriyoshi et al., 1991, Sucher et al., 1996). NMDARs were found to be expressed in neuronal cells of the brain areas, in particular in the cerebellum, cerebral cortex, hippocampus

and brain stem, (Moriyoshi et al., 1991, McBain and Mayer, 1994). However, they can also be found in many non-neuronal cells such as astrocytes, oligodendrocyte, kidney, pancreas and the heart (Hogan-Cann and Anderson, 2016).

NMDAR are tetramers of GluN1 and GluN2 subunits which come together to form an ion channel pore through the cell membrane (Hansen et al., 2018). NMDARs characteristically have a high permeability to Ca^{2+} (MacDermott et al., 1986) voltage-dependent blockade by Mg^{2+} (Mayer et al., 1984), blockade via Zn^{2+}, coactivation by glutamate and either glycine or serine (McBain and Mayer, 1994, Hansen et al., 2018), and slow gating kinetics (Lester, 1990). These characteristics underpin the actions of these receptors in the modulation of synaptic plasticity forms involved in learning and memory (Purves et al., 2008). NMDARs are the only neurotransmitter receptors whose activation requires two molecules of either glycine or serine bind to GluN1 (Kleckner and Dingledine, 1988) and two molecules of agonist glutamate bind to GluN2 (Clements and Westbrook, 1991) (see Figure 1.10). The ion channel is strongly blocked at resting or hyperpolarised potentials by extracellular Mg^{2+}, but this Mg^{2+} ion blockade is removed given sufficient depolarization (Kandel et al., 2000, Purves et al., 2008), which leads ion channels to open selectively for Na^{+}, K^{+} and Ca^{2+}, though the permeability for calcium is approximately 10 times greater than for other cations (Na^{+}) (Mayer and Westbrook, 1987, MacDermott et al., 1986) and three to four times higher compared the permeability of AMPA or kainate receptors to Ca^{2+} influx as well (Traynelis et al., 2010). This activity can be blocked with high selectivity using competitive antagonists such as DL-AP5 or D-CPPene (Watkins and Evans, 1981, Eblen et al., 1996) or non-competitive antagonists such as ketamine or MK801 (Wong et al., 1986, Wallach et al., 2016).

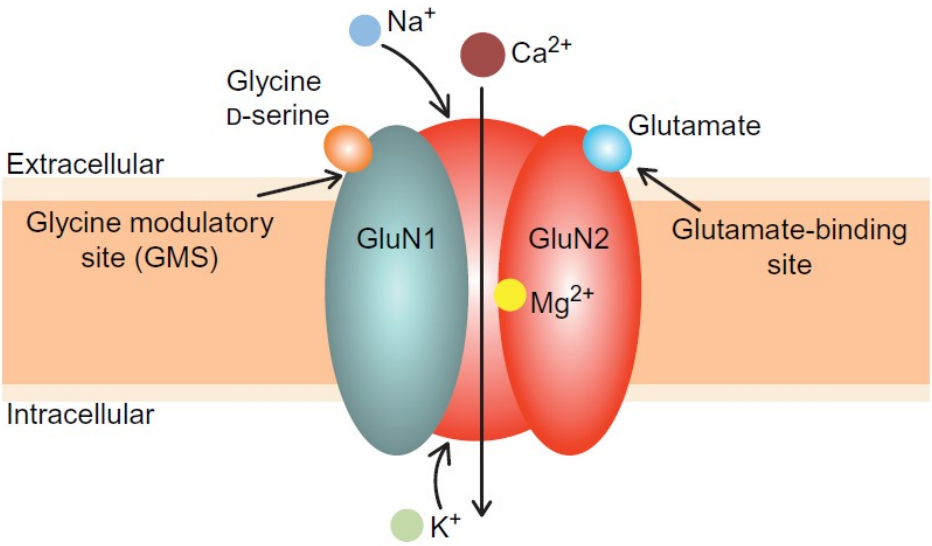

Figure 1.10. Schematic representation of the structure and NMDAR activation. This representation shows the NMDA receptor, which consists of GluN1 and GluN2 subunits. These receptors are also known as coincidence detectors due to their opening requirements, glutamate and either glycine or D-serine, to bind its subunits and gain sufficient depolarization to remove the Mg^{2+} ion blockade. Upon ion channel opening, Ca^{2+} and Na^{+} cations enter the neuron whereas K^{+} exits. However, the channel has a much higher Ca^{2+} permeability compared to other cations. Adapted from Balu (2016).

Among the ionotropic glutamate receptors, NMDARs are principally permeable to Ca^{2+} ions, which of course play a pivotal physiological role in synaptic plasticity and neuronal development (Collingridge, 1987, Purves et al., 2008, Hunt and Castillo, 2012, Flores et al., 2013). Abnormal NMDAR activity has been implicated in psychiatric disorders such as epilepsy, depression, stroke, schizophrenia and several neurodegenerative diseases which include Alzheimer's and Huntington's disease (Jewett and Thapa, 2018, Liu et al., 2019). For these roles in both biology and pathophysiology, NMDARs have been widely studied over the last few decades (Vyklicky et al., 2014). Most NMDAR functions in the cerebellum are traditionally thought to be located exclusively postsynaptically at brain synapses. However, multiple lines of evidence suggest that NMDARs expressed at presynaptic terminals modulate neurotransmitter release and plasticity and this evidence will be briefly described in the following paragraphs.

1.5.1 Evidence for NMDAR located on presynaptic elements modulating synaptic release

NMDARs have until fairly recently been considered to exclusively mediate postsynaptic effects at brain synapses. In recent years, there has been accumulating anatomical and physiological evidence to suggest that NMDARs are also present at the presynaptic membrane, and implicated in the regulation of forms of synaptic plasticity. It is expressed in many brain regions such as the cerebellum, hippocampus, brain stem, spinal cord and amygdala, amongst others (Duguid, 2013, Bouvier et al., 2015, Banerjee et al., 2016). The activation of presynaptic NMDARs (preNMDARs) is required for the induction of long-term plasticity in different structures of the brain (Sjöström et al., 2003, Suárez et al., 2005, Casado et al., 2002). However, the role of preNMDARs at cerebellar synapses in modulating synaptic transmission and plasticity remain controversial and unclear. At the PF-PC synapses, adult PCs seem to be an exception as they lack functional NMDA receptors after 2-3 weeks (Farrant and Cull-Candy, 1991, Llano et al., 1991). Therefore, their involvement in synaptic plasticity at these synapses was initially overlooked.

Multiple recent lines provide immunohistochemical and electrophysiological evidence for NMDARs on PF terminals in the cerebellum; Bidoret et al. (2009) reported that there is a clear expression of NMDARs on PF boutons but no such expression on PC in cerebellum acute slices from young adult rats (17 to 24 days of age). The study of Casado et al. (2000) and Casado et al. (2002) has elucidated the fact of the activation of NMDAR at PF–PC synapses by NMDA (in the presence of its co-agonist, glycine) leading to inhibition of synaptic transmission at the PF-PC synapse in slices of young adult rats (at an age where functional postsynaptic NMDARs on PCs are absent). Contrasting with other forms of synaptic plasticity, which are dependent on preNMDARs, no change in PPR was found after stimulation of preNMDARs suggesting a postsynaptic locus of expression. This depression was also found to be NMDAR dependent, indicating that NMDARs located on PF terminals are stimulated during the synaptic activity that leads to trigger depression and that this participates in the postsynaptic expression of depression through an NO-dependent mechanism (see Figure 1.11). However, under the same conditions,

Dobson and Bellamy (2015) found that activation of NMDA produced a reversible depression of synaptic plasticity and an associated increase in PPR, suggesting a decrease in the probability of presynaptic release. Furthermore, at PF-PC synapses, a form of potentiation can be triggered by a high frequency of PF activation that was found to be presynaptic in origin was inhibited by the NMDAR antagonist, AP5 (Jacoby et al., 2001). Activation of NMDARs can also cause an increase in the frequency of miniature excitatory postsynaptic currents (mEPSCs) without affecting their amplitude or rate of decay, similarly indicating an effect on presynaptic release (Lonchamp et al., 2012).

There is also accumulating immunohistochemical and electrophysiological evidence for the existence of NMDAR at GABAergic terminals; Bidoret et al. (2015) found that NMDARs are expressed in cerebellar ML interneurons in cerebellar slices taken from rats. Duguid and Smart (2004) and Rossi et al. (2012) found that NMDARs were expressed in cerebellar ML interneurons in cerebellar slices taken from rats. Furthermore, these studies also found that activation of NMDARs caused a decrease in PPR, indicating a presynaptic effect. It was also observed that activation of NMDARs caused a selective increase in the frequency of miniature inhibitory postsynaptic currents without affecting their amplitude, indicating an effect on presynaptic boutons (Glitsch and Marty, 1999).

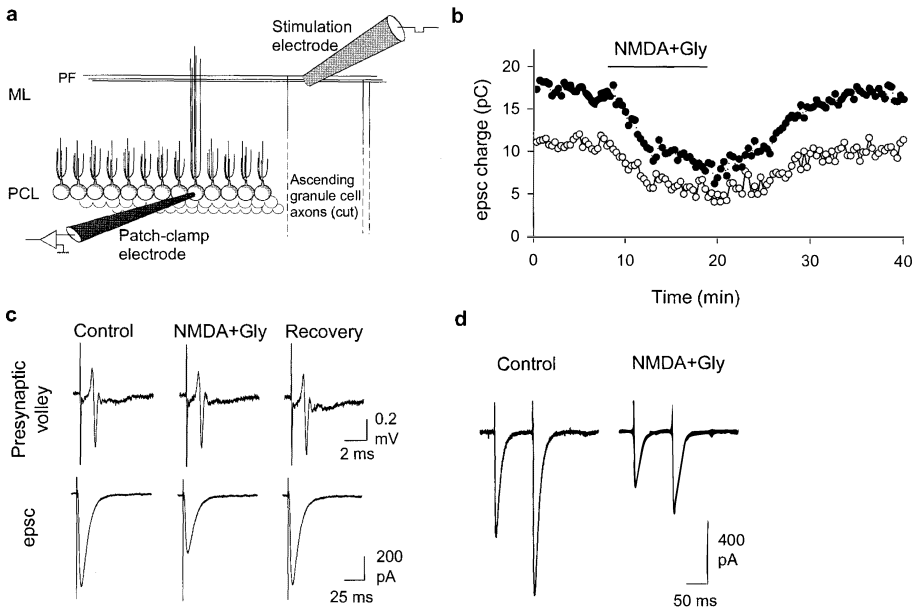

Figure 1.11. Inhibition of synaptic release linked to NMDA receptor activation. (a) Schematic representation of a transverse slice of the rat cerebellum showing recording and stimulating electrode positions. (b) Effect of applications of NMDA (30 µM), with its co-agonist glycine (10 µM) on EPSC recordings. Paired stimulation of first to second pulses are shown by the empty and filled colours in the circle, respectively. (c) Simultaneous recordings of the EPSC and presynaptic fibre volley during the baseline, after 10 minutes of applications of NMDA (30 µM), with its co-agonist glycine (10 µM) and 20 minutes after NMDA/glycine washout (recovery). (d) Paired-pulse ratio is not affected. Traces under control conditions and during NMDA/glycine perfusion. Adapted from Casado et al. (2000).

1.5.2 Evidence for CB1R located on presynaptic elements modulating synaptic release

Natural products of the cannabis plant such as marijuana, ganja, hashish and bhang, have been used widely throughout the world for millennia for medicinal and recreational purposes. Δ9-tetrahydrocannabinol (Δ9-THC) is the main psychoactive component of cannabis (Adams and Martin, 1996, Xu and Chen, 2015). Endocannabinoids are derivatives of arachidonic acid, which is derived from endogenous lipids. They have recently been shown to play major modulatory roles in CNS of mammals, and are involved in regulating a wide range of physiological and cognitive pathways such as memory and motor tasks, stress and emotions, neuronal development, appetite, fertility, physical exercise, pain sensation and

mood (Aizpurua-Olaizola et al., 2017, Schwitzer et al., 2015). Two Gi/o protein-coupled cannabinoid receptors (GPCRs) have been identified in the mammalian brain which are CB1, first discovered in 1990, and CB2 discovered in 1993, (Matsuda et al., 1990, Devane et al., 1992). CB2 receptors (CB2Rs) are widely distributed in the immune system, while CB1 receptors (CB1Rs) are present in the central nervous system with their highest densities in the cerebellum, hippocampus, hypothalamus, thalamus, basal ganglia and brain stem. In addition, CB1Rs are also present in the peripheral nervous system (Howlett et al., 2002, Kendall and Yudowski, 2017, Sun et al., 2011, Núñez et al., 2004, Ehrler et al., 2015). In the cerebellar cortex, the highest densities of CB1Rs are expressed in the excitatory terminals of PFs and CFs (Lévénès et al., 1998, Kawamura et al., 2006, Núñez et al., 2004, Takahashi and Linden, 2000), and inhibitory terminals such as basket and stellate cell terminals (Diana et al., 2002, Tsou et al., 1998). These receptors are not detected in the somata or dendrites of PCs (Kreitzer and Regehr, 2001b, Diana et al., 2002, Szabo et al., 2004, Taura et al., 2007).

In hippocampal neurons, CB1Rs are also expressed in the presynaptic terminal (Hájos et al., 2000, Wilson and Nicoll, 2001, Kawamura et al., 2006). CB1Rs are activated by Δ9-THC (Taura et al., 2007, Wilson and Nicoll, 2002, Zimmer et al., 1999, Aizpurua-Olaizola et al., 2014) as well as by synthetic cannabinoids such as [1-(5-fluoropentyl)-1-hindol-3-yl](4-methyl-1-naphthalenyl)-methanone (MAM-2201), (-)-cis-3-[2-hydroxy-4-(1,1-dimethylheptyl)phenyl]-trans-4-(3-hydroxypropyl)cyclohexanol (CP 55,940) and (R)-(+)-[2,3-dihydro-5-methyl-3-(4-morpholinylmethyl)pyrrolo[1,2,3-de]-1,4-benzoxazin-6-yl]-1-naphthalenylmethanone mesylate (WIN55,212-2) (Irie et al., 2015, Kendall and Yudowski, 2017). It is widely known that endogenous cannabinoids such as anandamide (N-arachidonoylethanolamine; AEA) and 2-arachidonoyl-glycerol (2-AG) (Stella et al., 1997) can be released from postsynaptic neurons by depolarization of the postsynaptic site by neurotransmitter release that stimulates Gq-protein and voltage-dependent calcium channels.

The raised concentration of calcium activates the synthesis of endocannabinoids through phospholipase D (PLD) and phospholipase C (PLC). These enzymes are involved in the synthesis of endocannabinoid from the precursors of the lipid when activated, as the activation of PLD leads to the formation of AEA from N-

arachydonoylphosphatidylethanolamine (NAPE), whereas the stimulation of PLC leads ultimately to the production of 2-AG from diacylglycerol. These cannabinoids then move in a retrograde direction at the synapses, activating CB1Rs on the excitatory or inhibitory presynaptic terminals and consequently activating the Gi/o proteins which negatively regulate adenylyl cyclase, leading to activation of potassium channels (Daniel et al., 2004) and inhibition of calcium channels (N, P/Q and R type) (Brown et al., 2004). (For more information, see Figure 12). These processes ultimately lead to the inhibition of presynaptic Ca^{2+} entry and, consequently, modulate synaptic transmission. These effects can impact homeostatic and/or long- and short-term plasticity at synapses, supporting results that suggest the endocannabinoid signalling pathway appears to be implicated in learning and memory (Hampson and Deadwyler, 2000, Ehrler et al., 2015). Recent studies have provided strong evidence that activation of CB1Rs by endocannabinoids leads to a transient inhibition of excitatory transmission at the PF-PC synapse (Kreitzer and Regehr, 2001b, Kawamura et al., 2006, Irie et al., 2015, Maejima et al., 2001b, Lévénès et al., 1998) and a transient inhibition of inhibitory synaptic transmission at the BC-PCs in the cerebellum (Yoshida et al., 2002, Szabo et al., 2004, Takahashi and Linden, 2000); however, the mechanisms underlying this inhibition are not fully understood. It is possible to hypothesize that a decrease in neurotransmitter release arises from activation of potassium channels by endocannabinoids as the activation of CB1R may shorten the duration of the AP and thereby indirectly reduce Ca^{2+} influx (Daniel and Crepel, 2001, Diana and Marty, 2003, Robbe et al., 2001, Daniel et al., 2004). An alternative hypothesis is that endocannabinoids directly inhibit all calcium channels in presynaptic terminals (Brown et al., 2004, Liang et al., 2004, Huang et al., 2001) or even only N-type Ca^{2+} channels (Wilson and Nicoll, 2001). Another alternative hypothesis is that endocannabinoids directly inhibit the vesicular release machinery (Takahashi and Linden, 2000, Szabo et al., 2004). Previous studies by Ito (1993), Linden (1994), Hémart et al. (1995), Lamont and Weber (2012), and Purves et al. (2008) hypothesized that LTD is considered to occur through postsynaptic regulation resulting from the loss of the AMPA receptor through internalization by endocytosis, which ultimately reduces the response of the postsynaptic PC to the glutamate release from the terminals of the presynaptic PFs. However, there may well be other forms of depression on the synapses. For example, recent studies have found

evidence that the action of endocannabinoids on PF mediated EPSCs is presynaptic regulation. These studies found an increase in the PPR and a reduced frequency of miniature postsynaptic currents recorded without affecting their amplitude in the presence of endocannabinoids (Lévénès et al., 1998, Takahashi and Linden, 2000, Kreitzer and Regehr, 2001b, Azad et al., 2003, Haj-Dahmane and Shen, 2009, Irie et al., 2015).

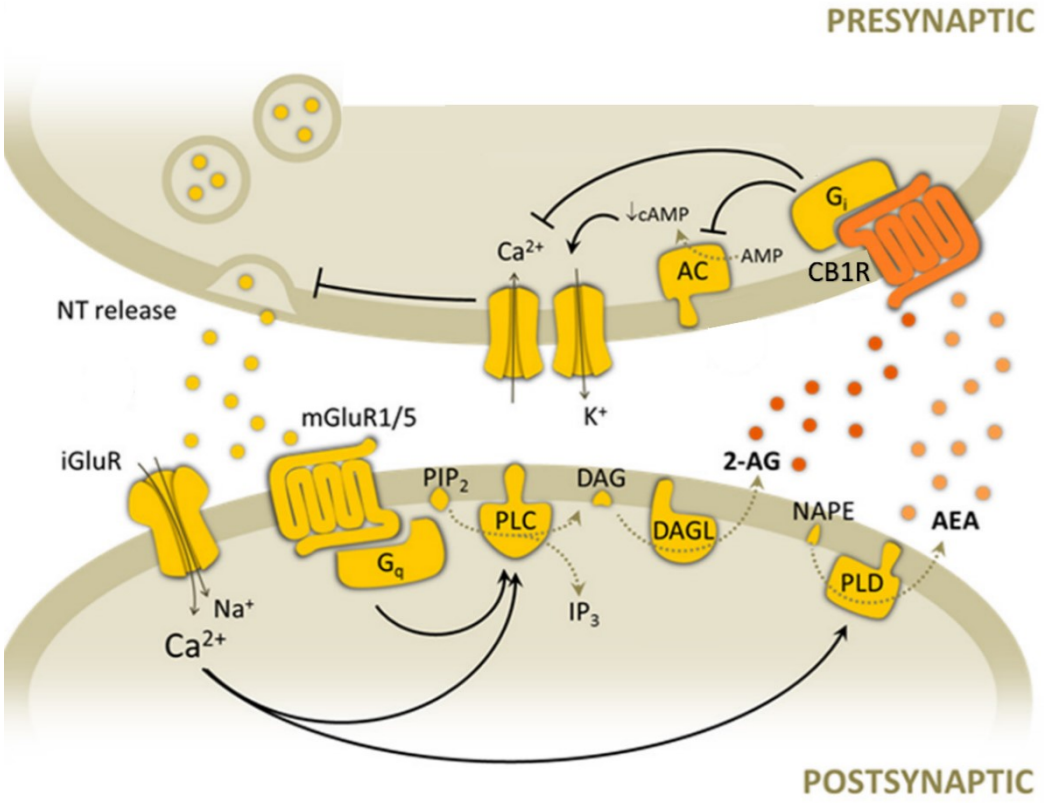

Figure 1.12. Possible model for endocannabinoid mechanisms of action. Depolarization of the postsynaptic site leads to the activation of voltage-dependent calcium channels and Gq-protein. Calcium influx leads to the activation of phospholipase C (PLC) and phospholipase D (PLD), which are both involved in the formation of endocannabinoids from the precursors of the lipid. The action of PLD on *N*-arachidonoyl phosphatidylethanolamine (NAPE) leads to the creation of anandamide (AEA). In addition, the activation of mGluR1/5 in the postsynaptic site can also produce 2-arachidonylglycerol (2-AG) by activating phospholipase C and creating diacylglycerol and, ultimately, diacylglycerol lipase will cleave the diacylglycerol to form 2-AG. Thereafter, the endocannabinoids bind to CB1Rs and consequently activate Gi/o proteins which down-regulate adenylyl cyclase (AC), leading to the activation of potassium channels and inhibition of calcium channels. Modified from Flores et al. (2013).

1.6 Summary of aims

The primary goal of this study was to use a novel, transgenic mouse, referred to as SyG37, to examine the contributions of presynaptic calcium to synaptic transmission within different circuits of the cerebellum. Therefore, it was necessary to first confirm the expression patterns of SyGCaMP2-mCherry within the cerebellum and then to establish whether our optical responses originated from presynaptic terminals and, assuming so, what fraction might originate from PF terminals. Having established the above, we then used the new transgenic mouse to: 1) characterize the properties of synapses formed by ascending axon and PF segments of granule cell axons to different patterns of stimulation; 2) examine the presynaptic role of NMDA receptors (NMDARs) in modulating synaptic release and plasticity at PF-PC synapses, where in particular we examined weather activation of NMDARs affect presynaptic Ca^{+2} levels and release probability; and finally 3) establish the presynaptic role of CB1 receptors in modulating synaptic release and plasticity at PF-PC synapses, in particular whether activation of CB1R affects presynaptic Ca^{2+} levels and release probabilities.

Chapter 2: Materials and methods

2.1 Experimental animals used in this study

Male and female wildtype (C57 Blk6) and transgenic mice, aged between 3 and 10 weeks, were used in this study. The transgenic mouse strain, referred to here as SyG37, expresses the genetically encoded calcium indicator (GECI), SyGCaMP2-mCherry, at presynaptic terminals (Al-Osta et al., 2018). SyGCaMP2-mCherry was created through the fusion of mCherry to the C-terminus of GCaMP2, which was then tethered to the extravesicular facing membrane of synaptic vesicles via fusion to the C-terminus of the vesicular protein synaptophysin (see Figure 2.1; Dresosti et al., 2009). The spectrally distinct red fluorescent protein mCherry was added to SyGCaMP2 to help identify presynaptic terminals because SyGCaMP2 itself has a low fluorescence intensity at resting concentrations of calcium (Mao et al., 2008, Tallini et al., 2006). In addition, mCherry enables a ratiometric standardisation of the sensor which allows, if required, calibration and measurement of absolute calcium concentrations. The thy1.2 promoter was used to promote SyGCaMP2-mCherry expression specifically in neurones (Caroni, 1997). The SyG37 transgenic mouse strain used in the experiments described in this thesis was produced in our lab by Dr. Mariusz Mucha. The SyG37 mouse line was bred within the preclinical research facility (Animal Unit) of the University of Leicester. Mice were genotyped before experimental use using primers to target SyGCaMP2 and a ubiquitous section of DNA extracted from the same sample as a control (for more details see section 2.2 Genotyping). SyGCaMP2 is expressed in all brain regions, but expression is particularly high in the hippocampus, cerebellum, thalamus and brainstem. Our colleagues in the lab have previously demonstrated that the sensor is expressed in both excitatory and inhibitory synaptic terminals in hippocampal brain slices (Al-Osta et al., 2018).

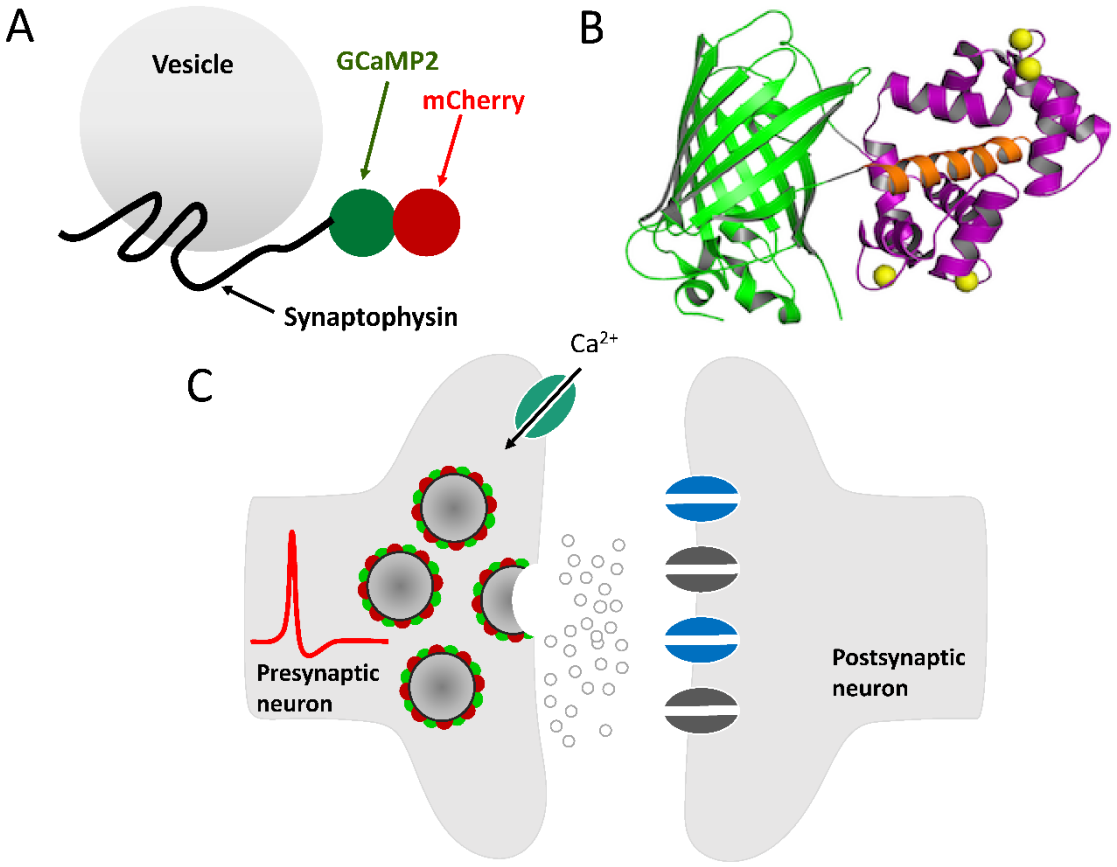

Figure 2. 1. Schematic diagram of SyGCaMP2-mCherry construction. (A) The fusion of mCherry to GCaMP2, which was then tethered to synaptic vesicles via fusion to the vesicular protein synaptophysin. (B) The structure of GCaMP sensor which consists of two components the first (on the left) is the circularly permuted enhanced green fluorescent protein (cpEGFP) attached to N-terminal of calmodulin and the second (on the right) is an M13 myosin light chain kinase attached to the N-terminus of cpEGFP. Up to four calcium ions (yellow circles) bind to calmodulin in a cooperative manner, leading to a conformational change in the calmodulin domain which induces another conformational change in the cpEGFP that strongly enhances its fluorescence intensity upon application of a suitable wavelength of excitation light. (C) A diagram illustrating the location of SyGCaMP2-mCherry which can be used to monitor changes of calcium levels in presynaptic terminals. Panel B is adapted from Akerboom et al. (2009).

2.2 Genotyping

Our colony of SyG37 mice was maintained by breeding positive and negative mice together. It was therefore necessary to genotype animals in order to identify mice in our SyG37 colony that expressed SyGCaMP2-mCherry. Ear snips of SyG37 mice colonies were taken from mice 2-3 weeks after birth and frozen until use. Genotyping was performed using the PCR technique. Before starting the genotyping, the working area and equipment were carefully cleaned and sterilised using 70% ethanol in order to avoid contamination. In addition, plugged tips were used and changed for each sample. Moreover, gloves were worn in order to ensure safety and to prevent contamination.

Ear snips in an Eppendorf tube were incubated using 70 µl 0.05 M NaOH and heated to 94°C for 22-24 minutes in order to extract genomic DNA, after which 7 µl Tris HCL at pH 7.5 was added to each tube in order to neutralise and halt the process of digestion. The resultant solution in the Eppendorf was then pulse spun to help take down debris and allow only the top of this solution to be used in subsequent PCR.

Identification of an individual genotype of extracted DNA was then performed using the PCR technique using 2x Reddymix, nuclease-free water and the following primers: SyGCaMP2 (forward primer 5'-CGACAACCACTACCTGAGCA; reverse primer 5'-GAACTTCAGGGTCAGCTTGC) was used to target SyGCaMP2 DNA, whereas primers of the cytidine monophospho-*N*-acetyl-neuraminic acid hydroxylase (Cmah) (forward primer 5'-CAGCTTGCTTATCACGTGTG; reverse primer 5'-TGGTGCTCACGTCTAACTTC) were used to target DNA as controls to confirm that the DNA had indeed been recovered from the same samples. DNA samples, 2x Reddymix, nuclease-free water and primers were then added to each PCR tube, which were then placed in the PCR machine (Bibby Scientific Techne TC-512, UK). The PCR machine was run using what we describe as 'the SyGCaMP2 protocol'. This protocol includes heating to activate the polymerase for 5 minutes at 94°C, followed by 35 cycles of 94°C for 30 seconds (to denature the DNA), 60°C for 30 seconds (to anneal the primers) and 72°C for 30 seconds (for elongation). This was finally followed by one round of 5 minutes at 72°C (final elongation). When the cycles of PCR had finished 3g agarose was added to 100 ml

TAE buffer to make the agarose solution that was required for the gel. This solution was boiled and 10 µl (1:1000) SYBR® were added to 100 ml agarose. The gel chambers were then formed by inserting a comb and placing tape to the required height. The gel was carefully poured into a casting tray and allowed to set for approximately 25-30 minutes. The comb was then removed gingerly. The gel was then placed in a gel tank and covered with 1 X TAE buffer. 18 µl of sample per well was added from PCR tubes and the gel run at 80 V and 400 mA for 42-45 minutes. The power was then turned off and the electrodes removed. The gel buffer was decanted, and the gel was dried gently. Finally, the gel was visualised using a blue light chamber and the results recorded in the lab book as appropriate.

In general, the PCR technique led to the production of double the DNA for every cycle, leading to the generation of a large number of copies (an exponential amplification) of the target DNA segment. Thus, the genotype can be deduced by looking at the differential bands formed through flanking primers. Flanking primers are used to differentiate between the alleles of transgenic and wildtype mice via amplicon length (Bartlett and Stirling, 2003).

Figure 2.2 illustrates the results of a typical example of the genotyping. It shows the results of electrophoresis in agarose gel, which shows two potential columns for each sample from a single mouse. The first two columns in the agarose gel always show a control transgenic mouse, which was already known from the previous genotyping experiment. The first lane in each pair represents the results obtained from the control primer to ensure that the DNA had been successfully extracted. The presence of a second band in the right-hand lane of each pair indicates the presence of DNA encoding SyGCaMP2.

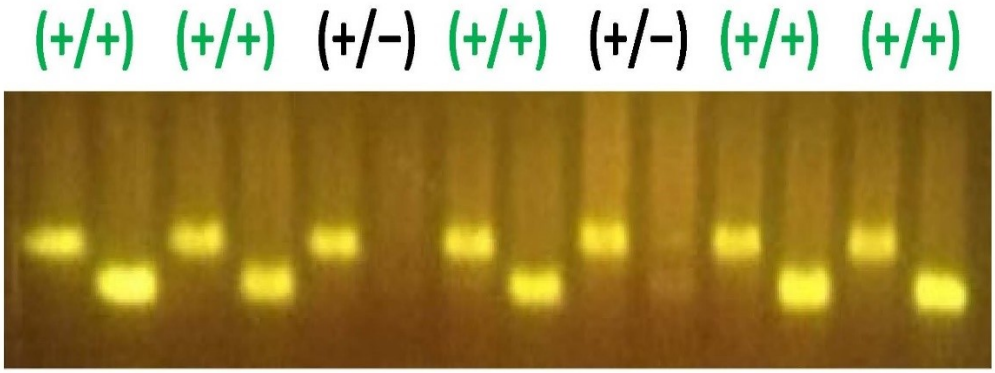

Figure 2.2. Typical example of a genotyping gel used for identification of transgenic mice from SyG37 colonies. Each sample from a single mouse is illustrated with two columns. The first lane in each pair represents the result of the control primer to ensure that the DNA was successfully extracted. The presence of a second band in the right-hand lane of each pair indicates the presence of DNA encoding SyGCaMP2. In this case, the third and fifth samples were from WT mice (coloured black, +/−). The mouse is transgene when both columns are bright (coloured green, +/+).

2.3 Preparation of acute brain slices

2.3.1 Solutions and equipment

An artificial cerebrospinal fluid (aCSF) was used for the incubation and perfusion of brain slices. The aCSF composition was in (in mM): 2.7 KCl; 1.2 $MgSO_4.7H_2O$; 120 NaCl; 25 $NaHCO_3$; 1.2 NaH_2PO_4; 11 D-Glucose; 2.5 $CaCl_2.2H_2O$ and equilibrated with 95% O_2 and 5% CO_2 (pH 7.4) at room temperature, whereas an ice-cold sucrose solution was used for cutting brain slices. The ice-cold sucrose solution was composed of (in mM); 2.5 KCl; 10 D-Glucose; 1.2 NaH_2PO_4; 0.5 ascorbic acid; 26 $NaHCO_3$; 250 sucrose; 0.1 $CaCl_2.2H_2O$; 4 $MgCl_2$ and then equilibrated with 95% O_2 and 5% CO_2 at room temperature. Various tools were also required for the preparation of brain slices such as a small spatula, small surgical scissors, fine tip forceps, large scissors, blades, petri dishes, filter papers, super glue, Pasteur pipettes, a small glass beaker (60-80 ml), plastic transfer pipettes, small syringes, a standard tissue platen and blocks of agar which were made in advance using 4.5 to 6.0% agarose in a 0.9% solution of NaCl which were kept in the fridge until use.

2.3.2 Dissecting and slicing

The mice were deeply anesthetised in a small animal chamber using isoflurane in 100% oxygen until the pedal reflexes were absent. The mice were then removed from the chamber and decapitated (according to an approved Schedule 1 procedure). The skull was removed, and the brain exposed. A small spatula was used to quickly remove the brain and place it in a glass beaker containing an ice-cold sucrose solution bubbled with 95% O_2 and 5% CO_2, as described above. A sharp blade was used to separate the cerebellum from the rest of the brain and the brain stem was cut away from the cerebellum. After that, the cerebellum, in the coronal or sagittal plane as appropriate, was glued onto the cutting stage (standard tissue platen) facing towards the blade, and an agar block glued behind the cerebellum in advance for support. Filter paper was also used to briefly dry the cerebellum to remove any excess fluid before gluing. A Pasteur pipette containing cold sucrose solution was used to add some drops to the top of the cerebellum to avoid any drying or any glue going up to the tissue edges, and then the standard tissue platen was placed quickly in the chamber of the vibrating blade tissue slicer which contained ice-cold sucrose solution that was continuously bubbled with 95% O_2 and 5% CO_2 to cover the tissue for the entire period of cutting. Slices were prepared by using a vibrating microtome (Model 7000smz-2; Campden Instruments Ltd; UK). 300 µm thick slices were then cut using an amplitude of 1 mm and a frequency of 90 Hz at an advancing speed of 0.05 mm/sec. The reverse end of a Pasteur pipette was used to transfer the slices (5-6 slices) to the incubation chamber which was filled with aCSF and equilibrated with 95% O_2 and 5% CO_2 to maintain a pH of 7.4. Slices were maintained in the incubation chamber at room temperature for at least one hour (Pereda et al., 2019, Al-Osta et al., 2018) and then a selected slice was transferred to a recording chamber on the microscope and perfused with carbogenated aCSF at room temperature at a rate of flow 1 to 2 ml per minute using a laboratory peristaltic pump (Gilson Minipuls; France). The slices were kept from floating by using a harp which consisted of a flattened U-shaped ring of silver wire over which nylon fibres were stretched and glued thin at intervals of about 1-2 mm.

2.4 Reagents

Unless stated otherwise, drugs were obtained from Sigma Aldrich. Isoflurane (IsoFlo®) was obtained from Abbott Laboratories (USA), while ReddyMix PCR master mix was obtained from Thermo Scientific (USA). Primers for genotyping, namely Cmah R, Cmah F, SyGCaMP2 R, and SyGCaMP2 F, were obtained from Invitrogen (USA), as was the SYBR® safe DNA gel stain. Other chemicals, including sucrose, $MgSO_4.7H_2O$, NaH_2PO_4, $NaHCO_3$, KCl and D-glucose were purchased from Fisher Scientific (USA), whereas *N*-methyl-D-Aspartate receptor (NMDA) was obtained from Cayman Chemical (USA). DL- AP5, DNQX, picrotoxin (PTX), bovine serum albumin, NBQX and tetrodotoxin (TTX) were obtained from Tocris Cookson (UK). WIN 55,212-2 and AM251 were purchased from Cambridge Bioscience (UK).

2.5 Extracellular field potential recordings

Thin-walled borosilicate glass capillaries (1.5 mm OD X 1.17 mm ID; Harvard Apparatus) were used as a material for preparing electrodes. The stimulation and recording electrodes were produced using a Flaming-Brown micropipette puller (P-97, Sutter; USA). Tip resistances of 1-3 MΩ were used for the stimulating electrode and resistances of 2-4 MΩ for the recording electrodes with both electrodes filled with aCSF. These electrode resistance ranges were used for all experiments. The stimulating electrode was formed by filling the capillary with aCSF with two a silver wire (Ag-AgCl); one placed inside and a second wire wrapped around the outside of the barrel. The recording electrode was formed by inserting an Ag-AgCl wire inside the pipette and a bath reference electrode was used. When the slices were ready to be used for running experiments, a selected slice was placed in a recording chamber on the fluorescence microscope and perfused with aCSF and oxygen at a flow rate of 1-2 ml per minute to keep the slices healthy. In order to keep the slices in place and prevent them from moving during recordings, a silver harp was (Al-Osta et al., 2018) placed on the top of slice during stimulation as described previously in section 2.3. A micromanipulator was used to lower the tip of the stimulating electrode onto the surface of the ML between the pial surface

and the middle of the molecular layer (see Figure 2.6 A) in order to activate the PFs. This electrode was also linked to an isolated stimulator (Digitimer; UK), which was used to supply a constant voltage electrical stimulus. The recording region selected was in the ML, just above the PCL, to record field potentials originating from the PC dendrites. Using motorised patch-clamp micromanipulators, the recording electrode was advanced carefully in this region of the slices until the clear, characteristic appearance of typical field potential signals were detected in response to PF activation (for further details, see Figure 2.3).The protocol of this activation constituted trains of 20-50 stimuli, delivered at a rate of 50 Hz at an intensity of 25-40 V. The typical field potential includes a stimulus artefact (SA), a presynaptic fibre volley (N1) and a postsynaptic component (N2) which may incorporate the activation of both excitatory and inhibitory neurones (Van den Burg et al., 2007, Kochlamazashvili et al., 2011) (see Figure 2.3). Extracellular field potentials were recorded using a patch clamp amplifier (HEKA; Germany) linked to the WinLTP data acquisition program (WinLTP version-2.01, U.K) (Anderson and Collingridge, 2007, Bliss and Lømo, 1973) via an M-series DAQ acquisition board (National Instruments, USA). WinLTP was also used to trigger Ca^{2+} imaging experiments which were controlled and collected using various software procedures (written by Prof Nick Hartell in Igor Pro 6; Wavemetrics, USA) running on a separate computer. Pairs of field potentials, stimulated at intervals of 50 ms, were collected every 10 s. Drugs were applied after recording a stable baseline for at least 10 minutes. Field recordings were filtered at 3 kHz and digitised at 10 kHz. These recordings then were saved on the computer for subsequent analysis.

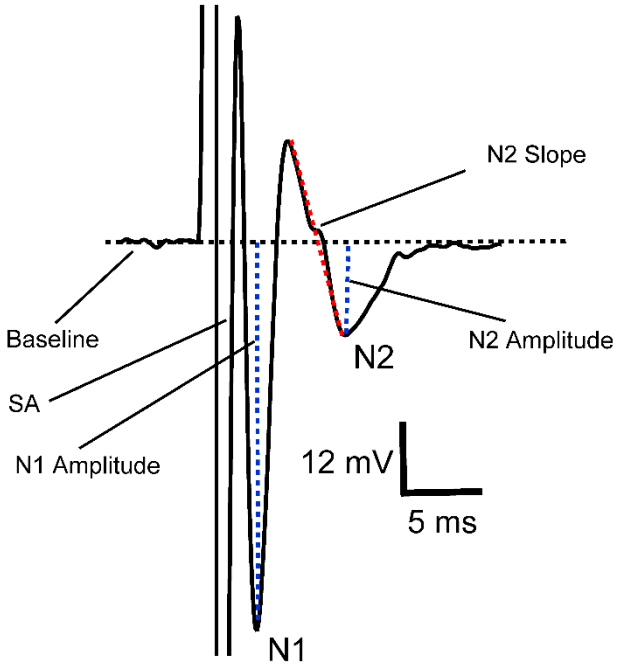

Figure 2.3. A typical trace for an extracellular field potential response evoked by the activation of the cerebellar PFs. The trace shows the characteristic appearance of the synaptic components of a PF response, as evoked by electrical stimulation. After the stimulation is applied, the stimulus artefact (SA) will appear immediately, followed by N1 (also known as the fibre volley) which refers to the action potentials and N2 which is a postsynaptic potential that can only appear when a neurotransmitter has released from the presynaptic axon terminals. The peak amplitudes of N1 and N2 (blue dashed line) and the slope of N2 (red dashed line) are shown on the trace and can be measured using the WinLTP software. The scale bar, at 12 mV, 5 ms, illustrates typical magnitudes.

2.6 Ca^{2+} Imaging

2.6.1 Epifluorescence microscopy

Ca^{2+} imaging measurements were performed using a Nikon FNI upright microscope (Nikon: Japan) equipped with an optiMOS™ Scientific CMOS camera (QImaging; Canada). As already described, brain slices were placed in the custom-built recording chamber of the microscope, held in place using a silver harp and with carbogenated aCSF. A 20 x (0.5 NA) Plan Fluor objective (Nikon; JAPAN) water-immersion lens was used. A micromanipulator was used to place a stimulating electrode in ML or GCL as appropriate to activate their various regions. In the same field of view, recordings of fluorescence and electrophysiological responses were taken. An LED light source (Lumencor®; USA) was synchronised with the image capture such as to switch rapidly between the 470 ± 20 nm and 560 ± 20 nm excitation wavelengths to record a stack of interleaved images with emission wavelengths of 520 ± 20 nm and 620 ± 20 nm, which were measured as green (SyGCaMP2) and red (mCherry) images, respectively. Ca^{2+} imaging responses were collected using customised procedures written by Prof Nick Hartell in Igor Pro (Version v6.34A7; Wavemetrics, USA). Ca^{2+} imaging experiments were triggered using the WinLTP. Each image in a sequence consisted of 760 x 760 pixels (unless stated otherwise) exposed for 80 ms. Each image stack comprised 200 images and covered a total time of 20 seconds. Bursts of 20 or 50 stimuli at a rate 50 Hz and of 25 - 40 V were applied as electrical stimulation in these experiments. Image stacks were collected every 5 minutes. Stable baseline recordings were obtained for at least 10 minutes before applying any drugs. Image stacks were saved as TIFF files on a computer for subsequent offline analysis. Figure 2.4 illustrates the imaging setup coupled to the electrophysiological recording system.

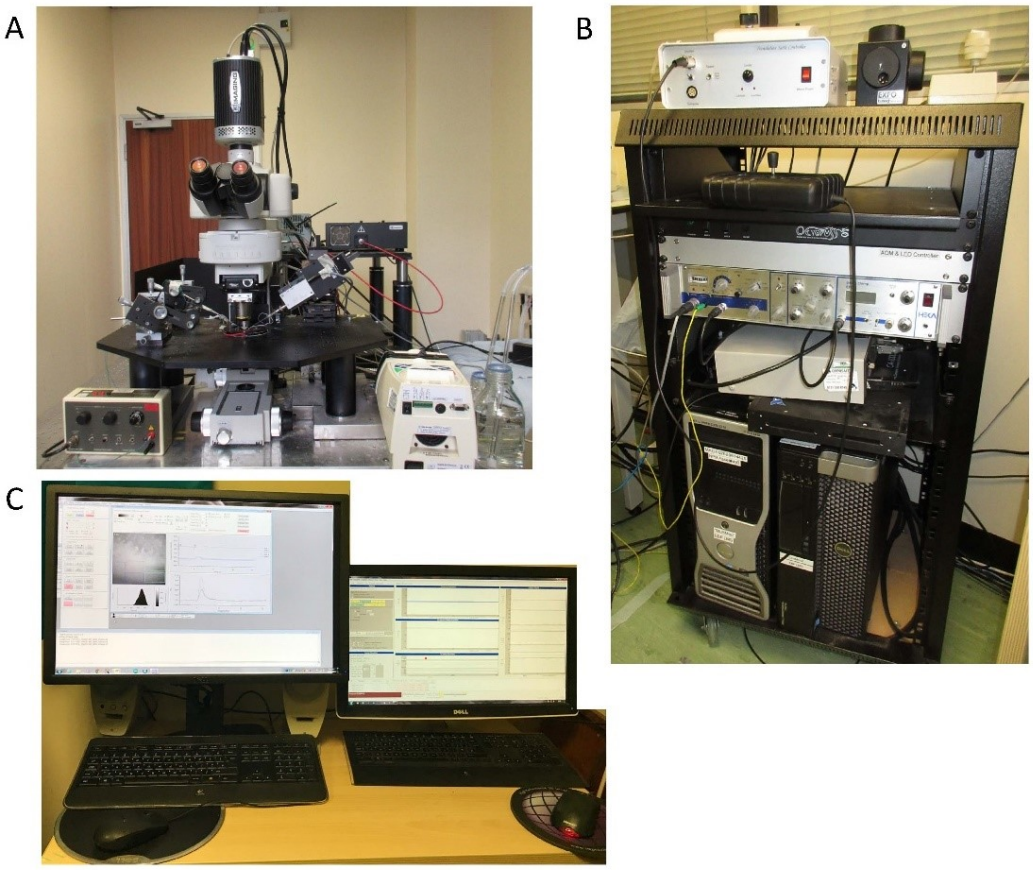

Figure 2.4. Photographs of the imaging and electrophysiological recording system used for experiments. (A) shows an upright microscope fitted with an sCMOS camera, micromanipulators, stimulating and recording electrodes, a recording chamber and a light source is shown. On the right-hand side is the automatic perfusion system used to perfuse the chamber with the appropriate solution. On the left-hand side is the stimulating electrode and manipulator which was used to electrically activate acute brain slices. (B) illustrates the control units for the motorised patch-clamp micromanipulators, remote focus accessory (Nikon), translation table controller, an M-series DAQ acquisition breakout box (National Instruments) and a patch clamp amplifier. (C) shows two computer monitors connected to computers running Igor Pro (left) and WinLTP software (right), which were used to control and record the calcium imaging and electrophysiology experiments, respectively.

2.6.2 Multiphoton microscopy imaging recordings

A multiphoton microscope (MP7; Carl Zeiss Microscopy GmbH; Germany) was used to perform single bouton Ca^{2+} imaging experiments. As described previously, slices were placed in the recording chamber of the upright multiphoton microscope and held in place with a silver harp. Slices were perfused with carbogenated aCSF. Stimulating electrodes with resistances of 1-3 MΩ when filled with aCSF were inserted into slices as described previously and connected to an isolated stimulator (Digitimer; UK). A water immersion objective (x20, 1 NA; Carl Zeiss GmbH; Germany) was used. The microscope was fitted with a Mai-Tai HP Ti: Sapphire pulsed laser (Spectra-Physics, USA). The laser, and imaging experiments, were controlled using the Zen 2011 software. For relatively high-speed imaging experiments of single boutons, a digital zoom of x2 was used and stacks of 80-90 images of fields of single boutons were collected at intervals of 98 ms with sizes of 512 pixels x 64 lines (corresponding to 212.5 μm X 26.6 μm; unless stated otherwise). Electrical stimulation and image recording were triggered using an Arduino Uno controlled via the Igor Pro software. SyGCaMP2 was excited at 920 nm and the subsequent emission collected at 520 ± 20 nm (Drobizhev et al., 2009). Unless stated otherwise, the stimulating electrode was placed in the ML to activate the PFs, and a train of 20-50 stimuli were again applied at a rate of 50 Hz and 30-50 V, for which imaging data were collected at 5 minutes intervals in response to PF stimulation; stable baseline recordings were also obtained for at least 10 minutes before applying any drugs. Figure 2.5 shows the setup used for the multiphoton microscope system.

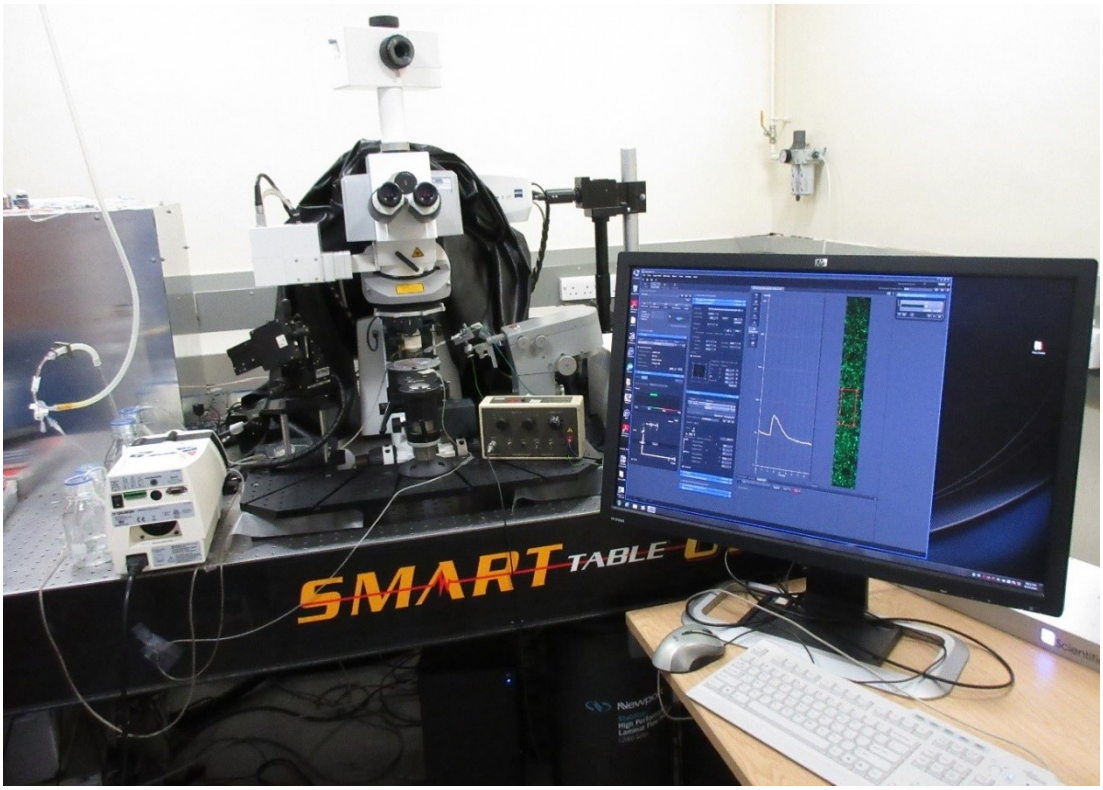

Figure 2.5. Multiphoton microscope system and control software used to obtain images of single boutons. This system comprised a multiphoton microscope (Zeiss LSM 7 MP; Carl Zeiss, Germany) equipped with a water-immersion lens (x20, 1 NA), a Mai Tai HP Ti: Sapphire pulsed laser, stimulating electrode and the chamber in the centre. On the left-hand side is an automatic perfusion pump. The computer used to control the experiments is shown on the right.

2.6.3 Expression of SyGCaMP2-mCherry in the SyG37 mouse's brain cerebellum slice

Coronal cerebellar slices, 300 µm thick, were prepared from SyG37 and aged matched, wildtype mice as previously described. Slices were placed on the recording chamber which was perfused slowly with aCSF at a rate of 1 ml/min at room temperature. The perfusion was switched off during image capture, as this helps to prevent any movement of the slices. A sCMOS camera attached to a fluorescence microscope was used to take images of the whole brain slice of the cerebellum from SyG37 and wildtype adult mice. This microscope was controlled by Igor Pro, as previously described. The individual wavelengths were control by a

universal illumination system (CoolLED Ltd; U.K.). The single band filter was set ET-EGFP/mCherry (Chroma Technology; U.S.A.). 470 ± 10 nm and 560 ± 10 nm excitation wavelengths were applied to record a stack of interleaved images with emission wavelengths of 520 ± 20 nm and 620 ± 20 nm (Drobizhev et al., 2009), which were measured as green and red images, respectively. A Nikon Plan (4X/0.20 NA) water-immersion lens was used to visualise the different areas of the cerebellum slice. The individual images of the whole cerebellum were acquired in a systematic manner to form a panoramic image that contained equally spaced overlaps among each image. This allows the FIJI software to recognise images during the process of stitching. Overlapping images of SyGCaMP2 and mCherry fluorescence were obtained over a panoramic image. Prior to stitching, overlapping was filtered without edges to produce a good approximation of the resolution and quality of the whole cerebellum. Sets of images of both the SyGCaMP2 and mCherry fluorescence of the cerebellum were stitched together using a stitching plugin in the FIJI software (Schindelin et al., 2012, Preibisch et al., 2009, Bankhead, 2014). Finally, these images were then presented with identical brightness settings using the Igor Pro software.

2.7 Data analysis

2.7.1 Field potential data

Field potential data were analysed using the WinLTP software (WinLTP version-2.01, U.K; Anderson and Collingridge, 2007). The peak amplitudes of the N1 and N2 components were routinely measured and analysed along with the initial slope of N2. In most cases, absolute values were converted into a percentage of the mean value measured during the baseline period. Microsoft Excel software was used for this purpose and to calculate the mean, standard deviation and standard errors of the mean (SEM) for multiple experiments. The PPR of the amplitude or slope of the second to the first pulse of the two stimuli applied at 50 ms intervals was also calculated and plotted over time. The change in PPR was used as evidence for presynaptic plasticity (Yang and Calakos, 2013). The results were reported as mean ± SEM, as shown in the results section.

2.7.2 Ca^{2+} imaging data

2.7.2.1 Epifluorescence imaging data

Imaging data were analysed using a combination of the Igor Pro and Microsoft Excel software. Interleaved image stacks were first split into two separate stacks, representing images from SyGCaMP2 (green) and mCherry (red). For SyGCaMP2 image analysis, regions of interest (ROIs) were identified as appropriate in either the ML or GCL or both. The absolute fluorescence from the ROIs was measured for each image in the stack, after which bleach compensation was applied. This was achieved by fitting traces before and after stimulation with a single or double exponential curve and then subtracting the fitted decay from the actual response. The bleach compensation of the baseline response was then reset to its original value before normalisation to F_0 (see Figure 2.6 C and D). The mean fluorescence prior to electrical activation (F_0) was calculated, and any subsequent change in absolute fluorescence, expressed as the ratio F/F_0, was plotted against relative time. The change in fluorescence was assessed in the ROIs. A similar methodology was used for all experiments, and the example shown (image data analysis) in the steps in Figure 2.6 reveal how the data were recorded and analysed. In this Figure, data from about twelve separate ROIs were arranged into two groups and averaged. ROIs 1, 2, 3, 4, 5, and 6 were grouped in the GCL, whereas ROIs 7, 8, 9, 10, 11 and 12 were grouped in the ML (Figure 2.6 B and C). Bleach compensation was applied as described above, and then image number was converted to time relative to the stimulus onset and normalised to the baseline average (see Figure 2.6E and F). Data from the ML and GCL groups were subsequently plotted against relative time and the peak intensity of the responses, and the initial slope and area under the curve was measured (see Figure 2.7). The Figure 2.6A also illustrates the position of the stimulating electrode, as placed in ML to activate the PFs. In this example, trains of 50 stimuli were applied at a rate of 50 Hz at an intensity of 35 V. The recording electrode was placed above the PC layer to record the N1 and N2 components of the field potentials.

Figure 2.7 illustrates the peak amplitude, the initial slope, the decay and AUC of SyGCaMP2 fluorescence on from the trace of the SyGCaMP2 fluorescence

response. The measurement of peak, slope, and AUC was achieved using Igor Pro software. Finally, unless stated otherwise, the raw data for each experiment were normalised to the baseline and expressed as percentages using Microsoft Excel software. The analysis of mCherry image was performed in the same way as for SyGCaMP2 the image.

For measurement of the baseline SyGCaMP2: mCherry ratio, the interleaved image stacks were first split into two separate stacks as mentioned above, where images from SyGCaMP2 (green) and mCherry (red) were then uploaded into Igor Pro, allowing for analysis to be conducted, also in the same manner as described above. The baseline for SyGCaMP2 and mCherry were then measured directly by Igor Pro and the baseline data then transferred to Microsoft Excel software to calculate the SyGCaMP2: mCherry ratio. Due to the decline in the baseline fluorescence as a result of photobleaching, the data were again transferred to Igor Pro software to allow fitting with a single exponential using the equation below, and then subtracting the fitted decay from the actual response. The bleach compensation to the baseline response was then reset to its original value, as mentioned earlier. Finally, the ratios for the SyGCaMP2 to mCherry baseline fluorescence were calculated using Microsoft Excel software. Data were normalised and presented as mean ± SEM.

$$y_0 + A \exp\left\{\frac{-(x-x_0)}{\tau}\right\}$$

(Y_0 is intercept, A is maximum, x is the time relative to x0, and τ is tau)

2.7.2.2 Multiphoton microscopy imaging data

For single bouton data analysis, image stacks in the Zeiss proprietary image format were converted into TIFF format using the FIJI software (Schindelin et al., 2012). These TIFF files were then imported into Igor Pro 7 for analysis. The Niman5_SarfiaAssistant (written by Prof Nick Hartell in Igor Pro) software was used to batch analyse the single bouton data. This software was adapted from semi-automated routines for functional image analysis (SARFIA) (Dorostkar et al., 2010). SARFIA contains a series of routines that allow detection and identification of punctate regions of interest that can be categorised according to the patterns of their responses to electrical stimulation. The stages of this analysis include: (A) images (TIFF format) were loaded and optionally a background fluorescence value subtracted from them; (B) image stacks were registered, if required, to correct for movement artefacts over time and then filtered over time; (C) the Laplace operator was used to transform the averaged images and to set the threshold level; (D) the ROIBeams2Traces command was used to group individual pixels into ROIs which corresponded to individual puncta; (E) bleach compensation was applied and data were subsequently normalised to baseline fluorescence (F/F_0). The results of peak fluorescence were reported in the form of mean ± SEM unless otherwise stated; (F) hierarchical clustering was applied to categorise the response or non-response of each ROI to electrical stimulation; and (G) the responding and non-responding puncta were displayed on the original image as green and red dots. Most of these stages of analysis, as mentioned above, were run automatically using Niman5_SarfiaAssistant with the exceptions that the background subtraction, hierarchical clustering, selecting responding and non-responding puncta, and normalisation to the baseline (F/F_0) required manual input.

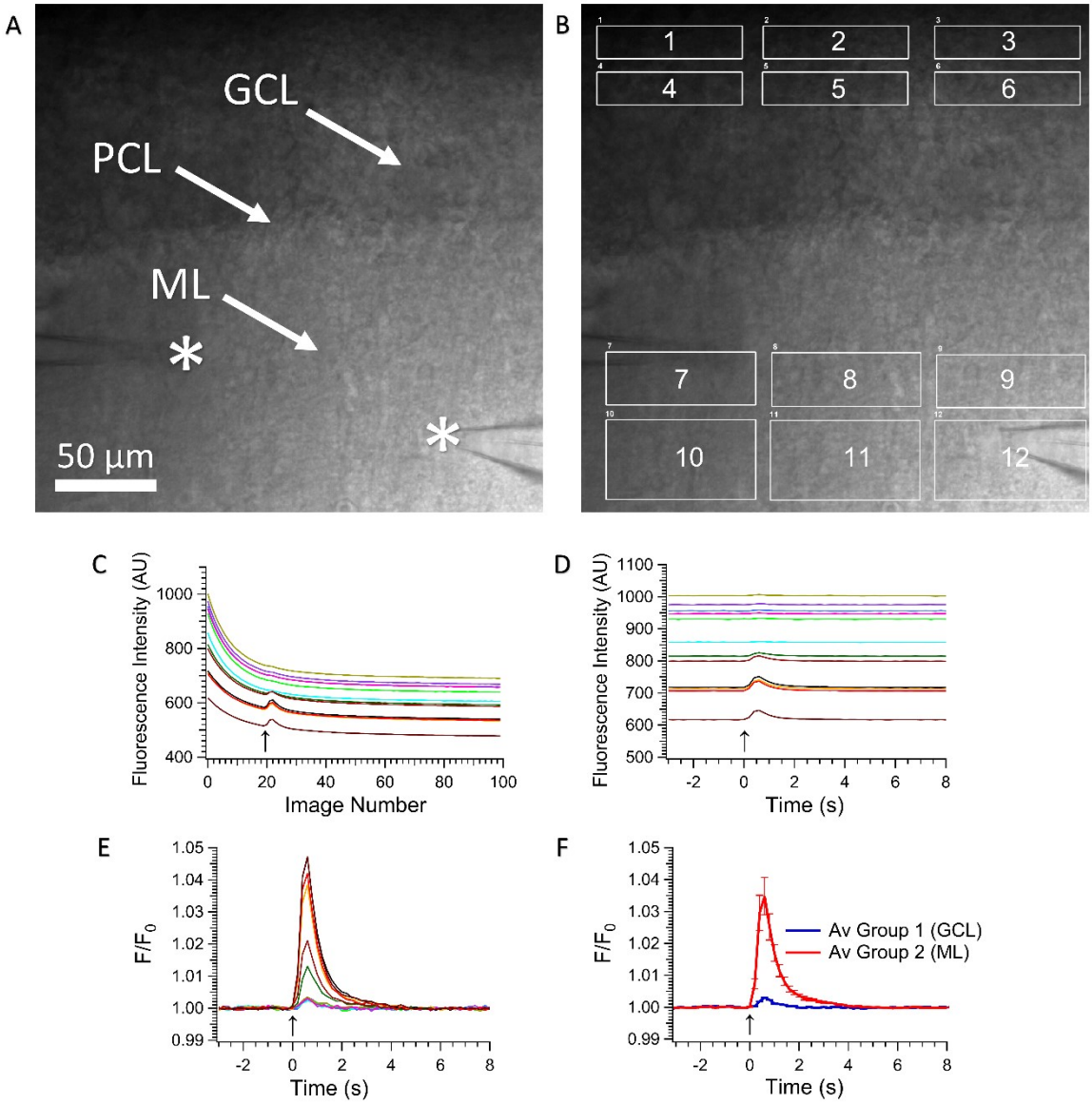

Figure 2. 6. Analysis steps for SyGCaMP2 imaging. (A) The white arrows identify the granule cell layer (GCL), Purkinje cell layer (PCL) and molecular layers (ML) on a light transmission image of a coronal cerebellar slice. The bottom-right asterisk shows the location of the stimulating electrode, whereas the top-left asterisk shows the location of the recording electrode. The scale bar represents 50 µm and the image size was 760 x 760 pixels. (B) shows twelve regions of interest positioned over the ML and GCL regions. These ROIs were later organised into two groups (GCL; ROIs 1-6; ML ROIs 7-12). (C) shows SyGCaMP2 fluorescence changes over time collected from the ML and GCL ROIs. (D) shows the effect of the bleach compensation protocol on the data presented in (C) and then the image number converted to time. (E) and (F) show data were normalised to baseline (F/F_0) and the averaged ROIs within the ML and GCL, respectively.

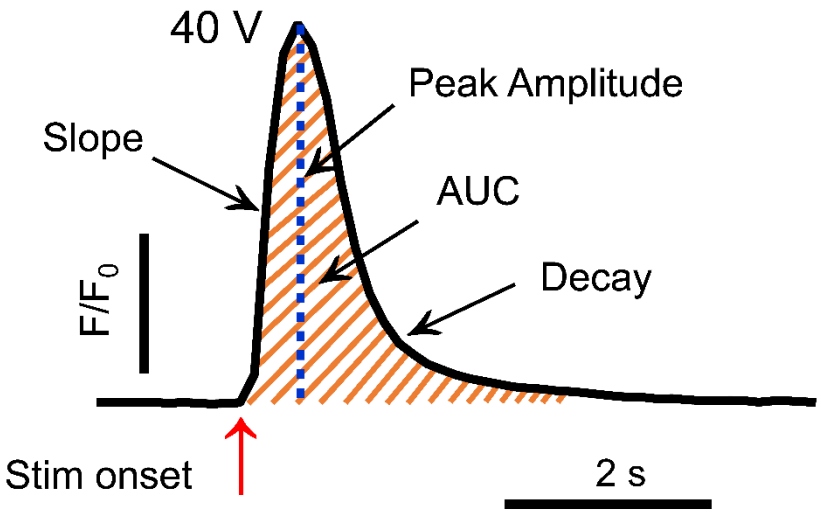

Figure 2.7. Typical trace for a SyGCaMP2 fluorescence response. This trace illustrates a characteristic response of SyGCaMP2 fluorescence to electrical activation (50 Hz, 50 stimuli and 40 V) of the ML in a cerebellar slice cut in a coronal orientation. Measurements were obtained from regions of interest (ROIs) sited within the molecular layer (ML) of the cerebellar cortex. SyGCaMP2 was excited at 470 ± 20 nm and its emission recorded at 520 ± 20 nm. The peak amplitude (blue dashed line in centre), AUC (brown solid lines), the initial slope (the black solid line in the left-hand side) and the decay (the black solid line in the right-hand side) for SyGCaMP2 fluorescence are shown on the graph. The red arrow indicates the onset of electrical activation.

2.7.2.3 Subtracting images

Igor Pro was also used to collect images of SyGCaMP2 fluorescence both before and during stimulation. The averages of three sequential SyGCaMP2 images were taken immediately before stimulation. These were subtracted from the peak responses taken during electrical stimulation to create a subtraction image. A warm/cold look-up table was used to highlight the difference in intensity between the two responses. The changes in calcium concentration can be seen in the brighter colours of the SyGCaMP2 images.

2.8 Experimental design and statistical analysis

In this study, the experiments were performed using acute brain slices from both genders of wildtype and transgenic C57 Blk6 mice, aged between 3 and 10 weeks. Unless stated otherwise, no more than two replicates were obtained from any one mouse. These replicates represent data from separate brain slices. Data were normalised to a baseline and expressed as mean ± SEM. Unless stated otherwise, the number of replicated experiments for each dataset are indicated in Figure legends and the levels of statistical significance are shown in the Figures. All experiments were performed at room temperature (Al-Osta, 2018, Casado et al., 2000, Pereda et al., 2019). Statistical analysis was undertaken using GraphPad Prism 7. All data were first tested to determine if they were normally distributed using the Shapiro-Wilk normality test followed by analysis using parametric (for normally distributed data) or non-parametric tests (for non-normally distributed data). The non-parametric tests included a Wilcoxon matched-pairs signed rank test, which was used to test the levels of statistical significance between two paired data groups, whereas the Mann-Whitney test was used for comparisons between two unpaired data groups. The Friedman test, with Dunn's post hoc tests, were used to test the levels of statistical significance between three or more paired data groups while the Kruskal-Wallis test, again with Dunn's post hoc correction test, were used to test the levels of statistical significance between three or more unpaired data groups. Parametric tests, when used, included the paired t-test, which was used to test the levels of statistical significance between two paired data groups, whereas the unpaired t-test was used to test the levels of statistical significance between two unpaired data groups. For comparison between three or more unpaired data groups, we used the ANOVA test with the Tukey post hoc test. The repeated measures ANOVA test with the Tukey post hoc test was used to test the levels of statistical significance between there or more paired data groups. P values greater than 0.05 were considered not to be significantly different (ns). However, if the P value was less than 0.05, 0.01, 0.001 or 0.0001 than it considered as significantly different and highlighted with asterisks *, **, *** and ****, respectively. Where possible, absolute P values are given.

Chapter 3: Expression patterns of SyGCaMP2-mCherry in the cerebellar cortex of the SyG37 transgenic mouse line

3.1 Introduction

Previous studies in our lab have reported that the SyGCaMP2-mCherry sensor is expressed within the hippocampus of SyG37 mice (Al-Osta et al., 2018). SyGCaMP2-mCherry was found to be expressed in both excitatory and inhibitory synaptic terminals in hippocampus brain slices (Al-Osta, 2018). The first part of the present study was to examine and characterise the expression levels of SyGCaMP2-mCherry in acute slices of the cerebellar and compare these with fluorescence patterns in wildtype (WT) mice. The purpose of this was to first establish whether SyGCaMP2-mCherry was present in the cerebellum and, if so, in which layers and cell types it was expressed based upon the characteristic anatomy of the cerebellar cortex. Second, we aimed to establish whether we could visualise neuronal activity within the cerebellar cortex and to examine how, in particular, PF activity is transmitted across the cerebellar cortex. Coronal and sagittally cut cerebellar brain slices of 300 µm thickness were used to compare the patterns of GC or PF activity in each plane. Slices were prepared from SyG37 or WT animals. An epifluorescence and multiphoton microscope were used to image SyGCaMP2-mCherry fluorescence, as described previously. Image data were analysed using Igor Pro and ImageJ. See Chapter 2 for a detailed description of the methods used in this chapter.

3.2 Results

3.2.1 Expression patterns of SyGCaMP2-mCherry in cerebellar coronal slices of SyG37 mice

As a first step in this project, we aimed to examine the patterns of fluorescence expression of SyGCaMP2 and mCherry components of SyGCaMP2-mCherry in acute coronal slices prepared from SyG37 mice and compare these with age-matched WT mice. The images for both SyGCaMP2 and mCherry fluorescence were obtained and stitched together as previously described (see Materials and Methods, section, 2.6.3). The illumination intensities for SyGCaMP2 and mCherry fluorescence were kept constant to facilitate comparison with coronal slices obtained from WT mice. The brightness levels for the images were also kept the same to allow for a semi-quantitative comparison of expression levels. The results, as shown in Figures 3.1A and B, indicate that green and red fluorescence were markedly brighter in the cerebellar cortex of SyG37 positive mice compared to WT mice. This indicates that the SyGCaMP2-mCherry sensor is expressed in the cerebellum of SyG37 mice.

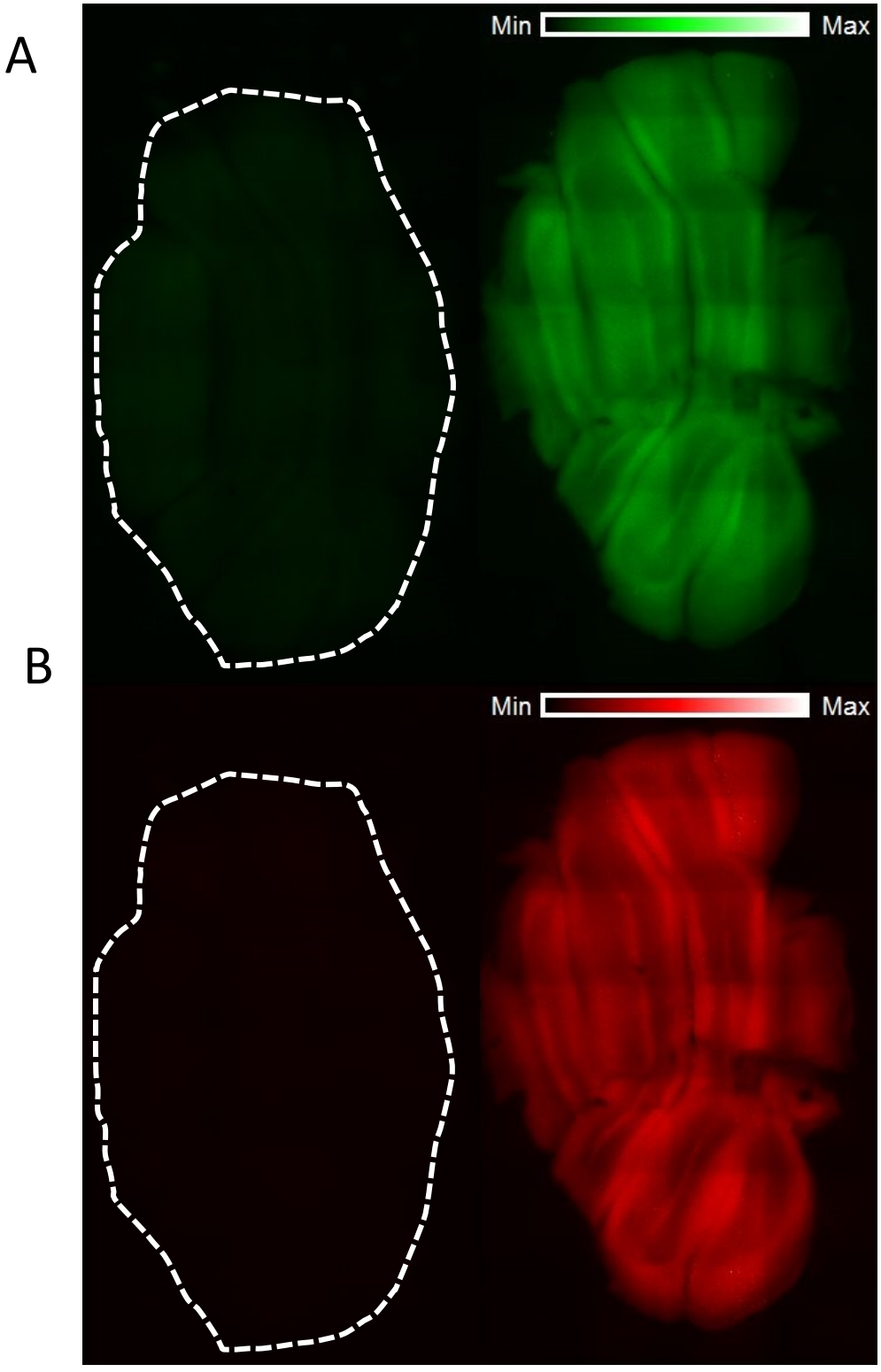

Figure 3.1. Expression pattern of SyGCaMP2-mCherry in cerebellar coronal slices of SyG37 and wildtype mice using an epifluorescence microscope. Epifluorescence microscope images of coronal cerebellar slices in SyG37 and wildtype mice. Images were stitched together and displayed as a complete cerebellar slice. (A) illustrates stitching of images of wildtype (left-hand side; white dashed lines outline slice contours) and SyG37 mice (right-hand side) that were

collected using an excitation wavelength of 470 nm. (B) illustrates stitched images of wildtype (left-hand side; white dashed lines outline slice contours) and SyG37 mice (right-hand side) obtained using an excitation wavelength of 550 nm. For the purposes of quantitative comparison, the same illumination intensities and brightness settings for WT and SyG37 positive mice were used. A green or red look-up table from minimum (Min) to maximum (Mix) in the top right panel A and B was used to illustrate the differences in the intensity in both.

We next repeated these experiments but used a multiphoton microscope to view the SyGCaMP2-mCherry expression patterns. We compared brain slices from WT and SyG37 mice. A wavelength of 920 nm was used to excite SyGCaMP2 and, as before, identical illumination intensities and brightness settings were applied to aid a semi-quantitative comparison between age-matched SyG37 positive and WT mice. Emission signals of 520 ± 20 nm were collected (Drobizhev et al., 2009). Images were then stitched together (see Materials and Methods, section 2.6.3). The results are shown in Figure 3.2. Green fluorescence was clearly much brighter in transgenic mice than the WT animals, further indicating that the SyGCaMP2 sensor is expressed in the cerebellum of SyG37 mice.

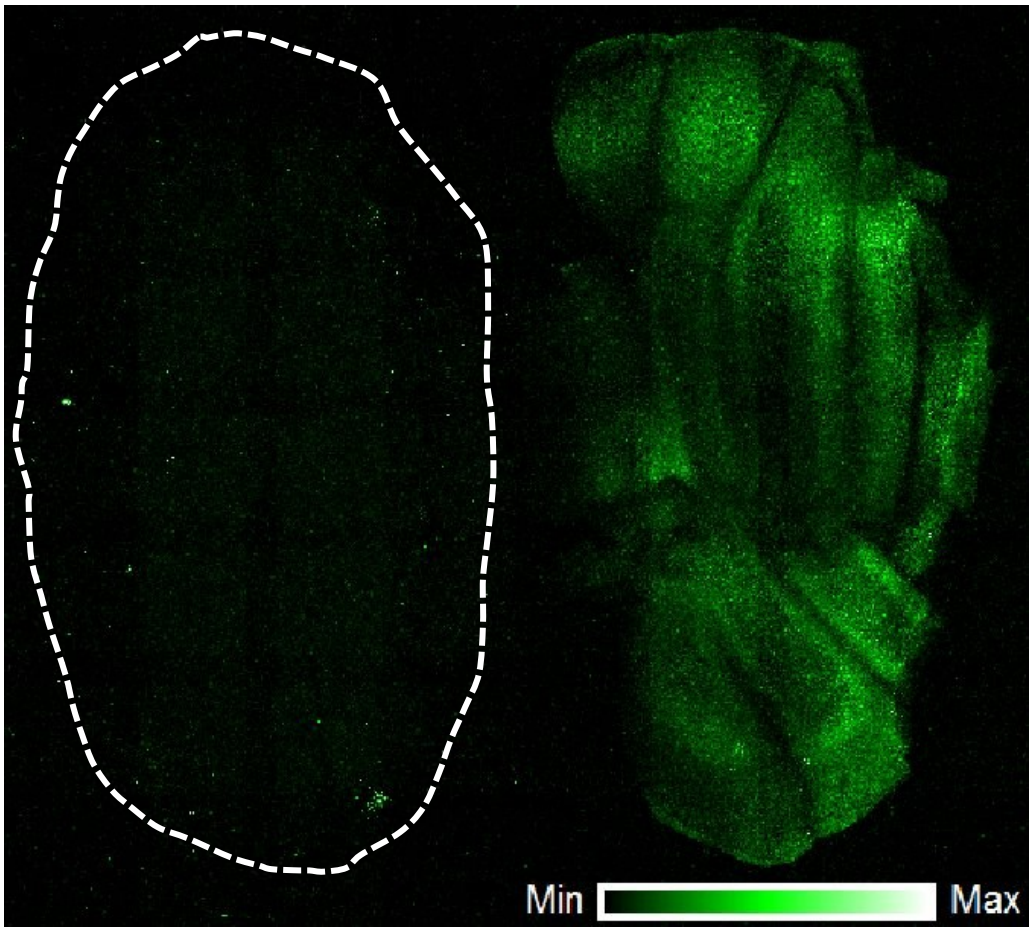

Figure 3.2. Expression pattern of SyGCaMP2 in cerebellar coronal slices as shown using multiphoton microscopy. The images presented here are as shown in Figure 3.1 except that images were collected with excitation wavelengths of 920 nm using a multiphoton microscope.

We next examined the expression patterns of SyGCaMP2 and mCherry using multiphoton microscopy at higher resolution to see in which cells and in which layers expression was evident; SyGCaMP2 was excited at 920 nm as before. mCherry has a two-photon absorption peak at 750 nm (Drobizhev et al., 2009) and so this wavelength was used to see if we could observe mCherry expression as well. Series of images with a resolution of 1024 x 1024 pixels were taken in the axial or Z plane at a digital zoom of 1 and 2 with a 20x magnification (NA 1.0) objective. The FIJI software was used to analyse and display the experimental images.

The results of the experiments carried out in sagittal cerebellar slices are summarised in Figure 3.3. Panels A ii, iii showed that the green and red fluorescence levels, respectively, were very much higher in the majority of

cerebellar regions, but are prominently expressed in the ML. These regions include the ML, which clearly has a high density of small punctate dots of sensor expression across the whole area of the ML (yellow arrows), whereas the GCL has a clear, larger concentrated sensor of expression (blue arrows), while the PCs show only dots of expression around their edges (white arrows). Panel iv illustrates the merging of the green (ii) and red fluorescence (iii). The merging shows apparent co-localisation of both green and red. It also clearly shows there are no areas that express red or green only, and that the two fluorescent proteins are expressed in the majority of cerebellar regions, indicating that the SyGCaMP2-mCherry sensor may express wholly in the presynaptic side of the cell types in the cerebellar cortex. In contrast, there was absence of expression patterns in WT mice (Figure 3.3 B). In fact, under the same brightness settings with A, autofluorescence detail in Figure3.3B cannot be seen, therefore the brightness was increased as much as possible, as shown in Figure 3.3 C. We found there was no expression of SyGCaMP2-mCherry sensor either in Figure 3.3 C ii or in 3.3 C iii, indicating that the SyGCaMP2-mCherry was only expressed in SyG37 mice. In general, therefore, it seems that expression in the ML is relatively high but it is not possible to see the characteristic tree-patterned branches of Purkinje cells, suggesting that expression is not within the PCs themselves. Moreover, in the PCL, there was no expression in PC somata, but expression was evident around cells bodies. Higher magnification images suggested that these might represent the axonal terminals of BCs which form complex synapses known as pinceau synapses around PC bodies (Tigyi et al., 1990, Buttermore et al., 2012). Given that the Thy1.2 promotor used to control the expression of SyGCaMP2-mCherry is neuronal specific, it is unlikely that these structures represent parts of the Bergmann glia, which also form close associations with PC somata within the PCL (Xu et al., 2013, Bellamy, 2006, Voogd and Glickstein, 1998). Expression was also observed in the GCL although not in the GCs themselves. Expression was not uniform, but related to structures that were in close association with GCs which could only be seen as “shadows” as they lacked expression. In the hippocampus, SyGCaMP2-mCherry expression was linked to both inhibitory and excitatory synapses (Al-Osta et al., 2018). Therefore, possible sources of expression include excitatory mossy fibre terminals which form rosettes with clusters of GCs, and the terminals of GoCs which reside within the GCL and form inhibitory contacts with GCs. We would expect that mCherry and SyGCaMP2

fluorescence would be overlapped since the two fluorescent proteins are fused together. This would appear to be the case, although it should be noted that when changing the excitation wavelength the axial position shifts and so the images are similar but not identical. Nevertheless, it is clear from images 3.3 A (iv) that the patterns of expression of green and red fluorescence are extremely similar, consistent with the two fluorophores being located in the same place.

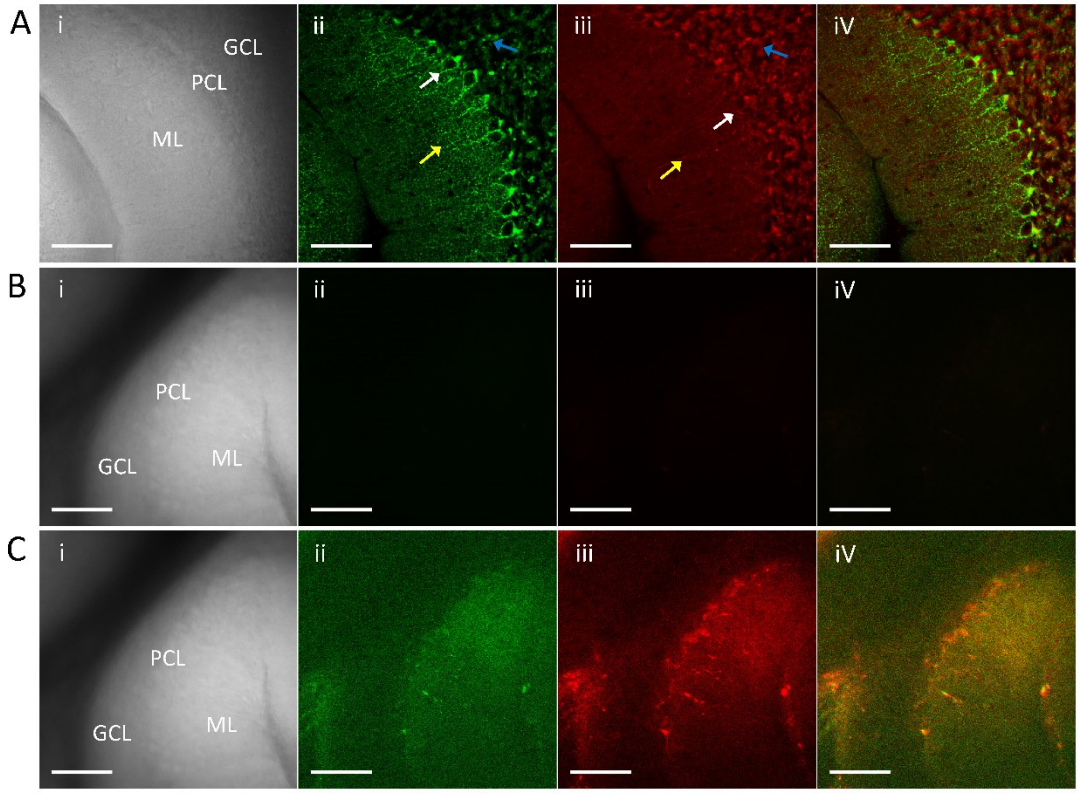

Figure 3.3. Expression pattern of SyGCaMP2-mCherry in sagittal slices of SyG37 and WT mice using multiphoton microscopy. (A) shows images of slices from SyG37 mice. From left to right images represent a transmission image (i), SyGCaMP2 (ii), and mCherry (iii) and SyGCaMP2-mCherry merged together (iv). The molecular layer (ML), granule cell layer (GCL) and Purkinje cell layer (PCL) are labelled in the transmission image and represented with yellow, blue and white arrows, respectively, in the fluorescence images. Each image is of the same region of the cerebellum and at the same magnification. Images in panel B were obtained from an aged matched WT animal and illustrated in a similar manner to those in A. The images in row B have much lower intensity than that in SyGCaMP2 mice. Therefore, the image acquisition intensity in row B had to be increased in order to see the any fluorescence (C). The scale bars in A, B and C are 100 µm.

We next repeated the experiments in 300 µm-thick coronal slices from SyG37 and aged-matched WT mice (Figure 3.4). We also finally attempted to examine the

expression pattern in coronal slices from SyG37 mouse using a zoom of 2 to get more detail in the expression patterns in the different layers.

As shown in Figures 3.4 and 3.5, the results were very similar to those for the sagittal slices illustrated in Figure 3.3. SyGCaMP2 and mCherry were expressed in the in majority of cerebellar regions of SyG37, but prominently in ML. However, there was no such expression in WT mice, as described above. As for sagittal slices, there was no sign of expression in obviously postsynaptic structures such as PC bodies or dendrites, or GC bodies or cell bodies of inhibitory interneurons within either the molecular or CG layers. Moreover, there was no obvious sign of expression in glial cells, including the Bergmann glia, which are characteristic within the cerebellar cortex.

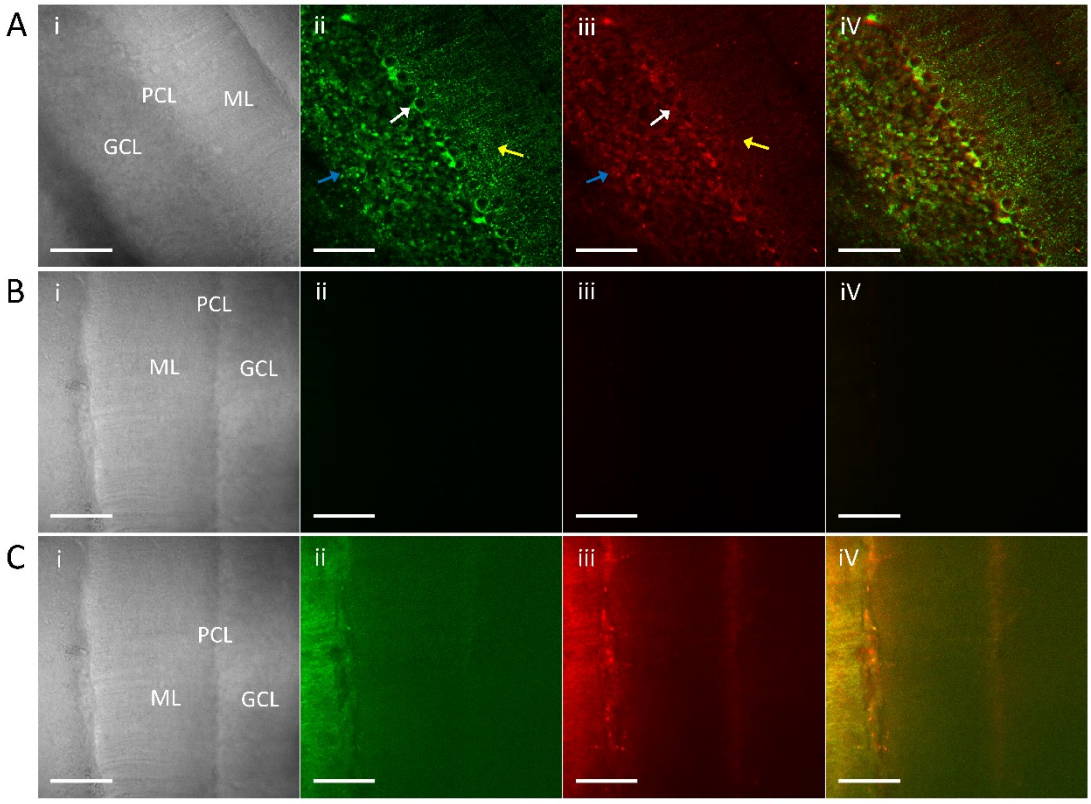

Figure 3.4. Expression pattern of SyGCaMP2-mCherry in coronal slices of SyG37 and WT mice using multiphoton microscopy. Data are shown in the same manner as described in Figure 3.3.

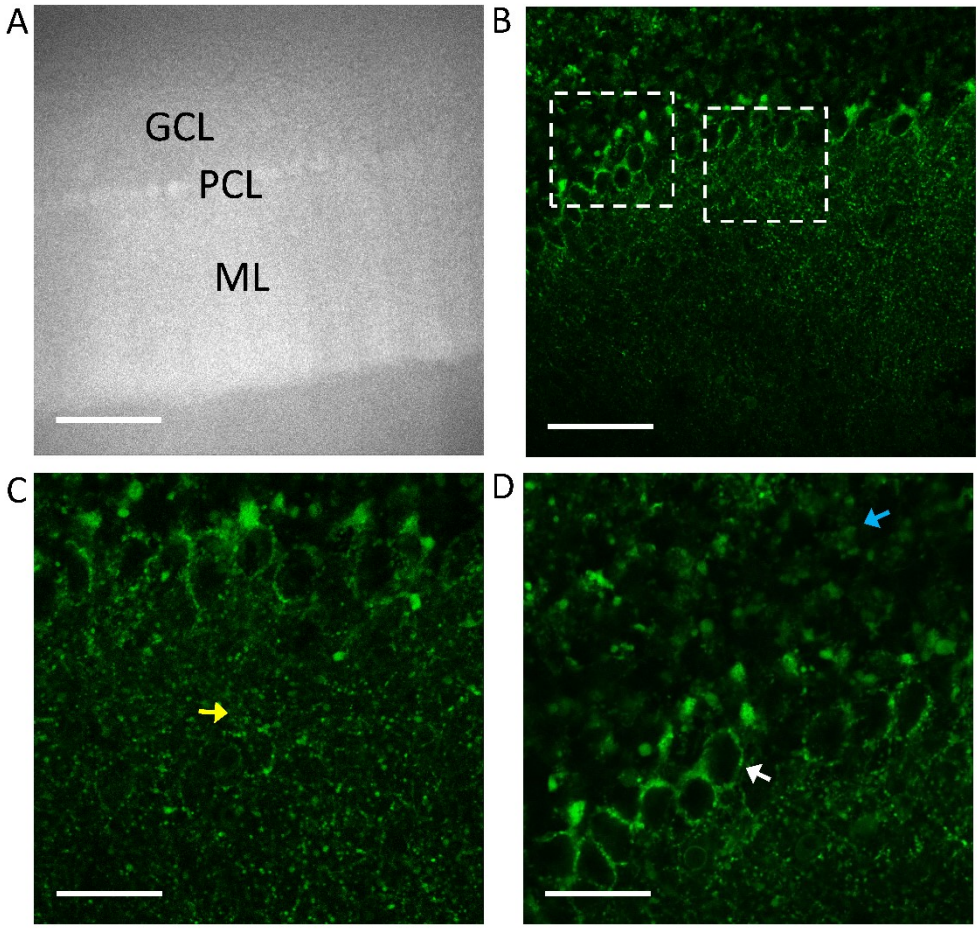

Figure 3.5. Expression pattern of SyGCaMP2 in coronal slices of SyG37 mice obtained using multiphoton microscopy. Images represent a transmission image (A) and SyGCaMP2 expression in the three layers of the cerebellum (B). Inset in C illustrates the magnified image of the boxed area in the top- right of (B; focus mainly in ML using a zoom of 2). Inset in (D) illustrates the magnified image of the boxed area in the top- left of (B; focus mainly in GCL and PGL using a zoom of 2). The scale bars represent 100 µm (panels A and B) and 50 µm panels C and D).

3.2.2 Visualisation of neuronal activity in the cerebellar cortex in SyG37 mice using a wide-field epifluorescence microscope

Having established that SyGCaMP2-mCherry was expressed within the cerebellar cortex, we next examined whether we could detect changes in fluorescence activity in response to electrical stimulation of GCs or direct activation of their PFs. Trains of 20 stimuli, delivered at a rate of 50 Hz and an intensity of 30 V, were applied. An example of the fluorescent changes that occurred in response to electrical activation

of the ML in sagittal slices is shown in Figure 3.6. Whilst mCherry fluorescence did not change, electrical activation produced a large increase in fluorescence that reached a peak response during stimulation and then returned to baseline over the next few seconds (for more details of this analysis, see Materials and Methods, section 2.7.2).

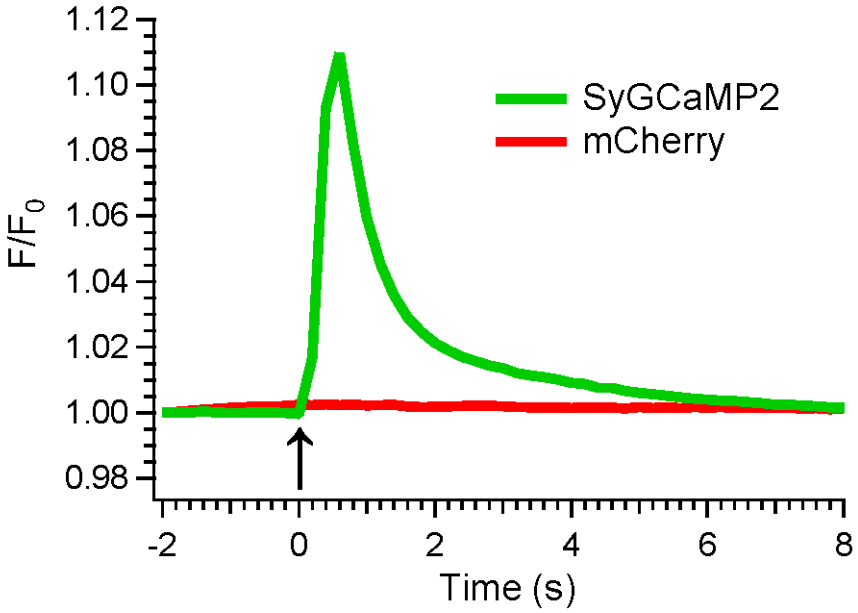

Figure 3.6. The time course of changes in SyGCaMP2 and mCherry fluorescence in response to electrical stimulation of the ML of the cerebellum of SyG37 mice. This Figure illustrates the average responses of SyGCaMP2 (green) and mCherry (red) to 20 stimuli, 30 V at 50 Hz, made from ROIs placed in the ML of sagittal slices of cerebellum as plotted against time. An LED light source (Lumencor®, USA) was synchronised with the image capture such that it switched rapidly between 470 ± 10 nm and 560 ± 10 nm excitation wavelengths to record a stack of interleaved images with emission wavelengths of 520 ± 20 nm and 620 ± 20 nm, which are measured as green and red images, respectively. The arrow indicates the start of electrical stimulation.

In order to highlight the spatial patterns of neuronal activation in response to stimulation in different orientations of cerebellar slices, the average of three sequential SyGCaMP2 images was taken immediately prior to stimulation and these were subtracted from the average of three images taken around the peak response

to electrical stimulation to create a subtraction image (Figure 3.7). A fixed scale with a warm/cold look-up table was used to highlight the spatial patterns of responses for each of the different conditions of spatial stimulation in both sagittal and coronal slices.

Figure 3.7A illustrates the pattern of SyGCaMP2 responses to electrical stimulation of the ML in sagittal slices. In this orientation, PFs are expected to run in the direction of the thickness of the slice. Consistent with the activation of PFs, subtraction images showed that activation occurred in a circular pattern around the stimulus point. Stimulation of the GCL of sagittal slices did not show the same pattern of response as the ML. A more diffuse pattern of activity was seen with a small number of brighter areas which might represent activation of MF terminals or GoC terminals. Although GCs send their axons vertically into the ML, we did not reliably here see evidence of activation of the ascending segment of the granule cell axon (Figure 3.7B). When electrodes were placed in the ML of coronal slices, a change in activity was observed along the length of the ML. This is consistent with the activation of PFs which run in beams in this slice orientation (Figure 3.7C).

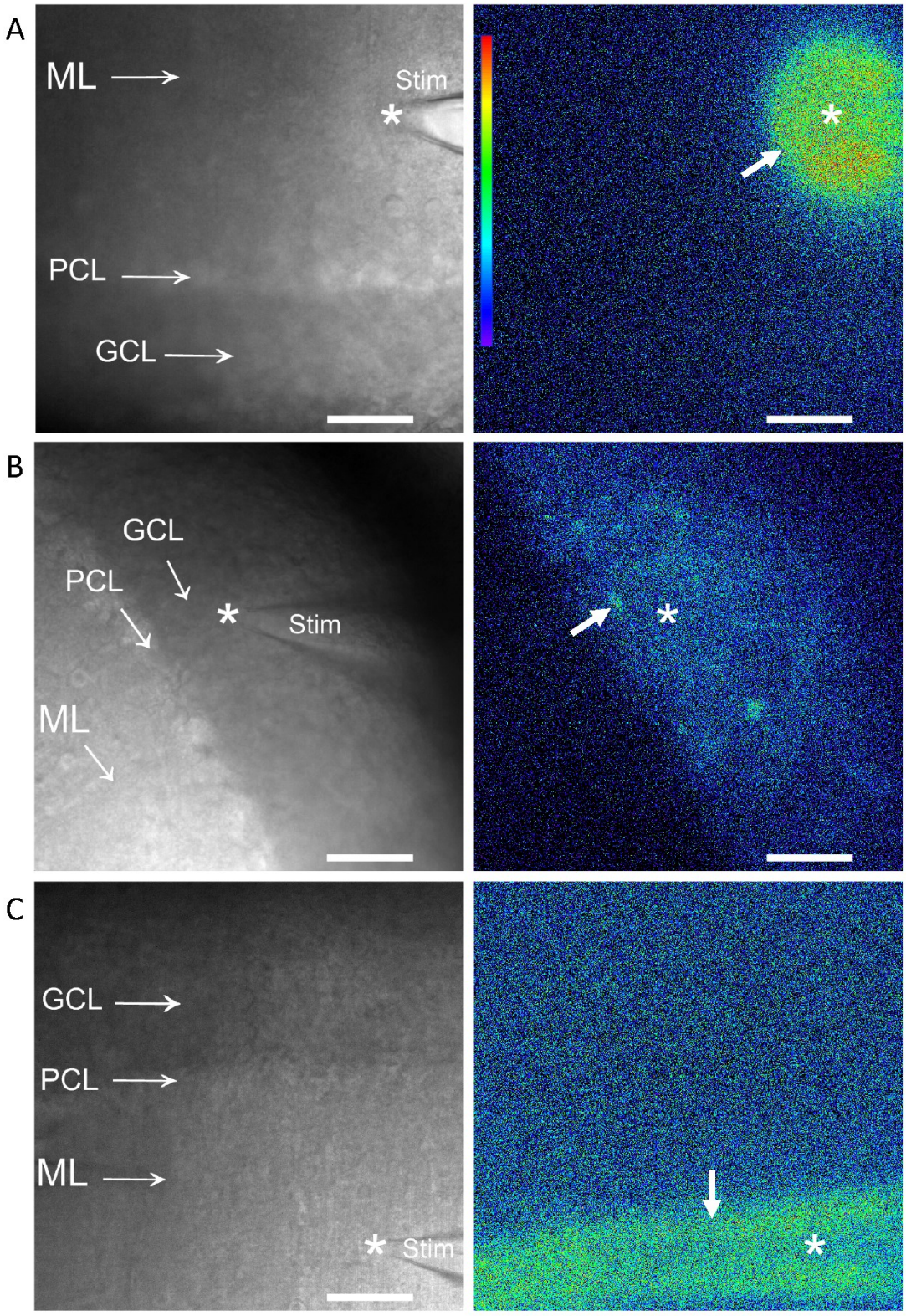

Figure 3.7. Visualisation of neuronal activity in the cerebellar cortex in SyG37 mice using epifluorescence microscopy. Shown on the left-hand side (panels A, B and C) are transmission images. Panels A and B are images of a sagittal slice and panel C is from a coronal slice (C). These images illustrate positions of stimulating electrodes with respect to the different layers of the

cortex (white arrows). The asterisks (white) indicate the tip of the stimulating electrode in each case. Shown on the right are the images that were created from averages of three sequential SyGCaMP2 images obtained immediately prior to stimulation and subtracted from the peak responses taken during electrical stimulation. The white arrows highlight the SyGCaMP2 responses in each of the panels (right-hand side A, B and C). A fixed scale with a warm/cold look-up table was used to highlight the areas of under each of the different conditions of spatial stimulation. The scale bar in all panels represents 50 μm.

We next repeated these experiments using a multiphoton microscope, the results of which are shown in Figure 3.8. The results were qualitatively similar to those obtained using standard epifluorescence microscopy. In sagittal slices, a circular pattern of activity was seen around the stimulation electrode placed in the ML. No sign of activation of intrinsic interneurons within the ML was observed. Stimulation of the GCL increased fluorescence in patches that might suggest activation of MF rosettes. In coronal slices, ML activation again produced activation along a beam in the direction that PFs would be expected to run.

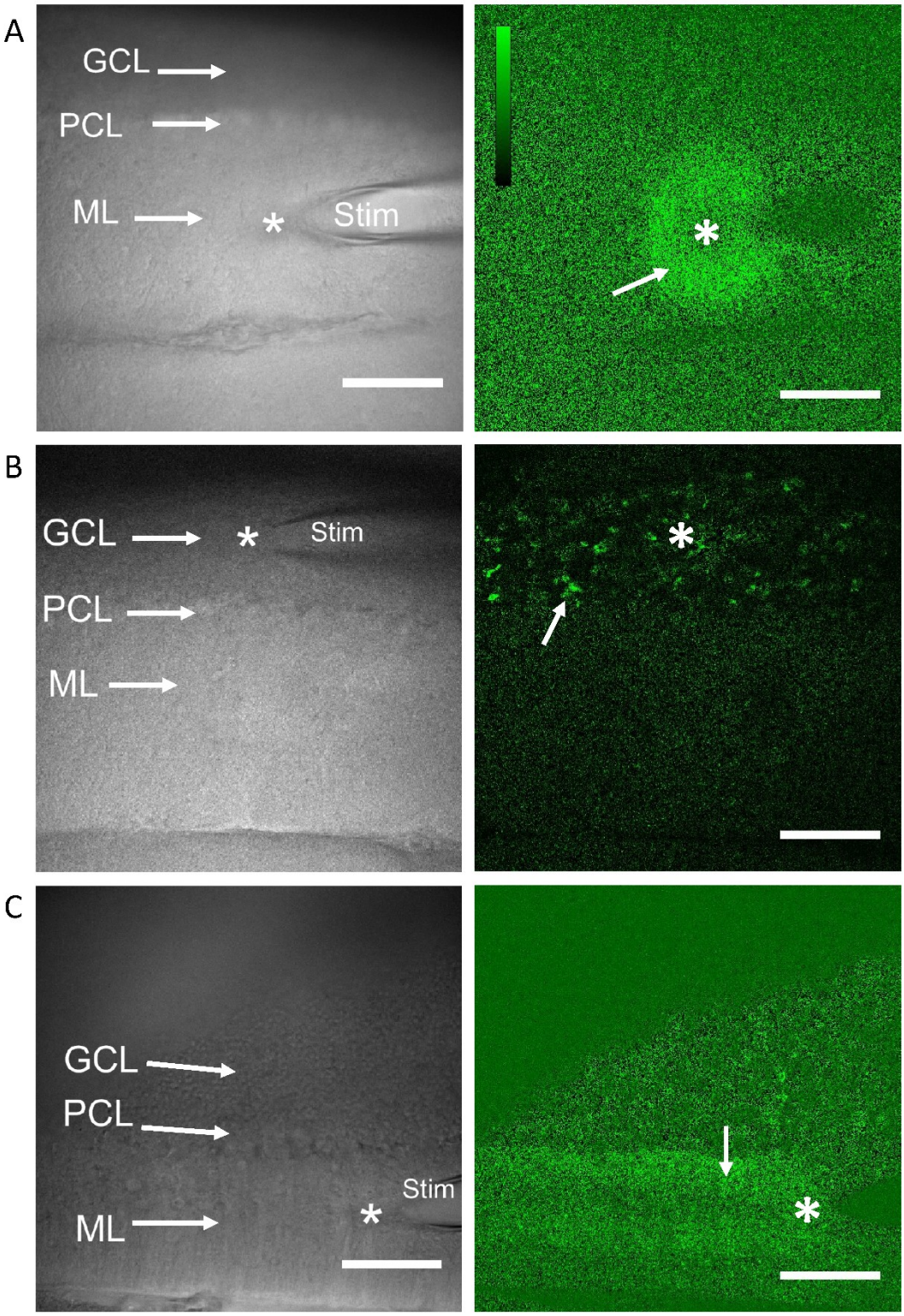

Figure 3.8. Visualisation of neuronal activity in the cerebellar cortex of SyG37 mice using multiphoton microscopy. Data are shown in the same manner as Figure 3.7. Images were of 512 x 512 pixels in size and were captured using an excitation wavelength of 920 nm with a multiphoton microscope. The scale bar in all panels represents 100 µm.

3.3. Discussion

The aim of this series of experiments was to verify that SyGCaMP2-mCherry was expressed in the cerebellar cortex and to carry out a number of pilot experiments to establish if expression was sufficiently high and in appropriate cell types and structures to observe patterns of neuronal activity in response to electrical activation. Both wide-field epifluorescence and multiphoton imaging methods were tested since we wished to test their utility for subsequent experiments. In order to view expression in a whole cerebellar slice, arrays of images were taken in a grid pattern and the images stitched together using a FIJI plugin (Schindelin et al., 2012, Preibisch et al., 2009). Figures 3.1 and 3.2 clearly show that fluorescence from SyGCaMP2-mCherry is evident. When plotted at the same intensity, there was no significant green or red fluorescence from age-matched WT mice. These results extend those from previous work carried out in our laboratory which showed expression in the hippocampus as well as mCherry protein expression in brains of SyG37 mice using Western blotting (Al-Osta et al., 2018). Higher magnification and resolution images taken with a multiphoton microscope showed that SyGCaMP2 and mCherry fluorescence were present in the three layers of the cerebellar cortex in both sagittal and coronal cerebellar slices (Figures 3.3, 3.4 and 3.5). Expression was punctate and uniform in the ML. whilst we did not attempt to establish the precise location of fluorescence in these experiments, these results are consistent with expression in presynaptic structures. Electrical stimulation studies suggest that these may be PF terminals, but we cannot exclude the possibility that SyGCaMP2-mCherry could also be expressed in the presynaptic terminal of SCs and BCs. We found no evidence for expression in overtly post-synaptic structures such as PC somata or dendrites or stellate or BC somata. The sensor was expressed around the edges of PCs. This could represent the axon terminals of BCs which form pinceau synapses onto PCs (Szentágothai et al., 1966, Tigyi et al., 1990, Kandel et al., 2000). We cannot exclude expression within CFs which contact PCs close to the soma and then along their proximal dendrites (Strata and Rossi, 1998, Dittman and Regehr, 1998). However, we did not see any obvious evidence for activation of CFs from electrophysiological stimulation of the CGL. Finally, SyGCaMP2-mCherry was also expressed in the GCL, suggesting that the sensor could be expressed in

the terminals of MFs, GoCs or even unipolar brush cells, although their distribution within certain lobules of the cerebellum is considered quite sparse (Nunzi et al., 2001, Rossi et al., 1995, Dino et al., 2000, Diño et al., 2000).

It will be necessary to carry out immunohistochemistry experiments to show it conclusively, but these results strongly suggest that expression is high within PF terminals, though we cannot rule out expression in other cell types including inhibitory terminals.

Lastly, we found that neuronal activities within the cerebellar cortex in SyG37 mice can be monitored using optical measurements of SyGCMP2 fluorescence. It was possible to detect robust and reproducible responses to stimulation in the cerebellar cortex. In sagittal slices, ML stimulation produced a circulatory pattern of activation. In coronal slices, stimulation caused activation along parallel beams. These results are consistent with activation of PFs but do not exclude contributions from BC or SC terminals. This result is consistent with the studies of Díez-García et al. (2005), who found that direct activation of ML triggered a beam-like responsive area that extended along PFs in frontal slices using a G-CaMP2 sensor whose expression was restricted to GCs.

In summary, SyGCaMP2-mCherry was found to be expressed in all layers of the cerebellar cortex but expression was prominently in the ML. These results lay the foundation for those presented in the following chapters where we characterise the patterns of stimulation that activate SyGCaMP2 in SyG37 mice in considerably more detail.

Chapter 4: Pharmacological and electrophysiological investigation of the characteristics of SyGCaMP2 signalling in the cerebellar cortex of SyG37 mice

4.1 Introduction

Work from this laboratory has previously revealed that in SyG37 mice, SyGCaMP2-mCherry is colocalised with the presynaptic protein bassoon, indicating that it is expressed in presynaptic terminals (Al-Osta et al., 2018). It colocalises with both the vesicular GABA transporter vGAT and the glutamate transporter vGluT, indicating that it is expressed at both the excitatory and inhibitory synaptic terminals in the hippocampus**.** The experiments carried out in chapter 3 demonstrated that SyGCaMP2-mCherry is also expressed in the cerebellar cortex. The pattern of expression suggested that it was similarly expressed presynaptically, and that expression was likely to be in both excitatory and inhibitory synaptic terminals. In response to electrical stimulation of the ML in coronal and sagittal slices, the results strongly suggested that the sensor is expressed in GC PFs, but these results do not rule out expression in terminals in other excitatory or inhibitory cell types.

One of the aims of this thesis was to establish whether it was possible to use SyG37 mice to measure calcium-dependent signalling from PFs and, if so, to use this model to investigate the contributions of endocannabinoid receptors and NMDARs to presynaptic signalling. In the first part of this chapter, we undertook a pharmacological investigation to test whether our optical responses originated from presynaptic terminals and, assuming so, what fraction of these responses might have originated from GC axons. This was done by combining optical imaging of SyGCaMP2 responses with electrophysiological measurements of field potentials (fEPSPs) in response to electrical activation with pharmacological manipulation. The approach used was to systematically block elements of pre- and post-synaptic synaptic transmission. Tetrodotoxin is a blocker of sodium channel (Catterall, 1992, Moore and Narahashi, 1967), and as such can be used to prevent the formation of APs in the presynaptic terminal and prevent transmitter release. It is therefore

expected to completely abolish synaptic transmission and indeed has been shown to block fEPSPs in the cerebellar cortex (Sutton, 1999, Bergerot et al., 2013).

Data from several studies suggest that lowering the extracellular calcium concentration on PF response to ML stimulation leads to a rapid block of synaptic transmission (Mintz et al., 1995, Margrie et al., 1998, Dittman and Regehr, 1998). Therefore, we next examined whether removing extracellular calcium led to a reduction of synaptic transmission of PF responses within the ML region of the cerebellum being blocked and, further, whether this was accompanied by a reduction of SyGCaMP2 fluorescence responses.

Fast excitatory transmission between PFs and PCs is mediated by AMPARs (Crépel and Audinat, 1991). The AMPAR antagonist DNQX was used to inhibit excitatory transmission via this receptor subtype as a result of ML stimulation (Bergerot et al., 2013, Sgobio et al., 2014). Electrical stimulation of the ML may not only activate PFs but it could also activate intrinsic inhibitory neurones within this layer, i.e. BCs and SCs. These are activated by PFs via AMPARs and NMDARs and then form inhibitory GABA-ergic synapses with PCs (Eccles et al., 1976, Cohen and Yarom, 2000). So, in addition to blocking AMPARs, we also examined what effects the inhibition of NMDA receptors with the selective antagonist DL-AP5 and GABA/Glycine receptors with PTX had. With this combination, we expected to block the majority of synaptic transmission between PFs and other cell types (Bergerot et al., 2013, Sgobio et al., 2014). NMDARs are not present on PCs in adult circuits (Farrant and Cull-Candy, 1991, Llano et al., 1991), but there is mounting evidence that suggests NMDARs play some role in modulating plasticity via actions at PF terminals within the cerebellar cortex. Therefore, we also examined the effect of DL-AP5 alone on fEPSPs and SyGCaMP2 responses in the cerebellar cortex. The cerebellum is highly regular in structure with three main layers (chapter 1, Figure 1.3), which are the ML, PCL and the GCL. MFs supply GCs that form ascending axons that bifurcate to form PFs which extend for several millimetres in either direction in the ML. Synapses between GCs and PCs are formed by both the PFs and ascending GC axons (Sims and Hartell, 2005, Sims and Hartell, 2006). Plasticity at synapses formed between GCs and PCs represents the main mechanism for learning in this system. Furthermore, anatomical and electrophysiological evidence suggests that there may be certain fundamental

differences between these two types of synapse. Work from this laboratory has previously shown that there are fundamental differences in the properties of synapses formed between the ascending and the PF segment of GC axons (Sims and Hartell, 2005, Sims and Hartell, 2006). Very little is currently known about monitoring presynaptic terminals at synapses formed between cerebellar GCs and PCs. One might hypothesise that this is most likely due to the presynaptic effects of neuromodulators being hard to measure because the synaptic terminals are too small to record electrical signals at these synapses. Therefore, in the second part of this chapter, we have first performed a physiological characterization of ascending axon and PF synapses in response to increasing stimulus intensity, number and frequency in ML and GCL of SyG37 mice using an epifluorescence microscope. After that, we attempted to measure presynaptic calcium at individual presynaptic boutons in the ML area to different patterns of stimulation using multiphoton microscopy.

4.2 Results

4.2.1 Pharmacological and electrophysiological investigation of SyGCaMP2 responses to ML stimulation

4.2.1.1 The effects of the sodium channel blocker tetrodotoxin (TTX) on SyGCaMP2 fluorescence and field potential responses to ML stimulation

In a first set of experiments, we aimed to examine the effects of bath application of the sodium channel blocker TTX on SyGCaMP2 fluorescence responses and fEPSPs elicited by electrical activation of the ML. To achieve this goal, stimulating electrodes were placed in the ML to activate PFs whereas recording electrodes were placed in the ML, above the PC layer to record field potentials originating from the PC dendrites (see Figure 4.1).

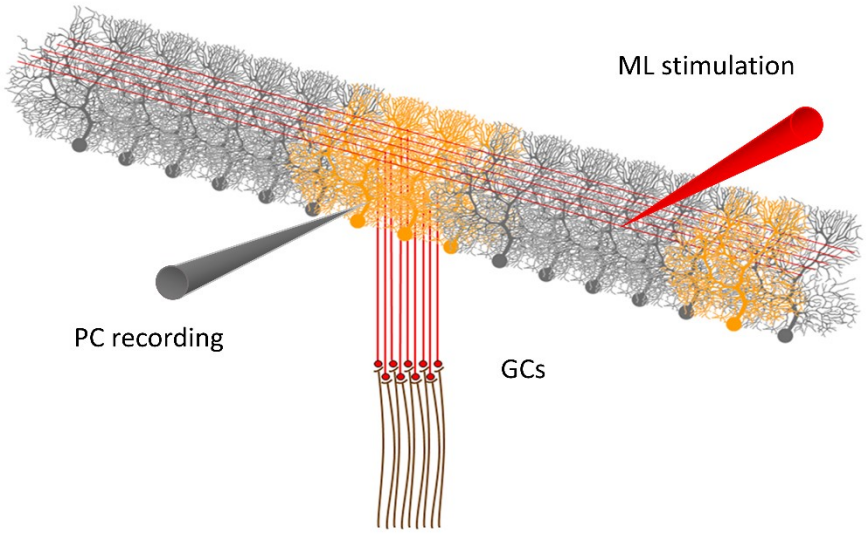

Figure 4. 1. Schematic diagram of parallel fibres - Purkinje cell synapses. This scheme shows the somatic recording from above the PC layer (using a patch pipette; grey). Parallel fibre burst (20 stimuli at 50 Hz) was performed using a stimulating electrode (red, top) placed in ML. Granule cells (GCs) form ascending axons which bifurcate to form parallel fibres. Adapted from Rokni et al. (2008).

Synaptic activity was evoked in sagittally cut cerebellar slices by delivering pairs of stimuli at 50 ms intervals every 10 seconds as described previously (see Materials and Methods, section 2.5). SyGCaMP2 responses were recorded every 5 minutes in response to PF stimulation (20 stimuli, 50Hz & 30 - 40V) using an epifluorescent microscope (see Materials and Methods, section 2.6.1).

A stable baseline of synaptic and SyGCaMP2 responses to PF activation was recorded for at least 10 minutes prior the perfusion of 0.1 µM TTX. TTX was applied for 10 minutes and then replaced with a standard aCSF solution so that its washout could be followed for at least 50 minutes. Imaging and electrophysiological data were analysed using Igor Pro and WinLTP, respectively, as described previously (see Materials and Methods, section 2.7). Data from separate experiments were combined and statistical tests performed. The results of these experiments are presented as mean ± SEM from eight separate experiments (Figure 4.2).

SyGCaMP2 fluorescence (expressed as F/F_0 % baseline) and the field potential response were measured over time from the ML in response to electrical stimulation before, during and after washout of TTX (Figure 4.2 A and B).

As shown in Figure 4.2 C, application of 0.1 μM TTX abolished the peak SyGCMP2 fluorescence response. SyGCMP2 responses recovered after washing for 50 minutes with the standard extracellular solution, but not to their original extent. TTX negated the peak amplitudes of both the N2 and N1 fEPSPs (Figures 4.2 E-H). The N1 component recovered close to baseline levels after 50 minutes (Figures 4.2 G and H); however, the N2 response did not completely recover (Figures 4.2 E and F). Figures 4.2 D, F and H show that TTX caused a significant reduction in the peak amplitudes of the SyGCMP2 responses compared to pre-application levels, and reduced the N2 and N1 components of the field potential to 5.54 ± 2.33%, 4.70 ± 1.09% and 3.92 ± 1.07% of their respective baseline levels (SyGCaMP2 Peak, P = 0.0004; N2, P = < 0.0001; N1, P = 0.0003; Friedman test followed by Dunn's multiple comparison post-hoc test; n = 8). Recovery of these components (after 50 min) reached 77.73 ± 6.31%, 62.20 ± 6.20% and 90.06 ± 5.95%, respectively, of baseline levels (SyGCaMP2 Peak, P = 0.26; N2, P = 0.0003; N1, P = 0.47; Friedman test followed by Dunn's multiple comparison post-hoc test; n = 8). This result clearly indicates that SyGCaMP2 responses depend upon sodium channel activation and hence require AP activity within the presynaptic bouton.

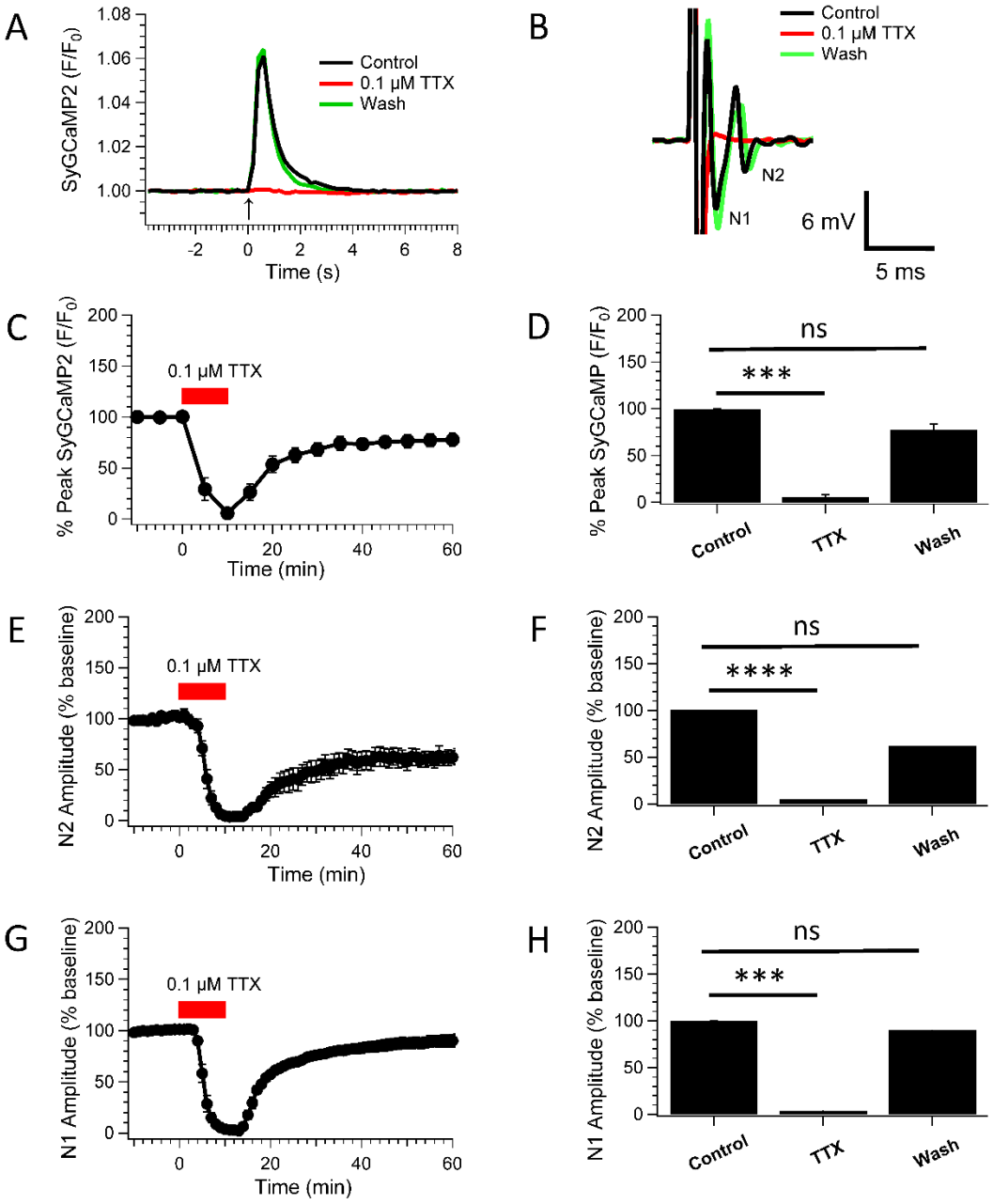

Figure 4. 2. Effects of 0.1 µM TTX on SyGCaMP2 fluorescence and corresponding field potential responses to ML stimulation in sagittal cerebellar slices. (A) illustrates average responses of SyGCaMP2 fluorescence before (black), during (red) and 50 minutes after washout of 0.1 µM TTX (green). Measurements were obtained from regions of interest (ROIs) placed within the ML of the cerebellar cortex. (B) shows field potential responses to molecular layer stimulation. (C) illustrates the effect of 0.1 µM TTX on peak SyGCaMP2 responses to molecular layer stimulation over time, expressed as a percentage of baseline peak values. The red horizontal bar shows the 10-minute period of TTX application. (E) and (G) illustrate the effects of 0.1 µM TTX on the N2 and N1 amplitude components of the responses to ML stimulation, respectively. (D), (F) and (H)

illustrate bar charts summarising the data before, during and after washout of TTX. Data are presented as normalized mean ± SEM (n = 8).

4.2.1.2 The effects of lowering extracellular calcium on SyGCaMP2 fluorescence and field potential responses to ML stimulation

Neurotransmitter release is mediated by a calcium-dependent synaptic vesicular release process. At the nerve terminal, rapid Ca^{2+} influx through voltage-gated calcium channels (VGCCs) triggers release ready vesicles to fuse with the terminal membrane and release neurotransmitters into the synaptic cleft, which ultimately activates receptors in the postsynaptic membrane (Katz and Miledi, 1968, Südhof, 2013). In other words, calcium is responsible for transforming the action potential into actual neurotransmitter release. Therefore, in this section, we aimed to first examine whether removing extracellular calcium chloride dehydrate ($CaCl_2.2H_2O$) from aCSF would block synaptic transmission of PF responses within the ML region of the cerebellum and, second, whether this was accompanied by a reduction in SyGCaMP2 fluorescence as would be expected from this GECI. Experiments were performed as previously described. After a 10-minute period of recording baseline fEPSP and SyGCaMP2 responses, a solution containing zero calcium was applied for 30 minutes and washed off for a further 25 minutes with standard aCSF. Data were obtained and presented as shown in previous sections (4.2.1.1). Example traces of SyGCaMP2 and fEPSP responses before, during and after washout of extracellular solution lacking calcium are shown in Figures 4.3 A and B, respectively. As shown in Figure 4.3 C, E and G, bath perfusion with an extracellular solution that lacked calcium produced 81.64% and 84.58% reductions in the peak SyGCaMP2 fluorescence responses and the N2 component of the fEPSP responses, respectively. These effects were statistically significant (Figure 4.3 D and F: peak SyGCaMP2, 18.36 ± 4.09% of baseline levels, P = 0.0003; fEPSP N2, 15.42 ± 4.88% of baseline levels, P = < 0.0001, n = 10, Friedman test). Interestingly, both responses completely recovered after 25 minutes of washing with standard aCSF.

These results were as expected as the removal of calcium should negate the response of the SyGCaMP2 calcium sensor and synaptic transmission.

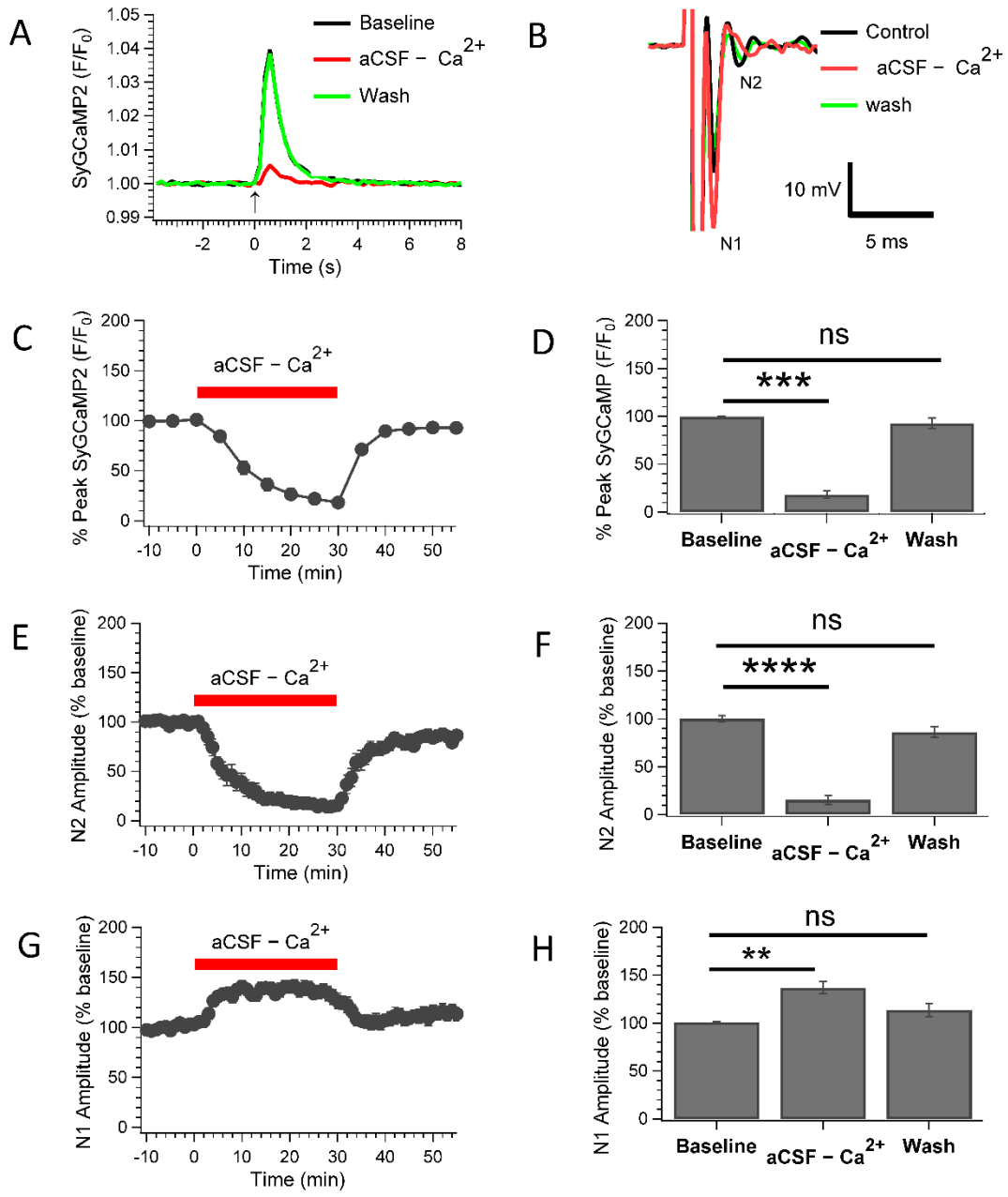

Figure 4.3. Effects of lowering extracellular calcium on SyGCaMP2 fluorescence and field potential responses to ML stimulation in sagittal cerebellar slices. Data are as illustrated as in Figure 4.2 except that the red horizontal bar shows the 30-minute period during which extracellular calcium was lowered, and where the washout period was 25 minutes. Mean and SEM are shown (n = 10).

We noticed that reducing extracellular calcium reversibly increased the peak amplitude of the N1 response to 130 ± 7.39% of baseline level (Figure 4.3 G). These effects were statistically significant (Figure 4.3 H: fEPSP N1, P = 0.0073, n = 10, Friedman test). One possible explanation for this result is that the perfusion of extracellular solutions that lacked calcium caused a change in the standard balance of divalent cations in the extracellular solution, which can alter the threshold for activation of fibres (Bahia et al., 2012). We therefore decided to repeat the experiment with a solution in which the extracellular magnesium concentration was increased to 3.7 mM to maintain the total concentration of divalent cations in our extracellular solution constant. The results in Figure 4.4 were indeed very similar to those already presented in Figure 4.3 except that, under these conditions, the peak amplitude of the N1 response remained stable throughout the experiments (see Figure 4.4 G). Statistical analysis showed there was no significant change (Figure 4.4 H: fEPSP N1, 102 ± 6.27% of baseline levels, P = 0.4, n = 11, Friedman test) indicating that the activation excites the same number of PFs before, during and after application of a solution containing a lowered concentration of calcium. The effects of lowering extracellular calcium here were as expected. As Figures 4.4 C and E show peak SyGCaMP2 and N2 responses were reduced significantly to 11.65 ± 3.56% of baseline (Figure 4.4D: P = 0.0002, n = 11, Friedman test) and 10.05 ± 2.28% of baseline (Figure 4.5F: P = 0.0022, N = 11, Friedman test), respectively. Together, the results of this section obviously show that SyGCaMP2 is only a calcium sensor, as we expected.

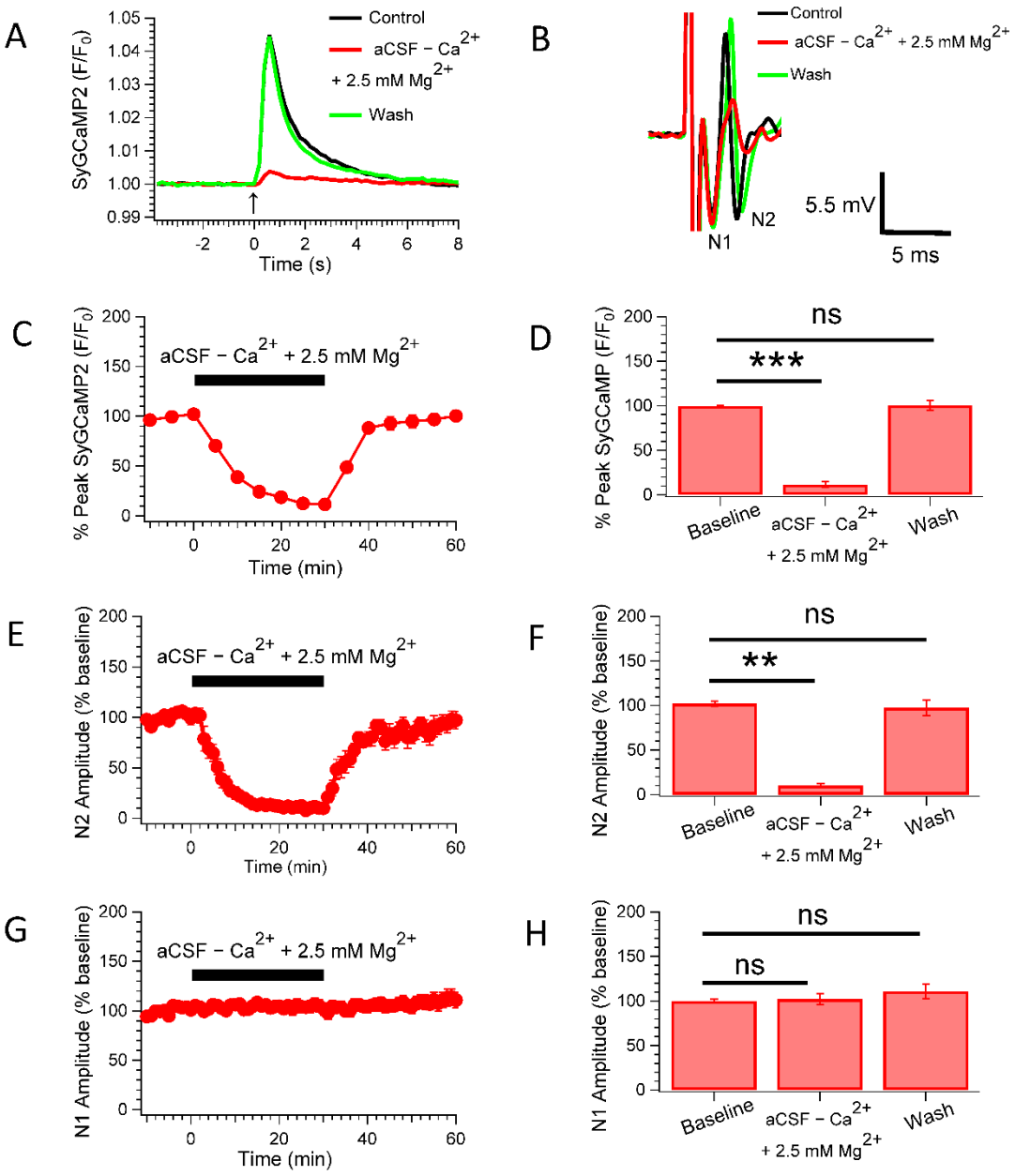

Figure 4. 4. The effects of lowering extracellular calcium with increased concentrations of magnesium on SyGCaMP2 fluorescence and field potential responses to ML stimulation in sagittal cerebellar slices. The data presented are as shown in Figure 4.3 except that the black horizontal bar illustrates the 30-minute application period of lowered extracellular calcium, and that of the washout period of 15 minutes. Data were presented as normalized mean ± SEM (n = 11).

4.2.1.3 The effects of pharmacological inhibition of AMPA, $GABA_A$ /Glycine and NMDA receptors on the SyGCaMP2 fluorescence and field potential of the PF responses to ML stimulation

In section 4.2.1.1, we showed that both fEPSPs and SyGCaMP2 responses to ML stimulation were negated by the sodium channel blocker TTX. In order to further define the origin of the SyGCaMP2 response, we next examined the effects of application of the GABA/Glycine receptor antagonist picrotoxin (PTX), and the AMPA receptor antagonists NBQX followed by AP5 to block NMDARs. Experiments were carried out and data presented as described previously in section 4.2.1.1 except that PTX and NBQX were applied for 30 minutes and then AP5 was added for 30 minutes in the presence of PTX and NBQX. All three drugs were then washed out for 50 minutes. Example traces of SyGCaMP2 and fEPSP responses before, during and after washout of these drugs are shown in Figures 4.5 A and B, respectively.

Applications of 10 μM NBQX with 10 μM PTX led to a small but non-significant decrease in SyGCaMP2 responses compared to pre-drug control values (Figures 4.5 C and D). After 30 minutes, peak responses were reduced to 77.37 ± 2.83% of baseline (P = 0.20, n = 6, Friedman test). Further addition of AP5 lowered responses by a further 9% in the peak SyGCaMP2 response but this reduction was not statistically significant compared to baseline levels (Figure 4.5 D, P = > 0.99, n = 6, Friedman test). SyGCaMP2 responses did not recover completely after washout, as shown in Figure 4.5 C. The N1 component of the fEPSP was not affected significantly by the addition of this cocktail of drugs (Figures 4.5 G and H). In contrast, as shown in Figure 4.5 E, applications of NBQX and PTX led to a significant decrease in the N2 amplitude responses of fEPSPs compared to the control, after 30 minutes with an approximately 86% reduction in the N2 component responses (Figure 4.5 F: 18.36 ± 6.55% of baseline levels, p = 0.043, n = 6, Friedman test). AP5 reduced N2 responses by a further 4%, where N2 responses did not fully recover on washout, as shown in Figures 4.5 E and F.

These experiments were also repeated with an alternative AMPAR antagonist DNQX in slices cut in a coronal orientation but we only recorded SyGCaMP2 fluorescence responses. We found that bath application of DNQX and PTX (10 μM,

30 min) reduced the SyGCaMP2 peak responses to 91.50 ± 4.65% of baseline, while further addition of 50 µM AP5 in the continued presence of 10 µM DNQX and 10 µM PTX (30 min) led to a further reduction of 8.3% in the peak SyGCaMP2 responses, although neither of these effects were statistically significant ($P > 0.9999$ and 0.08, respectively, $n = 6$, Friedman test) (data not shown). In summary, this result shows that the combined application of NBQX and picrotoxin selectively blocked the post-synaptic component of the field potential. These applications led to a reduction in SyGCaMP2 responses to ML stimulation to 77.37 ± 2.83% (in sagittal slices) and 91.50 ± 4.65% (in coronal slices) of baseline, indicating that about 23% (in sagittal slices) and 9% (in coronal slices) of the entire response originating from the presynaptic axon terminal of the neurones was synaptically driven by AMPA and GABA/Glycine receptors.

Overall, these data are consistent with the expected properties of SyGCaMP2 as a calcium indicator and, when considered alongside the effects of TTX, lowering extracellular calcium, AP5 and PTX/DNQX, strongly suggest that in the cerebellar cortex SyGCaMP2 responses represent calcium signals originating primarily, but not exclusively from PF terminals. Since there was an approximate 10 - 20% reduction in the size of SyGCaMP2 responses in the presence of PTX and NBQX or DNQX, we estimate that roughly 80 - 90% of the signal in the absence of blockers originates from PF terminals. The remainder presumably originates from terminals that are activated polysynaptically.

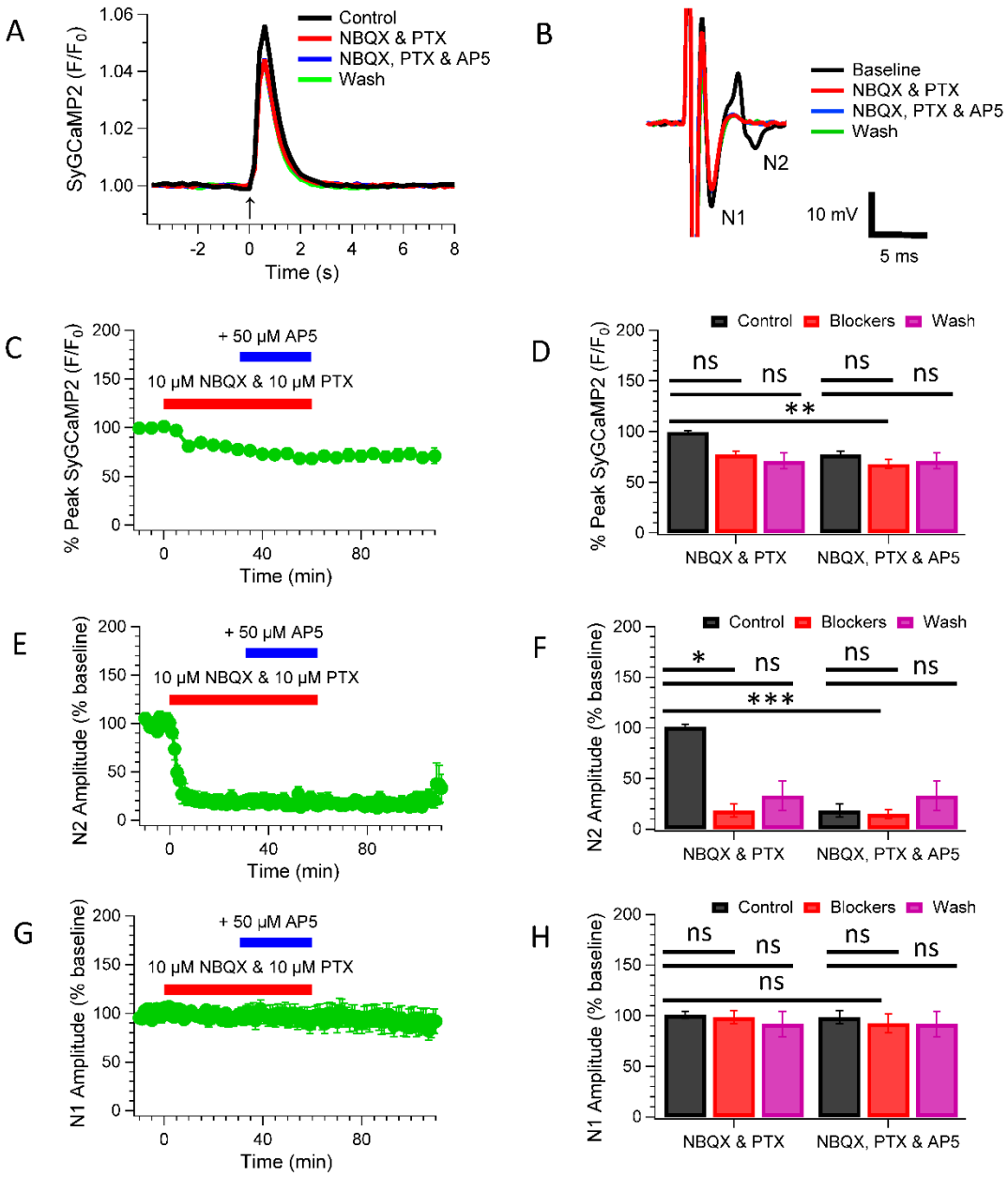

Figure 4. 5. Effects of 10 µM NBQX, 10 µM PTX then 50 µM DL-AP5 on SyGCaMP2 fluorescence and corresponding field potential responses to ML stimulation in sagittal cerebellar slices. Data are presented in the same way as Figure 4.2 except that the red horizontal bar shows the 60-minute period of application of 10 µM NBQX and 10 µM PTX and the blue horizontal bar shows the 30-minute period of application of 50 µM AP5 in the presence of 10 µM DNQX and 10 µM PTX. Data are presented as normalized mean ± SEM (n = 6).

4.2.1.4 The effects of the NMDAR antagonist DL-AP5 on SyGCaMP2 fluorescence and field potential responses to ML stimulation

We finally examined whether the inhibition of NMDA receptors with the selective antagonist DL-AP5 alone had any effect on fEPSPs or SyGCaMP2 responses. Experiments were carried out, and data were presented in the same manner as described in section 4. 2.1.1 except that 50 μM DL-AP5 was applied for 20 minutes and then washed for 15 minutes.

Example traces of SyGCaMP2 and fEPSP responses before, during and after washout of DL-AP5 are shown in Figures 4.6 A and B, respectively. The results in Figures 4.6 C, E and G showed that the application of DL-AP5 produced only a very slight decrease in the amplitude of the SyGCaMP2 fluorescence and the N2 competent of the fEPSP compared to the baseline level. However, there was no effect on the peak amplitude of the N1 competent (Figure 4.6 G). SyGCaMP2 fluorescence was reduced by about 5%, whereas the N2 component of the response was reduced by about 10%. Neither of these effects were statistically significant (Figures 4.6 D, F and H: SyGCaMP2 peak, P = 0.16; N2 competent, P = > 0.99; N1 competent, P = > 0.99; Friedman test; n = 6). Taken together, these results suggest that under these particular conditions of synaptic activation, there is little if any evidence that NMDA receptors contribute to either Ca^{2+} influx into presynaptic terminals, the PF volley, or the subsequent postsynaptic response.

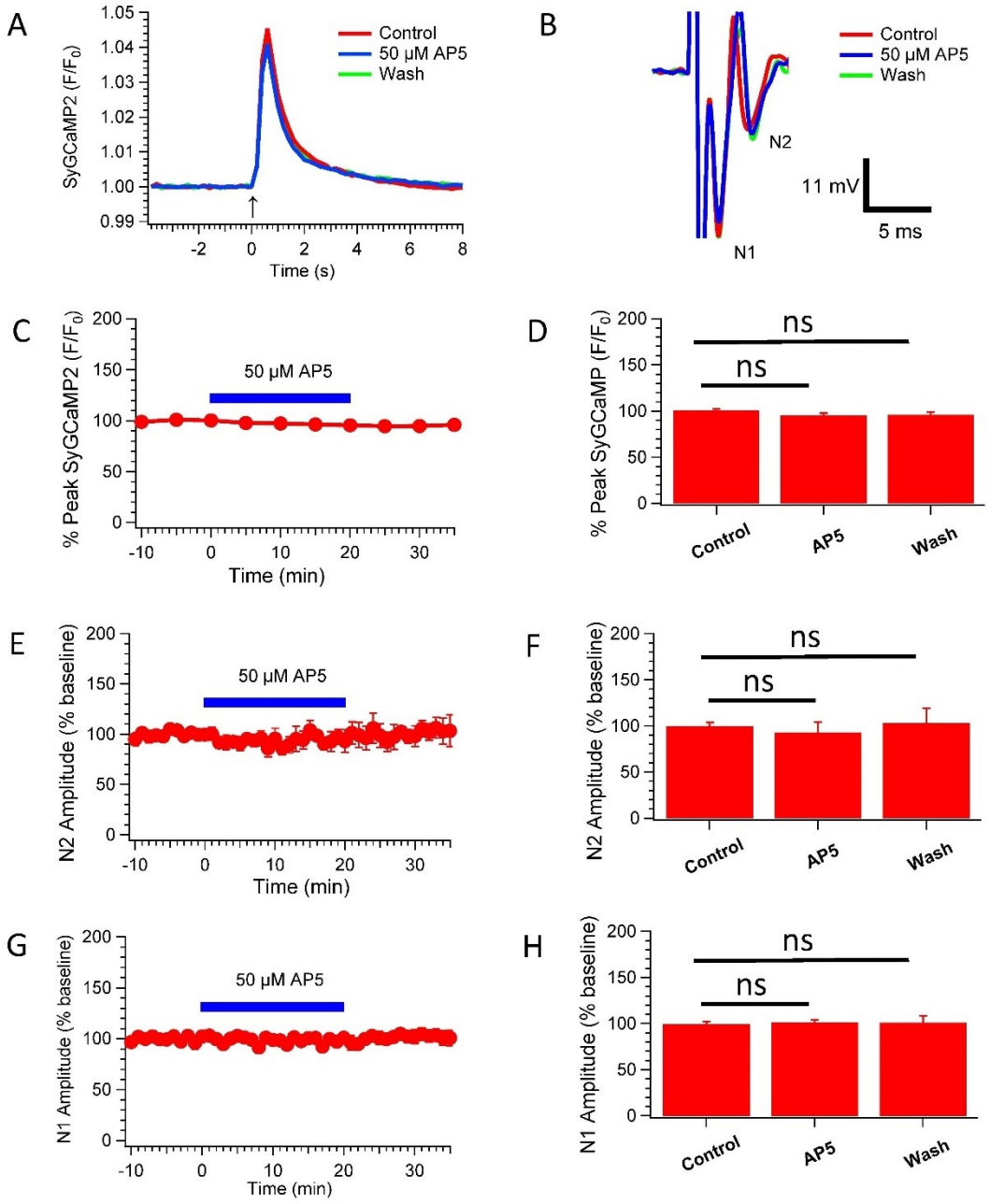

Figure 4.6. Effects of 50 µM DL-AP5 on SyGCaMP2 fluorescence and corresponding field potential responses to ML stimulation in sagittal cerebellar slices. The data presented are as shown in Figure 4.2, except that the blue horizontal bar illustrates the 20-minute period of 50 µM AP5 application, and the washout period was 15 minutes. Data were presented as normalized mean ± SEM (n = 6).

4.2.2 Measurements of calcium transients within the ML and GCL regions to different patterns of stimulation using the SyGCaMP2 sensor

In the second part of this study, we aimed to use SyG37 mice to characterize the response characteristics of different patterns of stimulation in the molecular and granule cell layers of the cerebellar cortex in coronal cerebellar slices. In this orientation, it is possible to activate beams of PFs directly by placing stimulating electrodes in the ML. Electrodes placed in the granule cell layer in this orientation activate GCs (see Sims and Hartell 2005). We wished to find out whether it was possible to use the SyG37 mouse to follow transmission along PFs and to see whether direct granule cell activation produced activation of synapses in the ascending segment of the granule cell axon and/or subsequent transmission along beams of PFs.

4.2.2.1 The effects of increasing stimulus intensity on both SyGCaMP2 fluorescence and fEPSP responses to direct stimulation of the ML

In this section, we first placed a stimulation electrode in the ML for direct activation of PFs in coronally cut slices (figure 4.7A). In this design, the SyGCaMP2 response was captured by recording images at a pixel resolution of 1200 x 450 positioned in layers of the cerebellum in response to ML stimulation (a train of 100 stimuli delivered at 50 Hz) using epifluorescence microscopy (see method section, 2.6.1). Finally, in order to visualise the pathways of the beam-like response that was induced by ML stimulation, images of SyGCaMP2 responses were subtracted as described previously (see chapter 2, section 2.7.2.3).

As shown in Figure 4.7 B, stimulation in the ML produced a clear beam-like response that flowed along the curved trajectory of PFs in both directions from the point of stimulation, whereas there is no evidence of a longitudinal beam into the GCL indicating that a direct activation within the ML may only induce propagation of an AP in the fibres in the ML, but not in the GCL.

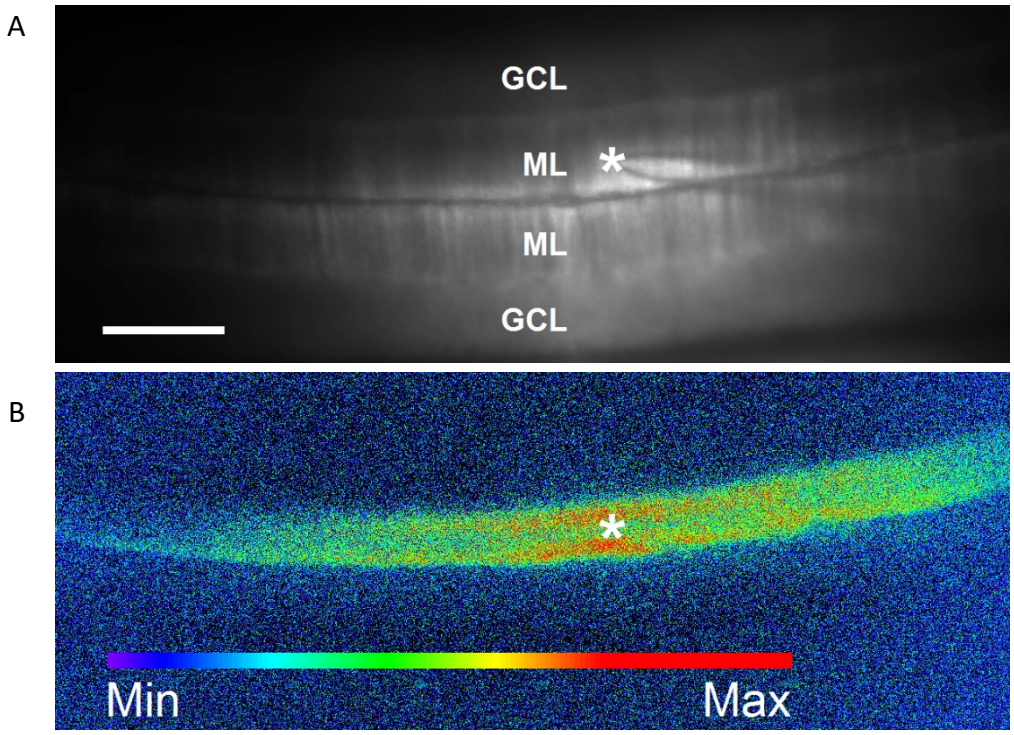

Figure 4.7. Visualization of the effects of direct activation in the ML of coronal cerebellar slices on SyGCaMP2 fluorescence. (A) shows a transmission image of a coronal cerebellar slices with a grey lookup table applied that shows the positions of stimulating electrodes with respect to the different layers of the cortex. The asterisks (white) indicate the positions of the stimulating electrodes in the ML. Activation was a train of 100 stimuli delivered at 50 Hz. The averages of five sequential SyGCaMP2 images were taken immediately prior to stimulation. These were subtracted from the peak responses taken during electrical stimulation to create a subtraction image in (B). A fixed scale with a warm/cold look-up table was used to show the differences in the magnitudes of each of the responses in both different conditions of spatial stimulation. The scale bar in A was 50 µm.

We next sought to further examine the effects of increasing the stimulus intensity within the ML region of the cerebellum on both SyGCaMP2 and field potential responses. Trains of 20 stimuli, delivered at 50 Hz, were applied over intensities of 0, 2, 5, 10, 15, 20, 30, 40, 50, 60 and 70 V, and fluorescence and fEPSP responses were measured. Responses were measured every 3 minutes. images of a coronal cerebellar slice were collected for each wavelength over a 20 s period using an epifluorescence microscope, as described in chapter 2, section 2.6.1.

The design of these experiments is explained by the schematic diagram shown in Figure 4.8. This diagram shows the locations of stimulating and recording electrodes with respect to the different layers of the cortex. A recording electrode was placed in the ML above the PC layer to record fEPSPs from the dendrites of PCs, and a micromanipulator was used to place the stimulating electrode in the ML to activate PFs. Measurements of SyGCaMP2 fluorescence were made from regions of interest (ROIs) located in the ML and GCL due to electrical stimulation in the ML. Finally, data were analysed and data from separate experiments were combined and results were presented as mean ± SEM, as described in chapter 2, section 2.7.2.1.

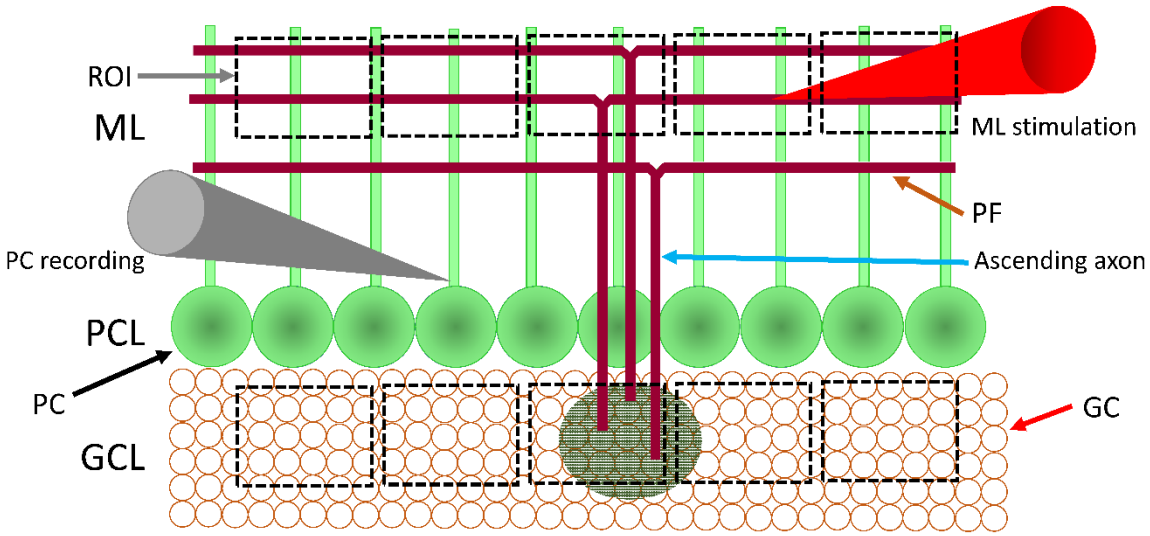

Figure 4.8. Schematic diagram for direct activation of the molecular layer in coronal cerebellar slices of SyG37 mice. This Figure shows the somatic recording from above the PC (using a patch pipette; grey). Molecular layer stimulation was performed using a stimulating electrode (red, top) placed in the molecular layer (ML). Granule cells (GC; red arrow) form ascending axons (blue arrow) which bifurcate to form parallel fibres (PF; brown). SyGCaMP2 fluorescence was made from regions of interest (ROIs; grey arrow) located in the ML and GCL for electrical stimulation in the ML.

Examples of individual SyGCMP2 responses in the ML and GCL to different intensities of direct stimulation of the ML are shown in Figures 4.9 A (ML) and 4.9 B (GCL). Figure 4.9 C shows pooled data for the peak SyGCaMP2 responses. The peak responses increased in a sigmoidal manner but did not reach saturation even

at an intensity of 70 V. There was comparatively little response within the GCL in response to ML activation, which was expected. Since these measurements were made using an epifluorescence microscope which does not allow optical sectioning, it is likely that the small increase in fluorescence in the GCL is simply light that spreads directly from the ML to the GCL.

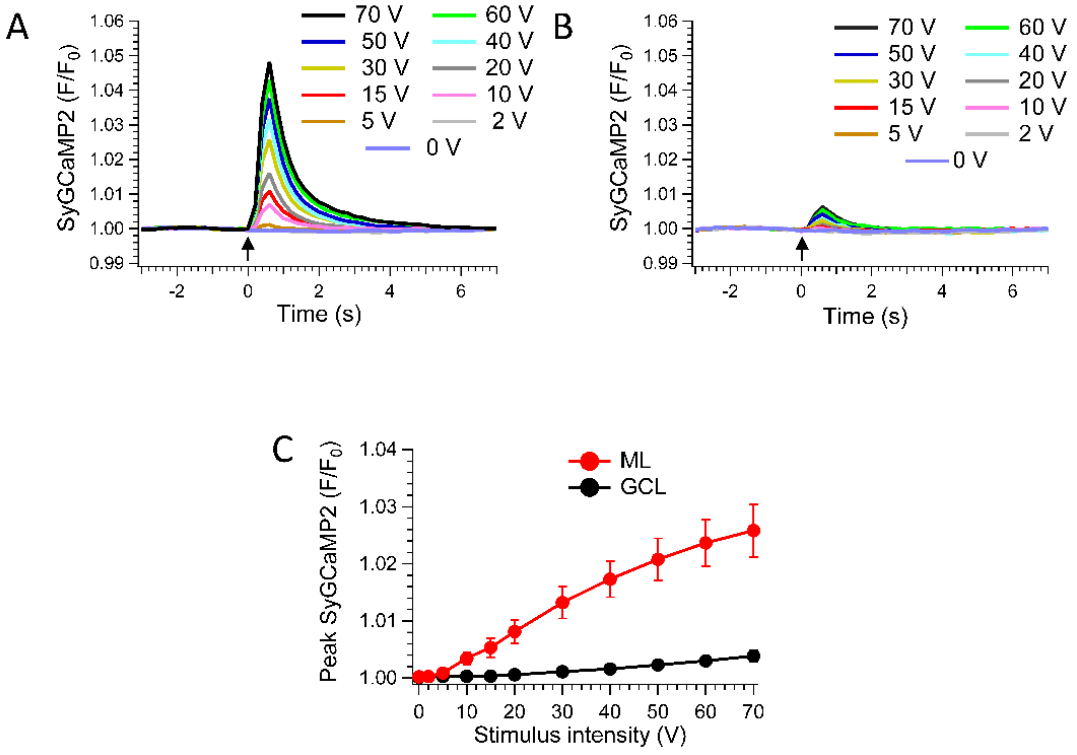

Figure 4.9. Effects of increasing stimulus intensity on SyGCaMP2 fluorescence within the ML and GCL regions to direct activation of the ML in coronal cerebellar slices of SyG37 mice. Bursts of 20 stimuli were applied at the fixed frequency at intensities between 0 V and 70 V. The panels (A and B) illustrate average responses of SyGCaMP2 fluorescence to the range of stimulus intensities of ML obtained from the ROIs located within the ML area (A) and GCL area (B) as plotted against time. Different colours are used to distinguish greater stimulus intensities. Panel (C) shows the effects of increasing intensity on peak of the SyGCMP2 responses within the ML (red) and GCL (black) to stimulation in the ML as plotted against intensity. Black arrows indicate the starting of the stimulation period. Mean and SEM are shown (n = 7).

As shown in Figure 4.10 B, C and D, the amplitudes and initial slopes of the N2 components of the fEPSP and the N1 amplitude also gradually increased with stimulus intensity in an entirely analogous manner to the SyGCaMP2 responses. To further determine if there was any relationship between the absolute amplitude of the field potential and calcium imaging (F/F_0) responses evoked by gradual stimulation of intensity at fixed frequency and number, comparisons of the presynaptic Ca^{2+} (peak of the SyGCaMP2 responses) and fEPSPs (the amplitudes of N1 and N2 and initial slope of N2) were made. Interestingly, there was a strong linear correlation between the peak calcium response and N1 and N2 peaks and N2 slope, as shown in Figures 4.10 E, F and G. Significant correlations were found between every one of the following two variables (Pearson correlation: SyGCaMP2 peak vs. N2, $r = 0.9869$, $P < 0.0001$; SyGCaMP2 peak vs. N2 slope, $r = 0.9969$, $P < 0.0001$; SyGCaMP2 peak vs. N1, $r = 0.\ 0.9884$, $P < 0.0001$).

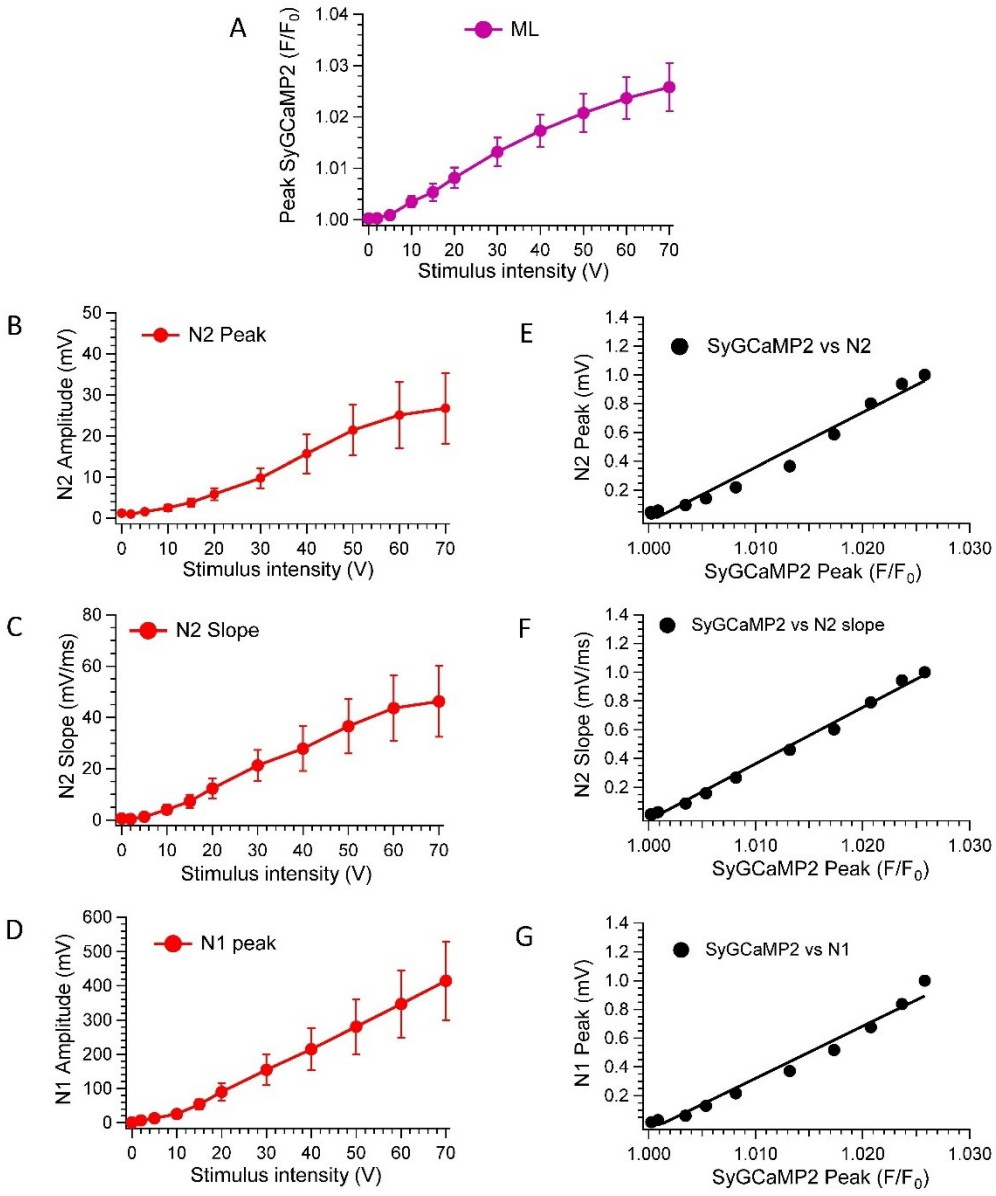

Figure 4.10. Effects of increasing stimulus intensity on peak SyGCaMP2 and fEPSP responses and the relationship between peak SyGCaMP2 and field of the PF responses to direct activation of the ML in coronal cerebellar slices of SyG37 mice. At a fixed frequency and at an intensity between 0 V and 70 V, trains of 20 stimuli were applied. Mean and SEM peak SyGCaMP2 fluorescence (A), and peak (mV) of N2 (B), the slope (mV/ms) of N2 and the peak (mV) of N1 are plotted against stimulus intensity (n = 7). Panels E, F and G are scatter plots illustrating approximately linear relationships between SyGCaMP2 peak (presynaptic calcium) and fEPSP of the N2 peak, N2 slope and N1 peak, respectively. Substantial correlation was found between each of the following two variables (Pearson correlation: SyGCaMP2 peak vs. N2, $r = 0.9869$, $p < 0.0001$; SyGCaMP2 peak vs. N2 Slope, $r = 0.9969$, $p < 0.0001$; SyGCaMP2 peak vs. N1, $r = 0.\ 0.9884$, $p < 0.0001$).

4.2.2.2 The effects of increasing stimulus intensity on SyGCaMP2 fluorescence responses to direct stimulation of the GCL

We next examined the effects of changing stimulus intensity on SyGCaMP2 fluorescence responses at the PFs and the ascending segments to direct stimulation of the GCL. For this, we have repeated the same experiments described in section 4.2.2.1 except that the stimulating electrode was placed in the GCL as opposed to the ML and we have here focussed only on recording SyGCaMP2 fluorescence responses.

We first tried to visualise the pathways of the beam-like response in coronal cut slices to direct activation of ascending segments in the coronal slice. To do so, the stimulating electrode was placed in the GCL to ensure direct activation of ascending segments in the coronal slice (Figure 4.11 A). As in the above section, stimulation was a train of 100 stimuli delivered at 50 Hz.

As shown in Figure 4.11 B, stimulation in the GCL induced diffuse patterns of activity around the point of stimulation, as seen from a small number of brighter areas, which could represent activation of MF terminals or GoC terminals as well as the responses which extended along the PFs. This result indicated that direct activation of GCL can propagate information directly above the point of stimulation through ascending axons to bifurcate along the PFs.

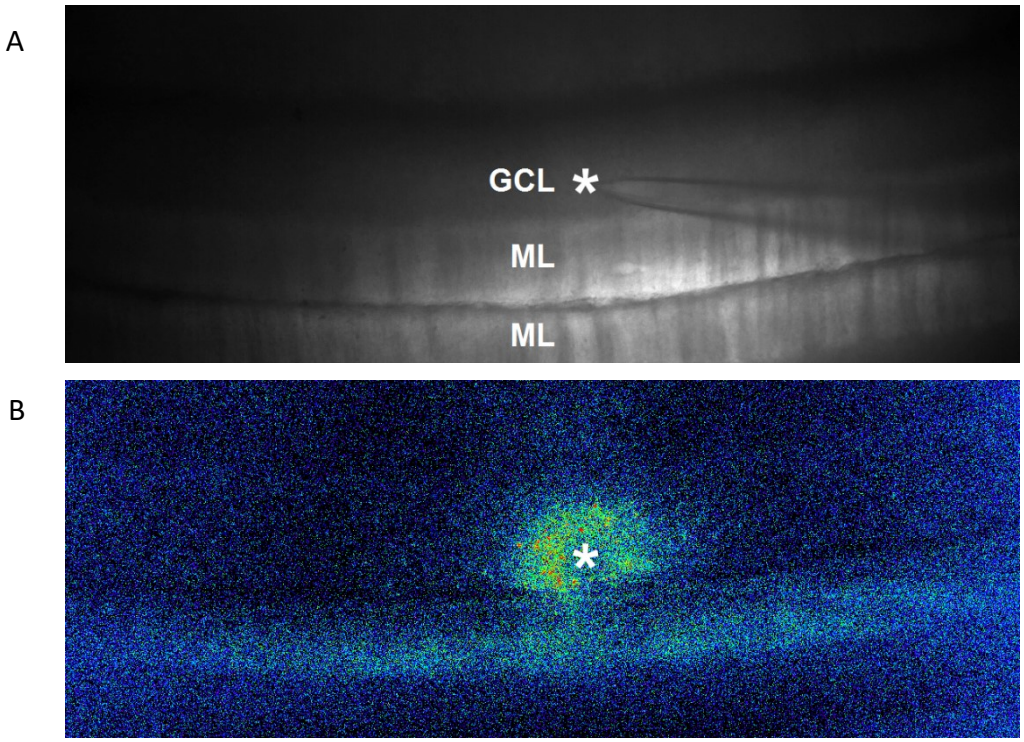

Figure 4.11. Visualization of the effects of direct activation in GCL of coronal cerebellar slices on SyGCaMP2 fluorescence. Images were illustrated as in Figure 4.7 except that the position of the stimulating electrodes positioned in GCL.

We next further examined SyGCaMP2 responses to increasing intensity stimulation of the GCL. The activation was increased (0, 2, 5, 10, 15, 20, 30, 40, 50, 60 and 70 V) at a fixed number of 20 and a fixed frequency of 50 Hz. The experimental protocol here is explained by the schematic diagram illustrated in Figure 4.12. This Figure shows the locations of the stimulating electrode with respect to the GCL. Measurements of SyGCaMP2 fluorescence were made from ROIs located in the ML, GCL and a column directly above the point of stimulation. Finally, data were presented as mean ± SEM as described in section 4.2.2.1.

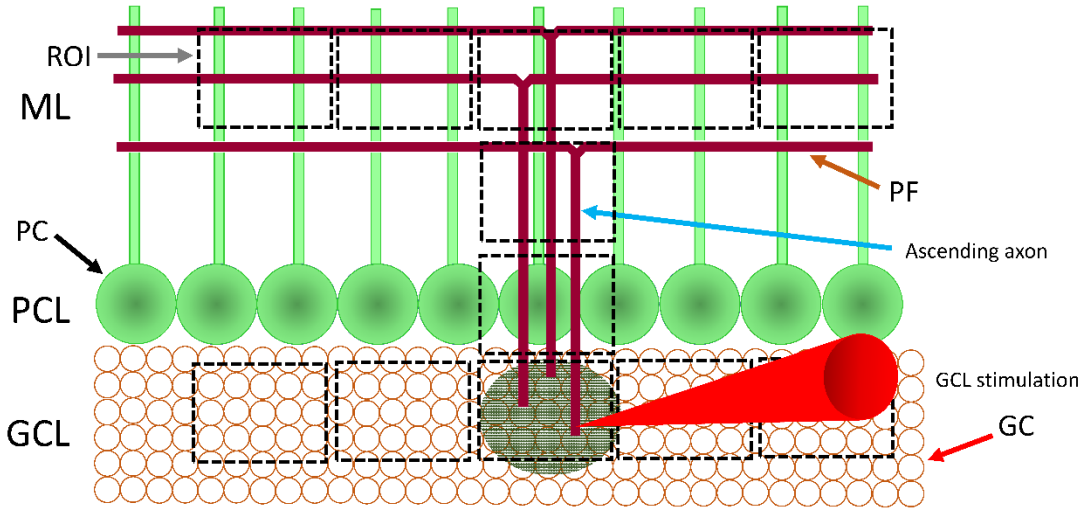

Figure 4.12. Schematic diagram for direct stimulation of the granule cell layer in coronal cerebellar slices of SyG37 mice. The diagram was presented in the same manner as described in Figure 4.7 except the stimulating electrode was placed in the granule cell (GCL), where the measurements here also include the column directly above the point of stimulation and there is no fEPSP recording.

Example traces of SyGCaMP2 responses at GCL, ML and column to different intensities of the direct stimulation of the GCL are shown in Figures 4.13 A, B and C, respectively.

As can be seen from Figure 4.13 D, the peak SyGCaMP2 responses (F/F_0) gradually increased with increasing intensity in an approximately sigmoidal fashion in the regions in a column directly above the point of stimulation and within the GCL. Interestingly, the responses at the ML were also gradually increased in the same manner. Responses did not indicate any saturation, even at an intensity of 70 V. Although we cannot exclude the direct spread of light between layers from these epifluorescence measurements, the responses in the ML and “column” were large, suggesting that activation of the GCL causes activity to propagate up the ascending segment of the GC axon and possibly spread along the PFs.

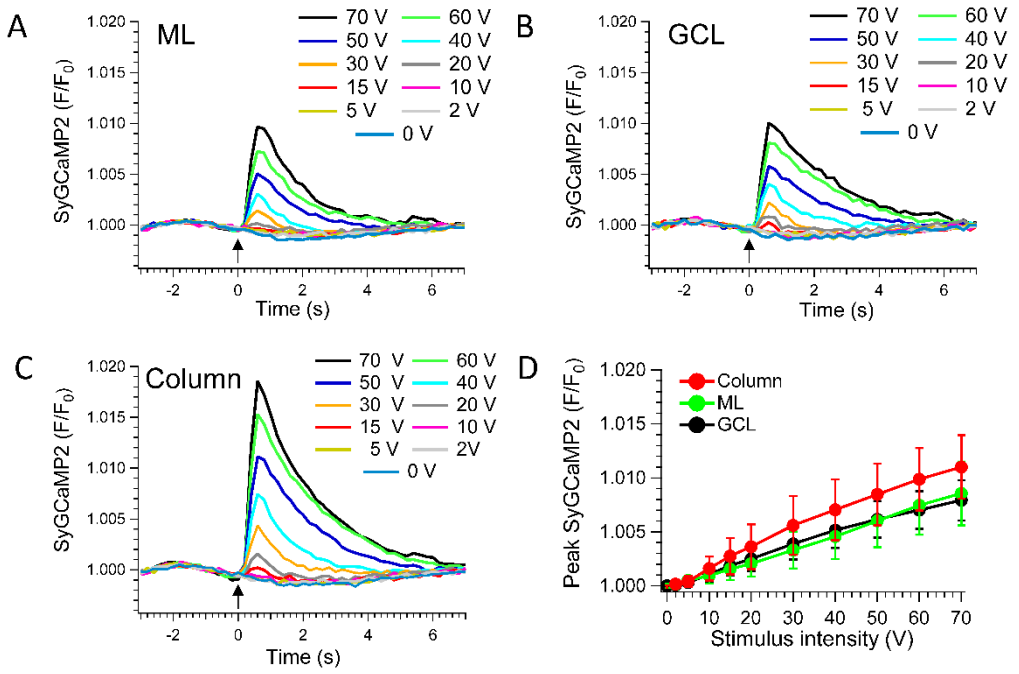

Figure 4.13 Effects of increasing stimulus intensity on SyGCaMP2 fluorescence within the GCL and ML regions to direct activation of the GCL in coronal cerebellar slices of SyG37 mice. The data presented are as shown in Figure 4.9, except Panels A, B and C illustrate average responses of SyGCaMP2 fluorescence to the range of stimulus intensities of the GCL obtained from the ROIs located within the ML area (A), GCL area (B) and "column" (C) (column refers here to the region directly above the point of stimulation). Panel D shows the effects of increasing intensity on peak of the SyGCMP2 responses within the column (red), ML (green) and GCL (black) to stimulation in the GCL as plotted against intensity. Black arrows indicate the starting of the stimulation period. Mean and SEM are shown (n = 7).

Figure 4.14 summarises that in coronal cerebellar slices, ML stimulation induced a clear response in the ML area but there was no associated response within the GCL. However, after moving the stimulating electrode into the GCL to activate the ascending segment, a clear response was induced in the ML, GCL and ascending segment. More importantly, the time course for SyGCaMP2 decay in PF recovery to baseline was clearly quicker after stimulation than for the ascending granule cell axon. These differences in rates of recovery between PFs and ascending granule cell axons may well reflect variances in the capabilities of PF and ascending granule cell axon synapses to homeostatically control Ca^{2+} levels after stimulation.

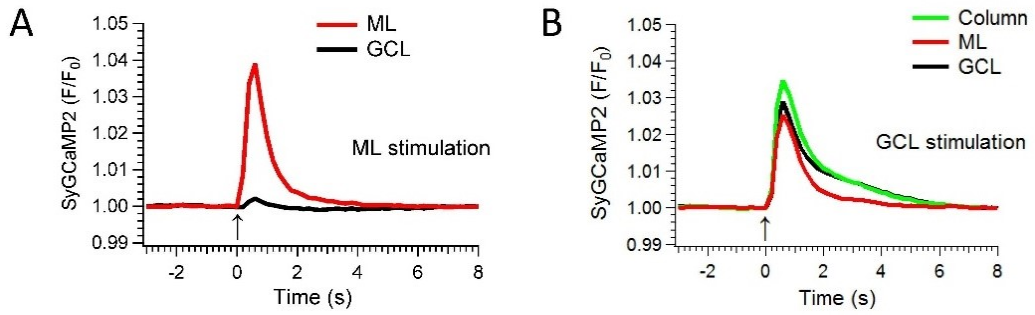

Figure 4.14. Direct and indirect stimulation in the ML and GCL of SyGCMP2 responses in coronal cerebellar slices of SyG37 mice. Activation was a train of 20 stimuli delivered at 50 Hz. Panels A and B illustrate average responses of SyGCaMP2 fluorescence (F/F_0) from ROIs placed within the ML (red traces), GCL (black traces) and column (green trace) to stimulation in the ML (left) and GCL (right) as plotted against time. Black arrows reveal the beginning of the stimulation period.

4.2.2.3 The effects of increasing stimulus number and frequency on SyGCaMP2 fluorescence within the ML and GCL to direct and indirect stimulation of GCL and ML

In this set of experiments, we first examined the effects of increasing stimulus number on SyGCaMP2 fluorescence within both the ML and GCL to stimulation of the GCL and ML. The stimulus number was increased over the range 1, 2, 5, 10, 15, 20, 30, 40, 50 and 100 stimuli at a fixed frequency of 50 Hz and an intensity of 30 V. The resultant SyGCaMP2 responses were measured at the ML and GCL following stimulation in the ML, GCL and responses from ROIs measured in the same way as for the effects of stimulus intensity (see sections 4.2.2.1 and 4.2.2.2). An example of individual SyGCMP2 responses at ML to different number of a direct stimulation of ML are shown in Figure 4.15 A.

Figure 4.15 B showed that application of an increasing number of stimuli at a fixed stimulus frequency and intensity to direct the activation of the ML led to an increased SyGCaMP2 peak response in an almost linear manner up to approximately 30 stimuli, after which a plateau was reached (i.e., at 40 stimuli). Not surprisingly, the effect was different for the AUC measurement (data not shown) as might be

expected since the duration of stimulation, and hence the duration over which the signal was elevated above baseline, increased with stimulus number (see Figure 4.15 A).

Similar to the results obtained by increasing the stimulus intensity, ML activation had relatively little effect on fluorescence in the GCL, indicating that ML activity did not propagate the AP into the GCL. On the other hand, direct activation of the GCL showed that SyGCaMP2 peak fluorescence responses with the GCL, ML and a column directly above the point of stimulation all increased in a similar manner (Figure 4.15 C). Again, this can be explained by orthograde propagation of an AP from the GCL via ascending axons to the PFs.

The next set of experiments involved examining the effects of increasing the stimulus frequency on SyGCaMP2 fluorescence responses to stimulation of the GCL and ML. Frequencies were increased over the range 1, 2, 5, 10, 20, 50, 100, 200, and 250 Hz at a fixed intensity of 30 V and a fixed number of 20 stimuli.

An example of individual SyGCMP2 responses in the ML to different frequencies of direct stimulation of the ML are shown in Figure 4.15 D. Figure 4.15 E shows the effects of increasing the frequency of ML stimulation on the peak of the SyG37 response. Responses increased in a roughly linear fashion up to 10 Hz after which they started to plateau, reaching a maximum at 100 Hz; they then declined in size at higher frequencies. As with previous experiments, there was only minimal response detected in the GCL, indicating that ML stimulation does not excite the GCL. These were then repeated but with stimulating electrodes placed in the GCL. Figure 4.15 F shows the results of these experiments. Responses peaked at a frequency of 50 Hz and then declined. There was no difference between responses measured in the GCL, ML or in the column directly above the point of stimulation.

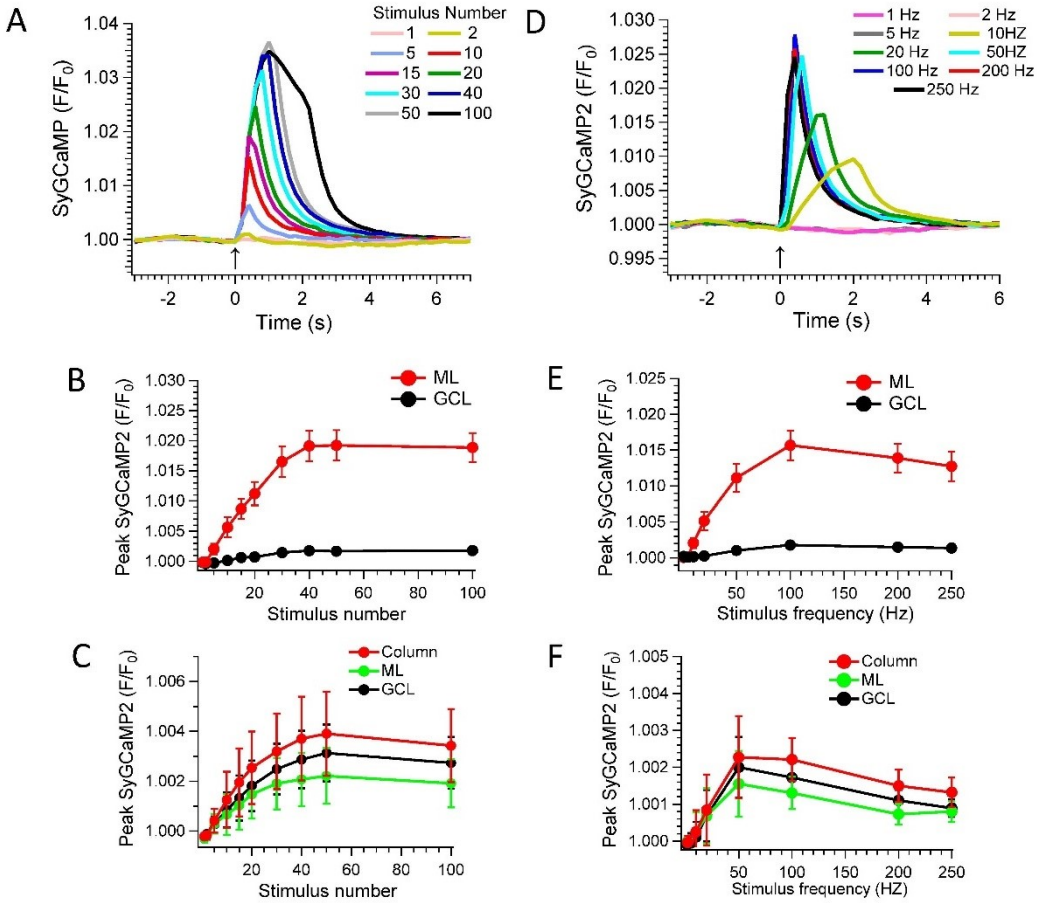

Figure 4.15. The effects of increasing stimulus number and frequency on SyGCaMP2 fluorescence to a direct and indirect stimulation of GCL and ML. Data are illustrated as in Figure 4.9 except Panels A and D which illustrate the average responses of SyGCaMP2 fluorescence to the range of stimulus number and frequency of ML obtained from the ROIs located within the ML area, respectively. Panels B and E show the effects of increasing stimulus number and frequency on SyGCaMP2 peak fluorescence responses within the ML (red) and GCL (black) to stimulation in the ML as plotted against number and frequency, respectively. Panels C and F show the effects of increasing stimulus number and frequency on the peak of the SyGCMP2 responses within the column (red), ML (green), GCL (black) to stimulation in the GCL as plotted against number and frequency, respectively. Black arrows show the beginning of the stimulation period. Mean and SEM are shown (n = 7).

4.2.2.4 The effects of increasing stimulus intensity on individual presynaptic boutons within the ML to direct stimulation of the ML

The results described in section 4.2.2.1 indicate that the amplitude of SyGCaMP2 responses gradually increased in the ML as a function of stimulus intensity, but this does not in itself clarify whether increasing stimulus intensity changes the size of the response per bouton and/or the number of boutons contributing to the total response. Therefore, the main aim of this section was to examine the effects of increasing intensity on individual boutons, as identified using multiphoton microscopy.

Stacks of 80 images consisting of 512 x 64 pixels were captured from the ML using a multiphoton microscope at rates of 98 ms per image (Figure 4.16 A). These images were collected in response to direct stimulation of the ML. A range of stimulation intensities between 0 V and 70 V were applied at a fixed frequency of 50 Hz and for a fixed number of 20 stimuli for each experiment. Stacks of images were background subtracted and averaged over time and a function of a threshold segmentation was used to automatically detect the putative individual puncta (Dorostkar et al., 2010), as described in more detail in Chapter 2. The SyGCaMP2 fluorescence (F/F_0) for each of these puncta were subsequently plotted against stimulus intensity. The number of puncta identified that responded to stimulation at each intensity were counted and the peak amplitudes of those responding puncta measured.

Figures 4.16 B and C show that as the intensity of the stimulus was raised, the number of responding puncta increased indicating that increasing the intensity of the stimulus led to the recruitment of new synaptic boutons.

In the same manner, the increase in intensity increased the average peak responses per individual puncta once the threshold for the detection of a response was reached (above 10 V) (Figures 4.16 B and D). However, this is surprising because one might believe that once a bouton reaches the threshold for stimulation, then it will respond in an ‘all or none’ manner and so the calcium increase in presynaptic boutons would not growth with increasing stimulus intensity.

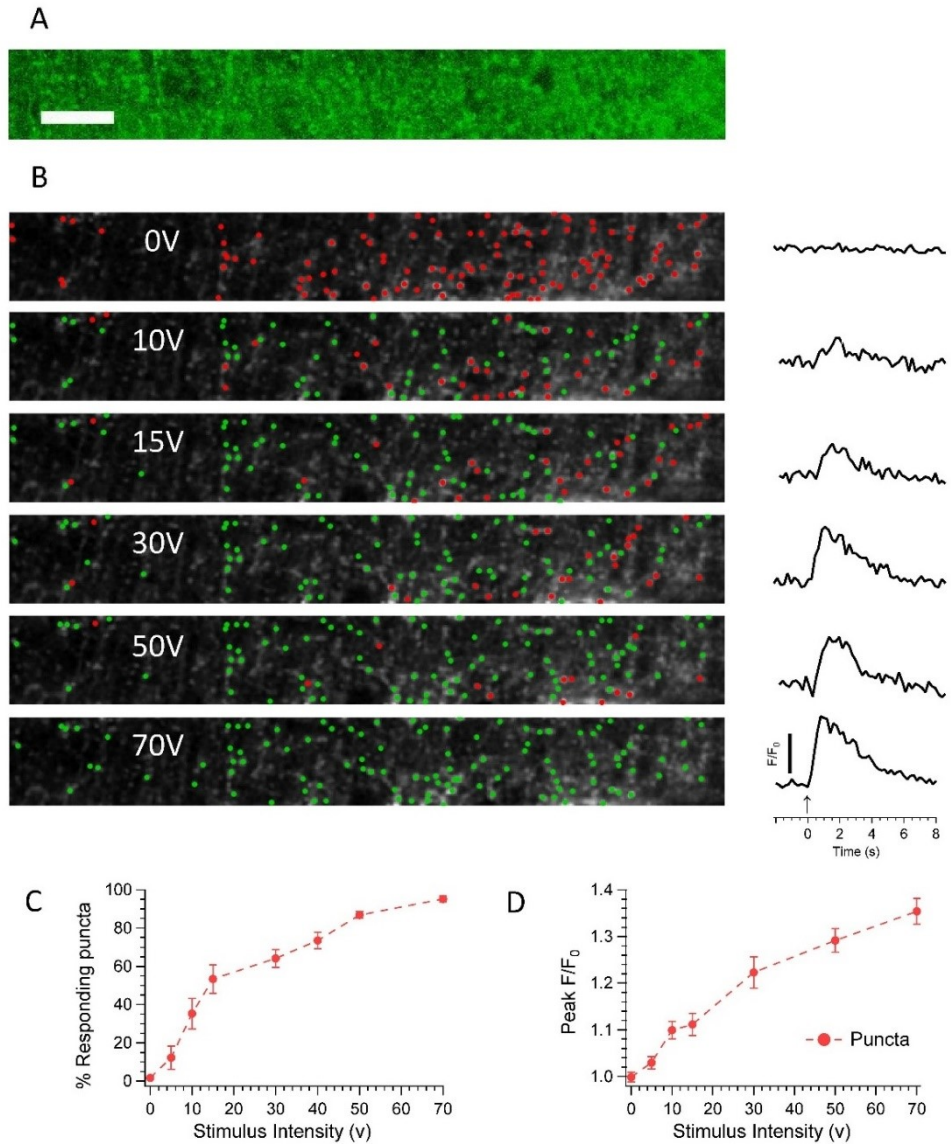

Figure 4. 16. Effects of increasing stimulus intensity on individual presynaptic boutons within the ML to direct stimulation of ML. Panel A shows the average of 80 images consisting of 512 x 64 pixels (corresponding to 212.55 x 26.57 µm) that were captured from the ML region to direct stimulation of ML using a multiphoton microscope. Panel B image stacks were obtained in response to trains of 20 stimuli at different intensities at a fixed frequency. These images were averaged, and then background subtracted. ROIs were also automatically identified using a Laplace operator threshold segmentation system. In the right-hand column, the black trace shows the average number of responding puncta (F/F_0) plotted against the time for each stimulus intensity shown here. The arrow shows the onset of electrical activation. Green and red dots are placed at each ROI indicating responding and non-responding, respectively. The scale bar shows 20 µm. Panel C shows the number of punctate regions that responded to stimulation as a proportion of the total number of ROIs identified by the threshold segmentation method. Panel D shows the effect of changing intensity on the peak responses (F/F_0) of responding puncta. Data in Panels C and D were presented as mean ± SEM (n = 7).

4.2.2.5 The effects of increasing stimulus number on individual presynaptic boutons within the ML to direct stimulation of the ML

We have previously observed in section 4.2.2.3 (Figure 4.15B), where experiments were performed using a sCMOS camera attached to an epifluorescence microscope, that the increasing stimulus number at a fixed stimulus frequency and intensity to the direct stimulation of ML produces an increase in the peak responses of SyGCaMP2 fluorescence in an almost linear fashion up to around 30 stimuli after which they reached a plateau with no any subsequent decline even at stimuli of 100. Therefore, the specific objective of the experiments performed using the multiphoton microscope in this section was to establish whether increasing stimulus number results in an increase in the amount of calcium per bouton and/or whether new boutons are recruited. The experiments in this section were repeated as described in the above section, with the exception that a burst of 1 to 100 stimuli were applied at 50 Hz at a fixed intensity (40 V). In contrast to the effects of altering stimulus intensity, the results as shown in Figure 4.17A and B indicated that the number of responding puncta gradually increased in an almost linear fashion up to 15 stimuli, after which the responses reached a plateau. Increasing the number of stimuli therefore increases the amount of calcium per bouton, rather than recruiting additional synaptic boutons.

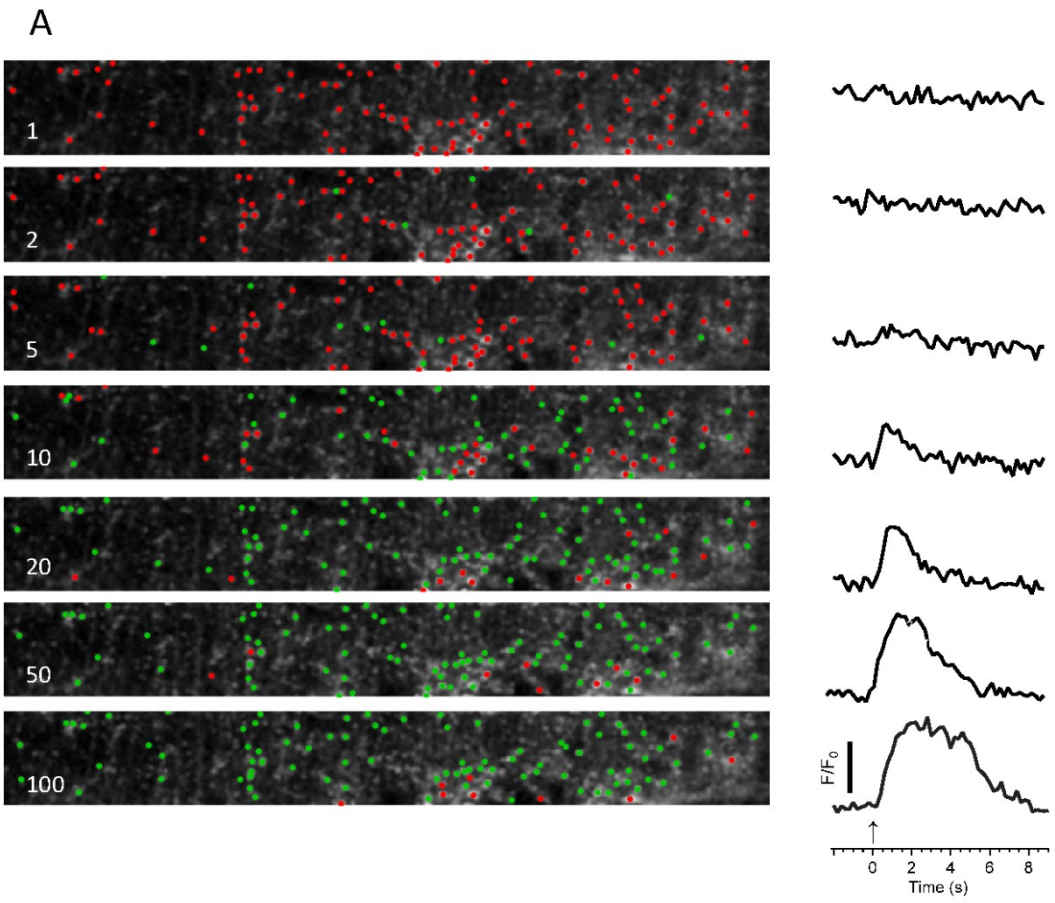

Figure 4. 17. Effects of increasing stimulus number on SyGCaMP2 responses in individual presynaptic boutons within the ML to direct stimulation of the ML. The data presented are as shown in Figure 4.16 except that image stacks of 512 x 64 pixels were obtained for trains of 1 to 100 stimuli applied at fixed frequency and intensity. Data in Panels B and C are presented as mean ± SEM (n = 7).

4.3. Discussion

4.3.1 SyGaMP2 as a sensor for measuring presynaptic calcium in the cerebellar cortex

In the first part of this study, we characterized the response characteristics of SyGaMP2 in the cerebellar cortex using pharmacological manipulation. We first examined the effects of tetrodotoxin (TTX) on fEPSP and SyGCaMP2 responses to ML stimulation. Voltage-gated sodium channels (VGSCs) are transmembrane proteins that conduct sodium ions across a membrane. TTX blocks voltage-gated sodium channels (VGSCs) as it is a selective inhibitor of Na^+ channel conductance, which is essential to the influx of sodium that both initiates and mediates the depolarising component of the action potentials in neurones (Kao, 1986, Akopian et al., 1999, Narahashi, 2008).

The best defined of the neurotoxin binding sites on VGSCs is neurotoxin site 1, which is located at extracellular sodium ion channel pores (Catterall, 1992). We found that application of TTX abolished SyGCMP2 responses and both the N2 and N1 components of the field potential response. Figures 4.2 E and G show that both the N2 and N1 components of fEPSPs were sensitive to TTX, in agreement with previous findings (Nakai et al., 2001, Hasan et al., 2004). SyGCaMP2 responses were also inhibited by TTX. These results indicate that SyGCaMP2 responses depend upon sodium channel activation and therefore require action potential activity within presynaptic terminals.

We secondly evaluated the effects of lowering extracellular calcium on SyGCaMP2 fluorescence and on field potential responses to ML stimulation. Perfusion of extracellular solutions that lacked calcium abolished SyGCaMP2 fluorescence responses and the N2 component, indicating that the optical response of SyGCaMP2 fluorescence and synaptic transmission in response to PF activation depends upon extracellular calcium. This observation is in perfect agreement with the theory regarding the GCaMP family action (Hasan et al., 2004, Nakai et al., 2001). This result is also consistent with previous results in the literature (Mintz et al., 1995), which found that the peak amplitude of dye furaptra was completely blocked when calcium was removed at the GC to PC synapses in slices of rat

cerebellum. These results are also extremely similar to those reported in numerous other studies (Dittman and Regehr, 1998, Margrie et al., 1998, Mintz et al., 1995), which illustrates that the effect of lowering extracellular calcium concentration on PFs to ML stimulation is one of the rapid blockage of synaptic transmission. Together, these data are consistent with the expected actions of SyGCaMP2 as a calcium indicator.

Since SyGCaMP2-mCherry is not selectively expressed in any particular cell type as our sensor was engineered under a Thy1–2 promotor for targeting expression to any neurons, we carried out a series of experiments to test whether the SyGCaMP2 response to ML stimulation arises from pre-synaptic terminals. We first blocked inhibitory (GABA/Glycine) and excitatory glutamatergic (AMPAR) transmission with PTX and NBQX, respectively, followed AP5 to block NMDARs. We reasoned that this would block the majority of synaptic transmission between PFs and their post-synaptic targets, namely PCs, BCs and SCs, as well as any polysynaptic transmission between these cell types. Inhibition of GABA/Glycine receptors and AMPARs completely abolished the N2 component of the fEPSP response, indicating that postsynaptic transmission was indeed blocked. The presynaptic volley was not affected. Further application of AP5 had no effect on either N1 or N2 fEPSP responses. These observations were completely consistent with previous findings (Bergerot et al., 2013, Sutton, 1999, Sgobio et al., 2014) and are consistent with the N2 component of PFs to ML stimulation being blocked by pharmacological blockade of AMPAR and GABA/GlycineRs. The N1 component was not affected by the presence of NBQX and PTX, indicating that the number of fibres activated was not affected. In contrast, the SyGCaMP2 response was reduced by roughly 10 and 25% in coronal and sagittal cerebellar slices, respectively, after receptor blockade, indicating that > 90% or >75% of the total response originated from PFs. Assuming that SyGCaMP2 is expressed exclusively in presynaptic terminals, there are two potential explanations for this. The first is that some of the total SyGCaMP2 response originates from synaptically connected presynaptic terminals on other cell types within the ML including, for example, SCs and BCs. The second possibility is that AMPA/Glycine/$GABA_A$ or NMDARs may be present on the presynaptic terminals of PFs and so are directly modulating calcium influx at the terminal. It should also be noted that these two possibilities are not mutually exclusive.

Regardless of explanation, these data, combined with the results for TTX and lowering extracellular calcium, show that the majority (~75% in the sagittal slice; ~90 % in the coronal slice) of the SyGCaMP2 response originates from the PFs. The larger percentage contribution of PFs to the total SyGCaMP2 response in coronal slices most likely reflects the fact that PFs are intact in this orientation. Indeed, we showed that ML stimulation in this orientation produced beams of activation along the ML. In sagittal slices, ML stimulation is likely to activate not only PFs but any other fibres in the local vicinity such as the terminals of BCs and SCs.

We finally set out to test whether the blockade of NMDARs by AP5 alone without any other blockers had any effects on fEPSPs and SyGCaMP2 fluorescence. Application of AP5 did not have any statistically significant effects on either the presynaptic fibre volley (N1) or the synaptic N2 components of fEPSPs. No effect on SyGCamP2 responses was seen. These results agree with the study by Díez-García et al. (2005), who reported that in a different transgenic mouse that expressed GCaMP2 selectively in GCs, paired pulse-induced presynaptic Ca^{2+} transients in PF terminals were not affected by inhibition of NMDA receptors. This result does not demonstrate that NMDA receptors do not exist or have any functional role at this synapse because Casado et al. (2000) found that activation of NMDA receptors with NMDA and its co-agonist, glycine, reduced the size of whole-cell EPSCs recorded between PFs and PCs. The present study does suggest, however, that under our conditions of synaptic activation, there is little if any evidence of tonic NMDA receptor activity contributing to either calcium influx into presynaptic terminals, the PF volley, or the subsequent postsynaptic response. In conclusion, these results collectively strongly suggest it is highly likely that in the cerebellar cortex, SyGCaMP2 responses represent Ca^{2+} signals that originate primarily, but not exclusively, from PF terminals.

4.3.2 Using SyG37 mice to visualise activity in the cerebellar cortex

Having demonstrated that SyGCaMP2 responses reflect calcium activity in PF terminals, we characterized the patterns of responses to activation of GCs in coronal cerebellar slices. In this orientation, PFs are intact and run along the length of the ML.

Stimulation of the ML produced very clear bands of activity that remained entirely restricted to the ML. This is consistent with direct activation of PFs which transmit information along their length (Díez-García et al., 2005). In contrast, when placing the stimulating electrode in the GCL, SyGaMP2 responses were evident in the GCL layer and in a column directly above the point of stimulation. Responses also propagated along the ML. These results suggest that GCL stimulation activates a cluster of GCs, their ascending axon segments and the PFs running bidirectionally through the ML. These results confirm the activation patterns previously proposed by these configurations of cellular activation (Gundappa-Sulur et al., 1999, Sims and Hartell, 2005, Sims and Hartell, 2006, Díez-García et al., 2005). These results also consistent with the fact that PFs arise from a T- shaped bifurcation of axons of ascending granular cell. They relay information from the key afferent input which is MFs (Kandel et al., 1991, Heck, 1995, Purves et al., 2008). The amplitudes of SyGCaMP2 responses to increasing intensities of stimulation were much higher in response to direct stimulation of the ML compared to activation of the GCL. This is perhaps not surprising because GCL activation would be expected to activate GCs and a number of other cell types and presynaptic boutons in this layer, potentially including MF terminals, GoC terminals and UBCs. Of these, only GCs would be expected to activate presynaptic terminals of the ascending axon segment and PFs. Therefore, the density of terminals activated is likely to be relatively low compared to the direct activation of a beam of PFs.

Our findings also indicate that the time course for SyGCaMP2 decay in PF recovery to its baseline was quicker after stimulation than for the ascending segment of the GC axon (Figure 4.14). These observations suggest that PF and ascending axon synapses are heterogeneous in their properties. Therefore, these two GC axon synapses should be considered separately. These observations provide further evidence to support earlier studies by Sims and Hartell (2005), and Gundappa-Sulur

et al. (1999), and indeed others, who illustrated that there are fundamental differences in the transmission properties at ascending axon and PF synapses.

Using MP microscopy to examine the effect of stimulus intensity at the single bouton level, we found that increasing intensities of stimulation of the ML produced an increase in the number of boutons that contributed to the response (Figure 4.16 C). This was consistent with fibre volley recordings (Figure 4.10 D), which are proportional to the number of presynaptic fibres activated (Henze et al., 2000, Sutton, 1999). Therefore, at a specified number and frequency of stimuli, increasing the intensity of the stimuli leads to the recruitment of additional boutons and an increased Ca^{2+} influx to boutons in the ML region. When only responding puncta were measured, the single bouton responses appeared to increase as well (Figure 4.16 D). This is difficult to explain because one might expect that once a bouton reaches the threshold for activation, then it will respond in an 'all or none' manner and so the calcium increase per bouton would not increase with increasing intensity. Our observation may reflect a difficulty in identifying boutons that respond. It is also possible that stimulation may have a high failure rate at PFs, and so as the stimulation intensity increases the number of stimuli that lead to an AP increases, and so the likelihood of detecting a response increase.

We finally also set out to test the effect of increasing stimulus number at fixed intensity and frequency. The peak amplitudes of SyGCaMP2 fluorescence from individual presynaptic boutons increased linearly up to 5 stimuli, after which it reached a plateau at about 30 stimuli (Figure 4.17C). This plateau was not simply due to saturation of the sensor as the AUC response was not saturated (Figure 4.15 A) but is rather due the duration of stimulation as a function of stimulus number. Figure 4.17 B revealed that as the stimulus number increased, the numbers of puncta responding increased in a roughly linear manner up to 15, after which the number of puncta responding did not change. Thus, at a fixed frequency and intensity of stimuli, increasing the number of stimuli does not lead to the recruitment of new synaptic boutons but does increase the amount of Ca^{2+} mobilized per bouton. This result is entirely consistent with the study by Al-Osta et al. (2018), who reported that at a fixed number and intensity of stimuli, increasing the stimulus number increased the Ca^{2+} influx per peak bouton up to 20 stimuli (then responses become saturated) but did not recruit additional synaptic boutons, as found using

hippocampal brain slices of SyG37. This result is also largely consistent with previous observations (Dreosti et al., 2009), where it illustrated that at a given number and intensity of stimuli, the peak amplitude of the SyGCaMP2 response was increased in a roughly linear fashion up to about 5 APs, after which they plateaued at about 20 APs, but the AUC response of SyGaMP2 was not saturated in cultured hippocampal neurones. However, as shown in Figure 4. 17B, our sensor was failing to detect responses to 1 stimulus but was detecting responses to 5 stimuli in cerebellum brain slices of SyG37 mice. Does this potentially reflect the inability of our sensor to detect a single electrical stimulus? As discussed, early SyGCaMP2-mCherry was produced by the fusion of red fluorescent protein (mCherry) to the C-terminus of SyGCaMP2 which in turn tethered GCaMP2 to the C-terminus of the vesicular protein synaptophysin to form SyGCaMP2-mCherry. Synaptophysin was restricted to synaptic vesicles with comparatively short expression on the surface of the vesicle membrane. Therefore, this design restricted the sensor to appropriate and specific places where synaptic calcium transients increase rapidly. Therefore, our sensor should be able to detect a single stimulus. Indeed, it has been shown that our sensor was able to detect responses to single electrical stimuli of single boutons in hippocampal cultures but not in brain slices. The study by Dreosti et al. (2009) was also able to detect the responses to single stimuli in hippocampal cultures using SyGCaMP2. Therefore, the addition of red fluorescent protein (mCherry) had no effect on the sensitivity of our sensor compared to SyGCaMP2. The discrepancy to detect responses of single stimuli within single boutons in hippocampal neuronal cultures but not in cerebellar or hippocampal brain slice preparations could be interpreted by using various neuronal preparations, as the synapses in preparations of neuronal cultures may not be covered via cell structure such as glial membranes, which is not expressed by our sensor. Therefore, these synapses may be more easily expressed by SyGCaMP2-mCherry compared to those in brain slice preparations. Nevertheless, by using widefield fluorescence imaging, it was likely that responses to a single electrical stimuli would be identified. We have clearly demonstrated that our sensor is able to reliably detect responses from large populations of boutons to different ranges of electrical stimuli in coronal brain slice preparations of the cerebellum (Figures 4.15 A and D).

Chapter 5: Investigating the Role of Presynaptic NMDA Receptors at Cerebellar PF-PC Synapses

5.1 Introduction

NMDARs play a myriad of roles in the induction of various forms of synaptic plasticity within the CNS. Plasticity is considered to be a cellular substrate of learning and memory (Traynelis et al., 2010, Hammond, 2001, Purves et al., 2008). NMDARs also appear to be involved in a wide range of neurological and psychiatric diseases and phenomena such as pain, depression, epilepsy and various neurodegenerative disorders such as Alzheimer's and Parkinson's (Malinow, 2012, Liu et al., 2019). For instance, NMDARs antagonists have been reported to show some evidence for reducing symptoms of Alzheimer's disease (Mota et al., 2014). As outlined in the introduction (section 1.5.1) there is mounting evidence to suggest that NMDARs might be found at PF terminals in the cerebellum terminals, and that they contribute to the regulation of synaptic plasticity. However, there is also an increasing body of evidence in the fields of immunohistochemistry and electrophysiology that suggest the existence of NMDARs at GABAergic terminals of the cerebellum, and that they contribute to the regulation of synaptic plasticity. Our previous results in chapter 4 revealed the following: in coronal slices, ML stimulation produces SyGCaMP2 responses that are beam-like and that remain apparent in the presence of PTX/DNQX, suggesting a significant component is from the PFs themselves. Therefore, in this chapter, we are making the most of this to better understand whether NMDAR modulation affects presynaptic calcium. The specific aims of this chapter are: 1) to examine whether NMDARs presence on presynaptic terminals and modulate synaptic transmission. We therefore sought to examine the effects of activating NMDARs by NMDA in the presence of its co-agonist, glycine (Gly), on SyGCaMP2 fluorescence and synaptic field potentials recorded from the ML of the cerebellar cortex; 2) to establish how the proportion of the total SyGCaMP2 fluorescence signal in response to ML stimulation directly originates from the presynaptic PF terminals under these experimental conditions, in which aCSF contained a low concentration of magnesium ions in the presence of the GABA/glycine receptor antagonist PTX. Therefore, we examined the effects of

AMPA receptor inhibition on SyGCaMP2 fluorescence and the synaptic field potentials recorded from the ML; 3) to examine whether NMDARs were present on PF terminals – as opposed to presynaptic terminals – of synaptically connected interneurons such as BSs or SCs. We therefore sought to examine the effects of activating NMDARs with NMDA/glycine on SyGCaMP2 fluorescence and synaptic field potentials recorded from the ML in the presence of the AMPAR inhibitor DNQX and PTX; 4) to confirm whether the effects of NMDA/Gly on SyGCaMP2 fluorescence responses and whether the N2 component of fEPSPs are indeed mediated via NMDARs. Therefore, we examined the effects of NMDARs activation by NMDA and glycine in the presence of NMDA receptor antagonist AP5 on SyGCaMP2 fluorescence and synaptic field potentials recorded from the ML; 5) to test whether the activation of NMDARs changes the resting presynaptic calcium. Therefore, we sought to examine the effects of the activation of NMDAR with and without the presence of AP5 on the baseline SyGCaMP2: mCherry ratio; and 6) to establish whether the effects of NMDA/Gly are due to a reduction in the size of the SyGCaMP2 fluorescence response per bouton or whether there is a change in the number of boutons contributing to the total SyGCaMP2 fluorescence response. Therefore, we sought to examine the effects of activation of NMDAR on single presynaptic bouton responses.

As outlined in the introduction (section 1.4), localizing SyGCaMP2-mCherry to synaptic terminals allowed us to measure the activity of presynaptic calcium-dependent fluorescence across enormous groups of neurons in the coronal cerebellar slices by capturing images using an epifluorescence microscope. It also allowed us to measure the activity of presynaptic calcium-dependent fluorescence through individual presynaptic boutons using a multiphoton microscope. Using measurements of presynaptic calcium signalling alongside extracellular field potential recordings over time at PFs to PCs synapses with electrical stimulation and pharmacological manipulations provided a greater understanding of how the alteration of presynaptic calcium can influence synaptic transmission and plasticity in this region of the brain.

5.2 Results

NMDARs exhibit a voltage dependency due to their channels being blocked at resting membrane potentials by extracellular Mg^{2+} (Purves et al., 2012, Mayer et al., 1984). As a consequence, NMDARs' contribution to postsynaptic response is relatively small during normal synaptic activity. In chapter 4, it was demonstrated that under normal conditions of synaptic activation there was little if any evidence that NMDA receptors contributed to either calcium influx into presynaptic boutons, the PF volley, or the postsynaptic response. Therefore, in this chapter, experiments were performed using an extracellular solution that contained 0.6 mM of extracellular Mg^{2+} as we usually used extracellular solution which contained 1.2 mM of extracellular Mg^{2+}. The effects of NMDA and its co-agonist Gly were examined in response to high-frequency stimulation of PFs. For each of the experiments illustrated in this chapter, the reduced magnesium aCSF was also supplemented with picrotoxin to block $GABA_AR$ and glycine receptors. Coronal cerebellar slices (300 µm thick) were obtained from the brains of young adult SyG37 as previously described.

5.2.1 Effects of NMDA receptor activation with extracellular perfusion with NMDA and glycine

The aim of this section was to investigate the role of NMDARs in modulating synaptic transmission and plasticity. In order to do this, we first aimed to reproduce a set of previously published results (Casado et al., 2000), where the application of NMDA (30 µM) and Gly (10 µM) in a low magnesium solution (aCSF) was found to lead to a significant and transient reduction of the postsynaptic current (EPSC) between the PF and PC synapse in cerebellum slices of adult rats. We then attempted to determine whether this depression was accompanied by a change in SyGCaMP2 fluorescence responses within the cerebellar ML region as evidence for presynaptic calcium signalling. Coronal cerebellar slices were obtained from the brains of young adult SyG37 mice. Stimulating electrodes were placed on the surface of the ML to activate the PFs, while recording electrodes were placed in the

ML above the PC (for details see chapter 2, Figure 2.6 and chapter 4, section 4.2.1.1). The extracellular field potential technique was used to record synaptic activity in the ML in response to pairs of stimuli, separated by 50 ms at an intensity of 30 V and repeated every 10 s. In combination with these electrophysiological recordings, epifluorescence imaging was used to record SyGCaMP2-mCherry fluorescence as an indicator of presynaptic calcium signalling. Images that were 760 x 760 pixels in size were obtained from the same locations as the electrophysiological recordings using trains of 20 stimuli delivered at 50 Hz at 5-minute intervals. Stable baselines for extracellular field potentials and SyGCaMP2-mCherry responses were recorded for at least 10 minutes prior the perfusion of drugs. NMDA and Gly were applied for 10 minutes, then replaced with a low Mg^{2+} aCSF so that its wash out could be followed for a further 25 minutes. Data were normalized to a baseline and expressed as percentages. The PPR was also calculated and plotted over time. The change in PPR was used as a possible indicator of a presynaptic site of action (Debanne, 1996, Zucker, 1989). The results were presented as mean ± SEM.

Measuring SyGCaMP2 fluorescence (F/F_0) and fEPSP responses under baseline conditions and the application of perfusions of NMDA/Gly (as shown in Figure 5.1, 5.2 and 5.3) showed the clear effects on both the SyGCaMP2 fluorescence and fEPSP responses. Bath application of NMDA, with its co-agonist Gly, for 10 minutes led to a pronounced decrease in the fEPSP slope to paired stimulation of PFs, which averaged 40.33 ± 7.95% of the control value (Figure 5.3 B and C, N = 6, P = 0.0078, Friedman test followed by Dunn's multiple comparison *post-hoc* test). This depression was completely reversible by washing out the agonists. On the other hand, the N1 component remained unchanged, averaging 99.27 ± 2.36% of the baseline response (Figure 5.3 F and G, N = 6, P = 0.4964, Friedman test followed by Dunn's multiple comparison *post-hoc* test). These results corroborated previous findings reported in the literature (Casado et al., 2002, Casado et al., 2000), with the exception that the PPR was significantly increased (Figure 5.3, D and E, control: 0.94 ± 0.15 NMDA and Gly: 1.97 ± 0.39, n = 6, P = 0.02, repeated measures ANOVA test with the Tukey *post-hoc* test).

Perfusion of NMDA/Gly produced an initially insignificant increase (after 5 min) in the SyGCaMP2 fluorescence response (F/F_0) which averaged 102.05 ± 1.614 and

101.94 ± 1.56% relative to the baseline for the peak and slope of the SyGCaMP2 responses, respectively (SyGCaMP2 Peak: P = 0.9; SyGCaMP2 Slope: P = 0.9; n = 6, Friedman test followed by Dunn's multiple comparison *post-hoc* test). Then, in a manner consistent with that of N2 fEPSP (after 10 min), this perfusion produced a significant reduction in the SyGCaMP2 fluorescence response (F/F_0) which averaged 90.83 ± 2.68 and 92.02 ± 2.65% relative to the baseline for the peak and slope of the SyGCaMP2 responses, respectively, as shown in Figure 5.1 B, C, D and E (SyGCaMP2 Peak: P = 0.0058; SyGCaMP2 Slope: P = 0.0058; n = 6, Friedman test followed by Dunn's multiple comparison *post-hoc* test).

Figure 5.2 B, C and D show heat maps with identical scales that illustrate the spatial changes in SyGCaMP2 florescence in response to the electrical stimulation of ML under the control conditions (B), the perfusion of 30 μM NMDA and 10 μM Gly (C), and after washing out (D). In this map, SyGCaMP2 florescence was clearly sensitive to the application of NMDA/Gly as its fluorescence was found to decrease in the presence of NMDA/Gly compared with the control conduction. This decrease was recovered later after washing out, as shown in Figure D. In other words, Figure 5.2 shows that stimulation within the ML produced a beam-like responsive area that may well be PFs (B). NMDA affects the size of this beam (C), which is the recovery after washing out (D). This result suggests that NMDA may well be located on PFs.

To summarise, these results suggest that NMDA receptors are located on presynaptic terminals (most likely on PFs) and could potentially modulate synaptic transmission.

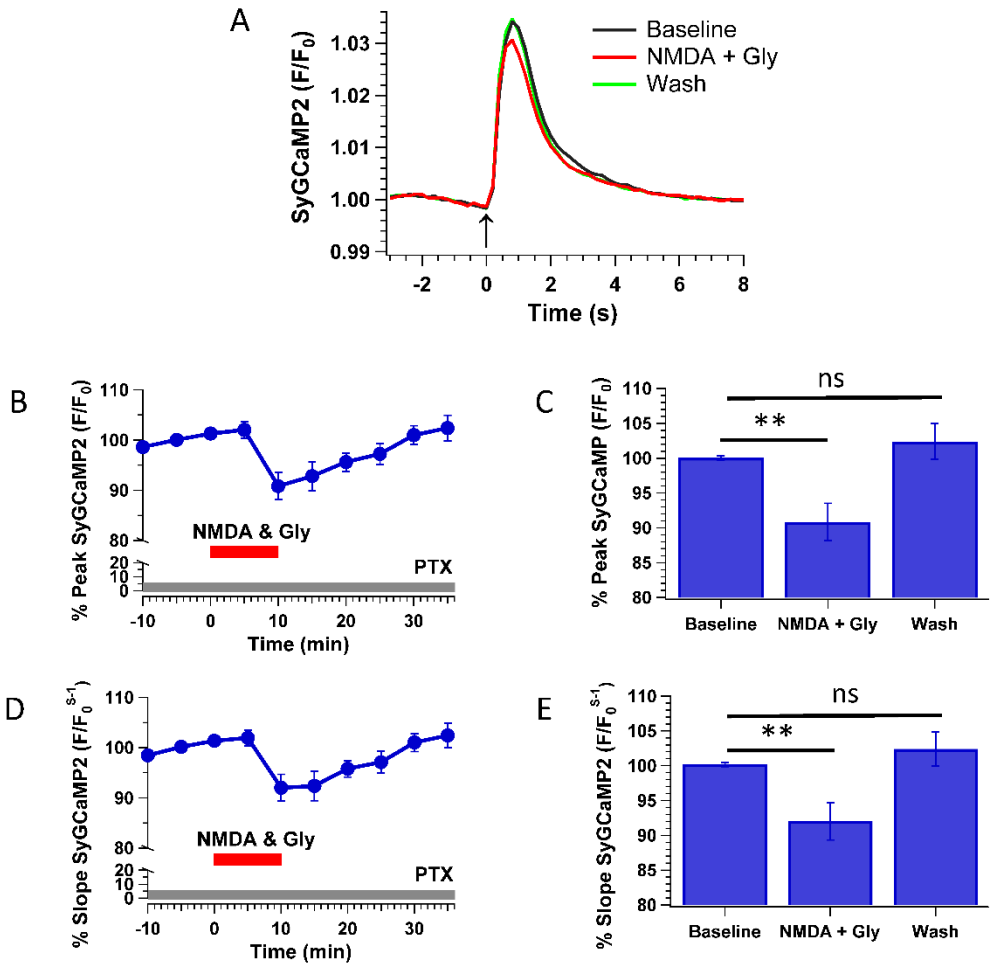

Figure 5.1. Effects of applications of NMDA and glycine on SyGCaMP2 fluorescence to ML stimulation. (A) shows examples of responses of SyGCaMP2 fluorescence in response to electrical stimulation during baseline conditions (black), application of NMDA/Gly (red) and 25 minutes after washout (green). Measurements were obtained from regions of interest (ROIs) placed within the molecular layer (ML) of the cerebellar cortex. (B, D) show the effects of NMDA/glycine on the peak and slope of the SyGCaMP2 responses expressed as a percentage of baseline values, respectively. The red horizontal bar shows duration of NMDA/glycine application. The grey horizontal bar illustrates that PTX was included in aCSF throughout. (C, E) show summaries of the data recorded during baseline conditions, drug application, and washout for the peak and slope SyGCaMP2 fluorescence responses, respectively. Arrow in (A) shows the onset of electrical stimulation. Data were presented as normalized mean ± SEM (n = 6).

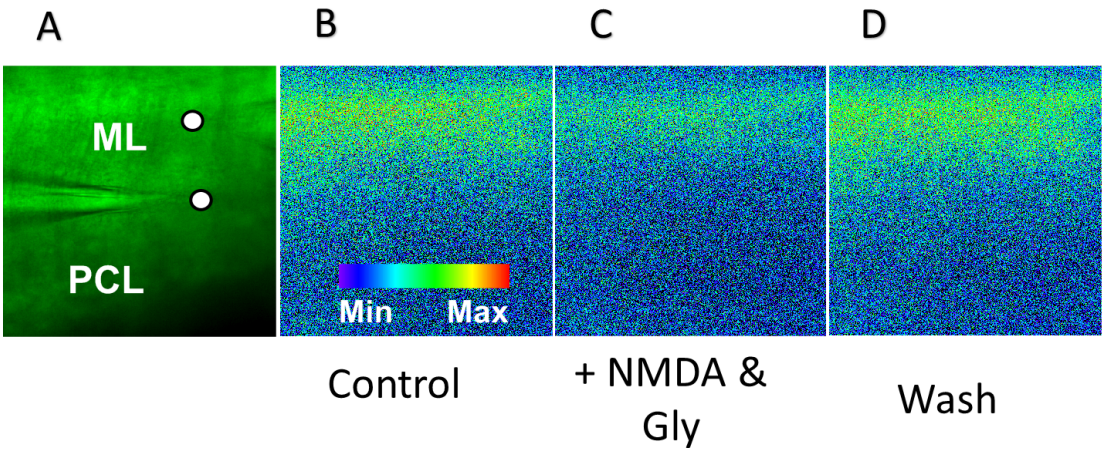

Figure 5.2. Visualization of the effects of NMDA/Gly on SyGCaMP2 fluorescence responses to cerebellar ML stimulation. (A) a transmission image of a coronal cerebellar slices with a green lookup table applied that shows the positions of stimulating and recording electrodes with respect to the different layers of the cortex. The upper white circle indicates the position of the stimulating electrode position and the lower circle indicates the position of the recording electrode. The averages of three sequential SyGCaMP2 images were taken immediately prior to stimulation. These were subtracted from the peak responses taken during electrical stimulation to create a subtraction image during baseline conditions (B). (C) shows the application of 30 µM NMDA and 10 µM Gly, and (D) after washout, respectively. A fixed scale with a warm/cold lookup table was used to show the differences in the magnitudes of each of the responses under each of these three different conditions.

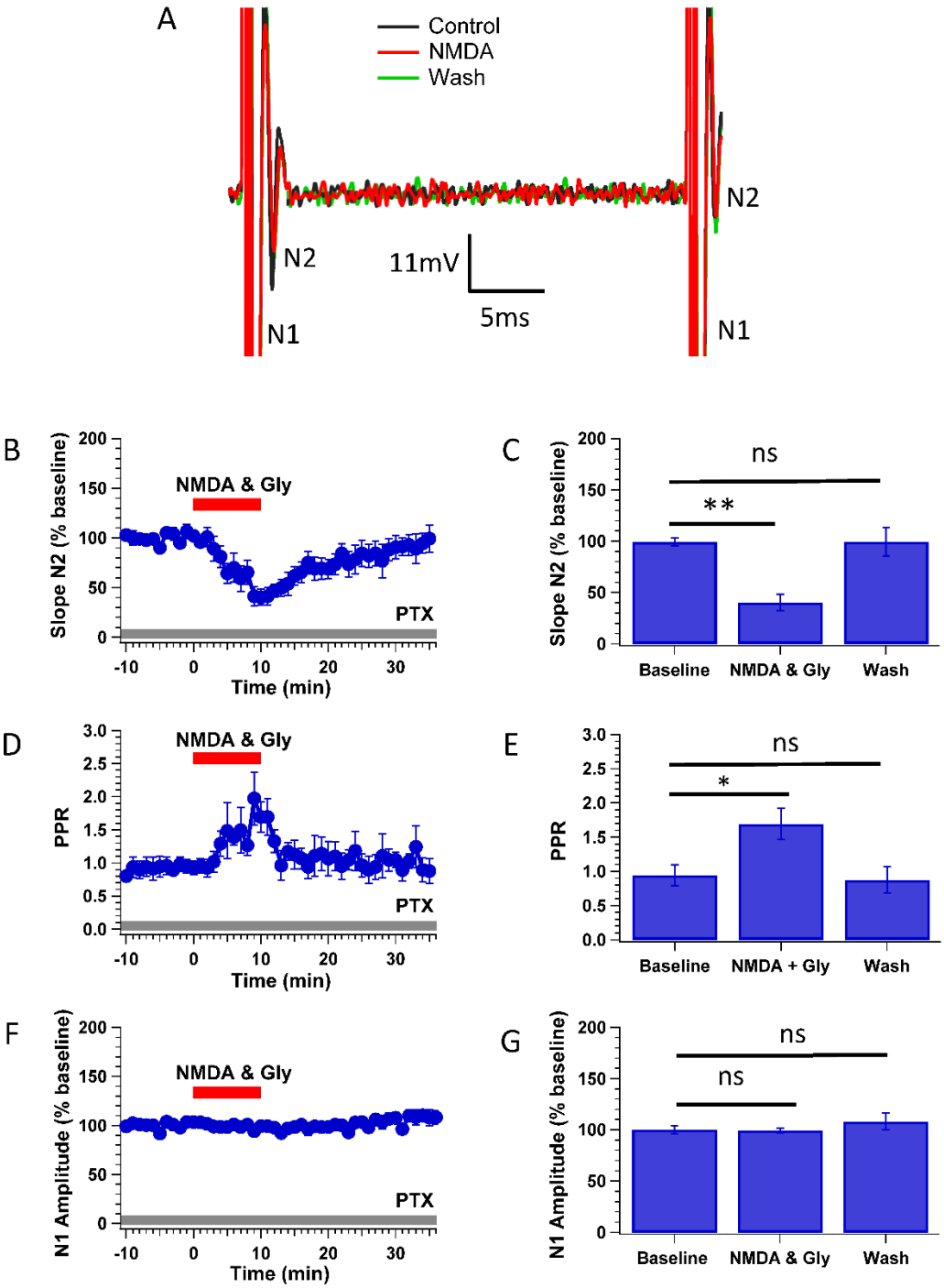

Figure 5.3. Effects of perfusion of NMDA and glycine on fEPSP responses. (A) shows examples of extracellular field potentials recorded simultaneously. The N1 component corresponds to the PF volley, whilst the N2 component represents the post-synaptic response to stimulation. The colour coding is the same for the data presented in panel 5.1A. (B, D and F) show the effects of applications of NMDA/Gly on the initial slope of the N2 component, the N2 PPR and the N1 amplitude of fEPSPs. As in previous Figures (Figure 5.1), the red horizontal bar shows the duration of NMDA/Gly application. The grey horizontal bar indicates that PTX was present throughout. (C, E and G) are bar charts summarising the results for baseline, drug application and washout for N2, PPR and N1. Data are presented as normalized mean ± SEM (n = 6).

5.2.2. Effects of AMPA receptor inhibition

My previous study demonstrated that the SyGCaMP2 response to ML stimulation was reduced by roughly 10% in coronal cerebellar slices after both $GABA_A$Rs and AMPARs blockade, indicating that > 90% of the total response originated from PFs. In this section, we sought to identify the total SyGCaMP2 fluorescence originating directly from first-order presynaptic terminals under these same experimental conditions. Accordingly, we repeated the experiments described in section 5.2.1 except that we applied the AMPAR antagonist, DNQX (10 µM, 30 min) instead of NMDA/Gly. DNQX is known to block synaptic transmission at the cerebellar synapses formed between PFs and PCs, as shown previously in chapter 4 (Bergerot et al., 2013). After recording a stable baseline for the synaptic activity that was evoked by stimulation of the PFs for at least 10 minutes, bath application of DNQX (10 µM) was used for 30 minutes and washed off for a further 45 minutes with standard aCSF which contained a lower concentration of magnesium ions and was supplemented with 10 µM PTX to inhibit $GABA_A$R, as mentioned above (section 5.2.1).

The results of these experiments are shown in Figure 5.4. Bath perfusion of DNQX for 30 minutes selectively blocked excitatory transmission as expected. The peak amplitude of the N2 component of the fEPSP decreased to 29.6 ± 7.57% of baseline levels after 30 minutes (Figure 5.4, C and D, n = 9, Friedman test followed by Dunn's multiple comparison post-hoc test: P = 0.0003).The N1 component of the fEPSP was not affected, indicating that the inhibition of AMPARs did not affect the size of the PF volley (Figure 5.4, E and F).

Perfusion of DNQX had no significant effect on SyGCaMP2 responses to ML stimulation (Figure 5.4 H, J, L). 30 minutes after DNQX application, the peak response was 92.81 ± 3.56% of baseline (P = 0.1979), the slope was 90.05 ± 4.61% of baseline, (P = 0.1187) and the AUC was 92.69 ± 3.58% of baseline (P = 0.1979; Friedman test followed by Dunn's multiple comparison *post-hoc* test; n = 9; Figure 5.4 G, I, K). These results indicate that the majority (> 90%) of the SyGCaMP2 florescence responses (F/F_0) originated from the presynaptic terminals of PFs. The remaining 10% of the total response most likely originated from synaptically

connected presynaptic terminals on other cell types within the ML that are driven via AMPARs.

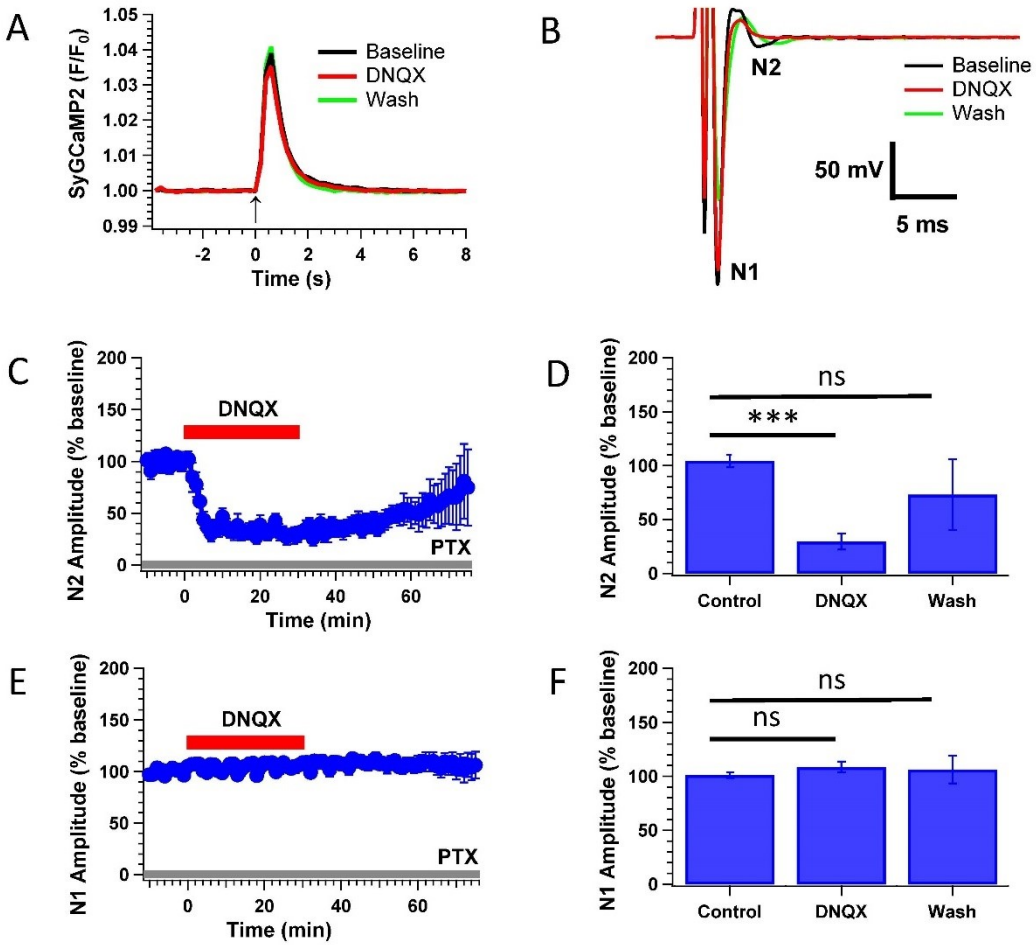

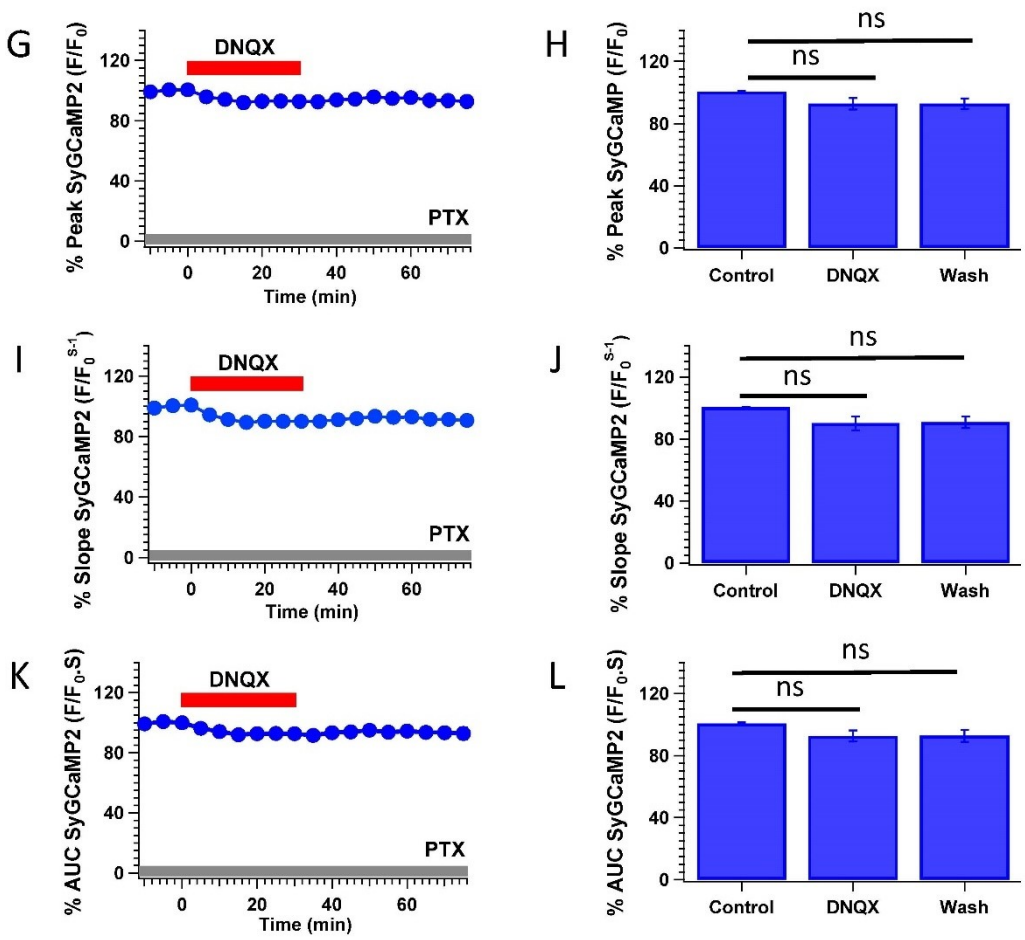

Figure 5.4. Effects of AMPA receptor inhibition. The data presented are as shown in Figure 5.1 and 5.3, except for the red horizontal bar which illustrates the 30-minute period of 10 µM DNQX application and the washout period of 45 minutes. Data are presented as normalized mean ± SEM (n = 9).

5.2.3 Effects of NMDA/Gly application in during pharmacological blockade of AMPA and $GABA_A$ receptors.

The results in section 5.2.1 established that applications of NMDA/Gly led to a reduction in SyGCaMP2 fluorescence (F/F_0), a reduction in N2 peak amplitude and increase in PPR. We next repeated these experiments but in the additional presence of the AMPAR antagonist, DNQX, to whether these effects originated from PF terminals or whether some of the total SyGCaMP2 fluorescence response originated from presynaptic terminals of other cell types within the ML and thus including that are connected via AMPA receptors, such as SCs and/or BCs. The inclusion of PTX and DNQX ensured that we blocked the majority of the excitatory

and inhibitory synapses that may have been activated as a result of direct stimulation of these cell types or indirectly via activation of PFs. Whilst the presence of DNQX and PTX prevented us from recording the N2 synaptic component of the fEPSP, we were able to record N1 whilst isolating the SyGCaMP2 fluorescence response that originated directly from the presynaptic terminals. Data were recorded and analysed and presented as for Figures 5.1 and 5.3. The results, as shown in Figure 5.5, illustrated that application of NMDA/Gly resulted in a significant reduction in the SyGCaMP2 fluorescence responses that could be raised directly from PF terminals, and which averaged 90.02 ± 2.78% and 91.03 ± 2.70% of the baseline in their peak and slope SyGCaMP2 responses, respectively (Figure 5.5 C and E, Peak: N = 9, P = 0.0039, Wilcoxon matched pairs test; slope: N = 9, P = 0.0039, Wilcoxon matched pairs test). This depression did not recover on washout of NMDA/Gly for 30 minutes. The N1 component of the fEPSP remained unchanged, averaging 102.17 ± 4.78% (Figure 5.5 G and H, N1: N = 9, P = 0.6523, Wilcoxon matched pairs test), indicating that the activation excites a similar number of PFs both before and during NMDA/Gly application.

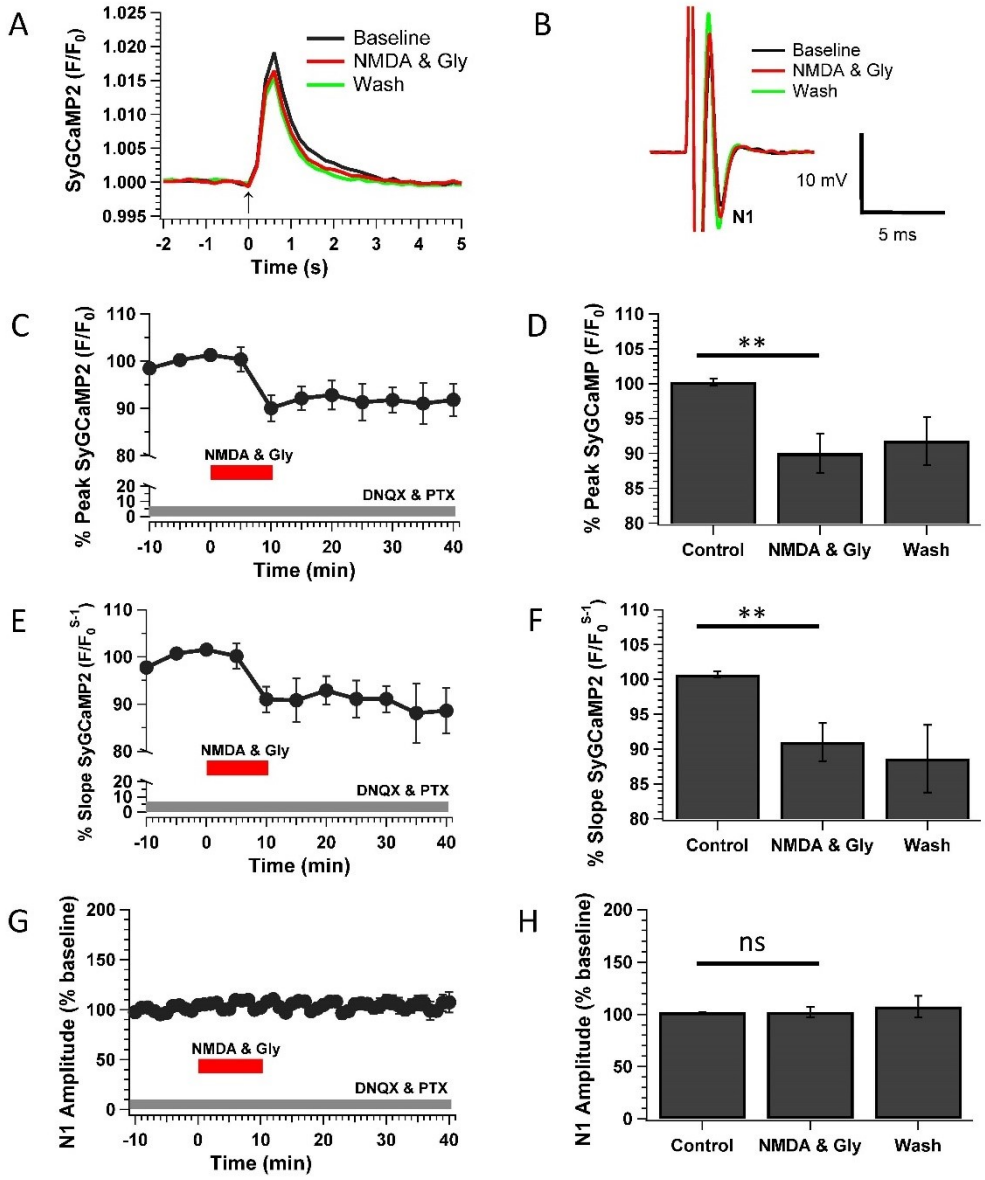

Figure 5.5. Effects of NMDA receptor activation in the presence of a pharmacological blockade of AMPA and $GABA_A$ receptors. Data are presented in the same manner as Figure 5.1 and 5.3 except that washing out the agonists took 30 minutes and colours here are black.

5.2.4 Effects of NMDAR activation in the presence of NMDAR antagonist AP5

We next aimed to confirm that the effects of NMDA/Gly on SyGCaMP2 fluorescence responses and the N2 component of fEPSPs were indeed mediated via NMDARs. A competitive antagonist of NMDAR, AP5, is known to prevent the effects of NMDA on the PF-PC EPSC in cerebellum slices of adult rats (Casado et al., 2000, Casado

et al., 2002). Therefore, we repeated the same experiments described in section 5.2.1 but in the continued presence of AP5. The results of these experiments showed that under these conditions, applications of NMDA/Gly failed to induce any depression in either SyGCaMP2 fluorescence (F/F_0) or fEPSP slope as shown in Figure 5.6 (SyGCaMP2 peak, P = 0.065; SyGCaMP2 slope, P = 0.065; slope N2, P = > 0.999; PPR, P = 0.570; N1, P= 0.314; n = 7, Friedman test followed by Dunn's multiple comparison post-hoc test).

Taken together, these data suggest that preNMDAR activation is indeed necessary to induce depression. Moreover, it suggests that preNMDARs indeed modulate synaptic transmission.

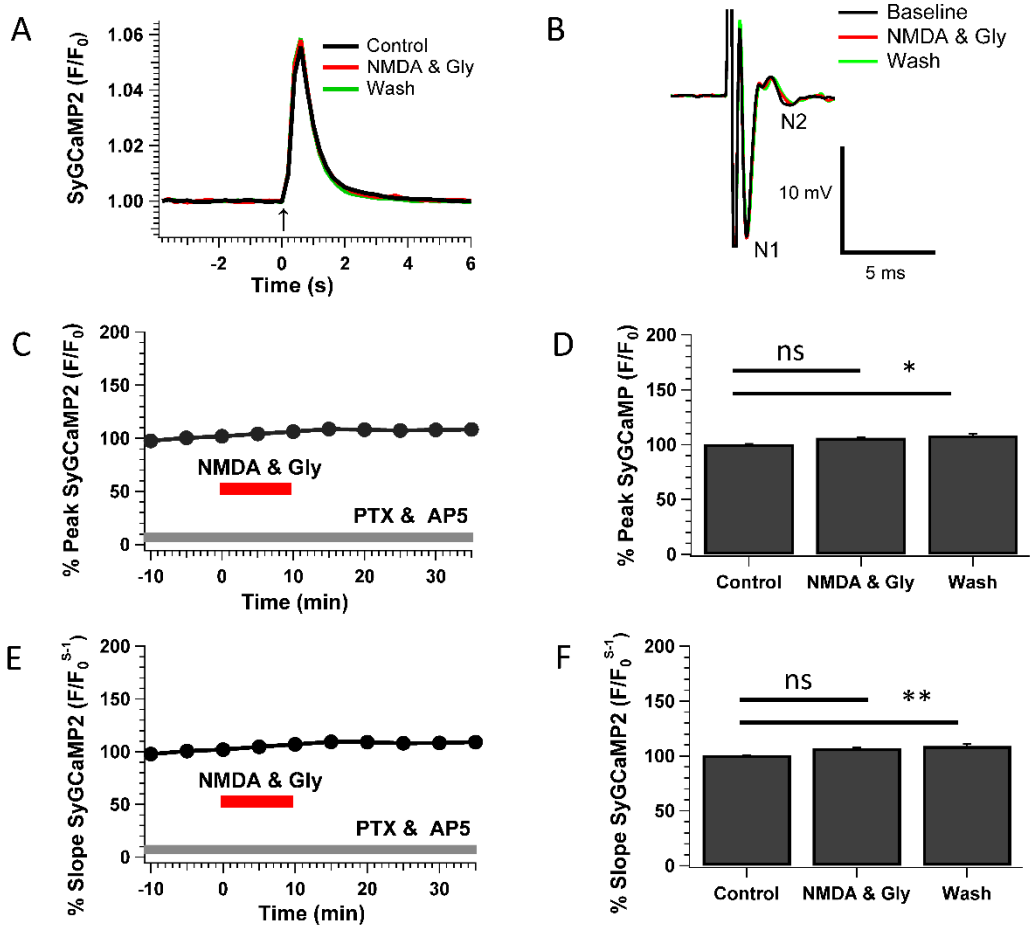

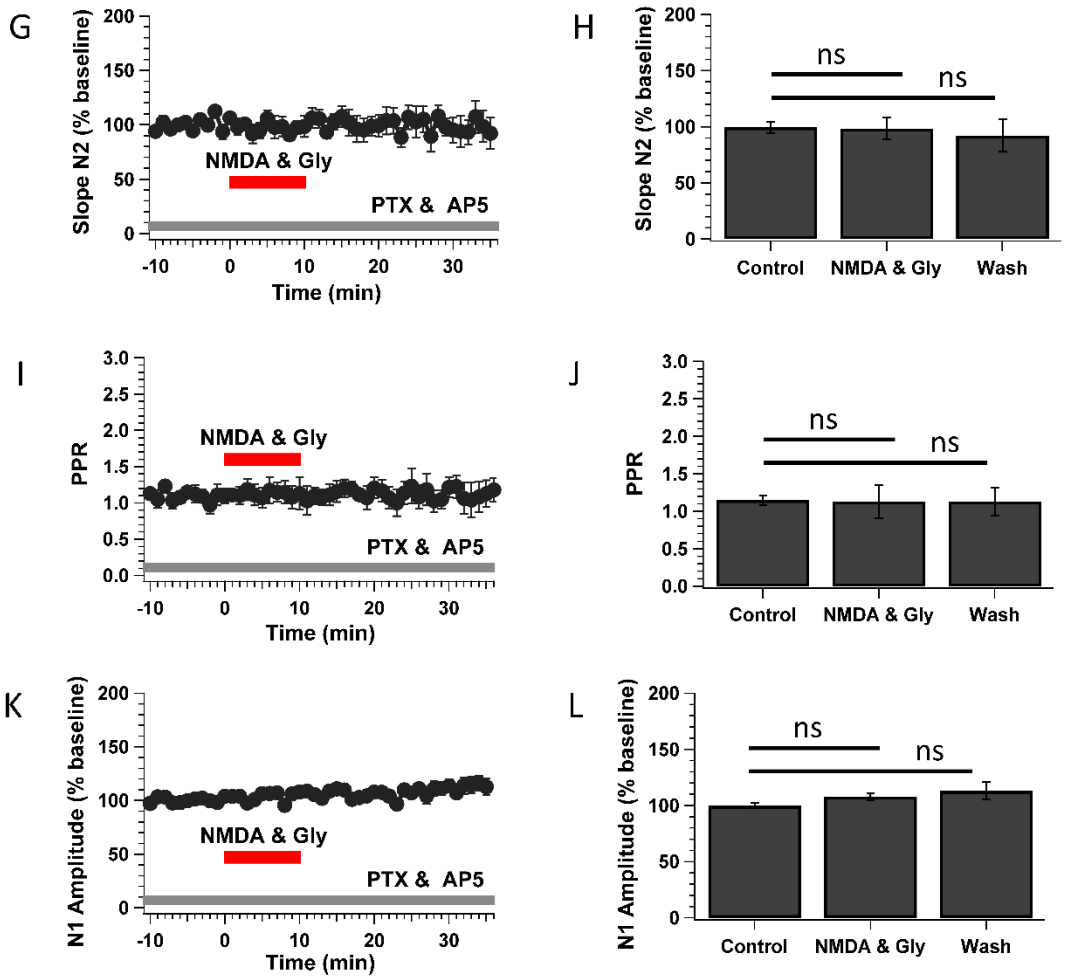

Figure 5.6. Effects of NMDA receptor activation in the presence of a pharmacological blockade of NMDA receptor blocker. Data are presented in the same manner as Figure 5.1 and 5.3 except that a low magnesium aCSF was also supplemented by AP5.

The bar charts in Figure 5.7 indicated that NMDA induced the depression of SyGCaMP2 (SyG) and initial slope of the fEPSP (N2) but not on the presynaptic fibre volley (N1). These effects were blocked in the presence of AP5. Together, these results suggest that NMDARs originate from PF terminals and modulated synaptic transmission. Moreover, it also suggests that presynaptic NMDAR activation is indeed necessary to induce depression. In the next section, we will examine whether activation of NMDAR has effect on baseline level of SyGCaMP2: mCherry ratio with and without the presence of AP5.

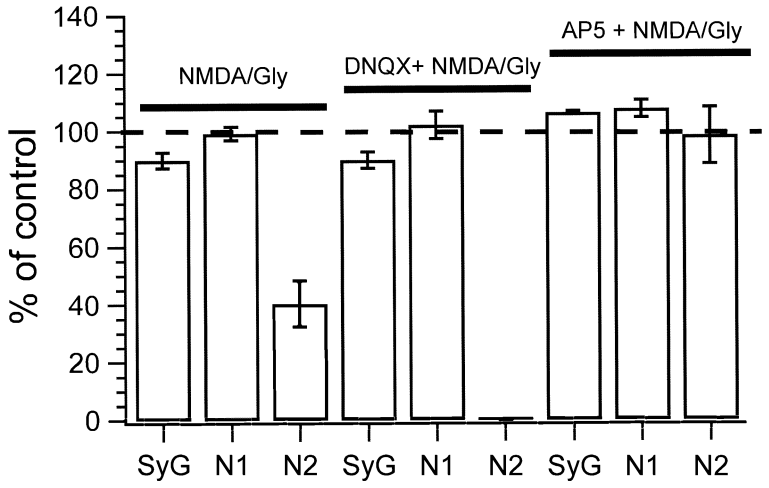

Figure 5.7. Pharmacological characterisation of the NMDA/Gly-induced depression of SyGCaMP2 and synaptic transmission responses. The bar chart illustrates the effects of (measured after 10 minutes of NMDA/Gly application) NMDA/Gly, NMDA/Gly in the presence of DNQX and NMDA/Gly in the presence of AP5 on peak SyGCaMP2 (SyG), a presynaptic fibre volley (N1) and the fEPSP slope (N2) under our experimental conditions. Data were presented as normalized mean ± SEM.

5.2.5 Effects of activation of NMDAR with and without the presence of AP5 on baseline level of SyGCaMP2: mCherry Ratio

We finally attempted to determine whether the activation of NMDAR has any effect on the baseline SyGCaMP2: mCherry ratio. To do so, we measured the ratio for the SyGCaMP2 to mCherry baseline fluorescence of the effects of NMDA receptor activation with and without the presence of the NMDA receptor antagonist, AP5, from previous data, as recorded in the experiments described in sections 5.2.1 and 5.2.4, respectively. The ratio was analysed and calculated using the Igor Pro software and Microsoft Excel, also as described previously (for details see Materials and methods, section 2.7.2.1). Finally, data were normalised and presented as mean ± SEM. The results, as illustrated in Figure 5.8 D (left), revealed that activation of NMDARs via the bath perfusion of NMDA/Gly for 10 minutes resulted in an initial and significant increase above baseline levels of resting calcium within presynaptic terminals, followed by a decline that washed off (Figure 5.8, baseline: 0.9996 ±

0.0008; NMDA/Gly: 1.0081: ± 0.0043, P = 0.0094; Wash: 1.0035 ± 0.0020, P= 0.3146; n = 9, Friedman test followed by Dunn's multiple comparison post-hoc test). These effects of NMDA were completely negated in the presence of the competitive NMDAR antagonist, AP5 (50μM), as per Figure 5.8 D (right), indicating that the effects of NMDA/Gly are mediated via NMDARs. Together, these results indicate that the activation of NMDARs led to an increase in the baseline fluorescence levels in the bouton. This led to the suggestion that the peak amplitude remains consistent. Therefore, when we measured the SyGCaMP2 fluorescence (F/F_0) response (section 5.2.1), it appeared that the response was going down but in actual fact it may just have been that the baseline was going up. Although the adjustment of the baseline ratio may still be unstable, both results in Figure 5.8 D (left and right) also indicated that NMDAR are located in presynaptic side and are responsible for modulation of SyGCaMP2 responses. More importantly, it indicated that the mCherry fluorescence was insensitive to calcium changes in the presynaptic boutons. In the next section, we will examine whether NMDA/Gly lowers bouton numbers or the amount of calcium per bouton or both.

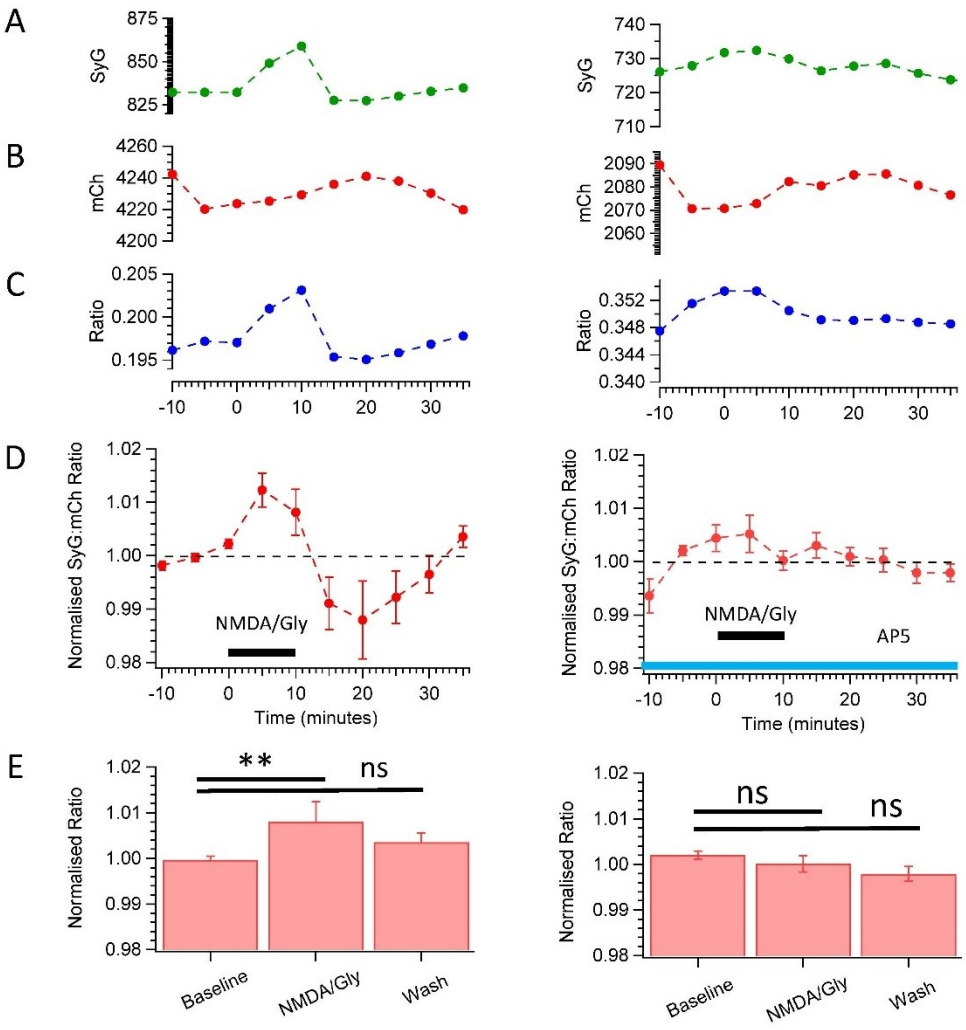

Figure 5.8. Effects of activation of NMDAR with and without the presence of AP5 on the baseline ratios. Panels (A, B, C) on the left show examples of the effects of 30 µM NMDA/10 µM Gly on the baseline fluorescence of SyGCaMP2 (A), mCherry (B), and the SyGCaMP2: mCherry ratio (C). Panels (A, B, C) on the right also present examples in the same manner, but as recorded in the presence of AP5. Panel (D) shows the effects of 30 µM NMDA/10µM Gly on the baseline fluorescence of SyGCaMP2: mCherry. Panel (D) on the right shows the effects of 10 µM NMDA/10 µM Gly on the baseline fluorescence of SyGCaMP2: mCherry in the presence of AP5. The black horizontal bar shows the 10-minute period during which 30 µM NMDA/10 µM Gly was applied, while the blue horizontal shows the 35-minute period over which AP5 was continuously applied. Panel (E) on the left and right summarises the data during baseline, NMDA application for 10 minutes, and after 25 minutes of washout of NMDA for each of these datasets. Data were presented as normalized mean ± SEM (n = 9).

5.2.6 Effects of NMDAR activation on single presynaptic bouton responses

The results presented so far indicate that activation of NMDARs leads to a decrease in SyGCaMP2 fluorescence originating from the presynaptic terminals of PFs. We next attempted to establish whether these effects of NMDA/Gly were due to a reduction in the size of the SyGCaMP2 fluorescence response per bouton or whether there was a change in the number of boutons contributing to the total SyGCaMP2 fluorescence response.

For these experiments, we used a multiphoton microscope since it is possible to detect single boutons responses in SyG 37 mice (Al-Osta et al., 2018). A low magnesium aCSF in the presence of picrotoxin was also used throughout. A stimulating electrode was placed onto the surface of the slice in the ML (Figure 5.9 A). Views of size 512 x 512 were selected at begging to help select a target size of 512 x 64 pixels at the ML (Figure 5.9 B). Then, stacks of images (of dimensions 512 x 64 pixels) were captured from the ML using a multiphoton microscope as described previously (see Materials and methods, section 2.6).

The data presented in Figure 5.10 indicate that the application of NMDA/Gly for 10 minutes resulted in a small reduction in the peak response of the responding puncta (Baseline: 1.193 ± 0.038; NMDA/Gly: 1.169 ± 0.027, Friedman test followed by Dunn's multiple comparison post-hoc test: P = 0.223, n = 6. See Figure 5.10, C and D) but that this did significantly reduce the number of responding puncta (Baseline: 92.33 ± 2.072; NMDA/Gly: 81.16.83 ± 3.279, Friedman test followed by Dunn's multiple comparison post-hoc test: P = 0.0023, n = 6, Figure 5.10A and B). Interestingly, peak response and the number of responding puncta completely recovered after washing for 25 minutes with the low magnesium aCSF in the presence of PTX. This result indicates that NMDA/Gly lowers bouton numbers significantly but has no effect on the amount of calcium per responding bouton. This led to the suggestion that the reduction in fluorescence from the whole frame that we observed during activation of NMDARs (Figure 5.1) was most likely due to a large reduction in the number of responding puncta as this leads to a reduction in the average fluorescence response.

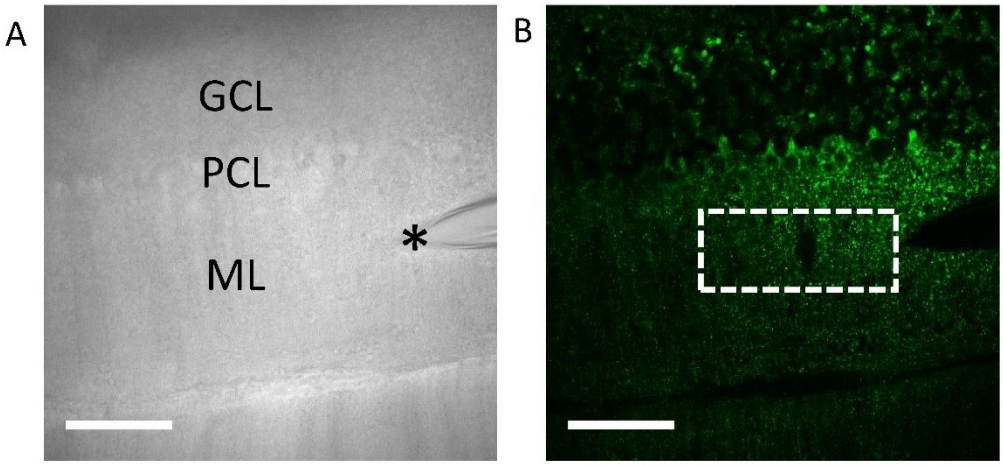

Figure 5.9. Positive modulation of NMDA reduces the number of responding puncta but fails to effect the puncta size in response to ML stimulation. Panel (A) illustrates a light transmission image of a coronal cerebellar slice (300 µm thick) including the ML, GCL and PCL regions. The asterisk (black) shows the location of the stimulating electrode at the ML. Panel (B) Higher magnification photomicrographs show expression patterns of SyGCaMP2 with different layers, as indicated by the images shown in panel (A). Images of 512 by 512 pixels were captured using an excitation wavelength of 920 nm. The scale bars in A and B are 100 µm.

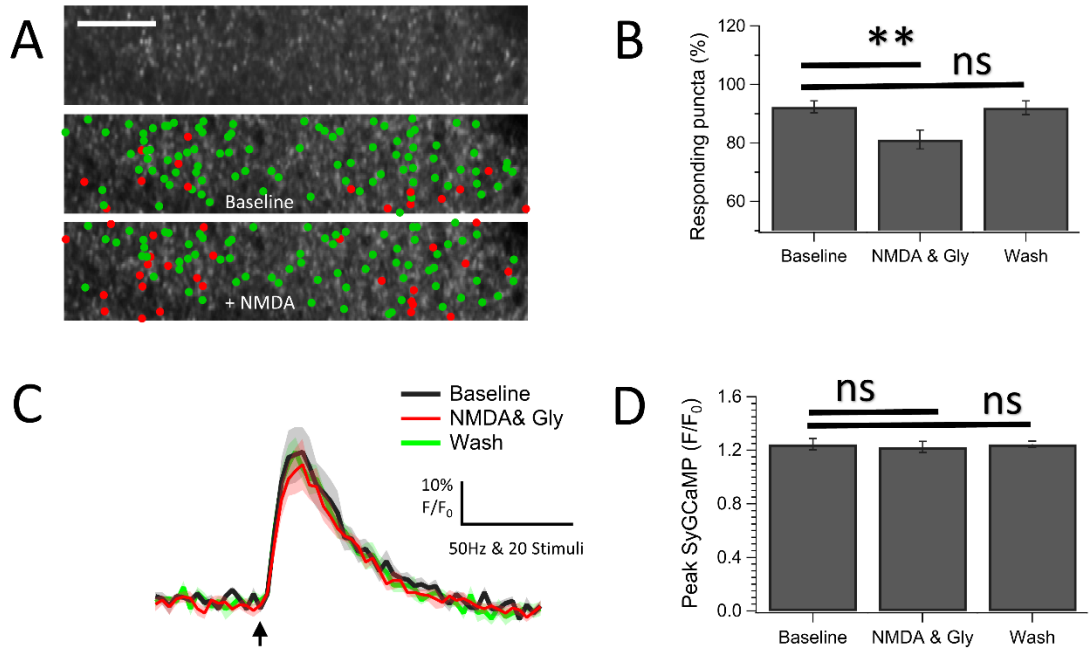

Figure 5.10. Positive modulation of NMDA reduces the number of responding puncta but fails to effect the puncta size in response to ML stimulation. (A) The grayscale image (size 512 x 64 pixels: corresponding to 212.5 x 26.6 µm) shows the typical punctate expression observed in ML cerebellum region, as indicated by the dashed box in the images shown in panel 5.9B. Shown below are images representing responding (green dots) non responding puncta (red dots) during control conditions (middle image) and following perfusion with NMDA and Gly (bottom image) in responses to 50 Hz (20 pulses) stimulation to the ML. The scale bar represents 10 µm. The fluorescence mean value prior to electrical activation (F_0) was calculated and any subsequent change in absolute fluorescence (F) expressed as a ratio of (F/F_0) and plotted against relative time. (C) illustrates the average of the responding puncta during baseline (black trace), application of NMDA/Gly (red trace) and for washout (green trace). Arrow indicates the onset of electrical stimulation. The bar chart (D) summarises the data during baseline, NMDA/Gly application and washout periods for each of these datasets, whereas the second bar chart (B) shows the number of puncta that responded to electrical stimulation during baseline, application of NMDA/Gly and washout. Data are presented as mean ± SEM (n = 6).

5.3 Discussion

The set of experiments in the present study were designed to investigate the role of presynaptic NMDA receptors at cerebellar PFs to PC synapses using a novel, transgenic mouse that expresses a SyGCaMP2-mCherry sensor selectively in its

presynaptic terminals. A combination of the extracellular field potential and optical techniques was carried out in the ML region to record the associated synaptic field potentials, and SyGCaMP2 fluorescence responses were induced via extracellular stimulation of the PFs using pharmacological manipulation to determine whether NMDAR were responsible for any presynaptic actions. Under our experimental conditions, imaging data indicated that inhibition of AMPARs by DNQX reduced the SyGCaMP2 fluorescence response (F/F_0) by only 10% (Figure 5.4 G, I and K), with an associated decrease of approximately 70% in synaptic transmission to PF stimulation (Figure 5.4, C and D). These findings suggest that, under these conditions, the majority (90%) of the total SyGCaMP2 fluorescence response arises directly from presynaptic terminals, with the remaining 10% arising through the contributions made by presynaptic terminals that are postsynaptic to the presynaptic terminals as a result of a synaptic excitation process driven by AMPARs. Therefore, in the presence of AMPAR blockade (and in the presence of PTX), the SyGCaMP2-mCherry sensor allows us to measure changes in calcium levels at the presynaptic PF terminals and by blocking $GABA_A$ and AMPARs to distinguish between the relative contributions of mono- and polysynaptic responses to synaptic activity.

Reduction of evoked SyGCaMP2 fluorescence responses with and without 10 µM DNQX at ML regains by NMDA as confirmed the presynaptic locus of the NMDAR.

In the present study, we have demonstrated that the activation of NMDAR via the bath application of NMDA and Gly produced a reversible decrease in SyGCaMP2 fluorescence (F/F_0) and a concomitant decrease in the N2 (post-synaptic) component of the fEPSP (Figure 5.1 B, D and Figure 5.3 B and C). This decrease in the N2 slope was accompanied by an increase in the PPR (Figure 5.3D and E), suggesting a presynaptic site of action. Electrophysiological recordings of the N1 component of the fEPSP were not affected by NMDA/Gly, suggesting that the baseline excitability of the parallel fibres was unaltered. The result in Figure 5.2 illustrated that the beam-like pattern of fibre activation following ML activation was not altered in the presence of NMDA/Gly but the intensity of the signal along the activated beam was clearly reduced. Along with the quantitative decreases in peak SyGCaMP2 responses, these observations suggest that NMDA/Gly has a

presynaptic effect that alters transmitter release but that this is not achieved by changing the excitability of PFs. Our data are consistent with the possibility that NMDAR activation reduces the amount of calcium that enters the terminal during stimulation, and this contributes to a reduction in transmitter release and, consequently, a reduced postsynaptic N2 response. Similar effects of NMDA/Gly were observed in the presence of the AMPAR inhibitor, DNQX, and the $GABA_A$/Glycine receptor blocker, PTX. One possible explanation for these effects is that NMDARs are located at the presynaptic terminals of PFs. However, we cannot rule out the alternative possibility that NMDAR are present on one or more postsynaptic cells and that their activation triggers the production of some retrograde messenger that affects calcium signalling in PF terminals. Although NMDARs are not thought to be present on PCs in the age range used in this study (Farrant and Cull-Candy, 1991, Llano et al., 1991), NMDARs are present on stellate and basket cells (Bidoret et al., 2015, Rossi et al., 2012, Duguid and Smart, 2004) and so their activation might trigger the release a diffusible, retrograde messenger. NMDA/Gly produced an increase in the baseline SyGCaMP2: mCherry ratio in the presence of AMPAR and $GABA_A$R inhibition. Whilst this rules out the possibility of an anterograde action of NMDAR activation on PF release properties via AMPARs or $GABA_A$Rs, we cannot rule out the possibility that a retrograde messenger is involved. Indeed, it has been shown that depolarisation of inhibitory neurones can lead to the production of endocannabinoids, which can act in a retrograde manner to inhibit release (Beierlein and Regehr, 2006, Kreitzer and Regehr, 2001b, Kreitzer and Regehr, 2001a). Also, we cannot discount the suggestion by Dobson and Bellamy (2015) that release of GABA from interneurons after NMDAR activation causes $GABA_B$ activation and a reduction in transmitter release from PFs. But what do the data on absolute ratio show? If GABA was acting at $GABA_B$ receptors on presynaptic terminals, then how could this lead to an increase in residual calcium? This is not impossible, but the main action of $GABA_B$ is to reduce transmitter release via activating K^+ channels, leading to hyperpolarisation. This would not be expected to increase residual calcium. Another mechanism is by inhibiting adenylate cyclase which could inhibit calcium channels. Again, whilst this could lower calcium influx via calcium channels, it would not be expected to elevate residual calcium. Therefore, there remains the possibility that NMDARs on the PF terminal are activated, and that this opens channels and allows calcium to enter to elevate

residual calcium. It is entirely possible that such an increase in residual calcium could lower calcium influx and hence reduce transmitter release. Furthermore, it also indicated the decrease in presynaptic calcium influx is independent of the AMPARs. Surprisingly, there is no clear recovery of this decrease when washing out the NMDAR agonists. This may indicate that the recovery property requires some form of contribution from the postsynaptic side. Together, these data strongly support the hypothesis that NMDAR receptors are located at presynaptic membranes (most likely on PFs) and that they modulate synaptic transmission. Furthermore, it also indicates that the presynaptic inhibition due to NMDA is not as a result of decreased excitability in an afferent PF. There have been many recent studies demonstrating that the cerebellar molecular layer has a high density of NMDA receptor subunits that may be located presynaptically on PFs (Bidoret et al., 2009, Bidoret et al., 2015, Rossi et al., 2012, Glitsch and Marty, 1999). Our data are largely consistent with previous findings reported in the literature (Dobson and Bellamy, 2015), where it was found that bath perfusion of NMDA (30 μM) and Gly (10 μM) induced a reversible decrease that was accompanied with an increase in the PPR at the PF-PC synapse in transverse cerebellar slices taken from young adult rats. However, it was suggested that this was due to release of GABA from interneurons which then acted on $GABA_B$ receptors to reduce transmitter release from PFs. Our data are also largely consistent with those of Casado et al. (2000), who found that the activation of NMDARs via application of 30 μM NMDA/10 μM glycine for 10 minutes resulted in a transient decrease in synaptic transmission (58% reduction), but that the number of fibres remained unaltered at the PF-PC synapse in slices taken from young adult rats under identical experimental conditions. The effect of NMDA on the PPR was, however, different, as this application of NMDA/Gly did not lead to any associated change in paired-pulse ratio. This led to the suggestion that the presynaptic calcium affecting presynaptic transmitter release was unchanged by pre-NMDAR activation. Therefore, the mechanism for this decrease is most likely postsynaptic expression through an NO-dependent action. There is no clear interpretation for this discrepancy in the effects on PPR found in Casado's study and our own, but we speculate that this might be due to one minor difference between our protocol and others, which is that we use a sucrose-based aCSF during brain slice preparation to help improve the survival of neuron cells. It would be interesting to explore this discrepancy in any later

studies. As described previously, PPF is based on the presynaptic calcium accumulation after the first stimulation. The first pulse of the stimulus triggers a calcium influx that can remain in the presynaptic side for several hundred milliseconds. This residual calcium then combines with the fresh calcium that enters during the second stimulation, leading to an increase in transmitter release PPF (Thomson, 2000, Katz and Miledi, 1968). PPF has previously been characterised in considerable detail at the PF-PC synapses, and is associated with the residual calcium transient in the PF (Atluri and Regehr, 1996) as the PPF can be changed by presynaptic calcium modulators that affect transmitter release (Dittman and Regehr, 1996). Therefore, these studies support our suggestion that preNMDARs modulate synaptic release.

Activation of NMDARs are responsible for modulation of SyGCaMP2-mCherry.

We have demonstrated that NMDA was not able to depress either the SyGCaMP2 (F/F_0) or fEPSP (N2) responses in the presence of the selective competitive antagonist, AP5 (50 μM), to the NMDA receptor. These findings suggest that the effects of NMDA are indeed mediated via preNMDARs. Our data were completely consistent with previous findings (Casado et al., 2000, Casado et al., 2002) that indicated that a perfusion of NMDA failed to induce any decrease in PF-PC synapses in the presence of the NMDA receptor antagonist, AP5, in slices taken from young adult rats. We have also shown that NMDA had no effect on the baseline SyGCaMP2: mCherry ratios in the presence of AP5, suggesting that the effects of NMDA are indeed mediated by NMDARs. However, in the absence of AP5, NMDA caused an initially significant increase in the response of the baseline ratio above normal baseline levels followed by a decline that washed off, suggesting that subsequent to the application of NMDA, there is an initially increase, followed by a decrease, in the resting ratio, and likely the presynaptic calcium in boutons. The absolute baseline ratio is proportional to absolute calcium levels (Al-Osta, 2018, Pereda et al., 2019). Therefore, the SyGCaMP2: mCherry fluorescence ratio clearly illustrates the calcium-dependent alteration in SyGCaMP2, indicating that SyGCaMP2-mCherry can be used to measure absolute levels of calcium. We believe that the SyGCaMP2: mCherry fluorescence ratio was, for the first time to

date, used to measure baseline ratio in these studies. Therefore, further investigation is necessary to study the SyGCaMP2: mCherry ratio in more detail, in particular with regard to the adjustment of bleaching SyGCaMP2 and mCherry fluorescence and background subtraction.

Activation of NMDAR significantly reduces the number of responding SyGaMP2 fluorescence buttons but fails to effect the size of individual boutons.

We have examined the effect of NMDA/Gly on SyGaMP2 fluorescence responses at the level of single presynaptic boutons using a multiphoton microscope (Al-Osta et al., 2018, Dreosti et al., 2009). We have shown that the activation of NMDARs resulted insignificant reduction in the size of individual boutons to ML stimulation. However, this also results in a significant reduction in the number of puncta that respond to ML stimulation. This may indicate a change in excitability which is in contrast to our previous results, where the PF action potential and excitability were not affected by the application of NMDA. One possible explanation for this apparent contradiction is that there is a reduction in SARFIA ability to detect responding boutons when the magnitude of responses is relatively low.

In summary, the results presented in this chapter strongly support the hypothesis that NMDAR receptors are located on PFs (see Figure 5.11), and further that preNMDARs modulate synaptic transmission. However, the mechanism by which preNMDARs modulate presynaptic calcium is not yet fully understood. Further investigations are clearly required to address the current gaps in our knowledge of NMDARs.

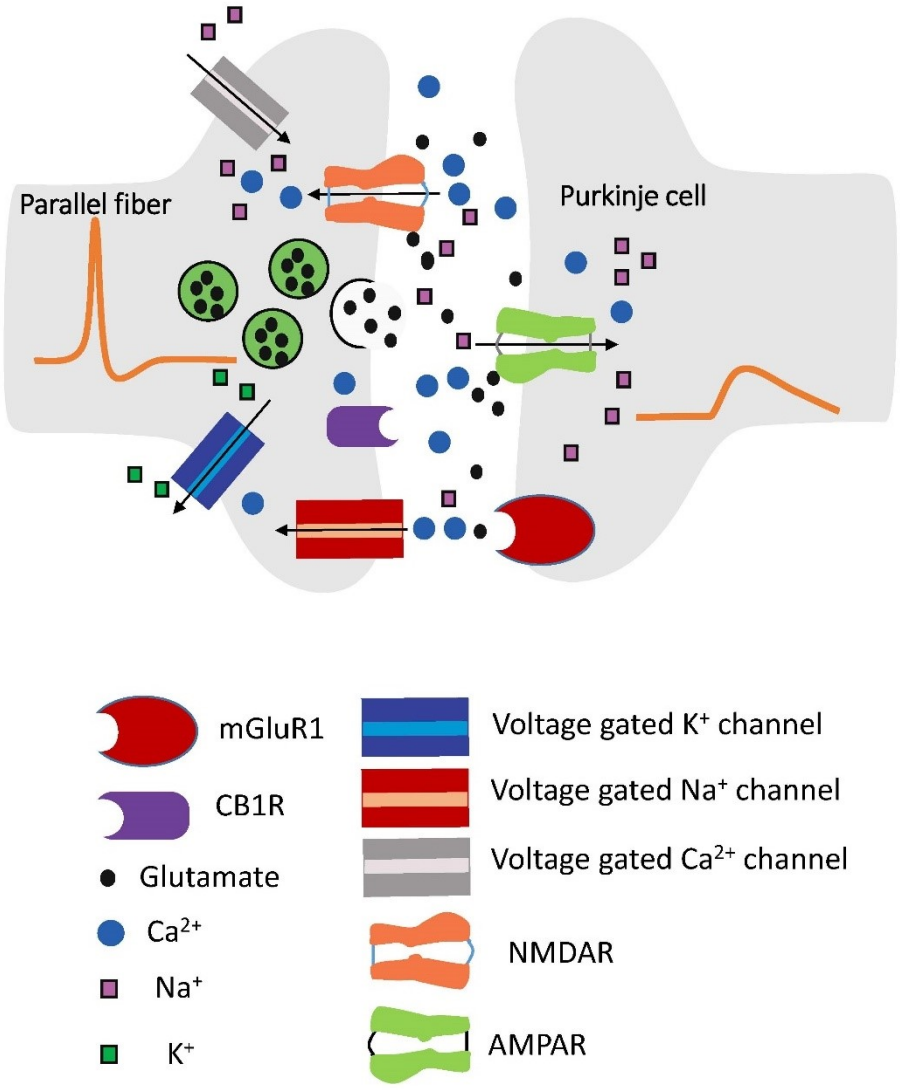

Figure 5.11. Schematic diagram showing the glutamatergic synapse between parallel fibres and the Purkinje cell, as well as illustrating the location of the NMDA receptors at parallel fibres.

Chapter 6: Investigating the Role of Presynaptic CB1R at Cerebellar PF-PC Synapses using SyG37 mice

6.1 Introduction

As outlined in Chapter 1 (section,1.5.2), endocannabinoids are implicated in retrograde signalling between neurons through G protein-coupled receptor cannabinoid 1 receptors (CB1Rs) found in the CNS with their highest densities in the cerebellum, hippocampus, hypothalamus, thalamus, basal ganglia and brain stem, amongst other locations. In the cerebellar cortex, the highest densities of CB1Rs are expressed in excitatory terminals of PFs and CFs (Lévénès et al., 1998, Kawamura et al., 2006, Núñez et al., 2004, Takahashi and Linden, 2000).

Activation of CB1Rs can lead to a transient inhibition of excitatory synaptic transmission at PF-PC synapses (Kreitzer and Regehr, 2001b, Kawamura et al., 2006, Irie et al., 2015, Maejima et al., 2001b, Lévénès et al., 1998). However, researchers have recently shown that activation of CB1R can also lead to a transient inhibition of inhibitory synaptic transmission basket cells to PCs indicating that they additionally regulate inhibitory synapses within the ML of the cerebellar cortex (Yoshida et al., 2002, Szabo et al., 2004, Takahashi and Linden, 2000).The mechanisms underlying this CB1R mediated inhibition at excitatory and inhibitory synapses are yet to be fully characterised. Part of the reason is the potential presynaptic effects of neuromodulators are hard to measure because the synaptic terminals are generally too small to record electrical signals directly. Our previous results showed that ML stimulation in cerebellar coronal slices produces SyGCaMP2 responses that are beam-like and that continue in the presence of synaptic transmission blockers, suggesting a significant component of the signal arises from the PFs themselves.

In the current chapter, we used SyGCaMP2 measurements in combination with electrophysiological recordings and pharmacological manipulation to help establish the site and mechanism of action CB1Rs at PF-PC synapses. In particular, the specific aims of this chapter were to:

1) confirm that CB1Rs modulate synaptic transmission between PFs and PCs. To address this objective, we studied the effects of the CB1R agonist WIN55, 212-2 on SyGCaMP2 fluorescence and the corresponding field potential responses recorded from the ML region of coronal cerebellar slices SyG37 mice in response to electrical activation of the ML.
2) test whether CB1Rs are present on PF terminals themselves as opposed to being located elsewhere in the polysynaptic cerebellar network such as between PFs and BCs or SCs. We therefore examined the effects of WIN55, 212-2 on SyGCaMP2 fluorescence and the corresponding presynaptic fibre volley (N1) responses recorded from the ML region of the cerebellum in SyG37 mice to electrical activation of the ML in the presence of DNQX, AP5 and PTX.
3) confirm whether the effects of WIN55, 212-2 on SyGCaMP2 fluorescence responses and the N2 component of fEPSPs are indeed mediated via CB1Rs. Therefore, we examined the effects of activation of CB1Rs in the presence of the CB1 receptor antagonist AM251 on SyGCaMP2 fluorescence and synaptic field potentials recorded from the ML
4) test whether activation CB1Rs can change the resting presynaptic calcium. Therefore, we sought to test the effects of activation of CBR1 with and without the presence of AM251 on baseline levels of the SyGCaMP2: mCherry ratio.
5) establish whether the effects of WIN55, 212-2 are due to a reduction in the size of the SyGCaMP2 fluorescence response per boutons or whether there is a change in the number of boutons contributing to the total SyGCaMP2 fluorescence response. Therefore, we sought to examine the effects of WIN55, 212-2 on SyGCaMP2 fluorescence recorded from the ML region in single presynaptic boutons of the cerebellum in SyG37 mice to electrical activation of the ML in the presence of synaptic transmission blockers.

6.2 Results

In this section, data were collected, analysed and displayed using the same approach as for chapter 5. All experiments were performed on coronal slices and

field potentials and SyGCaMP2-mCherry responses were recorded in the ML in response to ML stimulation (50 stimuli and 50Hz).

6.2.1 Effects of activation of CB1Rs with extracellular perfusion with endocannabinoid agonist WIN55, 212-2

Stable baselines of fEPSPs and SyGCaMP2 responses to ML activation were recorded for at least 10 minutes in standard aCSF before the CB1R agonist WIN55, 212-2 was perfused at a concentration of 10 μM for 30 minutes. Responses were recorded for a further 30 minutes in aCSF. As shown in Figures 6.1 and 6.2, WIN55,212-2 induced a significant, irreversible decrease in both the basal amplitude of N2 fEPSPs and SyGCaMP2 responses, which, after 30 minutes, averaged 58.76 ± 9.9% and 56.09 ± 9.2% of baseline in fEPSP peak and initial slope, respectively, and 78.72 ± 5.5%, 77.92 ± 5.2% and 75.63 ± 5.6% of baseline in peak, slope and AUC of SyGCaMP2 responses, respectively (SyGCaMP2 Peak: P = 0.0039; SyGCaMP2 Slope: P = 0.0039; SyGCaMP2 AUC: P = 0.0039; N2 peak: P = 0.0195; N2 slope: = 0.0039, n = 9, Wilcoxon signed rank test). No recovery of any of these responses was observed after a washout period of 30 minutes. The reduction in both synaptic and optical responses was slow, taking between 15 and 20 minutes to emerge, and irreversible, at least over the time course allowed for here. The suppression of fEPSPs and SyGCaMP2 responses was also accompanied by a significant rise in the paired pulse ratio of the N2 response compared to baseline control values from 1.07 ± 0.1 to 1.73 ± 0.31 (Wilcoxon test: P = 0.0039, n = 9, Figure 6.2 F & G). The amplitude of the presynaptic volley (N1) was unaffected by WIN55, 212-2 (P = 0.7344; n = 9; Wilcoxon matched-pairs signed rank test, see Figures 6.2 H and I). This depression by WIN55, 212-2 can be reversal by the CB1 receptor antagonist such as SR141716-A and AM251 (Lévénès et al., 1998, Szabo et al., 2004, Irie et al., 2015).

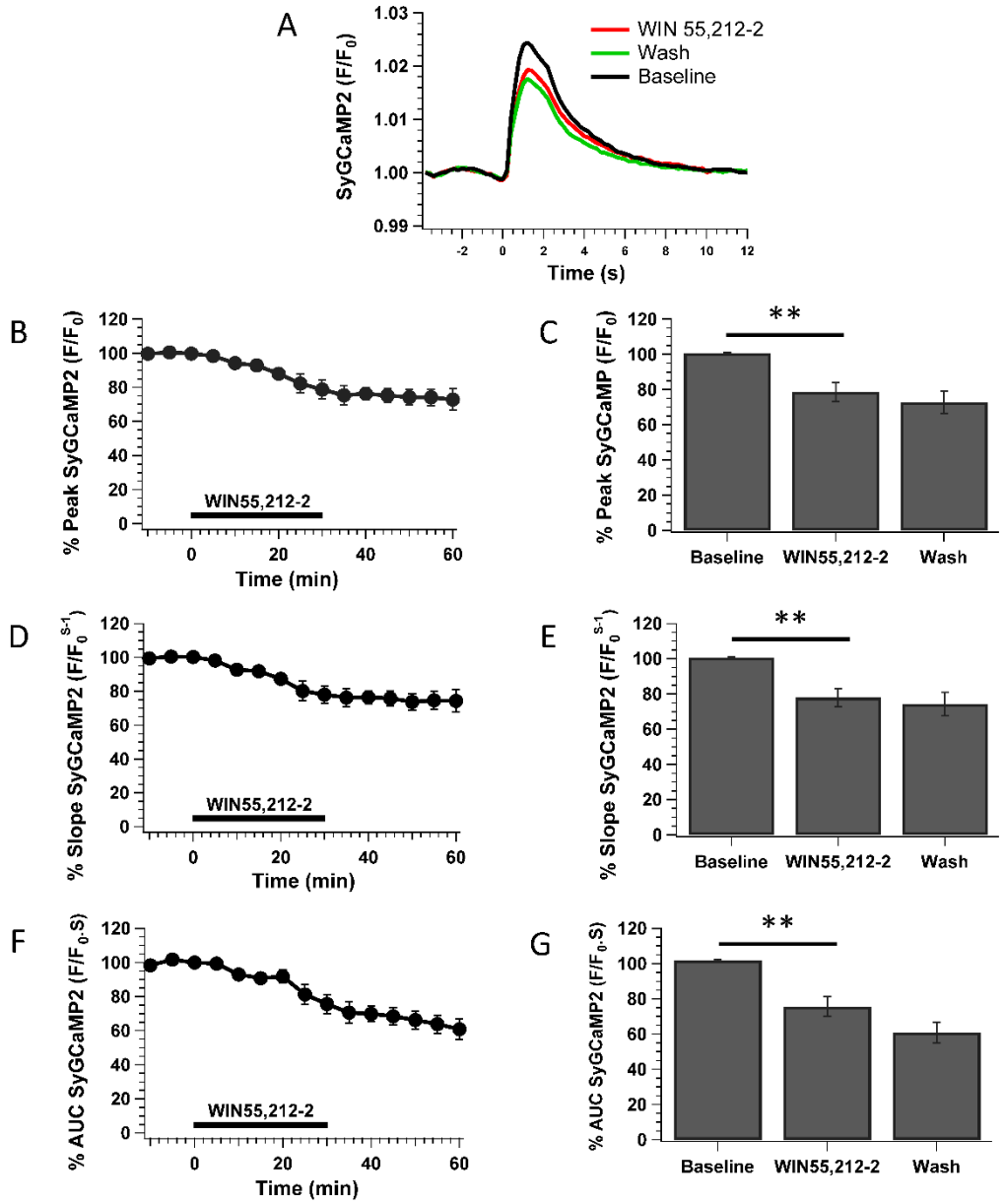

Figure 6.1. The effects of the CBR1 agonist WIN55, 212-2 on SyGCaMP2 fluorescence responses to ML stimulation in coronal cerebellar slices. (A) shows the averaged responses of SyGCaMP2 fluorescence during baseline (black), application of 10 µM WIN55, 212-2 (red) and after washout (green). Measurements were obtained from regions of interests (ROIs) placed within the molecular layer (ML) of the cerebellar cortex. Figures B, D and F illustrate the effects of 10 µM WIN55, 212-2 on peak, slope and AUC of SyGCaMP2 responses to ML stimulation expressed as a percentage of baseline values, respectively. The black horizontal bar shows the period of WIN55, 212-2 application. Figures C, E and G show bar charts which summarise the data during baseline, 30 minutes after WIN55, 212-2 application and after a 30-minute washout period for each of these datasets. Mean and S.E.M are shown (n = 9). This depression by WIN55,212-2 can be reversal by the CB1 receptor antagonist such as SR141716-A and AM251.

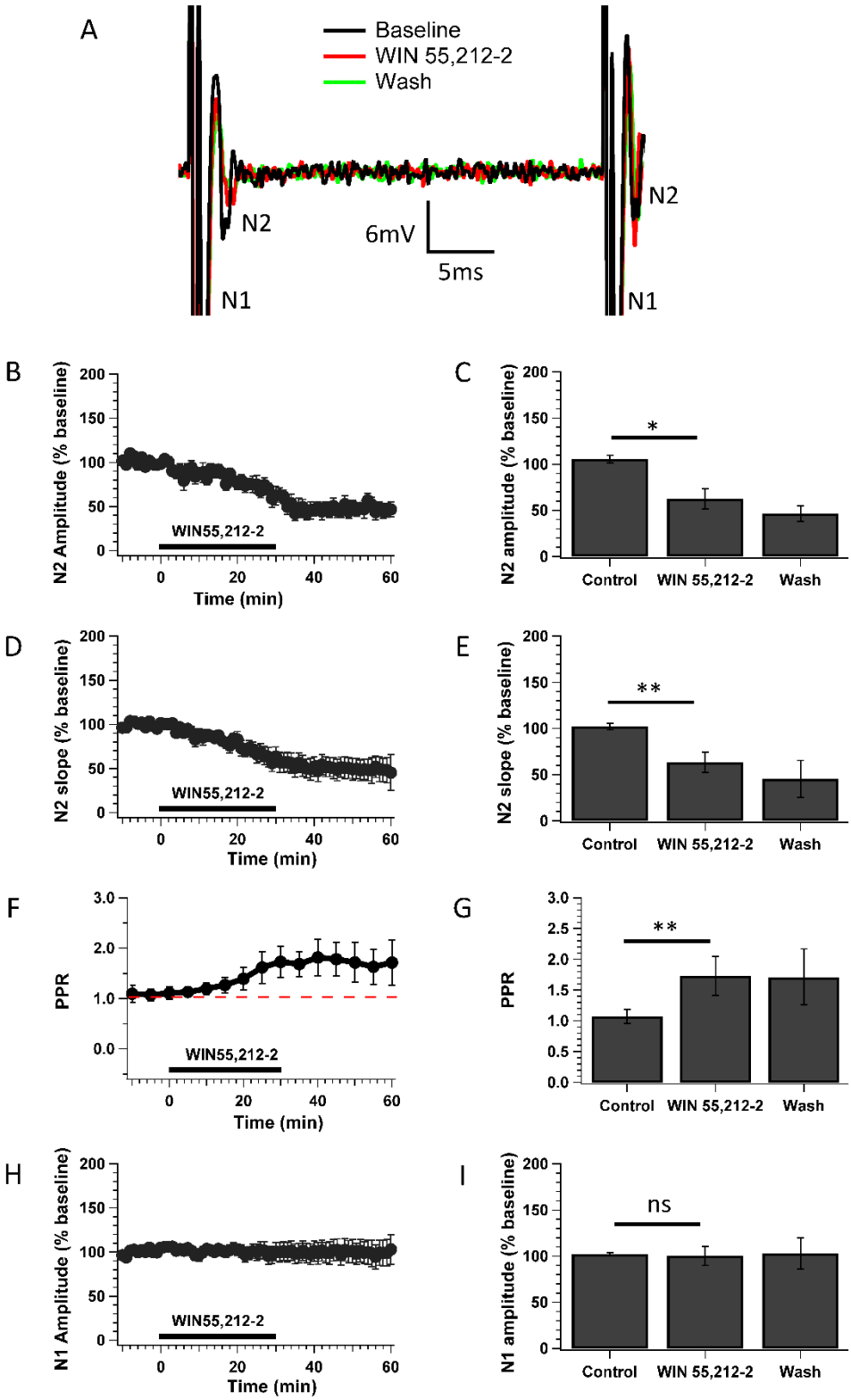

Figure 6.2. The effects of the CBR1 agonist WIN55, 212-2 on field potential responses to ML stimulation in coronal cerebellar slices. A illustrates representative field potential responses to ML stimulation during baseline (black), application of 10 µM WIN55,212-2 (red) and after washout (green). Figures B, D, F and H show the effects of WIN55, 212-2 on the peak and slope of N2, PPR and N1 amplitude components of the field potential responses before, during and

after WIN55,212-2 application respectively. The black horizontal bar shows the period of WIN55, 212-2 application. Figures C, E, G, and I show bar charts which summarise the data during baseline, WIN55,212-2 application and washout periods for each of these datasets. Data were presented as the mean percentage of baseline and S.E.M of N = 9 recordings. This depression can also be reversal by the CB1 receptor antagonist such as SR141716-A and AM251.

Figures 6.3 B-D illustrate the spatial changes in SyGCamP2 fluorescence using a 'hot-cold' look up table with identical settings that show the relative changes in SyGCaMP2 florescence in response to the electrical stimulation of ML before (B), during (C) and after WIN55,212-2 perfusion (D). Fluorescence clearly decreased irreversibly along a beam within the ML. This supports the idea that WIN55,212-2 is having its affect on PF terminals. Whilst the intensity of the beam clearly decreased, the size of the beam did not.

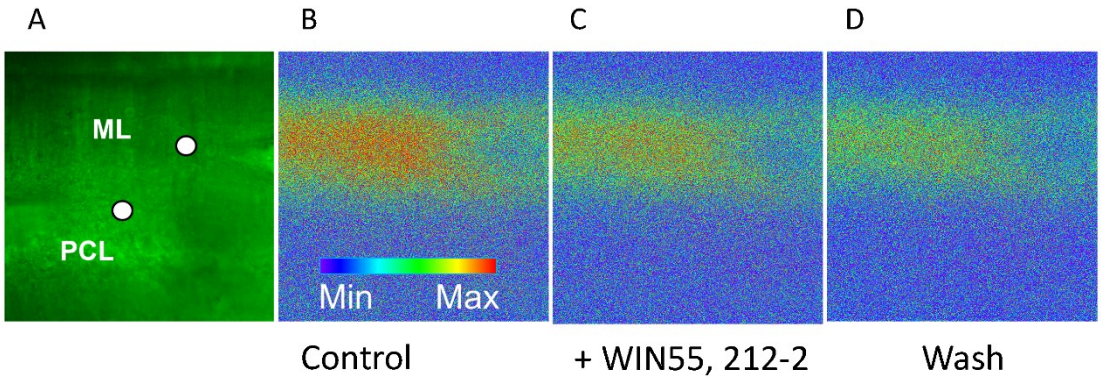

Figure 6.3. Visualization of the effects of WIN55, 212-2 on SyGCaMP2 fluorescence responses to cerebellar ML stimulation. The data presented are as shown in Chapter 5, Figure 5.2 except that bursts of 50 stimuli at a rate 50 Hz were applied, application of WIN55, 212-2 for 30-minute and the period of washouting was 30 minutes.

Together, these results show that WIN55, 212-2 reduced N2 fEPSPs responses and increase the PPR but did not affect N1, suggesting a presynaptic site of action but not via a change in PF terminal excitability. They also show that SyGCaMP2 florescence (F/F_0) responses were similarly reduced by WIN55, 212-2 indicating that calcium in presynaptic terminals reduces. These results led to the suggestions: first, CB1Rs are located on presynaptic terminals (most likely on PFs) and second, CB1Rs modulate synaptic transmission.

6.2.2 Effects of CB1R activation in the presence of pharmacological blockade of AMPA, NMDA and GABAA receptors

We next carried out experiments designed to test the effects of WIN55, 212-2 on SyGCaMP2 fluorescence and fEPSPs response recorded from the ML region to electrical activation of PFs in the presence of DNQX, AP5 and PTX to confirm that the recorded SyGCaMP2 fluorescence responses arose directly from ML stimulation rather than from anything postsynaptic to the PF terminals. In this set of experiments, we repeated the same experiment described in section 6.2.1 except we used the standard aCSF solution supplemented with DNQX (an AMPAR antagonist), AP5 (an NMDA antagonist) and PTX (a $GABA_A$ antagonist). Although the presence of these antagonists prevented us from recording the N2 component of the fEPSP because inhibitory and excitatory synaptic transmission was blocked, we were able to record the N1 (presynaptic volley) response without any contamination coming from the postsynaptic N2 responses (Lévénès et al., 1998). We were also able to record SyGCaMP2 fluorescence, but in the presence of this cocktail of synaptic blockers only fluorescence which originated directly from the presynaptic terminals of fibres activated through ML stimulation was recorded. In this set of experiments, we found that WIN55,212-2 significantly decreased the amplitude of the SyGCaMP2 fluorescence response to 79.77 ± 2.10% (Peak), 80.33 ± 1.85% (Slope) and 66.96 ± 4.69% (AUC) of the baseline response (Peak: P = 0.0039; Slope: P = 0.0039; AUC: P = 0.0039, n = 9, Wilcoxon matched-pairs signed rank test). In contrast, the PF volley (N1) was unaffected by the application of WIN55, 212 (N1: P = 0.1641, n = 9, Wilcoxon matched-pairs signed rank test) (see Figure 6.4). Overall, repeating experiments in the presence of PTX/DNQX and AP5 indicates that the effects are at presynaptic terminals that are activated directly through ML stimulation rather than through a synaptic process, leading to activation of presynaptic terminals that are postsynaptic to PF terminals. WIN55, 212-2 reduces SyGCaMP2 florescence (F/F_0) responses but did not affect N1 in similar way as in section 6.2.1, suggesting presynaptic calcium was reduced but not via a change in PF terminal excitability. These data led to the proposal that CB1R located on PFs are responsible for reducing presynaptic calcium at PF terminals.

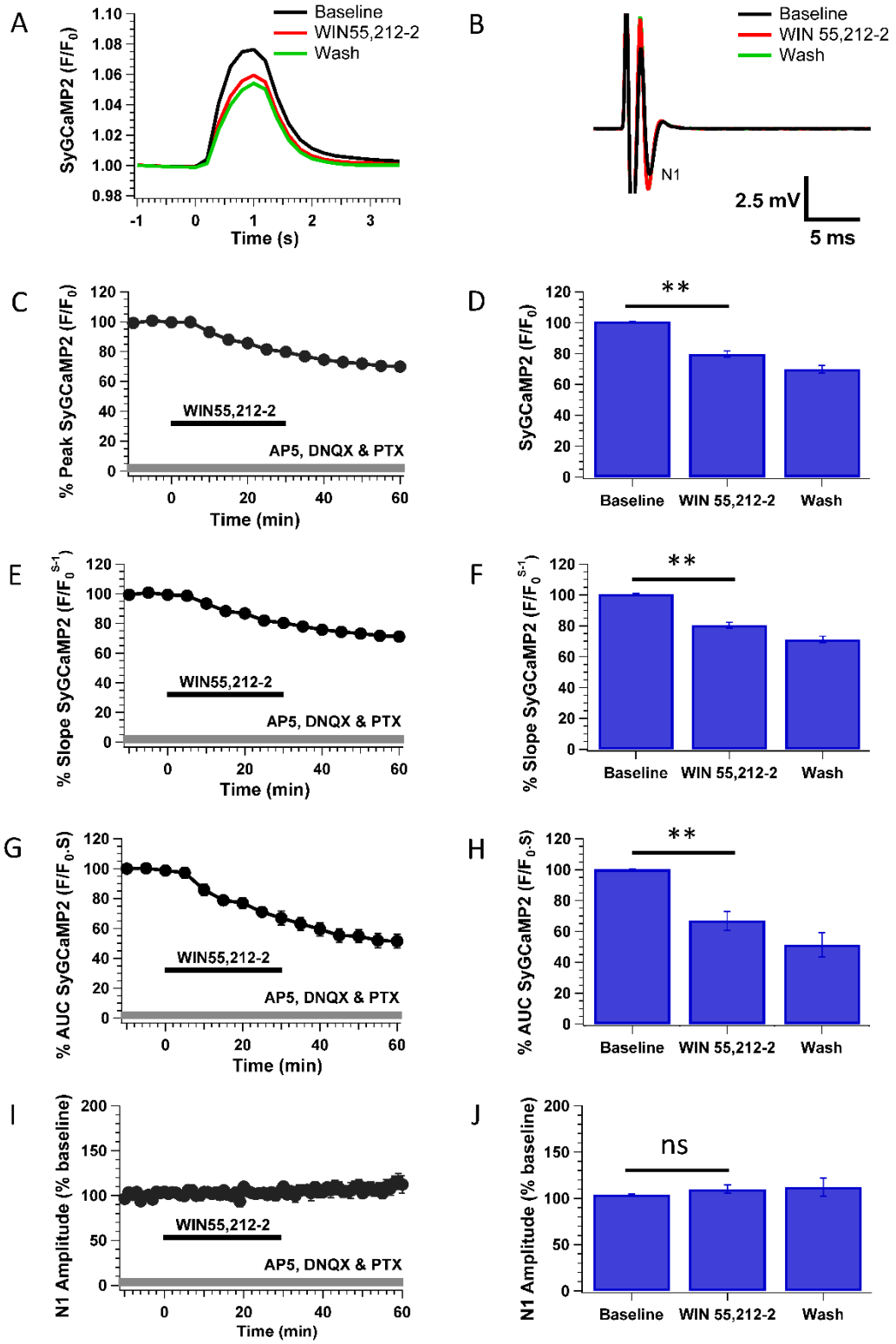

Figure 6.4. CB1R activation modulates SyGCaMP2 fluorescence responses to ML stimulation in the presence of DNQX, AP5 and picrotoxin. Figures (A–J) are shown in a similar manner as those in histograms 5.3.1 and 5.3.2 except for WIN55,212-2 application in the continued presence of 10 µM DNQX, 50 µM AP5 and 10 µM picrotoxin.

6.2.3 Effects of CB1R activation in the presence of pharmacological blockade of CB1R blocker

We next examined whether the effects of WIN55, 212-2 were mediated via CB1R by repeating the experiments in the presence of the CB1 antagonist AM251. It has been shown that the AM251 alone has no discernible effect on synaptic transmission between GCs and PCs in the cerebellum as well as reversing WIN55, 212-2-induced suppression of synaptic transmission in cerebella coronal slices, as described in previous studies (Lévénès et al., 1998, Szabo et al., 2004, Irie et al., 2015). Here, we examined the effects of WIN55, 212-2 in the presence of an extracellular solution containing 10 μM AM251. Slices were perfused for 15 - 20 minutes with aCSF containing 10 μM AM251 before starting to record the experiments to ensure that CB1R was blocked by AM251. A stable baseline of synaptic and SyGCaMP2 responses to PF activation was recorded for 10 minutes prior to the perfusion of WIN55, 212-2. The aCSF containing WIN55, 212-2 and AM251 (10 μM) was applied for 30 minutes. Because there was no recovery of suppression of endocannabinoids, as shown in section 6.2.1 and 6.2.2, no further washout was carried out after 30 minutes of WIN55, 212-2 application. Our results showed that AM251 completely prevented the effects of WIN55, 212-2 on both SyGCaMP2 fluorescence and its corresponding fEPSP (Figures 6.5 and 6.6, SyGCaMP2 Peak: 103.46 ± 1.74%, SyGCaMP2 Slope: 102.37 ± 2.03%, SyGCaMP2 AUC: 99.31 ± 1.71%, fEPSP N2: 101.39 ± 3.56%). In the same way, the PF volley was unaffected (fEPSP N1: 109.24± 8.14% of control).

Bar charts in Figures 6.5 and 6.6 (C, E and G) summarise the data during baseline and WIN55,212-2 application periods for each of these datasets (Peak SyGCaMP2: P = 0.1016; Slope SyGCaMP2: P = 0.3203; AUC SyGCaMP2: P = 0.4131, N1: P = 0.2031, N2: P = > 0.9999, n = 9, Wilcoxon matched-pairs signed rank test).Together, these results confirm that the effects WIN55,212-2 are indeed mediated via CB1Rs since the CB1R antagonist prevented the effects of WIN55,212-2.

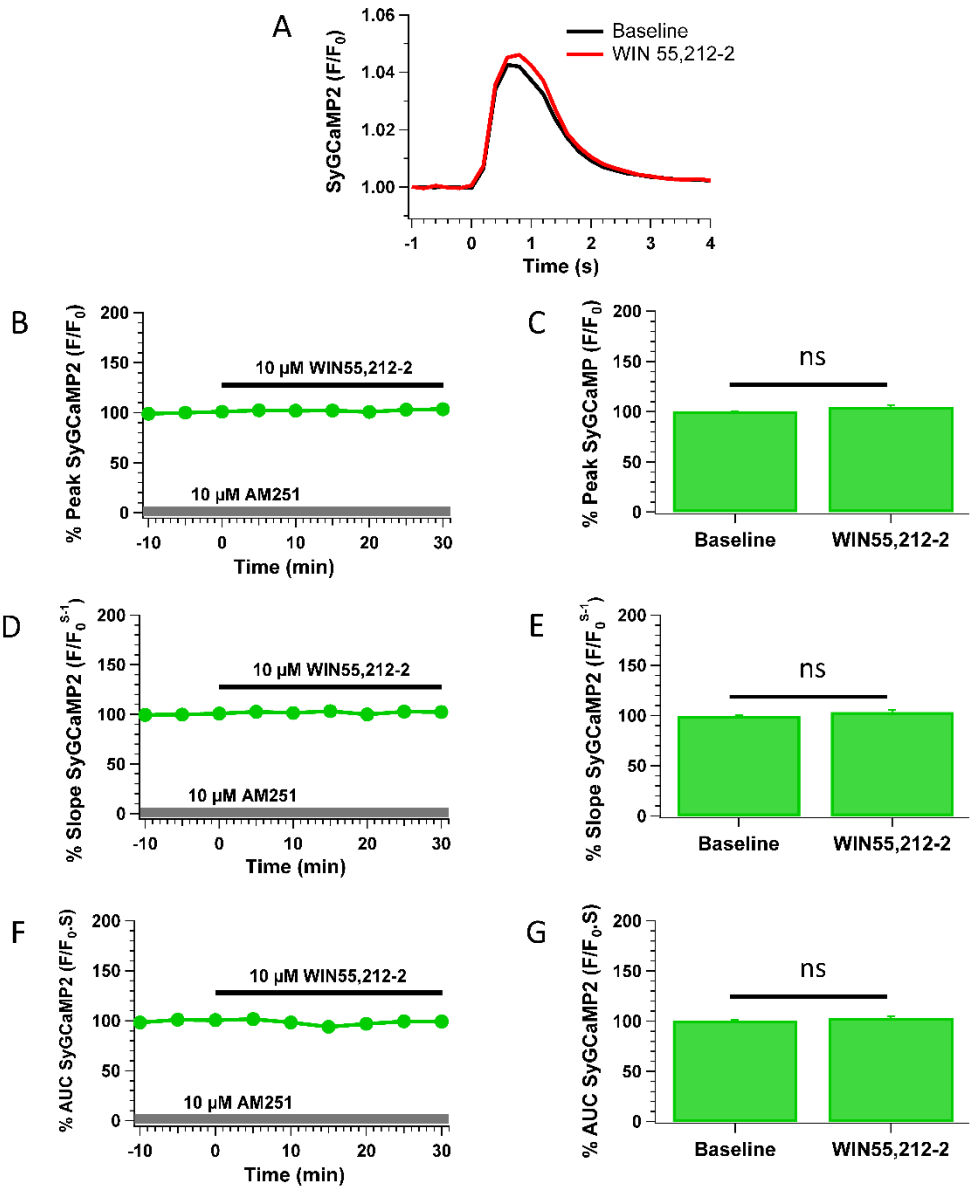

Figure 6.5. Prevention of WIN55, 212-2-induced suppression of SyGCaMP2 fluorescence responses recorded from the ML region to electrical activation of the ML by prior bath application of 10 µM AM251. Figures (A–G) are presented in a similar manner as those in histograms in 5.3.1 except that WIN55,212-2 application was in the continued presence of 10 µM AM251 and with no washing.

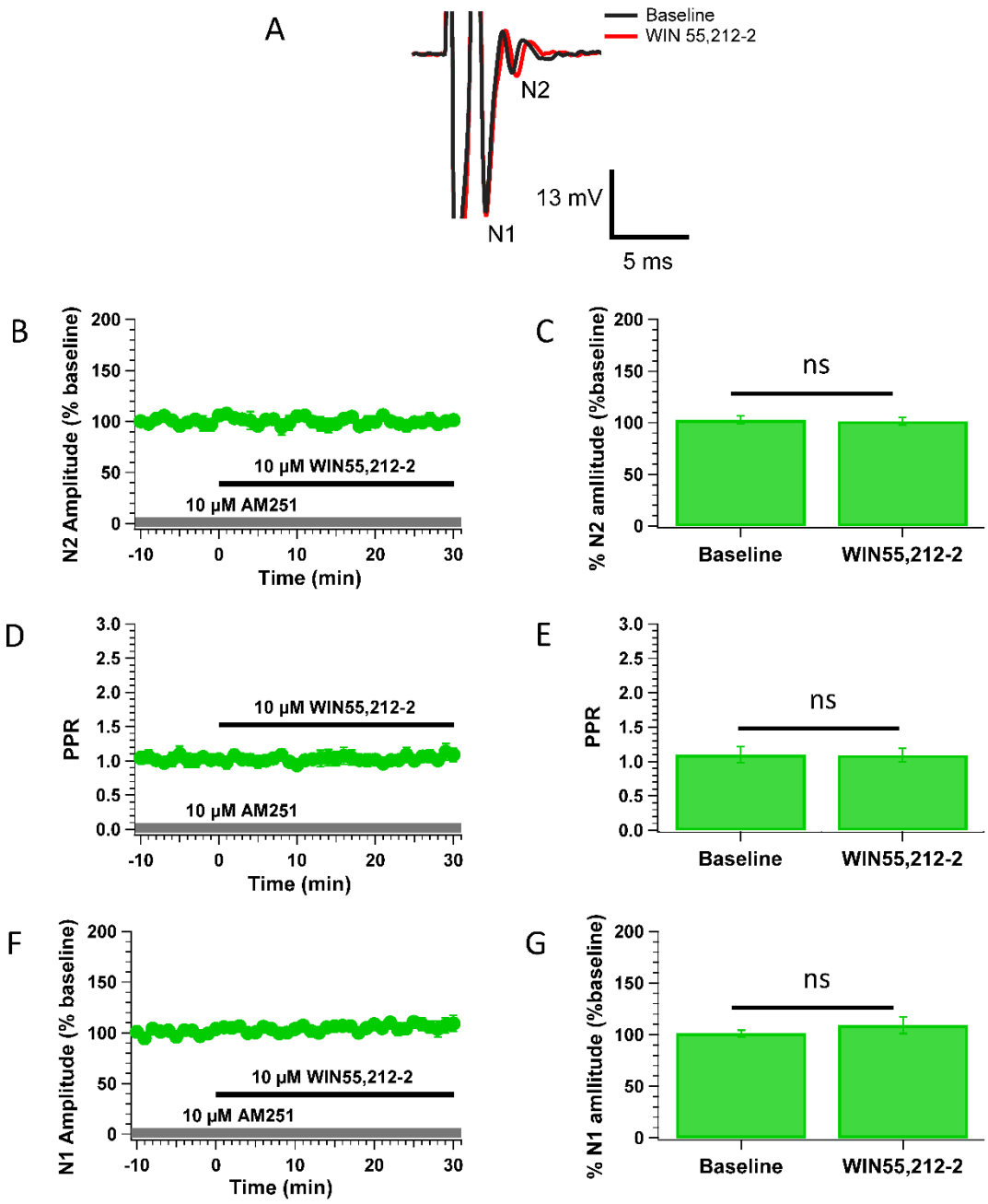

Figure 6.6. Prevention of WIN55, 212-2-induced suppression of PF amplitude recorded from the ML region to electrical activation of the ML by prior bath application of 10 µM AM251. Figures (A–G) are presented in a similar manner as those in the histograms in 5.3.2, except that WIN55, 212-2 application was in the continued presence of 10 µM AM251 and with no washing.

The bar charts in Figure 6.7 summarize the previous above results that WIN55, 212-2 triggered depression of peak SyGCaMP2 (SyG) and fEPSP N2. It also triggered depression of SyG responses in the presence of synaptic transmission blockers. However, there was no effect on the N1 component. These effects were totally prevented in the presence of AM251. Together, these data suggest that CB1Rs are located on parallel fibre terminals and that they modulate synaptic transmission. In the next section, we will study whether activation of CB1R has had any effect on baseline levels of the SyGCaMP2: mCherry ratio with and without the presence of AM251.

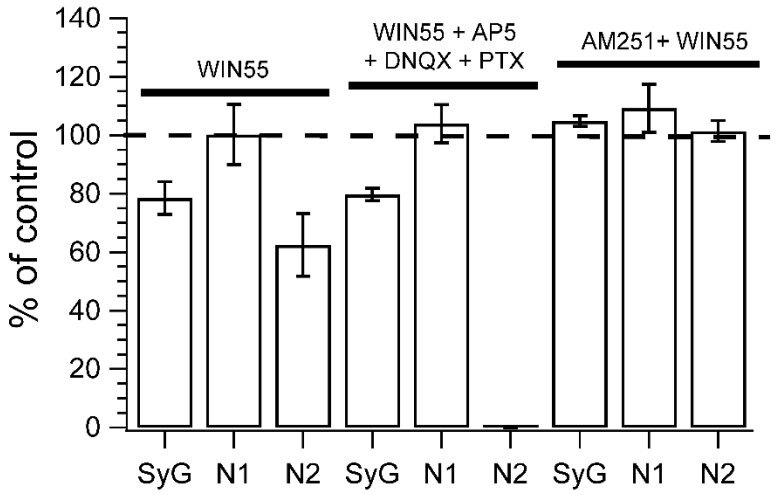

Figure 6.7. Pharmacological characterisation of the WIN55, 212-2 induced depression of SyGCaMP2 and synaptic transmission responses. Bar chart showing the effects (measured after 30 min application) of WIN55,212-2, the effect of WIN55,212-2 in the presence of DNQX ,AP5 and PTX, and the effect of WIN55,212-2 in the presence of AM251 on peak SyGCaMP2(SyG), a presynaptic fibre volley (N1) and the fEPSP peak (N2). Data were presented as normalised mean ± SEM.

6.2.4 Effects of activation of CB1Rs with and without AM251 on the baseline SyGCaMP2: mCherry Ratio

In this section, we attempted to establish whether the activation of CB1Rs has any effect on the resting levels of calcium inside presynaptic terminals. Therefore, we measured the ratio for the SyGCaMP2 to mCherry baseline fluorescence for the

effects of CB1R activation with and without the presence of the CB1R antagonist AM251 from previous data, as recorded in the experiments described in sections 6.2.1 and 6.2.3, respectively. The ratio of SyGCaMP2: mCherry was analysed and calculated as described previously (see Materials and methods, section 2.7.2.1). Finally, data were normalised and presented as mean ± SEM.

As shown in Figure 6.8D (left), bath perfusion of WIN55,212-2 for 30 minutes produced a significant decrease on the baseline level of the SyGCaMP2: mCherry ratio (Wilcoxon test, P = 0.039, n = 9). After washout of the drug, the baseline ratio fully recovered. However, perfusion of WIN55, 212-2 for 30 minutes in the presence of the competitive CB1R antagonist AM251 (10 μM) failed to produce any effects on the baseline ratio, as shown in Figure 6.8, D (right) (Wilcoxon test, P = 0.8904, n = 12).

As mentioned earlier, the SyGCaMP2: mCherry ratio is proportional to absolute calcium concentration in presynaptic terminals. Therefore, these results show calcium-dependent alterations in SyGCaMP2 and illustrates that after application of WIN55,212-2 there is a reduction in absolute residual presynaptic in the presynaptic boutons. This was consistent with the measurement of SyGCaMP2 fluorescence (F/F_0) response (sections 6.2.1 and 6.2.2) where we found application of WIN55, 212-2 led to a reduction in calcium influx into presynaptic terminals. In the next section will examine whether WIN55, 212-2 changes the amount of Ca^{2+} entering individual boutons and/or the number of boutons contributing to the total response.

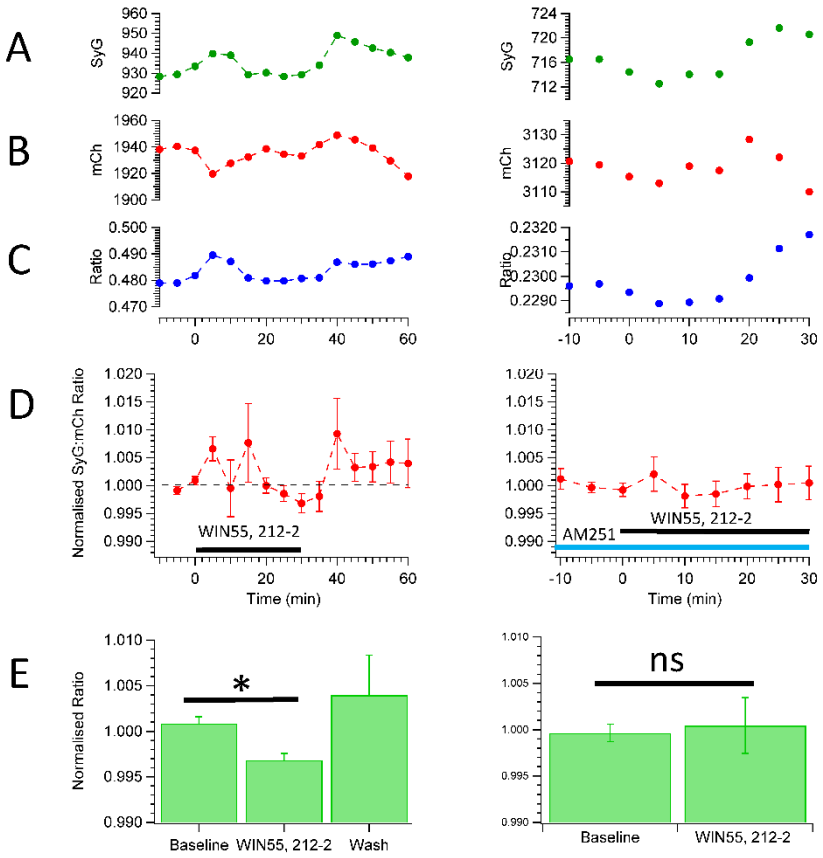

Figure 6.8. Effects of activation of CB1R in the absence and presence of AM251 on the resting ratios of SyGCaMP2: mCherry. Data are presented as per Figure 5.8 except that there was no washout of WIN 55,212-2 in the presence of the competitive CB1R antagonist AM251.

6.2.5 Effects of CB1R activation on single presynaptic bouton responses

We finally examined the effects of WIN55, 212-2 on SyGCaMP2 responses in single presynaptic boutons within the ML. The experiments described above indicate that WIN55, 212-2 reduces SyGCaMP2 responses but they do not reveal the mechanism. We therefore examined the effects on single, identified boutons using multiphoton microscopy to establish whether WIN55, 212-2 changes the amount of Ca^{2+} entering individual boutons and/or the number of boutons contributing to the total response. Experiments were performed in the same manner as for those described in Chapter 5, section 5.2.6 except for that application of WIN55, 212-2 was applied for 30 minutes in the presence of blockers (AP5, PTX and DNQX), and we took two additional measurements at different depths, which were the top and bottom of the first image recording by about 5 µM. There was then a break in

imaging that lasted for 30 minutes, during which stimulation and application of WIN55, 212-2 were continued without recording images. After this break, the responses were again recorded under the same conditions. Finally, imaging data were analysed using SARFIA software as in Chapter 5, section 5.2.6. Data were presented as the mean ± SEM. We found that bath application of 10 μM WIN55, 212-2 for 30 minutes produced a significant decrease in the peak response of responding puncta (Baseline: 100 ± 0.019; 10 μM WIN55, 212-2: 87.99 ± 3.22, Wilcoxon test: P = 0.0001, n = 27(three slices, with each slice replicated nine times). See Figure 6.9 C and D). More importantly, it also produced a significant reduction in the number of responding puncta (see Figure 6.9 A and B) (Puncta (Baseline): 76.52 ± 3.65; Puncta (10 μM WIN55, 212-2): 50.65 ± 3.58, Wilcoxon test: P value = 0.0039, n = 27. See Figure 6.9 B). Overall, these results indicate that WIN55, 212-2 significantly reduces the calcium mobilisation entering individual boutons. It also produces significant reduction in the number of boutons at PFs.

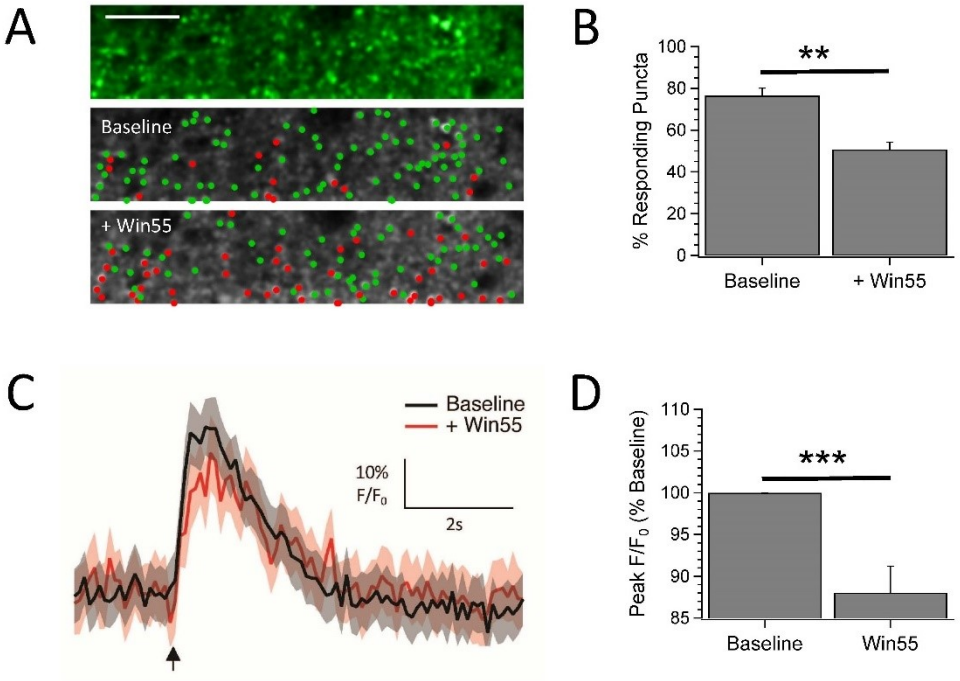

Figure 6.9. CB1Rs activation reduces the number and size of single puncta responses that respond to ML stimulation. The data presented as shown in Chapter 5, Figure 5.10, except for that, the red horizontal bar shows the 30-minute period of WIN55, 212-2 application and there is no washing of agonist.

6.3. Discussion

Although the highest densities of CB1Rs are expressed in inhibitory terminals such as those of basket and SCs (Diana et al., 2002, Tsou et al., 1998), there is evidence that CB1Rs are also expressed on the excitatory terminals of PFs and CFs (Lévénès et al., 1998, Kawamura et al., 2006, Núñez et al., 2004, Takahashi and Linden, 2000). In the present investigation, we tested the hypothesis that CB1Rs have a direct presynaptic mechanism of action at synapses formed between PFs and PCs. To do this, we combined SyGCaMP2-mCherry imaging with extracellular recording of fEPSPs recorded in the ML of coronal cerebellar slices in response to ML stimulation. We tested the effects of pharmacological modulation of CB1Rs in the absence and presence of synaptic blockade. We first confirmed that WIN55, 212-2 suppressed synaptic transmission and SyGCaMP2 fluorescence (F/F_0) in response to PF activation in coronal slices. This suppression was accompanied by a decrease in the N2 component of the fEPSP and a significant increase in the PPR of N2 (Figures 6.2 B, D & F). These results point towards a presynaptic site of action (Lévénès et al., 1998, Irie et al., 2015, Zhang and Linden, 2009). The effects of WIN55, 212-2 proceeded slowly and were irreversible; suppression of SyGCaMP2 responses and N2 required at least 15 to 20 minutes to be clearly apparent. It is generally accepted that the endogenous cannabinoids act slowly in most regions of the brain (Lévénès et al., 1998, Szabo et al., 2000, Azad et al., 2003, Szabo et al., 2004). Whilst this could reflect, in part, the time taken for the drug to reach its target, it is more likely that signalling pathway involved is slow. The results of the present investigation are comparable to the number of previous findings in various brain regions. For example, Azad et al. (2003) found that WIN55,212-2 (5 μM) significantly lowered the amplitude of the N2 fEPSPs of PFs to 52 ± 6% of the basal synaptic level in coronal slices of the mouse lateral amygdala using extracellular recording techniques. Similarly, Irie et al. (2015) and Lévénès et al. (1998) reported that WIN55, 212-2 (10 μM and 5 μM) decreased the amplitude of PF-PC EPSC in mouse and rat cerebellum to 46.8 ± 0.13% and 55·6 ± 13·5% of the baseline, respectively. Our findings showed that WIN55, 212-2 (10 μM) decreased the SyGCaMP2 response by roughly a quarter. This was consistent with the findings of Brown et al. (2004), who found that methanandamide (5 μM) reduced the

presynaptic calcium influx to 74 ± 1% of the control value of mouse cerebellar slices using magnesium green as the calcium indicator. In our experiments, the PF volley (N1) was unaffected by bath application of WIN55, 212-2 for 30 minutes (Figures 6.2H & I), indicating that, at least by this measure, the excitability of PFs did not change significantly. This is in agreement with several previous findings (Brown et al., 2004; Lévénès et al., 1998) which showed that the endocannabinoid system suppressed neurotransmitter release at PFs to Purkinje cell synapses by inhibiting presynaptic calcium influx through presynaptic calcium channels, but further that the excitability of the PFs did not change (Mintz et al., 1995). Our results were consistent with those of Takahashi and Linden (2000), who found that the application of WIN55, 212-2 (10 μM) had no detectable effects on presynaptic volley responses. It has been shown that endocannabinoids, in most regions of the brain studied so far, decrease inhibitory GABAergic synaptic transmission through CB1R activation (Yoshida et al., 2002, Szabo et al., 2004, Takahashi and Linden, 2000, Katona et al., 2001, Hájos et al., 2001). However, the role of CB1R in endocannabinoid in triggering a reduction of glutamatergic transmission is less clear (Hoffman and Lupica, 2000) for a more review see Wilson and Nicoll, 2002). Our findings showed that endocannabinoids reduced postsynaptic transmission (N2) but this did not confirm glutamatergic or GABAergic synaptic transmission as the N2 component could be a mixed excitatory/inhibitory synaptic response. Our observations also showed that endocannabinoids reduce SyGCaMP2 fluorescence (F/F_0). However, this experiment did not confirm unequivocally an effect exclusively at excitatory terminals of PFs. We have also demonstrated that the beam-like pattern of fibre activation following ML activation in coronal cerebellar slices was not changed in the presence of WIN55, 212-2 but the intensity of the signal, along the stimulated beam, was reduced. Along with the quantitative decreases in peak SyGCaMP2 responses (F/F_0), this finding suggests that CB1Rs may well be located on PFs. Repeating experiments in the presence of PTX, DNQX and AP5 to block $GABA_A$/Glycine, AMPA and NMDA receptors, respectively, further supports our contention that the effect of WIN55, 212-2 is on PF terminals that are activated directly through ML stimulation rather than through a synaptic process leading to activation of presynaptic terminals that are postsynaptic to PF terminals. Although these receptor antagonists help to minimise contamination of the presynaptic response from any polysynaptic responses (Lévénès et al., 1998; (Brown et al.,

2004), the applications of WIN55,212-2 (10 μM) again had no detectable effects on the (N1) presynaptic volley (Figures 6.4 I and J), indicating that fibre recruitment at ML regions were again not affected. The above notwithstanding, this is interesting as it shows that presynaptic change can occur without requiring effects on the presynaptic volley (N1) response itself. Data from several studies suggest that endocannabinoids inhibit synaptic transmission at the PF to PC synapses by lowering the probability of release at parallel fibre terminals (Lévénès et al., 1998). Our observation that presynaptic calcium signalling within PF terminals is reduced would provide a mechanism for this reduction in release probability, Maejima et al. (2001a), reported that endocannabinoids inhibit synaptic transmission at CF to PC synapses by reducing glutamate transmission. However, the mechanism underlying this essential means of synaptic control is not fully understood. We did not find any evidence for CF mediated SyGCaMP2 changes in fluorescence, but we did not explore this systematically. Our findings using the ratio of SyGCaMP2: mCherry to measure baseline residual calcium show that WIN55, 212-2 significantly reduced residual calcium (Figure 6.8). The ratiometric nature of sensor in SyG37 mice has enabled us to show for the first time that CBR1 activation not only reduces calcium mobilisation during synaptic activation, it lowers absolute presynaptic calcium. Taken together, our findings suggest that CB1R located on presynaptic PF terminals modulate resting calcium and calcium responses during synaptic transmission in the cerebellum. It has been shown at many synapses that endocannabinoids suppress neurotransmitter release by decreasing calcium influx within presynaptic terminals (Daniel and Crepel, 2001, Brown et al., 2004, Azad et al., 2003). However, our results do not rule out the possibility that endocannabinoids control synaptic transmission at the cerebellum by modulating both glutamatergic and GABAergic synapses via presynaptic actions, as suggested by Azad et al. (2003).

As our data demonstrate that WIN55, 212-2 reduces calcium in presynaptic terminals. However, the question still arises as to how the endocannabinoid system lowers calcium influx to stimulation and residual free calcium concentrations at PF boutons? How could this be possible? Theoretically, at least two hypothesise could account for these effects: first, cannabinoids activate potassium channels which could hyperpolarize presynaptic terminals and perhaps as a consequence lower

resting calcium levels as the probability of opening calcium channels is reduced. The primary evidence for this mechanism is that potassium channel antagonists eliminate the suppression following activation of CB1R (Daniel and Crepel, 2001, Diana and Marty, 2003, Robbe et al., 2001, Daniel et al., 2004). Endocannabinoids do not influence the amplitude of the presynaptic volley recorded extracellularly, suggesting that if potassium channels were activated this did not at least affect the threshold to electrical activation. Another possibility is that endocannabinoids direct modulate presynaptic calcium influx channels (Brown et al., 2004, Liang et al., 2004, Huang et al., 2001). Specifically, data from several studies suggest that N-type Ca^{2+} channels have an exclusive and privileged role in endocannabinoid-mediated suppression (Wilson and Nicoll, 2001, Alger, 2002). However, Daniel et al. (2004) found that CB1R-mediated inhibition of synaptic transmission at PF–PC synapses is independent of any direct effect on presynaptic calcium channels but does require the activation of potassium channels, making it again uncertain how direct inhibition of presynaptic Ca^{2+} channels (N, P/Q and R) can contribute to reduced calcium influx or absolute calcium levels per presynaptic terminal. In our study, although involvement of calcium and potassium channels was not investigated, we demonstrated that WIN55, 212-2 did not affect the presynaptic volley (N1) and largely decreased calcium mobilisation at PF terminals. Therefore, this is strongly supportive of the suggestion that the endocannabinoid system suppresses neurotransmitter release by inhibiting presynaptic calcium influx through presynaptic Ca^{2+} channels rather than potassium channels, since the fibre recruitment of PFs was not changed with the inhibition of presynaptic Ca^{2+} channels. In contrast, this absence of effect on PF excitability does not conflict with the postulated reduction of presynaptic Ca^{2+} channels by endocannabinoids, as blockade of these channels does not influence PF excitability (Mintz et al., 1995).

Activation of CB1Rs are responsible for the modulation of SyGCaMP2-mCherry responses.

AM251 completely prevented the effects of WIN55, 212-2 on both SyGCaMP2 fluorescence and its corresponding fEPSPs responses (see Figures 6.5 and 6.6) indicating that the effects of WIN55, 212-2 are mediated via CB1Rs. These results are consistent with the study of Lévénès et al. (1998), who found that SR141716A completely negated WIN55, 212-22-induced suppression of PF EPSCs in rat

cerebellar slices. It was also consistent with the study of Takahashi and Linden (2000), who illustrated that the effects of WIN55,212-2 application on PF EPSCs in rat cerebellar slices were completely prevented by prior application of SR141716-A. Moreover, it is also consistent with the study of (Irie et al., 2015), who showed that AM251 completely prevented MAM-2201-induced suppression of PF EPSCs in mouse cerebellar slices. Our results also agree with those of Azad et al. (2003), who found that WIN55,212-2 failed to induce depression of the amplitude of the N2 fEPSPs in coronal slices of the mouse lateral amygdala in the presence of the CB1R antagonist SR141716-A. Our result also corroborated a previous report showing that CB1Rs are expressed in excitatory terminals such as the PFs and CFs (Lévénès et al., 1998, Kawamura et al., 2006, Núñez et al., 2004, Takahashi and Linden, 2000). We have also shown that WIN55, 212-2 had no effect on the baseline SyGCaMP2: mCherry ratios in the presence of AM251, suggesting that the effects of WIN55, 212-2 are indeed mediated by CB1R. Taken together, the present investigation suggests that presynaptic CB1Rs activation is indeed necessary to induce synaptic inhibition by endocannabinoid agonists.

Activation of CB1Rs reduces the size of SyGaMP2 fluorescence responses in single boutons as well as the number of responding boutons

Finally, we looked at the effect of WIN55, 212-2 on single boutons within ML in the presence of PTX, DNQX and AP5. This study allowed us to test whether the decrease in the size of SyGCaMP2 responses described already were due to a decrease in the size of responses per bouton and/or a decrease in the number of contributing boutons. Our data showed that there was a clear decrease in calcium mobilisation in single terminals (see Figure 6.9 C and D). There was also a significant reduction in the number of boutons that responded to stimulation in the presence of WIN55, 212-2 (see Figure 6.9 A and B). There are two potential explanations for this. The first is that there is a change in excitability; However, this is not likely as we found the presynaptic volley (N1) was unaffected by the bath application of WIN55, 212-2. The second possibility relates to a technical limitation in detecting responding puncta when the size of these responses has been lowered by the application of WIN55, 212-2. Therefore, the reduction in the number of

boutons responding may simply have been due to a difficulty in detecting responding puncta. Nevertheless, we can conclude that WIN55, 212-2 decrease calcium mobilisation at individual PF terminals. These data also speak in favour of an inhibition of synaptic transmission by inhibition of voltage-dependent calcium channels (see Figure 6.10). Our results are in agreement with Zhang and Linden (2009), who reported that WIN55,212-2 significantly lowered the PF boutons using a loading dye method.

The results presented in this chapter strongly suggest that CB1R are present on PF terminals but cannot rule out the possibility that CB1R might also be found on interneuron terminals (such as basket and stellate cell terminals). WIN55, 212-2 clearly reduces calcium influx into boutons and additionally lowers resting levels of calcium inside presynaptic terminals. Further studies will be necessary to establish how CBR1 activation culminates in these effects.

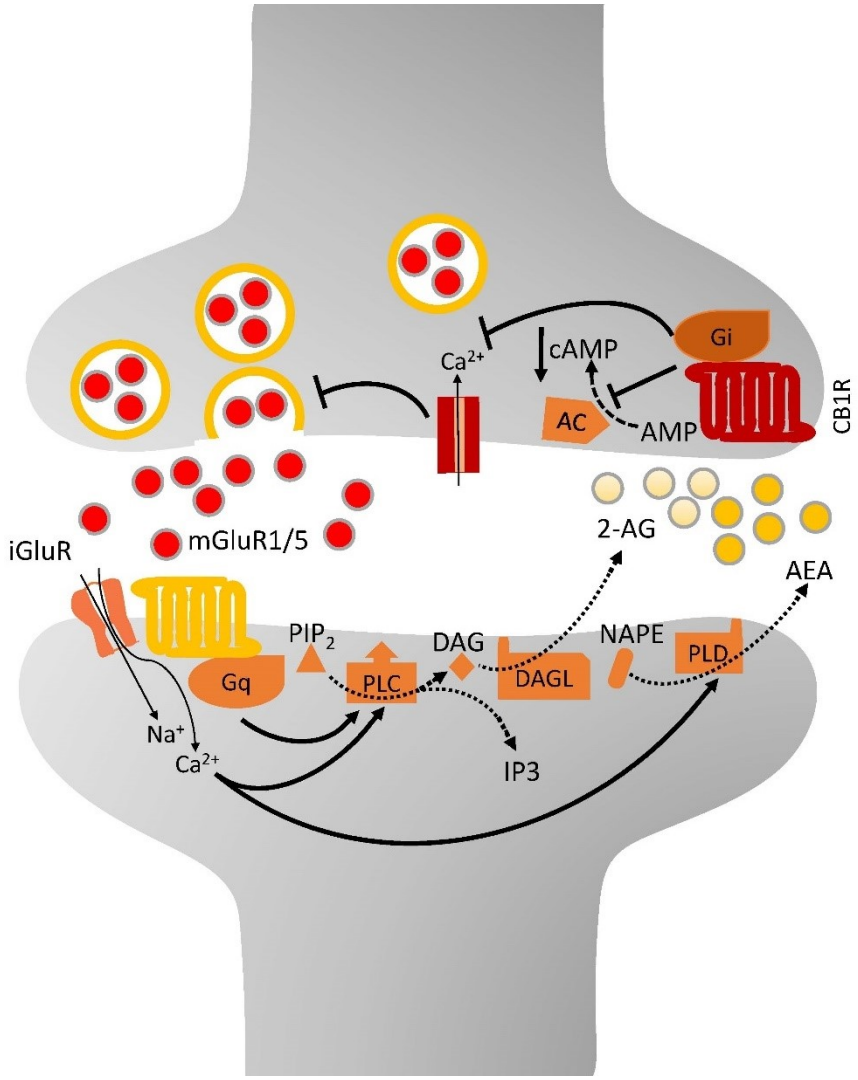

Figure 6.10. Proposed scheme overview for the endocannabinoid mechanism. Depolarization of the postsynaptic site leads to the activation of voltage-dependent calcium channels and the Gq-protein. Calcium influx leads to the activation of phospholipase C (PLC) and phospholipase D (PLD), which are both involved in the formation of endocannabinoids from the precursors of the lipid. The action of PLD on N-arachidonoyl phosphatidylethanolamine (NAPE) leads to the creation of anandamide (AEA). In addition, the activation of mGluRs in the postsynaptic site can also produce 2-arachidonylglycerol (2-AG) by activating phospholipase C and creating diacylglycerol and, ultimately, diacylglycerol lipase will cleave the diacylglycerol to form 2-AG. Thereafter, the endocannabinoids bind to CB1 receptors and consequently activate Gi/o proteins which down-regulate adenylyl cyclase (AC), leading to the inhibition of calcium channels.

Chapter 7: General Discussion

This PhD project aimed first to characterize the expression patterns and utility of a fluorescent protein-based genetically encoded calcium indicator (GECI), SyGCaMP2-mCherry, for measuring presynaptic calcium in sagittal and coronal cerebellar brain slices of SyG37 mice. Second coronal slices prepared from SyG37 mice were used to study the role of NMDARs and CB1Rs at synapses formed between PF and PCs.

Over the last few years, a new strain of a transgenic mice named SyG37 was created in this laboratory by fusing the fluorescent protein mCherry to the C-terminus of SyGCaMP2, which was in turn tethered to the C-terminus of the synaptic vesicle protein synaptophysin. This was engineered under the control of the Thy1-2 promoter for specific neuronal expression to avoid expression in glial cells, or indeed any other non-neuronal cell types present within the CNS (Dreosti et al., 2009, Moechars et al., 1999, Campsall et al., 2002). Although a Thy1.2 promoter is used to target expression of sensor to neurones, there is no control over which assemblies of neurones express the SyGCaMP2-mCherry. For example, SyGCaMP2-mCherry can be expressed in the GC axons (glutamatergic presynaptic terminals) but can also be expressed in the presynaptic terminals of BC and SC (GABAergic interneurons).

This model mouse was designed in part to monitor neural activities in populations of neurones. Not only can it be used to observe synaptic activity within neuronal pathways, it can be used to measure changes in presynaptic calcium signalling at the level of single synapses, even when synaptic transmission itself is blocked. To demonstrate this in the cerebellar cortex, we first examined the expression pattern of SyGCaMP2-mCherry using epifluorescent and multiphoton optical imaging techniques. Our study showed that SyGCaMP2-mCherry is expressed in all regions of the cerebellar cortex of SyG37 mice (chapter 3, Figures 3.1 and 3.2). SyGCaMP2-mCherry is expressed in each of the three main layers of coronal and sagittally cut cerebellar brain slices. It is prominently expressed in the ML. At low magnifications, expression is relatively uniform in this layer. At higher magnifications, expression is clearly punctate but without any obvious signs of

expression in post-synaptic structures such as dendrites or cell bodies. We did not see expression in stellate or basket cell somata (see for example Figures 3.3, 3.4 and 3.5), although it was possible to see “ghosts” of the cell bodies indicating an absence of expression. This is consistent with expression selective for presynaptic terminals although in future work, it would be useful to confirm this by demonstrating co-expression with presynaptic markers such as the presynaptic structural protein bassoon and with markers for inhibitory or excitatory synapses suchg as vGAT or vGlut. Experiments using electrical stimulation to activate specific cerebellar pathways within the ML were also consistent with expression of SyGCaMP2-mCherry in PF terminals. It was not possible to detect expression in the somata or dendrites of PCs, also suggesting that expression is not within the post-synaptic elements of PCs. Expression around PC somata was clear (Figures 3.3, 3.4 and 3.5). Expression patterns suggested that this most likely represented the axonal terminals of BCs which form complex synapses known as pinceau synapses around PC bodies (Tigyi et al., 1990, Buttermore et al., 2012).

Expression of SyGCaMP2 was also observed in the GCL. Again, there was no obvious sign of expression in post-synaptic structures, but the positions and patterns of expression suggested expression. Possible candidates for expression include presynaptic terminals of MFs, GoCs (Kandel et al., 1991) SCs and even UBCs. Together these data indicate that our sensor is expressed in the cerebellar cortex within presynaptic structures and importantly, for the subsequent parts of the thesis, it appears to be expressed within PF terminals. We cannot rule out the possibility of sensor expression in other cell types, including inhibitory terminals. Indeed, SyGCaMP2-mCherry is expressed at both inhibitory and excitatory terminals within the hippocampus (Al-Osta et al., 2018). Therefore, in future investigations it would be interesting to carry out immunohistochemistry experiments at this region of the brain to show conclusive expression of sensors on terminals of the cellular structure of the cerebellum region.

Our preliminary studies in Chapters 3 also showed that fluorescence responses could be reliably observed in sagittal and coronal cerebellar slices prepared from SyG37 mice in response to electrical stimulation of the ML or GCL (Figure 3.6) and the patterns of activity were again consistent with expression within PF terminals.

In the first part of chapter 4 we carried out a series of experiments using optical imaging techniques, in combination with extracellular recordings and pharmacological approaches, to examine whether our sensor can be used to measure presynaptic calcium in the cerebellar cortex. The results of these experiments suggested that SyGCaMP2 responses originated primarily, but not exclusively, from PF terminals. Preventing GABAergic and glutamergic synaptic transmission led to a reduction in the SyGCaMP2 responses to ML stimulation to roughly 80% in sagittal and 90% in coronal of pre-drug baseline levels. Therefore, it appears that about 10 - 20% of the total response arises from the polysynaptic activation of presynaptic axon terminals of neurones that have been driven via AMPA and GABA/Glycine receptors. Obvious possibilities are the axon terminals of BCs or SCs, both of which are driven by PF input. An alternative possibility is that AMPA and/or Glycine/$GABA_A$ receptors exist on the presynaptic terminals of PFs, and these are capable of directly modulating calcium influx at the terminal. I am not aware of direct evidence for this. To conclude, about 80 - 90% of SyGCaMP2 responses to ML activation in cerebellar slices appears to originate from PFs (Figures 4.5 and 5.4).

Our findings were in broad agreement with previous work from our laboratory in the hippocampus which found that blocking glutamergic synaptic transmission led to a reduction in SyGCaMP2 fluorescence to Schaffer collateral activation to 86% of baseline levels, suggesting that 14% of the total response originates from the presynaptic boutons of neurones, which are polysynaptically driven by AMPARs (Al-Osta et al., 2018).

Removal of calcium from our aCSF (with a corresponding increase in the concentration of magnesium ions to keep the proportion of divalent cations constant) abolished SyGCaMP2 responses as well as the N2 component of fEPSPs. The amplitude of the presynaptic volley was unaffected. These results were expected since GCaMP2 is a member of the GCaMP calcium sensor family (Akerboom et al., 2009, Hasan et al., 2004, Dittman and Regehr, 1998, Mintz et al., 1995, Nakai et al., 2001, Margrie et al., 1998) and removal of extracellular calcium prevents synaptic transmission (Figure 4.4). The sodium channel blocker TTX, which prevents action potential generation and as a result synaptic transmission, blocked SyGCaMP2 responses as well as N2 and N1 components of fEPSPs. Thus

SyGCaMP2 responses depend upon sodium channel activation and AP activity within the presynaptic terminals (Figure 4.2). In the second part of chapter 4 characterized SyGCaMP2 responses to different patterns of electrical stimulation and looked for evidence of differences in the different transmission patterns of granule cell ascending axon segment and PF synapses. In response to application of different intensities, numbers and frequencies of stimulation, SyGCaMP2 responses were not routinely detectable to single stimuli but could be reliably observed after 2-5 stimuli (Figures 4.9, 4.13, and 4.15). At a fixed frequency and intensity of stimulation, SyGCaMP2 responses increased in a reasonably linear manner up to about 10 stimuli after which responses started to reach a plateau (at about 40 stimuli). There was also a reasonably clear linear relationship between the peak SyGCaMP2 response and N2 fEPSP responses to ML stimulation (Figure 4.10 E, F and G). These observations indicated that our sensor can be used to reliably detect responses from populations of presynaptic boutons to a range of different electrical stimuli cerebellar brain slices. Whilst we could not detect responses to single stimuli, the fact that there was some linearity between stimulus number and SyGCaMP2 peak response suggests that it may be possible to use SyG37 mice to evaluate neuronal firing rates in situ from the amplitudes of responses.

Direct electrical stimulation of the ML in coronal cerebellar slices triggered beamlike responses across the cortex. We found no clear evidence for the propagation of the SyGCaMP2 response into the GCL which is expected if we are primarily activating PF terminals (see Figures 4.7B, 4.9C, 4.14A, 4.15B, and 4.15E). In contrast, direct electrical stimulation of the GCL produced response in GCL as well as responses in the ML. We found evidence for increases in fluorescence in the area directly above the point of stimulation and fluorescence extending in either direction along the ML (Figures 4.11B, 4.13D, 4.14B, 4.15C and 4.15F). These results suggest that direct activation of the GCL causes information to propagate directly above the point of stimulation by ascending axons to bifurcate along PFs; direct activation of the ML in contrast only propagate information along PFs. Although we did not have time to pursue this in more detail, the time course for SyGCaMP2 decay of responses to direct PF activation faster than those activated by activation of the GCL (Figure 4.14). These observations might provide additional evidence that PF and ascending axon synapses are heterogeneous in their properties. Indeed, as mentioned earlier,

it has been shown that there are differences in the characteristics between synapses formed by ascending and parallel fibre segments of granule cell axons of a presynaptic nature (Sims and Hartell, 2005, Gundappa-Sulur et al., 1999). Further investigation to identify other possible differences in transmission properties at ascending axon and PF synapses would be interesting.

Together, the results presented in the chapters 3 and 4 revealed in particular that, in coronal slices, ML stimulation induced SyGCaMP2 responses that are beamlike and that extended along PFs, and that these responses persist in the presence of synaptic transmission blockers, indicating a significant component arises from the PFs themselves. On this basis, we next decided to use SyG37 mice to examine the effects of modulation of two different receptor pathways that have been shown elsewhere to have presynaptic actions of synaptic transmission. We chose to examine the roles of NMDARs and CB1Rs as these have been shown to play myriad roles in learning and memory and to have retrograde actions at various synapse types including synapses within the cerebellum.

We first studied the possible role of presynaptic NMDA receptors in PF-PC synaptic transmission. Activation of NMDARs with NMDA produced a clear, reversible reduction in N2 fEPSP and SyGCaMP2 responses (Figures 5.1and 5.3). Given the apparent absence of NMDARs on adult PCs (Llano et al., 1991, Farrant and Cull-Candy, 1991) this suggests that pre-NMDARs modulate transmission at this synapse. Activation of NMDARs did not affect the N1 presynpatic volley but it did reversibly increase the PPR of the N2 response. PPR is commonly accepted as an indication of a presynaptic change in the probability of release, PPR can be influenced by other factors (Foster and Richardson, 1997). For example, PPR changes could arise following desensitization of the postsynaptic receptor and subsequent diffusion of transmitter (Trussell et al., 1993, Opazo et al., 2010), or it could also be affected by other modifications which are not associated with alterations in release probability (Shin et al., 2010, Geppert et al., 1997). These limitations may indicate that this method is inadequate on its own as evidence of a particular mechanism (Yang and Calakos, 2013) but when used in combination with SyGCaMP2 imaging, this may lend stronger support for a presynaptic mechanism of action.

Beam-like patterns of fibre activation following ML activation were clearly reduced in the presence of NMDA, also suggesting that NMDARs are located on PF terminals (Figure 5.2). These experiments alone cannot exclude the alternative possibility that NMDARs are present on postsynaptic cells (such as stellate and basket cells) and that their activation triggers the production of certain retrograde messengers that affect calcium signalling in PF terminals (Duguid and Smart, 2004, Rossi et al., 2012). However, NMDA-induced depression of SyGCaMP2 responses remained in the presence of the GABA/Glycine receptor antagonist picrotoxin and AMPA receptor blocker DNQX (Figure 5.5). The effects were sensitive to AP5, together (Figure 5.6) indicating that this was an NMDAR dependent process and that the receptors involved are most likely located on PF terminals as previously postulated (Casado et al., 2000). We did not have time to examine whether NMDAR activation may have caused $GABA_B$ activation and consequently a reduction in transmitter release from PFs.

NMDA significantly raised the baseline SyGCaMP2: mCherry ratio, indicating that the absolute calcium concentration in presynaptic terminals was indeed increased. This led to the suggestion that activation of NMDARs on the PF terminal led to its channels opening, allowing calcium to enter to increase residual calcium levels and consequently reduce transmitter release. One of the advantages of this sensor is that it provides unique opportunities for measuring absolute calcium.

Although we have provided strong evidence that pre-NMDARs exist on PF terminals and that their activation modulates synaptic transmission, the mechanism by which pre-NMDARs modulate presynaptic calcium is not yet fully understood. Further investigations are required to address the current – and significant – gaps in our knowledge of NMDAR function. It will also be interesting in future studies to use this sensor to examine NR2 subunit-selective NMDAR antagonists such as Ro 04-5595 hydrochloride (NR2B), PEAQX tetrasodium salt or zinc (NR2A) since NR2 subunits are found in axon terminals and presynaptic boutons (Petralia et al., 1994) to determine which subunits (NR2A and NR2B) are necessary to induce synaptic depression at this synapse (Bidoret et al., 2009).

CB1Rs are 7-transmembrane G protein-coupled receptors, which are the most abundant in the mammalian brain with high expression levels within the cerebellar

cortex (Kawamura et al., 2006, Herkenham et al., 1990) that are located primary on presynaptic terminals and whose activation leads to the inhibition of neurotransmitters (Azad et al., 2003, Irie et al., 2015, Daniel and Crepel, 2001, Brown et al., 2004).

In the final chapter, we investigated the role of CB1Rs in modulating synaptic release and plasticity at PF to PC synapses. Our findings demonstrated that WIN55, 212-2 reduced N2 fEPSP and increases PPR but did not affect the N1 component suggesting a presynaptic site of action but indicating that PF terminal excitability did not change (Figure 6.2). Moreover, our data showed that SyGCaMP2 responses were similarly reduced by WIN55,212-2 indicating that calcium in presynaptic terminals was reduced (Figure 6.1). WIN55,212-2 depressed SyGCaMP2 responses in the presence of synaptic transmission blockers, suggesting a direct effect via CB1Rs on PFs (Figure 6.4). Furthermore, our observations showed that WIN55,212-2 failed to depress either SyGCaMP2 responses or the N2 component of the fEPSP in the presence of the CB1R antagonist AM251 (Figure 6.5 and 6.6), indicating that the effect is actually mediated by CB1R (Daniel and Crepel, 2001, Irie et al., 2015, Brown et al., 2004). Endocannabinoids reduced both the size of SyGCaMP2 responses in single boutons and the number of boutons that responded to synaptic activation.

Once of the problems of SyGCaMP2 is that it lacks sufficient sensitivity to robustly identify a single response in a single bouton. Therefore, it is difficult to be sure from our results whether the reduction in the number of responding boutons was due to a change in the excitability of presynaptic terminals or a failure to detect very small responses in single boutons. Since the N1 component of the fEPSP did not change, then the most likely explanation for is that CB1R activation reduces calcium mobilisation during stimulation and hence represents a reduction in calcium per terminal (Brown et al., 2004). However, it is unclear from our studies exactly how calcium in presynaptic terminals is reduced and therefore would be something to explore in the future.

All experiments were performed at room temperature so it will be interesting to observe the effects of repeating some of our experiments at other physiological temperatures although all our responses were strongly active and stable during the

entire duration of the experiments. Both the N1 and N2 components of the PF waveforms were sensitive to TTX. The N2 component, but not the N1 component, was selectively abolished by the AMPA receptor blocker DNQX.

In conclusion, the findings presented in this PhD project demonstrate that SyGCaMP2-mCherry is expressed on presynaptic terminals in the cerebellar cortex and can be used to measure absolute and transient calcium signalling at presynaptic boutons of large populations of neurones. We have found evidence for NMDARs and CB1Rs being located on PF terminals and that each of these receptors is capable of modulating synaptic transmission at PF-PC synapses through presynaptic calcium modulation. This thesis furthers the understanding of the role of the CB1Rs and NMDARs at cerebellar PF-PC synapses that might underlie learning and memory processes.

References

ADAMS, I. B. & MARTIN, B. R. 1996. Cannabis: pharmacology and toxicology in animals and humans. *Addiction,* 91**,** 1585-1614.

AIZPURUA-OLAIZOLA, O., ELEZGARAI, I., RICO-BARRIO, I., ZARANDONA, I., ETXEBARRIA, N. & USOBIAGA, A. 2017. Targeting the endocannabinoid system: future therapeutic strategies. *Drug Discovery Today,* 22**,** 105-110.

AIZPURUA-OLAIZOLA, O., OMAR, J., NAVARRO, P., OLIVARES, M., ETXEBARRIA, N. & USOBIAGA, A. 2014. Identification and quantification of cannabinoids in Cannabis sativa L. plants by high performance liquid chromatography-mass spectrometry. *Analytical and bioanalytical chemistry,* 406**,** 7549-7560.

AKERBOOM, J., CHEN, T.-W., WARDILL, T. J., TIAN, L., MARVIN, J. S., MUTLU, S., CALDERÓN, N. C., ESPOSTI, F., BORGHUIS, B. G. & SUN, X. R. 2012. Optimization of a GCaMP calcium indicator for neural activity imaging. *Journal of Neuroscience,* 32**,** 13819-13840.

AKERBOOM, J., RIVERA, J. D. V., GUILBE, M. M. R., MALAVÉ, E. C. A., HERNANDEZ, H. H., TIAN, L., HIRES, S. A., MARVIN, J. S., LOOGER, L. L. & SCHREITER, E. R. 2009. Crystal structures of the GCaMP calcium sensor reveal the mechanism of fluorescence signal change and aid rational design. *Journal of biological chemistry,* 284**,** 6455-6464.

AKOPIAN, A. N., SOUSLOVA, V., ENGLAND, S., OKUSE, K., OGATA, N., URE, J., SMITH, A., KERR, B. J., MCMAHON, S. B. & BOYCE, S. 1999. The tetrodotoxin-resistant sodium channel SNS has a specialized function in pain pathways. *Nature neuroscience,* 2**,** 541.

AL-OSTA, I., MUCHA, M., PEREDA, D., PIQUÉ-GILI, M., OKOROCHA, A. E., THOMAS, R. & HARTELL, N. A. 2018. Imaging calcium in hippocampal presynaptic terminals with a ratiometric calcium sensor in a novel transgenic mouse. *Frontiers in cellular neuroscience,* 12.

AL-OSTA, I. M. S. 2018. *Visualising the role of presynaptic calcium in hippocampal circuits using a novel, genetically encoded calcium sensor.* University of Leicester.

ALGER, B. E. 2002. Retrograde signaling in the regulation of synaptic transmission: focus on endocannabinoids. *Progress in neurobiology,* 68**,** 247-286.

ANDERSON, W. W. & COLLINGRIDGE, G. L. 2007. Capabilities of the WinLTP data acquisition program extending beyond basic LTP experimental functions. *Journal of neuroscience methods,* 162**,** 346-356.

ATASOY, D. & KAVALALI, E. T. 2008. Neurotransmitter release machinery: components of the neuronal SNARE complex and their function. *Structural And Functional Organization Of The Synapse.* Springer.

ATLURI, P. P. & REGEHR, W. G. 1996. Determinants of the time course of facilitation at the granule cell to Purkinje cell synapse. *Journal of Neuroscience,* 16**,** 5661-5671.

AZAD, S. C., EDER, M., MARSICANO, G., LUTZ, B., ZIEGLGÄNSBERGER, W. & RAMMES, G. 2003. Activation of the cannabinoid receptor type 1 decreases glutamatergic and GABAergic synaptic transmission in the lateral amygdala of the mouse. *Learning & memory,* 10**,** 116-128.

BABA, A., YASUI, T., FUJISAWA, S., YAMADA, R. X., YAMADA, M. K., NISHIYAMA, N., MATSUKI, N. & IKEGAYA, Y. 2003. Activity-evoked capacitative Ca2+ entry: implications in synaptic plasticity. *Journal of Neuroscience,* 23**,** 7737-7741.

BAHIA, P. K., BENNETT, E. S. & TAYLOR-CLARK, T. E. 2012. Reductions in external divalent cations evoke novel voltage-gated currents in sensory neurons. *PloS one,* 7**,** e31585.

BAIRD, G. S., ZACHARIAS, D. A. & TSIEN, R. Y. 1999. Circular permutation and receptor insertion within green fluorescent proteins. *Proceedings of the National Academy of Sciences,* 96**,** 11241-11246.

BALU, D. T. 2016. Chapter Twelve - The NMDA Receptor and Schizophrenia: From Pathophysiology to Treatment. *In:* SCHWARCZ, R. (ed.) *Advances in Pharmacology.* Academic Press.

BANERJEE, A., LARSEN, R. S., PHILPOT, B. D. & PAULSEN, O. 2016. Roles of Presynaptic NMDA Receptors in Neurotransmission and Plasticity. *Trends in Neurosciences,* 39**,** 26-39.

BANKHEAD, P. 2014. Analyzing fluorescence microscopy images with ImageJ. *ImageJ,* 1**,** 195.

BARTLETT, J. M. & STIRLING, D. 2003. *PCR protocols*, Springer.

BECHER, A., DRENCKHAHN, A., PAHNER, I., MARGITTAI, M., JAHN, R. & AHNERT-HILGER, G. 1999. The synaptophysin–synaptobrevin complex: a hallmark of synaptic vesicle maturation. *Journal of Neuroscience,* 19**,** 1922-1931.

BEIERLEIN, M. & REGEHR, W. G. 2006. Local interneurons regulate synaptic strength by retrograde release of endocannabinoids. *Journal of Neuroscience,* 26**,** 9935-9943.

BELLAMY, T. C. 2006. Interactions between Purkinje neurones and Bergmann glia. *The Cerebellum,* 5**,** 116-126.

BERGEROT, A., RIGBY, M., BOUVIER, G. & MARCAGGI, P. 2013. Persistent posttetanic depression at cerebellar parallel fiber to Purkinje cell synapses. *PloS one,* 8**,** e70277.

BERRIDGE, M. J. 1998. Neuronal calcium signaling. *Neuron,* 21**,** 13-26.

BIDORET, C., AYON, A., BARBOUR, B. & CASADO, M. 2009. Presynaptic NR2A-containing NMDA receptors implement a high-pass filter synaptic plasticity rule. *Proceedings of the National Academy of Sciences,* 106**,** 14126-14131.

BIDORET, C., BOUVIER, G., AYON, A., SZAPIRO, G. & CASADO, M. 2015. Properties and molecular identity of NMDA receptors at synaptic and non-synaptic inputs in cerebellar molecular layer interneurons. *Frontiers in Synaptic Neuroscience,* 7.

BLISS, T. V. & COLLINGRIDGE, G. L. 1993. A synaptic model of memory: long-term potentiation in the hippocampus. *Nature,* 361**,** 31.

BLISS, T. V. & LØMO, T. 1973. Long-lasting potentiation of synaptic transmission in the dentate area of the anaesthetized rabbit following stimulation of the perforant path. *The Journal of physiology,* 232**,** 331-356.

BOURON, A. 2000. Activation of a capacitative Ca2+ entry pathway by store depletion in cultured hippocampal neurones. *FEBS letters,* 470**,** 269-272.

BOUVIER, G., BIDORET, C., CASADO, M. & PAOLETTI, P. 2015. Presynaptic NMDA receptors: roles and rules. *Neuroscience,* 311**,** 322-340.

BRODAL, P. 2004. *The central nervous system: structure and function*, Oxford University Press.

BROSE, N., ROSENMUND, C. & RETTIG, J. 2000. Regulation of transmitter release by Unc-13 and its homologues. *Current opinion in neurobiology,* 10**,** 303-311.

BROWN, S. P., SAFO, P. K. & REGEHR, W. G. 2004. Endocannabinoids inhibit transmission at granule cell to Purkinje cell synapses by modulating three types of presynaptic calcium channels. *Journal of Neuroscience,* 24**,** 5623-5631.

BRUNS, D. & JAHN, R. 2002. Molecular determinants of exocytosis. *Pflügers Archiv,* 443**,** 333-338.

BUTTERMORE, E. D., PIOCHON, C., WALLACE, M. L., PHILPOT, B. D., HANSEL, C. & BHAT, M. A. 2012. Pinceau organization in the cerebellum requires distinct functions of neurofascin in Purkinje and basket neurons during postnatal development. *Journal of Neuroscience,* 32**,** 4724-4742.

CAMPSALL, K. D., MAZEROLLE, C. J., DE REPENTINGY, Y., KOTHARY, R. & WALLACE, V. A. 2002. Characterization of transgene expression and Cre recombinase activity in a panel of Thy-1 promoter-Cre transgenic mice. *Developmental dynamics: an official publication of the American Association of Anatomists,* 224**,** 135-143.

CARLETON, S. C. & CARPENTER, M. B. 1983. Afferent and efferent connections of the medial, inferior and lateral vestibular nuclei in the cat and monkey. *Brain research,* 278**,** 29-51.

CARONI, P. 1997. Overexpression of growth-associated proteins in the neurons of adult transgenic mice. *Journal of neuroscience methods,* 71**,** 3-9.

CARR, C. M. & MUNSON, M. 2007. Tag team action at the synapse. *EMBO reports,* 8**,** 834-838.
CASADO, M., DIEUDONNE, S. & ASCHER, P. 2000. Presynaptic N-methyl-D-aspartate receptors at the parallel fiber–Purkinje cell synapse. *Proceedings of the National Academy of Sciences,* 97**,** 11593-11597.
CASADO, M., ISOPE, P. & ASCHER, P. 2002. Involvement of Presynaptic N-Methyl-D-Aspartate Receptors in Cerebellar Long-Term Depression. *Neuron,* 33**,** 123-130.
CATTERALL, W. A. 1992. Cellular and molecular biology of voltage-gated sodium channels. *Physiological reviews,* 72**,** S15-S48.
CATTERALL, W. A. & FEW, A. P. 2008. Calcium channel regulation and presynaptic plasticity. *Neuron,* 59**,** 882-901.
CESANA, E., PIETRAJTIS, K., BIDORET, C., ISOPE, P., D'ANGELO, E., DIEUDONNÉ, S. & FORTI, L. 2013. Granule cell ascending axon excitatory synapses onto Golgi cells implement a potent feedback circuit in the cerebellar granular layer. *Journal of Neuroscience,* 33**,** 12430-12446.
CHAN-PALAY, V. 1974. *The Cerebellar Cortex: Cytology and Organization*, Springer.
CHAUMONT, J., GUYON, N., VALERA, A. M., DUGUÉ, G. P., POPA, D., MARCAGGI, P., GAUTHERON, V., REIBEL-FOISSET, S., DIEUDONNÉ, S. & STEPHAN, A. 2013. Clusters of cerebellar Purkinje cells control their afferent climbing fiber discharge. *Proceedings of the National Academy of Sciences,* 110**,** 16223-16228.
CHEN, T.-W., WARDILL, T. J., SUN, Y., PULVER, S. R., RENNINGER, S. L., BAOHAN, A., SCHREITER, E. R., KERR, R. A., ORGER, M. B. & JAYARAMAN, V. 2013. Ultrasensitive fluorescent proteins for imaging neuronal activity. *Nature,* 499**,** 295.
CITRI, A. & MALENKA, R. C. 2008. Synaptic plasticity: multiple forms, functions, and mechanisms. *Neuropsychopharmacology,* 33**,** 18-41.
CLEMENTS, J. & WESTBROOK, G. 1991. Activation kinetics reveal the number of glutamate and glycine binding sites on the N-methyl-D-aspartate receptor. *Neuron,* 7**,** 605-613.
COESMANS, M., WEBER, J. T., DE ZEEUW, C. I. & HANSEL, C. 2004. Bidirectional Parallel Fiber Plasticity in the Cerebellum under Climbing Fiber Control. *Neuron,* 44**,** 691-700.
COHEN, D. & YAROM, Y. 2000. Cerebellar on-beam and lateral inhibition: two functionally distinct circuits. *Journal of neurophysiology,* 83**,** 1932-1940.
COLLINGRIDGE, G. 1987. The role of NMDA receptors in learning and memory. *Nature,* 330**,** 604-605.
COUTINHO, V. & KNÖPFEL, T. 2002. Book review: metabotropic glutamate receptors: electrical and chemical signaling properties. *The Neuroscientist,* 8**,** 551-561.
CRÉPEL, F. & AUDINAT, E. 1991. Excitatory amino acids receptors of cerebellar purkinje cells: Development and plasticity. *Progress in biophysics and molecular biology,* 55**,** 31-46.
D'ANGELO, E. & CASALI, S. 2013. Seeking a unified framework for cerebellar function and dysfunction: from circuit operations to cognition. *Frontiers in neural circuits,* 6**,** 116.
DANA, H., CHEN, T.-W., HU, A., SHIELDS, B. C., GUO, C., LOOGER, L. L., KIM, D. S. & SVOBODA, K. 2014. Thy1-GCaMP6 transgenic mice for neuronal population imaging in vivo. *PloS one,* 9**,** e108697.
DANIEL, H. & CREPEL, F. 2001. Control of Ca2+ influx by cannabinoid and metabotropic glutamate receptors in rat cerebellar cortex requires K+ channels. *The Journal of physiology,* 537**,** 793-800.
DANIEL, H., RANCILLAC, A. & CREPEL, F. 2004. Mechanisms underlying cannabinoid inhibition of presynaptic Ca2+ influx at parallel fibre synapses of the rat cerebellum. *The Journal of physiology,* 557**,** 159-174.
DEAN, P., PORRILL, J., EKEROT, C.-F. & JÖRNTELL, H. 2010. The cerebellar microcircuit as an adaptive filter: experimental and computational evidence. *Nature Reviews Neuroscience,* 11**,** 30.

DEBANNE, D. 1996. Guerineau NC, Gahwiler BH, and Thompson SM. *Paired-pulse facilitation and depression at unitary synapses in rat hippocampus: quantal fluctuation affects subsequent release. J Physiol,* 491**,** 163-176.

DEBANNE, D., GUERINEAU, N. C., GÄHWILER, B. & THOMPSON, S. M. 1996. Paired-pulse facilitation and depression at unitary synapses in rat hippocampus: quantal fluctuation affects subsequent release. *The Journal of physiology,* 491**,** 163-176.

DEVANE, W. A., HANUS, L., BREUER, A., PERTWEE, R. G., STEVENSON, L. A., GRIFFIN, G., GIBSON, D., MANDELBAUM, A., ETINGER, A. & MECHOULAM, R. 1992. Isolation and structure of a brain constituent that binds to the cannabinoid receptor. *Science,* 258**,** 1946-1949.

DIANA, M. A., LEVENES, C., MACKIE, K. & MARTY, A. 2002. Short-term retrograde inhibition of GABAergic synaptic currents in rat Purkinje cells is mediated by endogenous cannabinoids. *Journal of Neuroscience,* 22**,** 200-208.

DIANA, M. A. & MARTY, A. 2003. Characterization of depolarization-induced suppression of inhibition using paired interneuron–Purkinje cell recordings. *Journal of Neuroscience,* 23**,** 5906-5918.

DIETRICH, D., KIRSCHSTEIN, T., KUKLEY, M., PEREVERZEV, A., VON DER BRELIE, C., SCHNEIDER, T. & BECK, H. 2003. Functional specialization of presynaptic Cav2. 3 Ca2+ channels. *Neuron,* 39**,** 483-496.

DÍEZ-GARCÍA, J., AKEMANN, W. & KNÖPFEL, T. 2007. In vivo calcium imaging from genetically specified target cells in mouse cerebellum. *Neuroimage,* 34**,** 859-869.

DÍEZ-GARCÍA, J., MATSUSHITA, S., MUTOH, H., NAKAI, J., OHKURA, M., YOKOYAMA, J., DIMITROV, D. & KNÖPFEL, T. 2005. Activation of cerebellar parallel fibers monitored in transgenic mice expressing a fluorescent Ca2+ indicator protein. *European journal of neuroscience,* 22**,** 627-635.

DINO, M., SCHUERGER, R., LIU, Y.-B., SLATER, N. & MUGNAINI, E. 2000. Unipolar brush cell: a potential feedforward excitatory interneuron of the cerebellum. *Neuroscience,* 98**,** 625-636.

DIÑO, M. R., NUNZI, M. G., ANELLI, R. & MUGNAINI, E. 2000. Unipolar brush cells of the vestibulocerebellum: afferents and targets. *Progress in brain research.* Elsevier.

DITTMAN, J. S. & REGEHR, W. G. 1996. Contributions of calcium-dependent and calcium-independent mechanisms to presynaptic inhibition at a cerebellar synapse. *Journal of Neuroscience,* 16**,** 1623-1633.

DITTMAN, J. S. & REGEHR, W. G. 1998. Calcium dependence and recovery kinetics of presynaptic depression at the climbing fiber to Purkinje cell synapse. *Journal of Neuroscience,* 18**,** 6147-6162.

DOBRUNZ, L. E. & STEVENS, C. F. 1997. Heterogeneity of release probability, facilitation, and depletion at central synapses. *Neuron,* 18**,** 995-1008.

DOBSON, K. L. & BELLAMY, T. C. 2015. Localization of presynaptic plasticity mechanisms enables functional independence of synaptic and ectopic transmission in the cerebellum. *Neural plasticity,* 2015.

DOROSTKAR, M. M., DREOSTI, E., ODERMATT, B. & LAGNADO, L. 2010. Computational processing of optical measurements of neuronal and synaptic activity in networks. *Journal of neuroscience methods,* 188**,** 141-150.

DREOSTI, E., ODERMATT, B., DOROSTKAR, M. M. & LAGNADO, L. 2009. A genetically encoded reporter of synaptic activity in vivo. *Nature methods,* 6**,** 883-889.

DROBIZHEV, M., TILLO, S., MAKAROV, N., HUGHES, T. & REBANE, A. 2009. Absolute two-photon absorption spectra and two-photon brightness of orange and red fluorescent proteins. *The Journal of Physical Chemistry B,* 113**,** 855-859.

DUGUID, I. C. 2013. Presynaptic NMDA receptors: Are they dendritic receptors in disguise? *Brain Research Bulletin,* 93**,** 4-9.

DUGUID, I. C. & SMART, T. G. 2004. Retrograde activation of presynaptic NMDA receptors enhances GABA release at cerebellar interneuron–Purkinje cell synapses. *Nature neuroscience,* 7**,** 525.

EBLEN, F., LÖSCHMANN, P.-A., WÜLLNER, U., TURSKI, L. & KLOCKGETHER, T. 1996. Effects of 7-nitroindazole, NG-nitro-l-arginine, and D-CPPene on harmaline-induced postural tremor, N-methyl-d-aspartate-induced seizures, and lisuride-induced rotations in rats with nigral 6-hydroxydopamine lesions. *European Journal of Pharmacology,* 299**,** 9-16.

ECCLES, J., ITO, M. & SZENTAGOTHAI, J. 1967. The Cerebellum as a Neuronal Machine., Berlin: Springer-Verlag.

ECCLES, J. C., LLINÁS, R. & SASAKI, K. 1966. The mossy fibre-granule cell relay of the cerebellum and its inhibitory control by Golgi cells. *Experimental brain research,* 1**,** 82-101.

ECCLES, M., MCCARTHY, B., PROFFITT, D. & ROSEN, D. 1976. A programmable flying-spot microscope and picture preprocessor. *Journal of Microscopy,* 106**,** 33-42.

EHRLER, M. R., MCGLADE, E. C. & YURGELUN-TODD, D. A. 2015. Subjective and cognitive effects of cannabinoids in marijuana smokers. *Cannabinoid Modulation of Emotion, Memory, and Motivation.* Springer.

FARRANT, M. & CULL-CANDY, S. G. 1991. Excitatory amino acid receptor-channels in Purkinje cells in thin cerebellar slices. *Proc Biol Sci,* 244**,** 179-84.

FASSHAUER, D., SUTTON, R. B., BRUNGER, A. T. & JAHN, R. 1998. Conserved structural features of the synaptic fusion complex: SNARE proteins reclassified as Q-and R-SNAREs. *Proceedings of the national academy of sciences,* 95**,** 15781-15786.

FINKBEINER, S. & GREENBERG, M. E. 1998. Ca2+ channel-regulated neuronal gene expression. *Journal of neurobiology,* 37**,** 171-189.

FLORES, Á., MALDONADO, R. & BERRENDERO, F. 2013. Cannabinoid-hypocretin cross-talk in the central nervous system: what we know so far. *Frontiers in neuroscience,* 7**,** 256.

FOSTER, B. & RICHARDSON, T. L. 1997. Postsynaptic action potentials do not alter short-term potentiation in the dentate gyrus. *Brain research,* 758**,** 59-68.

GARNER, C. C., KINDLER, S. & GUNDELFINGER, E. D. 2000. Molecular determinants of presynaptic active zones. *Current opinion in neurobiology,* 10**,** 321-327.

GARNER, C. C., ZHAI, R. G., GUNDELFINGER, E. D. & ZIV, N. E. 2002. Molecular mechanisms of CNS synaptogenesis. *Trends in neurosciences,* 25**,** 243-250.

GEPPERT, M., GODA, Y., STEVENS, C. F. & SÜDHOF, T. C. 1997. The small GTP-binding protein Rab3A regulates a late step in synaptic vesicle fusion. *Nature,* 387**,** 810.

GLITSCH, M. & MARTY, A. 1999. Presynaptic effects of NMDA in cerebellar Purkinje cells and interneurons. *Journal of Neuroscience,* 19**,** 511-519.

GRANSETH, B., ODERMATT, B., ROYLE, S. J. & LAGNADO, L. 2006. Clathrin-mediated endocytosis is the dominant mechanism of vesicle retrieval at hippocampal synapses. *Neuron,* 51**,** 773-786.

GRIESBECK, O., BAIRD, G. S., CAMPBELL, R. E., ZACHARIAS, D. A. & TSIEN, R. Y. 2001. Reducing the environmental sensitivity of yellow fluorescent protein mechanism and applications. *Journal of Biological Chemistry,* 276**,** 29188-29194.

GUNDAPPA-SULUR, G., DE SCHUTTER, E. & BOWER, J. M. 1999. Ascending granule cell axon: an important component of cerebellar cortical circuitry. *Journal of Comparative Neurology,* 408**,** 580-596.

HAAG, J. & BORST, A. 2000. Spatial distribution and characteristics of voltage-gated calcium signals within visual interneurons. *Journal of Neurophysiology,* 83**,** 1039-1051.

HAJ-DAHMANE, S. & SHEN, R.-Y. 2009. Endocannabinoids suppress excitatory synaptic transmission to dorsal raphe serotonin neurons through the activation of presynaptic CB1 receptors. *Journal of Pharmacology and Experimental Therapeutics,* 331**,** 186-196.

HÁJOS, N., KATONA, I., NAIEM, S., MACKIE, K., LEDENT, C., MODY, I. & FREUND, T. F. 2000. Cannabinoids inhibit hippocampal GABAergic transmission and network oscillations. *European Journal of Neuroscience,* 12**,** 3239-3249.

HÁJOS, N., LEDENT, C. & FREUND, T. F. 2001. Novel cannabinoid-sensitive receptor mediates inhibition of glutamatergic synaptic transmission in the hippocampus. *Neuroscience,* 106**,** 1-4.

HAMANN, M., ROSSI, D. J. & ATTWELL, D. 2002. Tonic and spillover inhibition of granule cells control information flow through cerebellar cortex. *Neuron,* 33**,** 625-633.

HAMMOND, C. 2001. *Cellular and Molecular Neurobiology (Deluxe Edition)*, Academic Press.

HÁMORI, J. & SZENTÁGOTHAI, J. 1966. Identification under the electron microscope of climbing fibers and their synaptic contacts. *Experimental Brain Research,* 1**,** 65-81.

HAMPSON, R. E. & DEADWYLER, S. A. 2000. Cannabinoids reveal the necessity of hippocampal neural encoding for short-term memory in rats. *Journal of Neuroscience,* 20**,** 8932-8942.

HANSEN, K. B., YI, F., PERSZYK, R. E., FURUKAWA, H., WOLLMUTH, L. P., GIBB, A. J. & TRAYNELIS, S. F. 2018. Structure, function, and allosteric modulation of NMDA receptors. *The Journal of General Physiology,* 150**,** 1081-1105.

HASAN, M. T., FRIEDRICH, R. W., EULER, T., LARKUM, M. E., GIESE, G., BOTH, M., DUEBEL, J., WATERS, J., BUJARD, H. & GRIESBECK, O. 2004. Functional fluorescent Ca2+ indicator proteins in transgenic mice under TET control. *PLoS biology,* 2**,** e163.

HECK, D. 1995. Sequential stimulation of guinea pig cerebellar cortex in vitro strongly affects Purkinje cells via parallel fibers. *Naturwissenschaften,* 82**,** 201-203.

HENZE, D. A., BORHEGYI, Z., CSICSVARI, J., MAMIYA, A., HARRIS, K. D. & BUZSAKI, G. 2000. Intracellular features predicted by extracellular recordings in the hippocampus in vivo. *Journal of neurophysiology,* 84**,** 390-400.

HERKENHAM, M., LYNN, A. B., LITTLE, M. D., JOHNSON, M. R., MELVIN, L. S., DE COSTA, B. R. & RICE, K. C. 1990. Cannabinoid receptor localization in brain. *Proceedings of the national Academy of sciences,* 87**,** 1932-1936.

HIRONO, M., SAITOW, F., KUDO, M., SUZUKI, H., YANAGAWA, Y., YAMADA, M., NAGAO, S., KONISHI, S. & OBATA, K. 2012. Cerebellar globular cells receive monoaminergic excitation and monosynaptic inhibition from Purkinje cells. *PloS one,* 7**,** e29663.

HOFFMAN, A. F. & LUPICA, C. R. 2000. Mechanisms of Cannabinoid Inhibition of GABAASynaptic Transmission in the Hippocampus. *Journal of Neuroscience,* 20**,** 2470-2479.

HOGAN-CANN, A. D. & ANDERSON, C. M. 2016. Physiological Roles of Non-Neuronal NMDA Receptors. *Trends in Pharmacological Sciences,* 37**,** 750-767.

HOWLETT, A., BARTH, F., BONNER, T., CABRAL, G., CASELLAS, P., DEVANE, W., FELDER, C., HERKENHAM, M., MACKIE, K. & MARTIN, B. 2002. International Union of Pharmacology. XXVII. Classification of cannabinoid receptors. *Pharmacological reviews,* 54**,** 161-202.

HUANG, C. C., LO, S. W. & HSU, K. S. 2001. Presynaptic mechanisms underlying cannabinoid inhibition of excitatory synaptic transmission in rat striatal neurons. *The Journal of physiology,* 532**,** 731-748.

HUNT, D. L. & CASTILLO, P. E. 2012. Synaptic plasticity of NMDA receptors: mechanisms and functional implications. *Current opinion in neurobiology,* 22**,** 496-508.

INCHAUSPE, C. G., MARTINI, F. J., FORSYTHE, I. D. & UCHITEL, O. D. 2004. Functional compensation of P/Q by N-type channels blocks short-term plasticity at the calyx of held presynaptic terminal. *Journal of Neuroscience,* 24**,** 10379-10383.

IRIE, T., KIKURA-HANAJIRI, R., USAMI, M., UCHIYAMA, N., GODA, Y. & SEKINO, Y. 2015. MAM-2201, a synthetic cannabinoid drug of abuse, suppresses the synaptic input to cerebellar Purkinje cells via activation of presynaptic CB1 receptors. *Neuropharmacology,* 95**,** 479-491.

ITO, M. 2006. Cerebellar circuitry as a neuronal machine. *Progress in neurobiology,* 78**,** 272-303.

ITO, M. & ITŌ, M. 1984. *The cerebellum and neural control*, Raven press.

IWASAKI, S. & TAKAHASHI, T. 1998. Developmental changes in calcium channel types mediating synaptic transmission in rat auditory brainstem. *The Journal of physiology,* 509**,** 419-423.
JACOBY, S., SIMS, R. E. & HARTELL, N. A. 2001. Nitric oxide is required for the induction and heterosynaptic spread of long-term potentiation in rat cerebellar slices. *The Journal of physiology,* 535**,** 825-839.
JAEGER, D. 2003. No parallel fiber volleys in the cerebellar cortex: evidence from cross-correlation analysis between Purkinje cells in a computer model and in recordings from anesthetized rats. *Journal of computational neuroscience,* 14**,** 311-327.
JAKAB, R. & HAMORI, J. 1988. Quantitative morphology and synaptology of cerebellar glomeruli in the rat. *Anatomy and embryology,* 179**,** 81-88.
JEWETT, B. E. & THAPA, B. 2018. Physiology, NMDA Receptor. *StatPearls [Internet].* StatPearls Publishing.
JÖRNTELL, H. & EKEROT, C.-F. 2003. Receptive field plasticity profoundly alters the cutaneous parallel fiber synaptic input to cerebellar interneurons in vivo. *Journal of Neuroscience,* 23**,** 9620-9631.
KAESER, P. S. & REGEHR, W. G. 2014. Molecular mechanisms for synchronous, asynchronous, and spontaneous neurotransmitter release. *Annual review of physiology,* 76**,** 333-363.
KANDEL, E., SCHWARTZ, J. & JESSELL, T. 1991. Principles of Neural Science Third Edition, Chapter32 Hearing. Elsevier Science Publishing Co., Inc.
KANDEL, E. R., SCHWARTZ, J. H., JESSELL, T. M., BIOCHEMISTRY, D. O., JESSELL, M. B. T., SIEGELBAUM, S. & HUDSPETH, A. 2000. *Principles of neural science*, McGraw-hill New York.
KAO, C. Y. 1986. Structure-Activity Relations of Tetrodotoxin, Saxitoxin, and Analogues a, b. *Annals of the New York Academy of Sciences,* 479**,** 52-67.
KATONA, I., RANCZ, E. A., ACSÁDY, L., LEDENT, C., MACKIE, K., HÁJOS, N. & FREUND, T. F. 2001. Distribution of CB1 cannabinoid receptors in the amygdala and their role in the control of GABAergic transmission. *Journal of Neuroscience,* 21**,** 9506-9518.
KATZ, B. 1969. The release of neural transmitter substances. *Liverpool University Press***,** 5-39.
KATZ, B. & MILEDI, R. 1968. The role of calcium in neuromuscular facilitation. *The Journal of physiology,* 195**,** 481.
KAWAMURA, Y., FUKAYA, M., MAEJIMA, T., YOSHIDA, T., MIURA, E., WATANABE, M., OHNO-SHOSAKU, T. & KANO, M. 2006. The CB1 cannabinoid receptor is the major cannabinoid receptor at excitatory presynaptic sites in the hippocampus and cerebellum. *Journal of Neuroscience,* 26**,** 2991-3001.
KENDALL, D. A. & YUDOWSKI, G. A. 2017. Cannabinoid receptors in the central nervous system: their signaling and roles in disease. *Frontiers in cellular neuroscience,* 10**,** 294.
KLECKNER, N. W. & DINGLEDINE, R. 1988. Requirement for glycine in activation of NMDA-receptors expressed in Xenopus oocytes. *Science,* 241**,** 835-837.
KOCHLAMAZASHVILI, G., SENKOV, O. & DITYATEV, A. 2011. Extracellular Recordings of Synaptic Plasticity and Network Oscillations in Hippocampal Slices. *Neuronal Network Analysis.* Springer.
KOMURO, H. & RAKIC, P. 1998. Distinct modes of neuronal migration in different domains of developing cerebellar cortex. *Journal of Neuroscience,* 18**,** 1478-1490.
KOMURO, H., YACUBOVA, E., YACUBOVA, E. & RAKIC, P. 2001. Mode and tempo of tangential cell migration in the cerebellar external granular layer. *Journal of Neuroscience,* 21**,** 527-540.
KREITZER, A. C. & REGEHR, W. G. 2001a. Cerebellar depolarization-induced suppression of inhibition is mediated by endogenous cannabinoids. *Journal of Neuroscience,* 21**,** RC174-RC174.
KREITZER, A. C. & REGEHR, W. G. 2001b. Retrograde inhibition of presynaptic calcium influx by endogenous cannabinoids at excitatory synapses onto Purkinje cells. *Neuron,* 29**,** 717-727.

KREUTZ, M. R. & SALA, C. 2012. *Synaptic Plasticity: Dynamics, Development and Disease*, Springer Science & Business Media.
LAINÉ, J. & AXELRAD, H. 2002. Extending the cerebellar Lugaro cell class. *Neuroscience,* 115**,** 363-374.
LAMONT, M. G. & WEBER, J. T. 2012. The role of calcium in synaptic plasticity and motor learning in the cerebellar cortex. *Neuroscience & Biobehavioral Reviews,* 36**,** 1153-1162.
LEREA, L. S. & MCNAMARA, J. O. 1993. Ionotropic glutamate receptor subtypes activate c-fos transcription by distinct calcium-requiring intracellular signaling pathways. *Neuron,* 10**,** 31-41.
LESTER, A. 1990. JR, Clements, JD, Westbrook, G. L. &Jahr. CE.
LÉVÉNÈS, C., DANIEL, H., SOUBRIÉ, P. & CRÉPEL, F. 1998. Cannabinoids decrease excitatory synaptic transmission and impair long-term depression in rat cerebellar Purkinje cells. *The Journal of physiology,* 510**,** 867-879.
LI, L. & CHIN, L.-S. 2003. The molecular machinery of synaptic vesicle exocytosis. *Cellular and Molecular Life Sciences CMLS,* 60**,** 942-960.
LIANG, Y. C., HUANG, C. C., HSU, K. S. & TAKAHASHI, T. 2004. Cannabinoid-induced presynaptic inhibition at the primary afferent trigeminal synapse of juvenile rat brainstem slices. *The Journal of physiology,* 555**,** 85-96.
LIU, J., CHANG, L., SONG, Y., LI, H. & WU, Y. 2019. The Role of NMDA Receptors in Alzheimer's Disease. *Frontiers in Neuroscience,* 13.
LLANO, I., MARTY, A., ARMSTRONG, C. M. & KONNERTH, A. 1991. Synaptic-and agonist-induced excitatory currents of Purkinje cells in rat cerebellar slices. *The Journal of Physiology,* 434**,** 183-213.
LLINAS, R. & NEGRELLO, M. N. 2015. Cerebellum. *Scholarpedia,* 10**,** 4606.
LLINAS, R., STEINBERG, I. & WALTON, K. 1981. Relationship between presynaptic calcium current and postsynaptic potential in squid giant synapse. *Biophysical journal,* 33**,** 323-351.
LONCHAMP, E., GAMBINO, F., DUPONT, J. L., DOUSSAU, F., VALERA, A., POULAIN, B. & BOSSU, J.-L. 2012. Pre and post synaptic NMDA effects targeting Purkinje cells in the mouse cerebellar cortex. *PloS one,* 7**,** e30180.
MACDERMOTT, A. B., MAYER, M. L., WESTBROOK, G. L., SMITH, S. J. & BARKER, J. L. 1986. NMDA-receptor activation increases cytoplasmic calcium concentration in cultured spinal cord neurones. *Nature,* 321**,** 519.
MAEJIMA, T., HASHIMOTO, K., YOSHIDA, T., AIBA, A. & KANO, M. 2001a. Presynaptic inhibition caused by retrograde signal from metabotropic glutamate to cannabinoid receptors. *Neuron,* 31**,** 463-475.
MAEJIMA, T., OHNO-SHOSAKU, T. & KANO, M. 2001b. Endogenous cannabinoid as a retrograde messenger from depolarized postsynaptic neurons to presynaptic terminals. *Neuroscience research,* 40**,** 205-210.
MALENKA, R. C. & NICOLL, R. A. 1999. Long-term potentiation--a decade of progress? *Science,* 285**,** 1870-1874.
MALINOW, R. 2012. New developments on the role of NMDA receptors in Alzheimer's disease. *Current Opinion in Neurobiology,* 22**,** 559-563.
MAO, T., O'CONNOR, D. H., SCHEUSS, V., NAKAI, J. & SVOBODA, K. 2008. Characterization and subcellular targeting of GCaMP-type genetically-encoded calcium indicators. *PloS one,* 3**,** e1796.
MARGRIE, T. W., ROSTAS, J. A. & SAH, P. 1998. Long-term potentiation of synaptic transmission in the avian hippocampus. *Journal of Neuroscience,* 18**,** 1207-1216.
MATSUDA, L. A., LOLAIT, S. J., BROWNSTEIN, M. J., YOUNG, A. C. & BONNER, T. I. 1990. Structure of a cannabinoid receptor and functional expression of the cloned cDNA. *Nature,* 346**,** 561.

MAYER, A. 2001. What drives membrane fusion in eukaryotes? *Trends in biochemical sciences,* 26**,** 717-723.
MAYER, M. & WESTBROOK, G. 1987. Permeation and block of N-methyl-D-aspartic acid receptor channels by divalent cations in mouse cultured central neurones. *The Journal of physiology,* 394**,** 501-527.
MAYER, M. L., WESTBROOK, G. L. & GUTHRIE, P. B. 1984. Voltage-dependent block by Mg 2+ of NMDA responses in spinal cord neurones. *Nature,* 309**,** 261.
MCBAIN, C. & MAYER, M. 1994. N-methyl-D-aspartic acid receptor structure and function. *Physiological reviews,* 74**,** 723-760.
MENNERICK, S. & ZORUMSKI, C. 1995. Paired-pulse modulation of fast excitatory synaptic currents in microcultures of rat hippocampal neurons. *The Journal of physiology,* 488**,** 85-101.
MINTZ, I., SABATINI, B. & REGEHR, W. 1995. Calcium control of transmitter release at a cerebellar synapse. *Neuron,* 15**,** 675-688.
MOECHARS, D., DEWACHTER, I., LORENT, K., REVERSÉ, D., BAEKELANDT, V., NAIDU, A., TESSEUR, I., SPITTAELS, K., VAN DEN HAUTE, C. & CHECLER, F. 1999. Early phenotypic changes in transgenic mice that overexpress different mutants of amyloid precursor protein in brain. *Journal of Biological Chemistry,* 274**,** 6483-6492.
MOORE, J. W. & NARAHASHI, T. Tetrodotoxin's highly selective blockage of an ionic channel. Fed Proc, 1967. 1655-1663.
MORIYOSHI, K., MASU, M., ISHII, T., SHIGEMOTO, R., MIZUNO, N. & NAKANISHI, S. 1991. Molecular cloning and characterization of the rat NMDA receptor. *Nature,* 354**,** 31.
MOTA, S. I., FERREIRA, I. L. & REGO, A. C. 2014. Dysfunctional synapse in Alzheimer's disease–A focus on NMDA receptors. *Neuropharmacology,* 76**,** 16-26.
NAKAI, J., OHKURA, M. & IMOTO, K. 2001. A high signal-to-noise Ca 2+ probe composed of a single green fluorescent protein. *Nature biotechnology,* 19**,** 137.
NAPPER, R. & HARVEY, R. 1988. Number of parallel fiber synapses on an individual Purkinje cell in the cerebellum of the rat. *Journal of Comparative Neurology,* 274**,** 168-177.
NARAHASHI, T. 2008. Tetrodotoxin. *Proceedings of the Japan Academy, Series B,* 84**,** 147-154.
NIEUWENHUYS, R., VOOGD, J. & VAN HUIJZEN, C. 2007. *The human central nervous system: a synopsis and atlas*, Springer Science & Business Media.
NOLTE, J. 1988. The Cerebellum. *J. Nolte The Human Brain: An Introduction to its Functional Anatomy*.
NÚÑEZ, E., BENITO, C., PAZOS, M. R., BARBACHANO, A., FAJARDO, O., GONZÁLEZ, S., TOLÓN, R. M. & ROMERO, J. 2004. Cannabinoid CB2 receptors are expressed by perivascular microglial cells in the human brain: an immunohistochemical study. *Synapse,* 53**,** 208-213.
NUNZI, M. G., BIRNSTIEL, S., BHATTACHARYYA, B. J., SLATER, N. T. & MUGNAINI, E. 2001. Unipolar brush cells form a glutamatergic projection system within the mouse cerebellar cortex. *Journal of Comparative Neurology,* 434**,** 329-341.
OHKURA, M., SASAKI, T., SADAKARI, J., GENGYO-ANDO, K., KAGAWA-NAGAMURA, Y., KOBAYASHI, C., IKEGAYA, Y. & NAKAI, J. 2012. Genetically encoded green fluorescent Ca2+ indicators with improved detectability for neuronal Ca2+ signals. *PloS one,* 7**,** e51286.
OKOROCHA, A. E. 2016. *Fluorescent protein calcium sensor for monitoring synaptic transmission.* Department of Cell Physiology & Pharmacology.
OPAZO, P., LABRECQUE, S., TIGARET, C. M., FROUIN, A., WISEMAN, P. W., DE KONINCK, P. & CHOQUET, D. 2010. CaMKII triggers the diffusional trapping of surface AMPARs through phosphorylation of stargazin. *Neuron,* 67**,** 239-252.
PALAY, S. L. & CHAN-PALAY, V. 2012. *Cerebellar cortex: cytology and organization*, Springer Science & Business Media.

PALKOVITS, M., MAGYAR, P. & SZENTÁGOTHAI, J. 1971. Quantitative histological analysis of the cerebellar cortex in the cat: II. Cell numbers and densities in the granular layer. *Brain research,* 32**,** 15-30.

PANG, Z. P. & SÜDHOF, T. C. 2010. Cell biology of Ca2+-triggered exocytosis. *Current opinion in cell biology,* 22**,** 496-505.

PELLIONISZ, A. & SZENTA, J. 1973. Dynamic single unit simulation of a realistic cerebellar network model. *Brain research,* 49**,** 83-99.

PEREDA, D., AL-OSTA, I., OKOROCHA, A. E., EASTON, A. & HARTELL, N. A. 2019. Changes in presynaptic calcium signalling accompany age-related deficits in hippocampal LTP and cognitive impairment. *Aging cell,* 18**,** e13008.

PETRALIA, R., WANG, Y. & WENTHOLD, R. 1994. The NMDA receptor subunits NR2A and NR2B show histological and ultrastructural localization patterns similar to those of NR1. *Journal of Neuroscience,* 14**,** 6102-6120.

PREIBISCH, S., SAALFELD, S. & TOMANCAK, P. 2009. Globally optimal stitching of tiled 3D microscopic image acquisitions. *Bioinformatics,* 25**,** 1463-1465.

PURVES, D., AUGUSTINE, G., FITZPATRICK, D., HALL, W., LAMANTIA, A., MCNAMARA, J. & WHITE, L. 2012. Neuroscience. 4: e uppl. Sinauer Associates, Massachusetts USA.

PURVES, D., AUGUSTINE, G. J., FITZPATRICK, D., HALL, W. C., LAMANTIA, A.-S., MCNAMARA, J. O. & WHITE, L. E. 2008. Neuroscience. 4th. *Sunderland, Mass.: Sinauer. xvii,* 857**,** 944.

QIAN, J. & SAGGAU, P. 1999. Modulation of transmitter release by action potential duration at the hippocampal CA3-CA1 synapse. *Journal of Neurophysiology,* 81**,** 288-298.

REGEHR, W. G. 2012. Short-term presynaptic plasticity. *Cold Spring Harbor perspectives in biology,* 4**,** a005702.

ROBBE, D., ALONSO, G., DUCHAMP, F., BOCKAERT, J. & MANZONI, O. J. 2001. Localization and mechanisms of action of cannabinoid receptors at the glutamatergic synapses of the mouse nucleus accumbens. *Journal of Neuroscience,* 21**,** 109-116.

ROKNI, D., LLINAS, R. R. & YAROM, Y. 2008. The morpho/functional discrepancy in the cerebellar cortex: Looks alone are deceptive. *Frontiers in neuroscience,* 2**,** 36.

ROSSI, B., OGDEN, D., LLANO, I., TAN, Y. P., MARTY, A. & COLLIN, T. 2012. Current and calcium responses to local activation of axonal NMDA receptors in developing cerebellar molecular layer interneurons. *PLoS One,* 7**,** e39983.

ROSSI, D. J., ALFORD, S., MUGNAINI, E. & SLATER, N. T. 1995. Properties of transmission at a giant glutamatergic synapse in cerebellum: the mossy fiber-unipolar brush cell synapse. *Journal of neurophysiology,* 74**,** 24-42.

RUSSELL, J. T. 2011. Imaging calcium signals in vivo: a powerful tool in physiology and pharmacology. *British journal of pharmacology,* 163**,** 1605-1625.

SACHANA, M., MUNN, S. & BAL-PRICE, A. 2016. Adverse Outcome Pathway on binding of agonists to ionotropic glutamate receptors in adult brain leading to excitotoxicity that mediates neuronal cell death, contributing to learning and memory impairment.

SALIN, P. A., MALENKA, R. C. & NICOLL, R. A. 1996. Cyclic AMP mediates a presynaptic form of LTP at cerebellar parallel fiber synapses. *Neuron,* 16**,** 797-803.

SCHINDELIN, J., ARGANDA-CARRERAS, I., FRISE, E., KAYNIG, V., LONGAIR, M., PIETZSCH, T., PREIBISCH, S., RUEDEN, C., SAALFELD, S. & SCHMID, B. 2012. Fiji: an open-source platform for biological-image analysis. *Nature methods,* 9**,** 676.

SCHMAHMANN, J. D. 2004. Disorders of the cerebellum: ataxia, dysmetria of thought, and the cerebellar cognitive affective syndrome. *The Journal of neuropsychiatry and clinical neurosciences,* 16**,** 367-378.

SCHWEIGHOFER, N., DOYA, K. & KURODA, S. 2004. Cerebellar aminergic neuromodulation: towards a functional understanding. *Brain Research Reviews,* 44**,** 103-116.

SCHWITZER, T., SCHWAN, R., ANGIOI-DUPREZ, K., INGSTER-MOATI, I., LALANNE, L., GIERSCH, A. & LAPREVOTE, V. 2015. The cannabinoid system and visual processing: a review on

experimental findings and clinical presumptions. *European Neuropsychopharmacology,* 25**,** 100-112.
SEELIG, J. D., CHIAPPE, M. E., LOTT, G. K., DUTTA, A., OSBORNE, J. E., REISER, M. B. & JAYARAMAN, V. 2010. Two-photon calcium imaging from head-fixed Drosophila during optomotor walking behavior. *Nature methods,* 7**,** 535.
SGOBIO, C., KUPFERSCHMIDT, D. A., CUI, G., SUN, L., LI, Z., CAI, H. & LOVINGER, D. M. 2014. Optogenetic measurement of presynaptic calcium transients using conditional genetically encoded calcium indicator expression in dopaminergic neurons. *PLoS One,* 9**,** e111749.
SHIMOMURA, O., JOHNSON, F. H. & SAIGA, Y. 1962. Extraction, purification and properties of aequorin, a bioluminescent protein from the luminous hydromedusan, Aequorea. *Journal of cellular and comparative physiology,* 59**,** 223-239.
SHIN, R.-M., TULLY, K., LI, Y., CHO, J.-H., HIGUCHI, M., SUHARA, T. & BOLSHAKOV, V. Y. 2010. Hierarchical order of coexisting pre-and postsynaptic forms of long-term potentiation at synapses in amygdala. *Proceedings of the National Academy of Sciences,* 107**,** 19073-19078.
SHINODA, Y., SUGIUCHI, Y., FUTAMI, T. & IZAWA, R. 1992. Axon collaterals of mossy fibers from the pontine nucleus in the cerebellar dentate nucleus. *Journal of neurophysiology,* 67**,** 547-560.
SIEGEL, A. & SAPRU, H. N. 2015. *Essential neuroscience,* Philadelphia, Wolters Kluwer Health.
SIMONS, T. J. 1988. Calcium and neuronal function. *Neurosurgical review,* 11**,** 119-129.
SIMS, R. E. & HARTELL, N. A. 2005. Differences in transmission properties and susceptibility to long-term depression reveal functional specialization of ascending axon and parallel fiber synapses to Purkinje cells. *Journal of Neuroscience,* 25**,** 3246-3257.
SIMS, R. E. & HARTELL, N. A. 2006. Differential susceptibility to synaptic plasticity reveals a functional specialization of ascending axon and parallel fiber synapses to cerebellar Purkinje cells. *Journal of Neuroscience,* 26**,** 5153-5159.
SJÖSTRÖM, P. J., TURRIGIANO, G. G. & NELSON, S. B. 2003. Neocortical LTD via Coincident Activation of Presynaptic NMDA and Cannabinoid Receptors. *Neuron,* 39**,** 641-654.
STOODLEY, C. J. & SCHMAHMANN, J. D. 2010. Evidence for topographic organization in the cerebellum of motor control versus cognitive and affective processing. *cortex,* 46**,** 831-844.
STOSIEK, C., GARASCHUK, O., HOLTHOFF, K. & KONNERTH, A. 2003. In vivo two-photon calcium imaging of neuronal networks. *Proceedings of the National Academy of Sciences,* 100**,** 7319-7324.
STRATA, P. & ROSSI, F. 1998. Plasticity of the olivocerebellar pathway. *Trends in neurosciences,* 21**,** 407-413.
STRICK, P. L., DUM, R. P. & FIEZ, J. A. 2009. Cerebellum and nonmotor function. *Annual review of neuroscience,* 32**,** 413-434.
SUÁREZ, L. M., SUÁREZ, F., DEL OLMO, N., RUIZ, M., GONZÁLEZ-ESCALADA, J. R. & SOLÍS, J. M. 2005. Presynaptic NMDA autoreceptors facilitate axon excitability: a new molecular target for the anticonvulsant gabapentin. *European Journal of Neuroscience,* 21**,** 197-209.
SUCHER, N. J., AWOBULUYI, M., CHOI, Y.-B. & LIPTON, S. A. 1996. NMDA receptors: from genes to channels. *Trends in Pharmacological Sciences,* 17**,** 348-355.
SÜDHOF, T. C. 1995. The synaptic vesicle cycle: a cascade of protein–protein interactions. *Nature,* 375**,** 645.
SÜDHOF, T. C. 2004. The synaptic vesicle cycle. *Annu. Rev. Neurosci.,* 27**,** 509-547.
SÜDHOF, T. C. 2013. A molecular machine for neurotransmitter release: synaptotagmin and beyond. *Nature medicine,* 19**,** 1227.
SUN, Y.-G., WU, C.-S., LU, H.-C. & BEIERLEIN, M. 2011. Target-dependent control of synaptic inhibition by endocannabinoids in the thalamus. *Journal of Neuroscience,* 31**,** 9222-9230.

SUTTON, J. K. 1999. *An investigation into the synaptic conditions and celluar mechanisms underlying cerebellar synaptic plasticity.* Aston University.
SUTTON, N. G. 1971. *Anatomy of the Brain and Spinal Medulla: A Manual for Students*, Butterworths.
SZABO, B., THAN, M., THORN, D. & WALLMICHRATH, I. 2004. Analysis of the effects of cannabinoids on synaptic transmission between basket and Purkinje cells in the cerebellar cortex of the rat. *Journal of Pharmacology and Experimental Therapeutics,* 310**,** 915-925.
SZABO, B., WALLMICHRATH, I., MATHONIA, P. & PFREUNDTNER, C. 2000. Cannabinoids inhibit excitatory neurotransmission in the substantia nigra pars reticulata. *Neuroscience,* 97**,** 89-97.
SZAPIRO, G. & BARBOUR, B. 2007. Multiple climbing fibers signal to molecular layer interneurons exclusively via glutamate spillover. *Nature neuroscience,* 10**,** 735.
SZENTÁGOTHAI, J., HÁMORI, J. & TÖMBÖL, T. 1966. Degeneration and electron microscope analysis of the synaptic glomeruli in the lateral geniculate body. *Experimental Brain Research,* 2**,** 283-301.
TADA, M., TAKEUCHI, A., HASHIZUME, M., KITAMURA, K. & KANO, M. 2014. A highly sensitive fluorescent indicator dye for calcium imaging of neural activity in vitro and in vivo. *European Journal of Neuroscience,* 39**,** 1720-1728.
TAKAHASHI, K. A. & LINDEN, D. J. 2000. Cannabinoid receptor modulation of synapses received by cerebellar Purkinje cells. *Journal of Neurophysiology,* 83**,** 1167-1180.
TAKEI, K., SHIN, R.-M., INOUE, T., KATO, K. & MIKOSHIBA, K. 1998. Regulation of nerve growth mediated by inositol 1, 4, 5-trisphosphate receptors in growth cones. *Science,* 282**,** 1705-1708.
TALLINI, Y. N., OHKURA, M., CHOI, B.-R., JI, G., IMOTO, K., DORAN, R., LEE, J., PLAN, P., WILSON, J. & XIN, H.-B. 2006. Imaging cellular signals in the heart in vivo: Cardiac expression of the high-signal Ca2+ indicator GCaMP2. *Proceedings of the National Academy of Sciences,* 103**,** 4753-4758.
TAURA, F., SIRIKANTARAMAS, S., SHOYAMA, Y., SHOYAMA, Y. & MORIMOTO, S. 2007. Phytocannabinoids in Cannabis sativa: recent studies on biosynthetic enzymes. *Chemistry & biodiversity,* 4**,** 1649-1663.
TERUNUMA, M., REVILLA-SANCHEZ, R., QUADROS, I. M., DENG, Q., DEEB, T. Z., LUMB, M., SICINSKI, P., HAYDON, P. G., PANGALOS, M. N. & MOSS, S. J. 2014. Postsynaptic GABAB receptor activity regulates excitatory neuronal architecture and spatial memory. *Journal of Neuroscience,* 34**,** 804-816.
THESTRUP, T., LITZLBAUER, J., BARTHOLOMÄUS, I., MUES, M., RUSSO, L., DANA, H., KOVALCHUK, Y., LIANG, Y., KALAMAKIS, G. & LAUKAT, Y. 2014. Optimized ratiometric calcium sensors for functional in vivo imaging of neurons and T lymphocytes. *Nature methods,* 11**,** 175.
THOMSON, A. M. 2000. Facilitation, augmentation and potentiation at central synapses. *Trends in neurosciences,* 23**,** 305-312.
TIAN, L., AKERBOOM, J., SCHREITER, E. R. & LOOGER, L. L. 2012. Neural activity imaging with genetically encoded calcium indicators. *Progress in brain research.* Elsevier.
TIAN, L., HIRES, S. A., MAO, T., HUBER, D., CHIAPPE, M. E., CHALASANI, S. H., PETREANU, L., AKERBOOM, J., MCKINNEY, S. A. & SCHREITER, E. R. 2009. Imaging neural activity in worms, flies and mice with improved GCaMP calcium indicators. *Nature methods,* 6**,** 875.
TIBBETTS, P. E. 2013. Principles of Neural Science edited by Eric R. Kandel, James H. Schwartz, Thomas M. Jessell, Steven A. Siegelbaum, A. J. Hudspeth, and Sarah Mack. *The Quarterly Review of Biology,* 88**,** 139-140.
TIGYI, G., MATUTE, C. & MILEDI, R. 1990. Monoclonal antibodies to cerebellar pinceau terminals obtained after immunization with brain mRNA-injected Xenopus oocytes. *Proceedings of the National Academy of Sciences,* 87**,** 528-532.

TRAYNELIS, S. F., WOLLMUTH, L. P., MCBAIN, C. J., MENNITI, F. S., VANCE, K. M., OGDEN, K. K., HANSEN, K. B., YUAN, H., MYERS, S. J. & DINGLEDINE, R. 2010. Glutamate receptor ion channels: structure, regulation, and function. *Pharmacological reviews,* 62**,** 405-496.

TRUSSELL, L. O., ZHANG, S. & RAMANT, I. M. 1993. Desensitization of AMPA receptors upon multiquantal neurotransmitter release. *Neuron,* 10**,** 1185-1196.

TSIEN, R. Y. 1998. The green fluorescent protein. Annual Reviews 4139 El Camino Way, PO Box 10139, Palo Alto, CA 94303-0139, USA.

TSOU, K., BROWN, S., SANUDO-PENA, M., MACKIE, K. & WALKER, J. 1998. Immunohistochemical distribution of cannabinoid CB1 receptors in the rat central nervous system. *Neuroscience,* 83**,** 393-411.

VALTORTA, F., PENNUTO, M., BONANOMI, D. & BENFENATI, F. 2004. Synaptophysin: leading actor or walk-on role in synaptic vesicle exocytosis? *Bioessays,* 26**,** 445-453.

VAN DEN BURG, E., ENGELMANN, J. P., BACELO, J., GÓMEZ, L. & GRANT, K. 2007. Etomidate reduces initiation of backpropagating dendritic action potentials: implications for sensory processing and synaptic plasticity during anesthesia. *Journal of neurophysiology*.

VOOGD, J. & GLICKSTEIN, M. 1998. The anatomy of the cerebellum. *Trends in cognitive sciences,* 2**,** 307-313.

VRANESIC, I., IIJIMA, T., ICHIKAWA, M., MATSUMOTO, G. & KNÖPFEL, T. 1994. Signal transmission in the parallel fiber-Purkinje cell system visualized by high-resolution imaging. *Proceedings of the National Academy of Sciences,* 91**,** 13014-13017.

VYKLICKY, V., KORINEK, M., SMEJKALOVA, T., BALIK, A., KRAUSOVA, B., KANIAKOVA, M., LICHNEROVA, K., CERNY, J., KRUSEK, J. & DITTERT, I. 2014. Structure, function, and pharmacology of NMDA receptor channels. *Physiological research,* 63.

WALL, M. J., ATTERBURY, A. & DALE, N. 2007. Control of basal extracellular adenosine concentration in rat cerebellum. *The Journal of physiology,* 582**,** 137-151.

WALLACH, J., KANG, H., COLESTOCK, T., MORRIS, H., BORTOLOTTO, Z. A., COLLINGRIDGE, G. L., LODGE, D., HALBERSTADT, A. L., BRANDT, S. D. & ADEJARE, A. 2016. Pharmacological investigations of the dissociative 'legal highs' diphenidine, methoxphenidine and analogues. *PLoS One,* 11**,** e0157021.

WANG, Q., SHUI, B., KOTLIKOFF, M. I. & SONDERMANN, H. 2008. Structural basis for calcium sensing by GCaMP2. *Structure,* 16**,** 1817-1827.

WATKINS, J. & EVANS, R. 1981. Excitatory amino acid transmitters. *Annual review of pharmacology and toxicology,* 21**,** 165-204.

WILSON, R. I., KUNOS, G. & NICOLL, R. A. 2001. Presynaptic specificity of endocannabinoid signaling in the hippocampus. *Neuron,* 31**,** 453-462.

WILSON, R. I. & NICOLL, R. A. 2001. Endogenous cannabinoids mediate retrograde signalling at hippocampal synapses. *Nature,* 410**,** 588.

WILSON, R. I. & NICOLL, R. A. 2002. Endocannabinoid signaling in the brain. *Science,* 296**,** 678-682.

WONG, E., KEMP, J. A., PRIESTLEY, T., KNIGHT, A. R., WOODRUFF, G. N. & IVERSEN, L. L. 1986. The anticonvulsant MK-801 is a potent N-methyl-D-aspartate antagonist. *Proceedings of the National Academy of Sciences,* 83**,** 7104-7108.

WRIGHT, M., SKAGGS, W. & NIELSEN, F. A. 2016. The cerebellum. *WikiJournal of Medicine,* 3**,** 1.

XU, H., YANG, Y., TANG, X., ZHAO, M., LIANG, F., XU, P., HOU, B., XING, Y., BAO, X. & FAN, X. 2013. Bergmann glia function in granule cell migration during cerebellum development. *Molecular neurobiology,* 47**,** 833-844.

XU, J.-Y. & CHEN, C. 2015. Endocannabinoids in synaptic plasticity and neuroprotection. *The Neuroscientist,* 21**,** 152-168.

YACUBOVA, E. & KOMURO, H. 2002. Cellular and molecular mechanisms of cerebellar granule cell migration. *Cell biochemistry and biophysics,* 37**,** 213-234.

YANG, Y. & CALAKOS, N. 2013. Presynaptic long-term plasticity. *Frontiers in synaptic neuroscience,* 5**,** 8.

YOSHIDA, T., HASHIMOTO, K., ZIMMER, A., MAEJIMA, T., ARAISHI, K. & KANO, M. 2002. The cannabinoid CB1 receptor mediates retrograde signals for depolarization-induced suppression of inhibition in cerebellar Purkinje cells. *Journal of Neuroscience,* 22**,** 1690-1697.

ZAPATA-HOMMER, O. & GRIESBECK, O. 2003. Efficiently folding and circularly permuted variants of the Sapphire mutant of GFP. *BMC biotechnology,* 3**,** 5.

ZHANG, W. & LINDEN, D. J. 2009. Neuromodulation at single presynaptic boutons of cerebellar parallel fibers is determined by bouton size and basal action potential-evoked Ca transient amplitude. *Journal of Neuroscience,* 29**,** 15586-15594.

ZHANG, W. & LINDEN, D. J. 2012. Calcium influx measured at single presynaptic boutons of cerebellar granule cell ascending axons and parallel fibers. *The Cerebellum,* 11**,** 121-131.

ZIMMER, A., ZIMMER, A. M., HOHMANN, A. G., HERKENHAM, M. & BONNER, T. I. 1999. Increased mortality, hypoactivity, and hypoalgesia in cannabinoid CB1 receptor knockout mice. *Proceedings of the National Academy of Sciences,* 96**,** 5780-5785.

ZUCKER, R. S. 1989. Short-term synaptic plasticity. *Annual review of neuroscience,* 12**,** 13-31.

ZUCKER, R. S. & REGEHR, W. G. 2002. Short-term synaptic plasticity. *Annual review of physiology,* 64**,** 355-405.

ZUKIN, R. S. & BENNETT, M. V. L. 1995. Alternatively spliced isoforms of the NMDARI receptor subunit. *Trends in Neurosciences,* 18**,** 306-313.